



UNIVERSIDADE ESTADUAL DE CAMPINAS

Faculdade de Engenharia de Alimentos

TATIANA PORTO DOS SANTOS

MICROFLUIDICS AS A TOOL TO EVALUATE EMULSION STABILITY

MICROFLUIDICA COMO UMA FERRAMENTA PARA A AVALIAÇÃO DA  
ESTABILIDADE DE EMULSÕES

CAMPINAS

2021

TATIANA PORTO DOS SANTOS

MICROFLUIDICS AS A TOOL TO EVALUATE EMULSION STABILITY

MICROFLUIDICA COMO UMA FERRAMENTA PARA A AVALIAÇÃO DA  
ESTABILIDADE DE EMULSÕES

Thesis presented to the Faculty of Food Engineering of the University of Campinas in partial fulfillment of the requirements for the degree of Doctor in Food Engineering

Tese apresentada à Faculdade de Engenharia de Alimentos da Universidade Estadual de Campinas como parte dos requisitos exigidos para a obtenção do título de Doutora em Engenharia de Alimentos

Orientador: Profa. Dra. Rosiane Lopes da Cunha

ESTE TRABALHO CORRESPONDE À  
VERSÃO FINAL DA TESE DEFENDIDA  
PELA ALUNA TATIANA PORTO DOS  
SANTOS, E ORIENTADA PELA PROFA.  
DRA. ROSIANE LOPES DA CUNHA

CAMPINAS

2021

Ficha catalográfica  
Universidade Estadual de Campinas  
Biblioteca da Faculdade de Engenharia de Alimentos  
Claudia Aparecida Romano - CRB 8/5816

Santos, Tatiana Porto dos, 1990-  
Sa59m Microfluidics as a tool to evaluate emulsion stability / Tatiana Porto dos Santos. – Campinas, SP : [s.n.], 2021.

Orientador: Rosiane Lopes da Cunha.  
Tese (doutorado) – Universidade Estadual de Campinas, Faculdade de Engenharia de Alimentos.

1. Microcanais. 2. Desestabilização. 3. Antiespumantes. 4. Sistemas coloidais. 5. Avaliação dinâmica. I. Cunha, Rosiane Lopes da. II. Universidade Estadual de Campinas. Faculdade de Engenharia de Alimentos. III. Título.

Informações para Biblioteca Digital

**Título em outro idioma:** Microfluidica como uma ferramenta para a avaliação da estabilidade de emulsões

**Palavras-chave em inglês:**

Microchannels

Destabilization

Antifoams

Colloidal systems

Dynamic evaluation

**Área de concentração:** Engenharia de Alimentos

**Titulação:** Doutora em Engenharia de Alimentos

**Banca examinadora:**

Rosiane Lopes da Cunha [Orientador]

Maria Claudia Cuellar Soares

Lucimara Gaziola de La Torre

Carolina Siqueira Franco Picone

Márcio da Silveira Carvalho

**Data de defesa:** 20-04-2021

**Programa de Pós-Graduação:** Engenharia de Alimentos

**Identificação e informações acadêmicas do(a) aluno(a)**

- ORCID do autor: <https://orcid.org/0000-0002-9768-2006>

- Currículo Lattes do autor: <http://lattes.cnpq.br/9206317975691993>

## **FOLHA DE APROVAÇÃO**

### **COMISSÃO EXAMINADORA**

**Profa. Dra. Rosiane Lopes da Cunha**

Orientadora

FEA / UNICAMP

**Dra. Maria Claudia Cuellar Soares**

Membro

Pesquisador

**Profa. Dra. Lucimara Gaziola de La Torre**

Membro

FEQ / UNICAMP

**Profa. Dra. Carolina Siqueira Franco Picone**

Membro

FEA / UNICAMP

**Dr. Marcio da Silveira Carvalho**

Membro

Pontifícia Universidade Católica do Rio de Janeiro

*A Ata da defesa com as respectivas assinaturas dos membros encontra-se no SIGA/Sistema de Fluxo de Dissertação/Tese e na Secretaria do Programa da Unidade.*



*“Se eu vi mais longe, foi por estar sobre ombros de gigantes”.*

**Isaac Newton**

Dedico este trabalho ao meu companheiro

Cauki

## **AGRADECIMENTOS**

Neste documento, encontra-se um pouco da minha história científica decorrente desses últimos quatro (intensos) anos e que, de alguma maneira, contou com pessoas que foram essenciais para que tudo isso pudesse ser realizado. Assim, gostaria de expressar minha gratidão a estas pessoas que me auxiliaram não somente no âmbito científico, mas que também (e acima de tudo) compartilharam comigo momentos de alegria e foram meu alicerce nos momentos difíceis.

À professora Dra. Rosiane Lopes da Cunha, pela orientação e amizade. Não tenho palavras para expressar a gratidão que tenho pela Profa. Rosiane. Confesso que tive muita sorte em ter encontrado em meu caminho uma pessoa que não somente faz ciência com tanta propriedade, mas que também sabe ser orientadora, amiga e um ser humano incrível a todo momento. Só tenho a agradecer por todos os ensinamentos, conselhos e cuidado.

Aos meus pais Ana Livia e Osmar, pelo amor incondicional. Falar sobre o amor pelos meus pais e destacar o quanto eles me ajudam chega até ser redundante. Eles sabem o quanto me apoiam, me aconselham e estão sempre dispostos a me ajudar e a me colocar no colo. Nada que eu faça ou diga será suficiente para agradecer tudo o que fizeram, fazem e sei que farão por mim.

Ao meu marido Cauki, por tanto companheirismo. Obrigada por ser quem você é, pela paciência, pelo amor e cuidado inestimável presente em todos os momentos. Durante esta caminhada, não sei o que teria sido se não fosse você ao meu lado.

Aos meus sogros, Francisco e Gilcélia, pelo suporte e carinho de sempre. Agradeço por poder contar com vocês, na certeza que estarão sempre dispostos a ajudar.

À minha amiga Paula Okuro, por tantas memórias compartilhadas. Falar da Paula é falar de amor, carinho, cuidado, amizade. Obrigada, minha amiga.

À amiga Amanda, por ser uma pessoa tão caridosa e com tanta empatia que faz tudo ser bem mais leve. Obrigada pelas ajudas, conselhos e, acima de tudo, por sempre estar disposta a me ouvir, ajudar e partilhar comigo momentos memoráveis.

Às minhas queridas amigas Karen, Paula e Aline, que fizeram meu doutorado (e minha vida) mais leve e acolhedor. Obrigada por sempre me oferecerem colo e carinho.

Aos queridos do LEP que tive a feliz oportunidade de conhecer mais de perto e que tanto contribuíram comigo todos esses anos, Gabis, Jorge, Cris, Lary, Ana Carol, Ana Letícia, Andresa, Aureliano, Ana Caroline, Aninha, Fernando, Carol, Antônio, Cristhian, Monise, Raquel, Noádia, Karine, Flávia, Matheus, Thaís, Vanessinha, Zil, Rapha, Pier, Guilherme, Davi, Mariano e Nice.

Ao Mariano, por ter me acolhido para a realização das análises no Rio e por ser um amigo tão querido e sempre disposto a ajudar.

Aos amigos do *Microfluidics MEMS and Nanostructures Laboratory* (MMN), Maria, Marjan, Ilham, Maryam e Cesare por todo suporte emocional e científico durante minha estadia na França. Um especial agradecimento ao Cesare por estar sempre presente.

Ao Prof. Márcio Silveira Carvalho (PUC-Rio de Janeiro) por ter aberto as portas de seu laboratório para a realização de parte deste trabalho, provendo valiosas contribuições.

À *École Supérieure de Physique et de Chimie Industrielles de la Ville de Paris* e ao *Institut Pierre-Gilles de Gennes* por ter permitido a realização do meu doutorado sanduiche. E, um agradecimento especial ao meu supervisor na França, Prof. Patrick Tabeling, pela paciência e conhecimento compartilhado.

À Maria Helena de Oliveira Piazzetta e ao Angelo Gobbi do CNPEM (Centro Nacional de Pesquisa em Energia e Materiais) por sempre estarem disponíveis e dispostos a ajudar e a contribuir com o crescimento da pesquisa. E ao LNNano (Laboratório Nacional de Nanotecnologia - CNPEM) pela disposição da infraestrutura.

Aos membros da banca examinadora pelos conselhos e pelas correções que auxiliaram no aprimoramento da tese de doutorado aqui apresentada.

À Faculdade de Engenharia de Alimentos pelo acolhimento de tantos anos. São longos 12 anos compartilhados e que para sempre ficarão guardados na memória e no coração.

Aos professores e funcionários, pelos ensinamentos, suporte e paciência.

Agradeço também às agências de fomento.

Ao processo nº 2017/18109-0, 2018/18103-4 e 2019/07744-1, Fundação de Amparo à Pesquisa do Estado de São Paulo (FAPESP) pelo auxílio financeiro.

Ao Conselho Nacional de Desenvolvimento Científico e Tecnológico - CNPq (processo número 140700/2017-0) pelo auxílio financeiro.

O presente trabalho foi realizado com apoio da Coordenação de Aperfeiçoamento de Pessoal de Nível Superior - Brasil (CAPES) - Código de Financiamento 001.

Ressaltando que as opiniões, hipóteses e conclusões ou recomendações expressas neste material são de responsabilidade dos autores e não necessariamente refletem a visão das agências de fomento.

Enfim, meu muito obrigada a todos que, direta ou indiretamente, física ou emocionalmente, contribuíram para a realização deste trabalho.

## RESUMO

A capacidade de formação e estabilidade são características fundamentais a serem investigadas durante o desenvolvimento de emulsões visando aplicações tecnológicas. Por outro lado, em processos como os fermentativos e petrolíferos, em que ocorre a produção ou extração de compostos apolares, é desejada uma baixa estabilidade das emulsões inerentes ao processo, visando aumentar a recuperação eficiente do óleo. Neste contexto, a análise da estabilidade das emulsões é de suprema importância para se determinar a melhor composição dependendo das características da emulsão desejada. Ademais, desvendar os mecanismos de (des)estabilização seria de grande valia para o desenvolvimento destes importantes sistemas coloidais. Neste sentido, estratégias baseadas na microfluidica foram aplicadas para o estudo da (des)estabilização de gotas, uma vez que esta tecnologia pode alcançar tanto a formação das emulsões quanto sua separação eficiente das fases. Dentro deste viés, o presente estudo objetivou investigar a (des)estabilização de emulsões-modelo (usando surfactantes convencionais ou agentes tensoativos de sistemas fermentativos como estabilizantes) em microcanais. As estratégias aplicadas para tal foram, principalmente, alterações da geometria e das propriedades de parede dos canais, porém a adição de agentes externos (soluções aquosas) também foi realizada para induzir a desestabilização inclusive das emulsões mais estáveis. Por conseguinte, foi possível identificar os principais parâmetros relacionados aos mecanismos de (des)estabilização das emulsões, além de se determinar as condições de escoamento e os microcanais mais adequados para a indução deste fenômeno. De modo geral, foi observado que microcapilares de vidro não foram eficientes para a avaliação dos eventos de coalescência devido ao formato tridimensional, enquanto que os canais planares cujas dimensões são moduláveis foram mais adequados para a avaliação dos fenômenos de desestabilização. Ademais, constatou-se a dificuldade em se desestabilizar emulsões com alta concentração de estabilizantes utilizando microdispositivos que induzem o choque entre as gotas, todavia tal efeito foi alcançado através da injeção forçada de soluções aquosas em gotas concentradas. De fato, dependendo da solução aquosa adicionada (salina ou água deionizada), diferentes mecanismos de desestabilização foram visualizados (fratura, ruptura da gota na parede do canal e/ou coalescência). Tais mecanismos também foram modificados dependendo das propriedades de superfície dos microcanais (potencial zeta e hidrofobicidade). Desta maneira, o entendimento do papel da parede dos microcanais foi essencial para induzir tanto a formação quanto a desestabilização das gotas, permitindo modular a estabilidade cinética das emulsões. De modo geral, foi constatado que os estabilizantes carregados devem possuir cargas de mesmo

sinal que os microcanais para que as gotas sejam formadas, além de que a fase contínua da emulsão deve possuir a mesma natureza (polar ou apolar) que a parede dos canais. Em contrapartida, a aderência das gotas de óleo nas paredes dos dispositivos foi observada em duas ocasiões: (i) quando os microcanais possuíam uma alta hidrofobicidade e reduzida carga superficial e (ii) quando as gotas das emulsões possuíam cargas opostas às das paredes dos microcanais. Finalmente, este estudo permitiu indicar a utilização de microcanais em série para a determinação da estabilidade das gotas, no entanto ressalta-se que é necessário entender a priori as potenciais interações gotas-parede dos canais.

**Palavras-chave:** microcanais, desestabilização, antiespumantes, sistemas coloidais, avaliação dinâmica.

## ABSTRACT

The ability of formation and stability are fundamental attributes to be investigated during the development of emulsions aiming at technological applications. Notwithstanding, in other processes, such as fermentative and petroleum-related, in which the production or extraction of nonpolar compounds is triggered, the minimum stability of the emulsions inherent to the process is desirable in order to increase the oil recovery. In this sense, the evaluation of emulsion stability is of paramount importance to determine the optimized composition depending on the characteristics of the sought-after emulsion. Furthermore, unraveling the mechanisms of (de)stabilization would be of outmost value for the development of these important colloidal systems. In this light, strategies based on microfluidics were applied to the investigation of droplets (de)stabilization, since this technology can achieve both the formation of emulsions and their efficient separation of phases. Due to the above, the present study aimed to investigate the (de)stabilization of model emulsions (using conventional surfactants or tensoactive agents of fermentative systems as stabilizers) in microfluidic channels. In such devices, the applied strategies were mainly related to changes in the geometry and surface properties. However, the addition of external agents (aqueous solutions) was also performed to induce the destabilization even of the most stable emulsions. Therewith, it was possible to identify the main parameters related to the mechanisms of emulsion (de)stabilization, in addition to determining the flow conditions and set of channels most suitable for inducing this phenomenon. Overall, it was observed that glass microcapillaries were not efficient to evaluate the events of coalescence due to the 3D geometry, while planar channels (whose dimensions can be modified) were most suitable to assess the destabilization phenomena. Moreover, it was verified extreme difficulty in destabilizing emulsions (especially those with a high concentration of stabilizing agents) using microdevices inducing the contact between the droplets. Nonetheless, such destabilization was achieved through the forced injection of aqueous solution in concentrated droplets. Indeed, depending on the aqueous solution added (saline solution or water), varied mechanisms of destabilization were visualized (fracture, droplet burst on the channel surface and/or coalescence). Such mechanisms were also dependent on the surface properties of the microchannels (zeta potential and hydrophobicity). Therefore, understanding the role of the microchannel wall was essential to induce both formation and destabilization of the droplets, allowing modulating the kinetic stability of the emulsions. In general, it was found that charged stabilizing agents must have charges of the same signal as microchannels to allow droplets formation. In addition, the continuous phase of

the emulsions must have the same nature (polar or nonpolar) as the channel surface. On the other hand, adherence of oil droplets on the device walls was observed on two occasions: (i) when the microchannels possessed both high hydrophobicity and reduced surface charges and (ii) when the emulsion droplets had opposite charges to those of the walls of the microchannels. Ultimately, this study allowed indicating the use of channels coupled in series to determine the stability of the droplets; however, it was emphasized that a prior understanding of the potential interactions between the droplets and the channels needs to be accomplished.

**Keywords:** microchannels, destabilization, antifoams, colloidal systems, dynamic evaluation.



## SUMÁRIO

INTRODUÇÃO .....	14
OBJETIVOS.....	17
Objetivo geral.....	17
Objetivos específicos.....	17
ESTRUTURA DA TESE.....	18
CAPÍTULO 1 .....	20
Revisão de Literatura: Microfluidics as a platform to assess and induce emulsion destabilization .....	20
CAPÍTULO 2 .....	43
Designing biotechnological processes to reduce emulsions formation and improve oil recovery: Study of antifoams application .....	43
CAPÍTULO 3 .....	58
Microfluidic tools to observe (de)stabilization mechanisms of water-in-oil emulsions.....	58
CAPÍTULO 4 .....	81
Microfluidics for assessing the formation and stability of oil-in-water emulsions based on components of bioprocesses .....	81
CAPÍTULO 5 .....	108
Unraveling driving regimes for destabilizing concentrated emulsions within microchannels .....	108
CAPÍTULO 6 .....	128
Colloidal particle deposition on microchannel walls, for attractive and repulsive surface potentials.....	128
DISCUSSÃO.....	152
CONCLUSÃO.....	157
REFERÊNCIAS .....	159
ANEXO 1 .....	161
ANEXO 2.....	162
ANEXO 3 .....	163
ANEXO 4.....	164

## INTRODUÇÃO

Emulsões simples são dispersões coloidais compostas por dois líquidos imiscíveis que podem ser classificadas como água-em-óleo (A/O) ou óleo-em-água (O/A) de acordo com a natureza das suas fases dispersa e contínua. Estes sistemas, apesar de serem termodinamicamente instáveis, podem alcançar estabilidade cinética dependendo das suas propriedades físico-químicas, que são influenciadas por fatores como a presença de estabilizantes (surfactantes ou outros agentes com propriedades tensoativas) e as características das fases (MCCLEMENTS, 2005; MCCLEMENTS, 2015). Tal estabilidade é desejável considerando diversas aplicações nas indústrias alimentícia, farmacêutica e cosmética (emulsões O/A e A/O), no entanto, é considerada uma desvantagem quando a recuperação eficiente de óleo é necessária nos processos de fermentação (emulsão O/A), bem como na extração de petróleo (emulsão A/O) (AVEYARD et al., 1990; FURTADO et al., 2015; HEERES et al., 2014). Desta maneira, avaliar sistematicamente a estabilidade das emulsões é essencial em uma variedade de indústrias para escolher os componentes do sistema bem como obter *insights* sobre potenciais valores de concentração e, então, estabelecer suas possíveis aplicações. Além disso, o entendimento das interações entre os componentes da emulsão, interações gota-gota, interações gota-material em contato e susceptibilidade intrínseca é de grande importância para se estabelecer possíveis aprimoramentos na composição do sistema coloidal.

Neste contexto, os canais microfluidicos poderiam ser utilizados para avaliar sistematicamente a capacidade de formação e a estabilidade das emulsões através da indução da desestabilização, com baixo custo de capital, operação, reduzida quantidade de amostra e permitindo uma triagem de alto rendimento (*high-throughput screening*) devido à possibilidade de visualizar os fenômenos (tamanho, morfologia, inversão de fases) em tempo real (HINDERINK et al., 2020; KREBS; SCHROËN; BOOM, 2012; USHIKUBO et al., 2014). Além disso, tais dispositivos poderiam também ser aplicados para estudar a origem dos mecanismos de (des)estabilização das emulsões, a fim de se escolher as condições de processamento, o ambiente de armazenamento bem como a composição adequada da emulsão dependendo da sua aplicação final, ou da sua necessidade de separação de fases. Finalmente, como uma abordagem adicional, estes dispositivos poderiam também ser aplicados para a obtenção da separação de produto de alto valor agregado aprisionado em um sistema multifásico.

A desestabilização de gotas em microdispositivos pode ser alcançada através de dois métodos distintos, denominados de ativos e passivos. Os métodos passivos incluem mudanças na estrutura (*design*) e na superfície (molhabilidade e carga) do microcanal, enquanto os métodos ativos estão relacionados, por exemplo, ao uso de campos elétricos, magnéticos e/ou gradientes de temperatura para induzir a instabilidade interfacial das gotas. De modo geral, métodos passivos são mais viáveis e fáceis de serem aplicados devido à sua simplicidade e baixa contaminação. Por outro lado, é necessário projetar minuciosamente os microcanais (*design* e propriedades de superfície) e ajustar as condições de escoamento (vazão volumétrica, tempo de residência, etc.) com base nas propriedades dos fluidos do sistema multifásico (viscosidade, densidade e presença de estabilizantes), de modo a aumentar a eficiência da desestabilização (BREMOND; THIAM; BIBETTE, 2008; MAZUTIS; GRIFFITHS, 2012; SHEN et al., 2015).

Até o momento sabe-se que, além da escassa elucidação dos mecanismos de desestabilização de gotas em microcanais, tal fenômeno é principalmente alcançado para dispersões isentas de estabilizantes, pois ainda é considerado um grande desafio induzir a desestabilização de uma emulsão produzida com elevada concentração destes agentes. Ademais, na presença de surfactantes, o efeito Marangoni pode ocorrer, dificultando a drenagem da fase contínua e aumentando o tempo de desestabilização (SHEN et al., 2015), embora outros agentes tensoativos também promovam uma barreira física na interface. Além disso, considerando-se estudos de coalescência de emulsões em microdispositivos, diferentes métodos passivos baseados na modificação do projeto dos canais, manipulação da velocidade das gotas e alteração da molhabilidade superficial têm sido propostos nos últimos anos (BREMOND; DOMÉJEAN; BIBETTE, 2011; DENG et al., 2013; MENG et al., 2016). No entanto, não foram estabelecidas estratégias eficientes para se determinar o grau de estabilidade das emulsões, bem como para desestabilizar gotas contendo uma concentração de estabilizantes que promovam alta estabilidade, como previamente mencionado. Ademais, os mecanismos de desestabilização também necessitam de maior exploração. Sendo assim, um melhor entendimento sobre o comportamento das gotas e a desestabilização em diferentes dispositivos microfluidicos poderia ser alcançado a partir de um banco de dados contendo informações sobre emulsões com variados graus de estabilidade expostas a condições singulares dentro dos microdispositivos. Ademais, outros agentes (ex. água ou solução salina), se adicionados no interior dos microcanais, poderiam potencialmente induzir a desestabilização inclusive das emulsões mais estáveis (FURTADO et al., 2015), além de seus efeitos serem concomitantemente avaliados.

Desta maneira, este trabalho abordou tanto a formação quanto, principalmente, a desestabilização de emulsões em microcanais utilizando estratégias passivas com potencial adição de agentes externos. Este estudo promoveu a ampliação do conhecimento fundamental relacionado ao tema, elucidando conceitos que auxiliaram (i) no entendimento dos mecanismos envolvidos tanto na formação quanto na desestabilização das emulsões, sendo que este último pode ser relacionado às características intrínsecas da emulsão, às propriedades de compostos adicionados no sistema (desemulsificantes ou outros compostos químicos) e ao material em contato (superfície de parede do microcanal), (ii) na obtenção de conhecimento que permitirá avançar a tecnologia e, como perspectiva, desenvolver um analisador de estabilidade de emulsões visando sua aplicação em indústrias alimentícias, farmacêuticas, biotecnológicas e petrolíferas e, (iii) no desenvolvimento de um microcanal que possa ser utilizado para induzir a separação eficiente das fases da emulsão. Portanto, este trabalho possibilitou entender as peculiaridades de diferentes microcanais e assim, indicar aqueles mais adequados para emulsões com variados graus de estabilidade, dependendo da aplicação desejada, de forma a agregar a microfluidica como uma ferramenta interessante para se desvendar os mecanismos de des(estabilização) de emulsões.

## OBJETIVOS

### Objetivo geral

Desenvolver sistemas microfluidicos para avaliar a estabilidade das emulsões e os fenômenos que agem na desestabilização das gotas de modo a elucidar os mecanismos associados a tais efeitos.

### Objetivos específicos

- ❖ Produzir emulsões O/A contendo levedura e antiespumantes comumente utilizados em bioprocessos em agitador mecânico e em rotor-estator, e caracterizá-las de modo a entender os mecanismos de formação e estabilização destas emulsões para posteriormente correlacionar estes *outputs* aos resultados em microcanais;
- ❖ Projetar sistemas microfluidicos com diferentes geometrias e características de molhabilidade de parede, e avaliar nestes microcanais a formação e a desestabilização de emulsões produzidas com componentes de fermentação ou com surfactantes convencionais;
- ❖ Selecionar sistemas microfluidicos que mostrem melhor indução da desestabilização para diferentes sistemas emulsionados e adicionar água ou solução salina para desestabilizar e aferir a estabilidade inclusive das gotas das emulsões mais estáveis;
- ❖ Entender os mecanismos associados a cada tipo de desestabilização, incluindo relações entre as propriedades da emulsão, material de parede, molhabilidade dos canais e adição de solução aquosa como agente desestabilizante.

## ESTRUTURA DA TESE

De modo a compreender a estrutura da tese, uma breve contextualização dos objetivos iniciais se faz necessária. Inicialmente, esta tese tinha como finalidade estudar emulsões O/A estabilizadas por compostos presentes em sistemas fermentativos, visto que o papel deles na formação de emulsões indesejáveis e inerentes em tais processos biotecnológicos ainda não se encontrava elucidado na literatura. Estas emulsões seriam, então, aplicadas nos microdispositivos como sistemas-modelo que auxiliariam na construção de um analisador microfluidico. Com este viés, o **Capítulo 1** desta tese engloba a revisão de literatura que descreve as principais ferramentas microfluidicas até então aplicadas para a desestabilização de emulsões. Ainda no mesmo contexto inicial, a primeira etapa experimental descrita no **Capítulo 2** visou entender o papel de determinados componentes da fermentação (antiespumantes comumente utilizados e levedura) na formação e estabilização de emulsões O/A, simulando parcialmente os sistemas gerados em processos fermentativos. Após esta etapa exploratória, tais sistemas seriam produzidos e avaliados em microcanais. Assim, aplicando microcanais produzidos a partir da técnica mais comumente utilizada, litografia macia, experimentou-se produzir emulsões O/A. No entanto, tanto os microcanais produzidos através da técnica de corrosão em vidro (selados ao polidimetilsiloxano - PDMS), que possuiriam natureza majoritariamente hidrofílica, quanto aqueles fabricados com o próprio PDMS (selados ao vidro) geraram emulsões A/O. Tais resultados estão descritos no **Capítulo 3**. Diante de tais desfechos e visando aprofundar o conhecimento em áreas correlatas à microtecnologia, foi então decidido ampliar os objetivos deste projeto aplicando diferentes vertentes microfluidicas, focando no desenvolvimento de microcanais para uma aplicação geral na avaliação da (des)estabilização de emulsões, evoluindo ainda mais o conhecimento na área. Além disso, devido à complexidade do tema decidiu-se estudar também emulsões com surfactantes convencionais para melhor compreender os diferentes fenômenos. No entanto, emulsões O/A continuaram sendo o foco visto que emulsões A/O são pouco aplicadas nas indústrias alimentícias, farmacêuticas e biotecnológicas, além de que processos petrolíferos, apesar de serem importantes sistemas a serem investigados, geram emulsões naturalmente sem a possibilidade de evitá-las através da manipulação composicional, como nos demais casos. Desta maneira, a ainda constante necessidade de produzir emulsões O/A nos levou à busca por alternativas. Foi assim que os canais capilares de vidro inertes surgiram como uma abordagem interessante para a geração e estudo de emulsões O/A, que foram descritos no **Capítulo 4**. Contudo, ambos canais estudados nos Capítulos 3 e 4 não foram capazes de desestabilizar emulsões extremamente estáveis

através do choque entre as gotas durante o escoamento. Mais do que isso, os capilares também não permitiram uma visualização apropriada do fenômeno, além de não ser possível a alteração do *design* do canal. Com isso, para a produção de emulsões O/A uma terceira estratégia emergiu: a utilização de canais em PDMS tratados com plasma de oxigênio (alternativamente também tratados com compostos químicos). Tais emulsões foram coletadas, concentradas em canais de PDMS (2D com *design* apropriado) e testadas sob diferentes condições de molhabilidade de parede dos dispositivos, injeção de componentes, entre outras variáveis descritas no **Capítulo 5**. Adicionalmente, de modo a desvendar os mecanismos relacionados à carga superficial das paredes dos microcanais e das emulsões, foi realizado um estudo complementar relatado no **Capítulo 6**. Sendo assim, os resultados apresentados nesta tese guiaram as etapas experimentais a diferentes vertentes que, ao final, convergiram para um maior entendimento do assunto em questão, possibilitando obter conclusões e indicar possíveis próximos caminhos.

**Capítulo 1.** *Revisão de literatura: Microfluidics as a platform to assess and induce emulsion destabilization*

**Capítulo 2.** *Designing biotechnological processes to reduce emulsions formation and improve oil recovery: Study of antifoams application*

**Capítulo 3.** *Microfluidic tools to observe (de)stabilization mechanisms of water-in-oil emulsions*

**Capítulo 4.** *Microfluidics for assessing the formation and stability of oil-in-water emulsions based on components of bioprocesses*

**Capítulo 5.** *Unraveling driving regimes for destabilizing concentrated emulsions within microchannels*

**Capítulo 6.** *Colloidal particle deposition on microchannels walls, for attractive and repulsive surface potentials*

## **CAPÍTULO 1**

**Revisão de Literatura: Microfluidics as a platform to assess and induce emulsion destabilization**

Artigo a ser submetido no periódico “Lab on a Chip”: Santos, T. P., Cejas, C. M., Cunha, R. L. Microfluidics as a platform to assess and induce emulsion destabilization.



## Microfluidics as a platform to assess and induce emulsion destabilization

Tatiana Porto Santos <sup>a</sup>, Cesare M. Cejas <sup>b</sup>, Rosiane Lopes Cunha <sup>a\*</sup>

<sup>a</sup>Department of Food Engineering and Technology, School of Food Engineering, University of Campinas (UNICAMP), 13083-862 – Campinas, SP, Brazil

<sup>b</sup>MicrofluidX Ltd, Gunnels Wood Road, Stevenage Bioscience Catalyst, Stevenage SG1 2FX UK

\* E-mail addresses: rosiane@unicamp.br (Rosiane L. Cunha); tatiana.porto90@gmail.com (Tatiana P. Santos); cesare.cejas@gmail.com (Cesare M. Cejas)

### ABSTRACT

Microfluidic technology enables a judicious control of the process parameters on a small scale, which in turn allows speeding up the destabilization of emulsion droplets interface in microfluidic devices. In this light, microfluidic channels can be used as an efficient tool to assess emulsion stability and to observe the behavior of the droplets immediately after their formation, enabling to determine whether or not they are prone to re-coalescence. Observation of the droplets after emulsifier adsorption also allows the investigation of emulsion stability over time. Both evaluation would contribute to determine emulsion stability aiming at specific applications in food and pharmaceutical industries. Furthermore, emulsion coalescence can also be performed under extremely controlled conditions within the microfluidic devices in order to explore emulsion droplets as micro-reactors (for regulated biological and chemical assays). Such microfluidic procedures can be performed in either confined environments or under dynamic flow conditions. Under confined environments, droplets are observed in fixed positions simulating different environmental conditions. On the other hand, with the scrutiny of emulsions under dynamic flow processes, it is possible to determine the behavior of the droplets when subjected to shear forces, comparable to those experienced in conventional emulsification techniques or even in pumping operations. Given the above, this paper reviews different microfluidic techniques (such as changing channel geometry or wettability) hitherto used to destabilize emulsions, mainly focusing on the specificities of each study, whether the droplets are destabilized in confined or dynamic flow processes. Thereby, by going deeper into this review, readers will be able to identify different strategies for emulsion destabilization (in order to understand stabilizing mechanisms or even to apply these droplets as micro-reactors), as this paper shows the particularities of the most recent studies and elucidates the current state-of-the-art of this microfluidic-related application.

**Keywords:** coalescence, geometry, wettability, passive strategies, microchannels

## 1. Introduction

Microfluidics is defined as the science and technology of designing, manufacturing, and operating either processes or devices with small quantities of fluids ( $10^{-9}$  to  $10^{-18}$  liters), with typical dimensions ranging from tens to hundreds of micrometers (or even a few millimeters), but it must exhibit at least one dimension smaller than 1 mm (Fang & Cathala, 2011; Ushikubo et al., 2015; Whitesides, 2006). This technique presents several advantages, but the most important are related to the application of devices with small sizes, reduced sampling, low energy consumption and dissipation and, consequently, relatively low cost. Such advantages arise from an interplay of unique features related to laminar and diffusive flow, such as very small molecular diffusion distances, large surface areas, high-performance heat transfer, precise control of flow conditions and so on (Roques-Carnes et al., 2014). Thus, microfluidics provides a powerful strategy for exploring the behavior of small-scale fluids, where diffusion, viscous, and interfacial forces predominate (Atencia & Beebe, 2005). These characteristics steer the technique towards industrial and research applications, which has led to its swift development in recent years (Shen et al., 2015).

The use of microfluidics in multiphase systems enhances the precise control of the formation of a defined interface between fluids (Ushikubo et al., 2015). Indeed, emulsion droplets produced in microfluidic devices have a highly monodisperse size distribution because they are not only formed one-by-one, but also generated under milder conditions when compared to high-energy techniques (Sugiura et al., 2004; Ushikubo et al., 2014). Overall, the mean size of droplets formed in shear-based geometries (micro-capillaries and planar) is in the range of tens to hundreds of micrometers (Liu et al., 2013; Nisisako & Torri, 2008; Ren et al., 2010; Ushikubo et al., 2014). Nevertheless, depending on the composition, some emulsions may exhibit complex rheological behavior that cause channel obstruction and difficulties in both fluid injection and flow stabilization. In addition, different components of the emulsions (such as oil and surfactants) can interact with the surface of the channels (Santos et al., 2021), impairing the formation of the droplets. Therewith, the development and application of microfluidic devices that can operate in high-throughput conditions remain a major challenge for expanding the use of this technology. To overcome such drawback, different techniques (laser ablation, micromachining and soft lithography), materials (glass, polydimethylsiloxane (PDMS) and thermoplastic) and surface wall treatments (plasma and covalent modifications) have been used to produce a wide range of microfluidic devices (Costa et al., 2017; Santos et al., 2021). The choice of approaches to be applied depends on whether the objective is to assess

and/or produce an oil-in-water (O/W) or a water-in-oil (W/O) emulsion.

In addition to droplets production and development of emulsions, microfluidic technology is growing in other fields in the study of multiphase systems. Particularly, microfluidic platforms have been used either for the separation of emulsion phases or to trigger the merge of the emulsion droplets for a better understanding of the droplet coalescence mechanism. Generally, to foster droplets coalescence, the instability of their interface must be induced. It is interesting to study the stability or to induce the fusion of the droplets within microfluidic channels, as these devices can provide visualization of the droplet interface and the precise control of the droplet formation and destabilization process. Microfluidics also operates at high shear rates due to their reduced length-scale (Baret, 2012), which can positively influence droplet destabilization. Therefore, microfluidic tools can be applied to induce droplet coalescence, which is especially important considering many facets, such as:

(i) Evaluation of emulsion (in)stability using lab-scale experiments - The performance of systematic studies using different components to improve emulsion stability is a growing demand in many industries (Krebs et al., 2012a), which can be achieved by observing emulsion droplets and their respective destabilization within microfluidic devices. However, the application of different conditions to investigate emulsion stability will provide specific information. Observing the coalescence immediately after droplets formation provides insights on the probability of re-coalescence in classic shear emulsification processes (Baret et al., 2009), which is paramount because it usually defines the final droplet size (Zhou et al., 2016). On the other hand, the destabilization study performed after a period of time from emulsion production (Santos et al., 2021) can be used to identify long-term kinetic stability of droplets under specific conditions (e.g., during storage or in contact with different matrices as well as wall materials) or even during simulated gastrointestinal environment.

(ii) Application of the droplets as micro-reactors, when the process of droplet fusion triggers chemical or biological reactions - Due to the short time-scales and the efficient heat and mass transfer typically involved in microfluidic systems, the droplets can be used as micro-reactors. However, in this specific case, a judicious control of the droplet coalescence is targeted to allow a proper mixture of reagents (Mazutis et al., 2012; Shen et al., 2015; Tullis et al., 2014; Xu et al., 2011). In this light, microfluidics can be applied as a miniaturized platform to modulate both reactions and product synthesis (Deng et al., 2013).

(iii) Phase-inversion induction - The study of concentrated droplets using *in situ* analysis is fundamental to understand the origin of the shear-induced phase inversion and to determine which factors can drive the triggering of this phenomenon (Bremond et al., 2011).

(iv) Study of interaction of emulsion droplets with different components - Observation of droplets inside microfluidic devices when in contact with other compounds is of paramount interest to observe real-time kinetics and specific synergistic/antagonistic effects (Marze et al., 2014; Santos et al., 2021) in processes and formulations.

Overall, droplet destabilization is triggered in microfluidic devices by applying two different approaches: active and passive methods. Passive methods are associated with changes in microchannel structure and wettability, while active methods include external energy (e.g., electric or magnetic fields) to induce interfacial instability (Mazutis et al., 2012; Shen et al. 2015). Normally, passive methods are more feasible due to their simplicity and reduced inter-droplet contamination, but they require the design of the microchannel network and the adjustment of flow conditions based on the properties of the fluids to increase separation efficiency (Mazutis et al., 2012; Shen et al. 2015). In this sense, this review sheds light on the fundamentals of droplet destabilization in microfluidic devices as well as the passive strategies currently applied to promote such phenomenon, systematically showing an overview of the main advances, the specificities of each study and the challenges to be overcome. With this set of information, we intend to show the gaps and the current state-of-the-art of the subject, aiming at the implementation of these microfluidic platforms in both fundamental and applied research.

## **2. Mechanisms to promote droplet destabilization in passive microfluidic devices**

Passive strategies present remarkable advantages (ease of production, use of different materials, low cost, amongst others) when compared to active methods, in addition to being directly associated with changes in the microfluidic channels themselves. The liquid film drainage model is usually used to describe the process of passive fusion between two spherical droplets in contact within microfluidic channels. Typically, when two spherical droplets come into contact, they initially slide one over each other, rotating so that the line connecting the droplet centers is no longer parallel to the flow axis. In the meantime, the membrane between the droplets (constituted by the continuous phase) begins to drain, favored by the excess of capillary pressure between the films (Christopher et al., 2009; Shen et al., 2015). When the liquid film is thin enough, the interfacial tension is unbalanced (if there is a surfactant) and van der Waals forces, as well as other interactions, start to play a fundamental role in the membrane

disruption, leading to the fusion of the droplets. Therefore, in an ideal scenario, the droplet coalescence mechanism in microfluidic channels includes three main steps, as illustrated in Figure 1: (i) two-droplet approach, collision and deformation, (ii) drainage of the film constituted by the continuous phase, and (iii) rupture of the interfacial film and fusion of the droplets (Bremond et al., 2008; Christopher et al., 2009; Shen et al., 2015).

In general, several factors affect droplet destabilization in microfluidics devices, including the inlet velocity and viscosity of the phases, as well as the presence and absence of surfactants. However, surface wall wettability and design of the channels can definitely play a fundamental role on droplet destabilization (Santos et al., 2021). Droplet coalescence in microfluidic devices is more suitable for surfactant-free dispersions and despite many efforts, it is still a challenge to induce the coalescence of an emulsion stabilized with surface-active compounds (Mazutis et al., 2012). In these surfactant-based systems, the Marangoni effect can occur, hindering the drainage of the continuous phase and, thereby, increasing the coalescence time (Shen et al., 2015). In view of the numerous attempts to induce destabilization of emulsion droplets within microfluidic devices, the following sections (Section 2.1 and its subsections) show the fundamentals of passive strategies and the respective studies based on this approach.

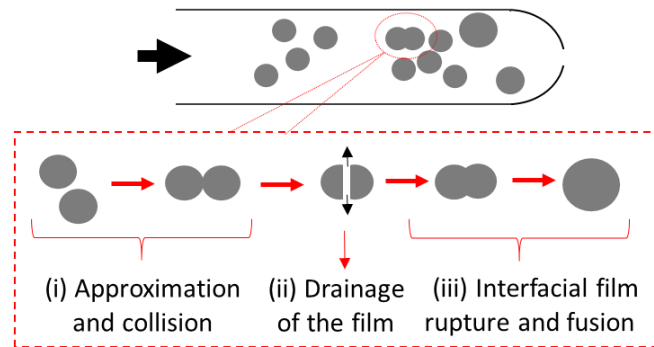


Figure 1. Illustration of the main steps of the coalescence process within microfluidic devices (based on Heeres, 2016; Krebs et al., 2013).

## 2.1 Passive strategies to induce droplet destabilization

Passive methods can be divided into two different approaches: i) changing fluid dynamics based on channel configurations and ii) modifying channel surface properties. According to the literature, changing the channel configuration includes, for instance, manipulating the path or inserting an expansion chamber (Shen et al., 2015) to increase the collision of the droplets, reducing the amount of continuous phase between them. Changes in the surface properties of the channels, on the other hand, can compromise the stability of the droplets due to repulsive/attractive forces between the walls and either the continuous or the

dispersed phase of the emulsion (Fidalgo et al., 2007; Santos et al., 2021). As a result, the wall can immobilize the continuous phase, triggering droplets collision, or even attract the dispersed phase, inducing the droplet to “burst” onto the wall (Fidalgo et al., 2007; Santos et al., 2021). Despite progress in understanding the different mechanisms and ways of achieving emulsion destabilization, promoting the coalescence of kinetically stable emulsions still remains a major challenge as previously mentioned. In this sense, several studies have emerged showing different techniques to induce emulsion destabilization, also seeking to identify the role of each parameter in driving the droplet coalescence or the separation of emulsion phases.

Considering these approaches, in this review, we divide passive methods into two different group-concepts (confined and dynamic flow processes). Techniques based on flow-induced coalescence were classified as dynamic flow processes (DFP), wherein the droplets are in constant flow while different strategies are applied to allow their merge/destabilization (Table 1). In general, the coalescence of droplets in this type of process can be hampered by the relatively ‘long film drainage times’ compared to the ‘short residence times’ experienced in microfluidic devices. Thus, it is clear that coalescence happens easily in microfluidic devices if there is enough time for droplet collisions to occur (Meng et al., 2016; Shen et al., 2015). However, the effect of the intrinsic emulsion properties must also be taken into account, especially because coalescence time can be influenced by droplet size and deformation, viscosity ratio and interfacial tension between the phases (Christopher et al., 2009; Shen et al., 2015). Therefore, such information can be interesting indicators of the stability of emulsions within microfluidic devices.

Confined processes (CP) have also emerged as a pivotal strategy to induce emulsion destabilization and coalescence, but, unlike DFP techniques, they are still scarcely explored. However, application of CP techniques can be a rational strategy to manipulate the residence time of the droplets in microfluidic devices. In such cases, the droplets are usually confined within either a small trap/anchor or a reservoir and destabilization is observed over time (Table 2) (Bremond et al., 2011; Marze et al., 2014; Nguyen et al., 2019ab; Scheuble et al., 2017; Tullis et al., 2014). As they are confined systems, the effect of the channel surface or external components on the droplets has also been evaluated (Marze et al., 2014; Santos et al., 2021; Scheuble et al., 2017; Tullis et al., 2014).

Table 1 and Table 2 summarize and illustrate different passive strategies to destabilize emulsion droplets that have been proposed in recent years. DFP strategies were classified as (1) single direction of droplets approach, (2) multiple directions of droplets

approach, (3) insertion of other microstructures and (4) tailoring the wettability. CP studies, on the other hand, were classified as (1) droplets confinement, (2) reservoir and also (3) tailoring the wettability. Regardless of the flow conditions, both strategies (DFP and CP) are typically associated with modifying the design and/or the surface of the channels. However, a direct comparison between the different techniques presented in Tables 1 and 2 is not possible because the materials used either to compose the emulsions or to manufacture the devices were different. Notwithstanding, these outcomes allowed to better elucidate the process of droplet destabilization, providing important details of each approach and specific information about the different studies.

### **2.1.1 Dynamic Flow Processes (DFP)**

The processes in which the emulsions are destabilized during the continuous flow of the droplets are denominated in this review as dynamic flow processes (DFP). In such circumstances, droplets generally experience shear stresses that can be compared to those applied in conventional emulsification processes, due to the reduction in the length-scale of the devices (Baret, 2012). As aforementioned, we divide these processes in different approaches. In the first strategy - (1) single direction of droplets approach - the droplets flow only on the “x” axis (i.e. in the main direction of the flow) throughout the observation process, colliding with each other and potentially experiencing coalescence. On the other hand, in the second perspective - (2) multiple directions of droplets approach -, instead of flowing on the same “x” axis, droplets flow coming from multiple directions and a forced head-on faced collision of the droplets is usually observed. In the latter, either a T- or a Y-junction is typically applied. Considering the “(3) insertion of other microstructures” and “(4) tailoring the wettability”, a scarce number of studies have emerged. For instance, in the former case, we can point to an example related to the addition of a tip inside the channel to induce local instabilities on the surface of the droplets (Deng et al., 2013). On the other hand, in the strategy related to the manipulation of channel wettability, specific regions are created to immobilize the droplets (Fidalgo et al. 2007; Meng et al., 2016). In the next section, we pinpoint some examples of these techniques, and the main characteristics related to the emulsion coalescence. In addition, Table 1 shows the strategies (either channel geometry or wettability modification) and fundamental information considering each study.

### ***Single direction of droplets approach***

The single direction of droplets approach is the most widely used concept for studying droplet coalescence in microfluidic devices. In this strategy, a flow resistance is introduced along the channel, which can be any type of flow perturbation occurring over a one-dimensional flow. Therefore, based on the premise that fluid must be removed from between the two colliding droplets, different techniques have been proposed (Table 1). Examples of such techniques include an increase in the area of the microchannel section (Baret et al., 2009; Bremond et al. 2008; Gunes et al., 2013; Krebs et al., 2012a; Tan et al., 2004; Tan et al., 2007) or the addition of a geometrical constriction for a single droplet (Chokkalingam et al. 2010). In this context, *Tan et al* (Tan et al., 2004) investigated the fusion of water droplets (W/O emulsion) using three different geometries, including straight and tapered expansions as well as a flow rectifying design. In both expansions, the configuration of the channels allowed to decrease the distance separating the droplets, leading to their approach and consequent collision. In the tapered expansion, undesired multiple coalescence was triggered, while the flow rectifying design enabled a more controlled fusion of the droplets, which was associated to the regulated drainage of the continuous phase imposed by the insertion of an upper and a lower channel with identical resistances (Table 1) (Tan et al., 2004). Therefore, it is possible to modulate judiciously the number of merged droplets using a flow-rectifying structure. Overall, one can affirm that if the aim is to coalesce and determine the stability of the droplets, these strategies are quite interesting. However, when the objective is to collide only two droplets (for their application as micro-reactors); especially the geometries based on expansions leave much to be desired due to the difficulty in controlling flow conditions (Xu et al., 2011). Similarly, *Tan et al* (Tan et al., 2007) applied a rectifying geometry, but testing a trifurcating channel with varied width in order to guarantee an even more controlled fusion of water droplets, emphasizing that the platform can be applied to either study coalescence rate or perform the mixing of chemicals. In the same vein of the successful principle above, *Gunes et al* (Gunes et al., 2013) implemented a main channel containing several channels on both lateral walls (see Table 1) and, by properly controlling the flow conditions in these vertical (lateral) channels, the drainage of the oil film (in W/O emulsions) could be manipulated and the coalescence of droplets achieved as desired. The main advantage of this strategy is the adaptation of the separation of the droplets by playing only with the influx and the outflux of the lateral channels.

Resembling the straight geometry used by *Tan et al* (Tan et al., 2004), *Baret et al* (Baret et al., 2009) proposed a microfluidic strategy based on a collision chamber to observe



the coalescence of W/O emulsions. In summary, they studied the droplet re-coalescence and quantitatively determined the influence of the adsorption dynamics of the surfactant at the water-oil interface on the emulsion stabilization. Using the same approach, *Krebs et al* (Krebs et al., 2012a) evaluated the demulsification kinetics by applying a simple experimental setup that consisted of a microfluidic chamber, but testing an O/W emulsion. They cautiously analyzed the interactions and trajectories of the droplets, which allowed measuring the coalescence rate under varying flow conditions, suggesting that the method could provide an easy-to-use tool to determine the stability of emulsions. Furthermore, they also pointed out that although the applied glass chips are only suitable for analyzing oil-in-water emulsions, these same devices can also be treated with alkylsilanes to evaluate water-in-oil emulsion systems (as in native PDMS material). Ultimately, *Dudek et al* (Dudek et al., 2020) also used the concept of coalescence chamber, but with a design capable of evaluating the contact time as well as the speed of approach of the colliding droplets. The geometry consisted of a straight chamber similar to that used in other studies (Dudek et al., 2018; Hinderink et al., 2020; Krebs et al., 2012b; Krebs et al., 2013; Muijlwijk et al., 2017; Schroder et al., 2018) but with an additional division separating the droplets into two streams. After separation, these droplets were subsequently introduced into a square channel, where the coalescence of even thousands of droplets could be evaluated.

Another solid strategy that contradicted expectations was performed by *Bremond et al* (Bremond et al., 2008), who demonstrated that coalescence of W/O emulsions could not take place with droplets impact in the expansion channel, but only occurred during droplets separation due to instantaneous instability and the formation of two-facing nipples. They also showed that in a compact system (with a train of droplets), once destabilization was triggered, a cascade of coalescence could be achieved even in surfactant-stabilized emulsions (with Span 80) (Bremond et al., 2008). To explain better the results, *Lai et al* (Lai et al., 2009) performed, in a later study, an in-depth characterization of the phenomenon and concluded that the nipple formation led to an increase of local contact area, which unleashed momentary instabilities.

Finally, in addition to the chamber-related strategies, this section also encompasses the addition of geometrical constrictions for the fusion of the droplets. In such structures, a droplet is immobilized and instabilities are promoted on its surface meanwhile a rear droplet flows towards it. *Chokkalingam et al* (Chokkalingam et al., 2010) applied this strategy for sol-gel reactions, triggering chemical synthesis by the precise synchronization and coalescence of the droplets.

### ***Multiple directions of droplets approach***

In multiple directions of droplets approach, a junction structure is usually proposed, but unlike the one direction strategy, most of these designs need meticulous synchronization of the droplets to allow their contact at the junction, which is a challenge (Shen et al., 2015). However, as with unidirectional flow strategies, coalescence takes place when the continuous phase is drained, enabling droplets fusion. Therefore, the controlled pattern of these structures allows the droplets to be efficiently merged one-by-one (Mazutis et al., 2012), while inducing a coalescence cascade is difficult in these microfluidic systems. As a result, the droplets can be used as micro-reactors in which reactions are triggered once the droplets are merged. Nevertheless, the physicochemical properties of the droplets and the process parameters, mainly the viscosity and the flow rate of the phases, seem to play a pivotal role in either improving or preventing the fusion of the droplets (Shen et al., 2015).

Considering the junction strategy, *Christopher et al* (Christopher et al., 2009) analyzed the role of droplet size and flow rate in triggering the coalescence of a pair of droplets in a perpendicular T-junction. Within these channels, the authors observed the transition between different mechanisms (coalescence, splitting, slipping, late coalescence, multiple splitting, and late splitting), which depended on the applied variables (droplet size and flow rate). In general, coalescence occurred easily using slow collision speeds, while splitting and slipping of the droplets could be visualized when faster velocities were established. Therefore, they concluded that the local velocity and droplet curvature were the control parameters, since both typically influence the drainage time of the liquid film. However, although the aforementioned study was able to induce coalescence, it indeed presented an inherent issue related to droplets synchronization. To overcome this impasse, *Shen et al* (Shen et al., 2017) developed a T-junction geometry coupled with a rectangular microgroove, which enabled a better coalescence efficiency of water-in-oil emulsion droplets. Moreover, in addition to the perpendicular-based structures, *Liu et al* (Liu et al., 2015) and *Wang et al* (Wang et al., 2013) also tested other angles (30°, 60°, 120°, 150° and 180° for the former and 60°, 120° and 180° for the latter) and both found that, by reducing the junction angle, coalescence efficiency could be improved. *Liu et al* (Liu et al., 2015) further corroborated the fact that, when droplets are in conditions of low flow rate, they easily undergo coalescence.

*Simone* (Simone, 2015) also used the shock-induced approach to promote droplet coalescence, but an extra “shuffling element” (or “coalescence element”) was inserted into the channel, which allowed the process to be independent of both the phases of the emulsions and

the synchronization of the droplets. In order to prove the versatility of the channel, she also applied this “lab-on a-chip” to fuse the droplets and mix different components. Later, *Simone et al* (Simone et al., 2019) applied the same geometry to investigate the effect of the rheological and physical properties of the phases on the occurrence of coalescence, concluding that the viscosity ratio of the phases has a direct influence on the coalescence dynamics. Ultimately, *Mazutis et al* (Mazutis et al., 2012) implemented a different approach based on the hydrodynamic flow to trigger coalescence. In addition to the T-junction strategy, where two droplets collide in a widening channel, they also applied droplets with different sizes (playing with droplet polydispersity). In this scenario, the droplets did not coalesce during the collision. Instead, a more spontaneous fusion was reproduced due to the flow field that induced the smaller droplet to rotate on the surface of the larger droplet, which consequently changed the shape of the smaller droplet, unbalancing the interfacial tension and triggering coalescence.

### ***Insertion of other microstructures***

In DFP methods, another different approach is to insert other classes of structures within the microchannels in order to induce local-points of instability on the surface of the droplets. *Deng et al* (Deng et al., 2013) classified their study as a surgery-like strategy, in which they explored structures called micro-lancets, manipulating their shape and hydrophilicity. The authors found that adequate wettability can make these lancets able to scratch the droplets and, consequently, unbalance the surfactants deposited on the water-oil interface. Such phenomenon may have led to a local scattering of surfactants in two contacting droplets, inducing their destabilization. As expected, hydrophilic structures and sharp tips easily induced coalescence of water-in-oil emulsions, while when using hydrophobic tips, the droplets did not fuse. In fact, hydrophilic tips triggered an easier droplet destabilization because the oil phase did not wet the surface and the water droplets could be scratched. The main advantage of this technique is the independence of droplet synchronization, since the tip has the capacity to partially immobilize the first droplet until the other arrives, allowing long-term processing.

### ***Tailoring the wettability***

Another method that has been studied is the change on the wettability of the channel surface. This technique is based on the surface energy pattern that initially induces droplets entrapment (in regions where the continuous phase of the emulsion has no affinity with the surface of the channel), followed by the detachment of droplets in a region of easy flow. The

droplet entering the modified region is expected to slow down and even stop until another droplet reaches the “surface-inducing trap”. As soon as the drag force exceeds the surface energy, immobilized droplets are released (Figaldo et al., 2007; Xu et al., 2011). In a first study (Fidalgo et al., 2007), the authors observed the behavior of W/O emulsions in a patterned PDMS produced with hydrophilic poly (acrylic acid), which was grafted via UV-induced photopolymerization. A second study (Meng et al., 2016), on the other hand, observed O/W emulsions in a glass capillary device with a heterogeneous surface-pattern, presenting a segment of hydrophobic wall. Interestingly, this latter work demonstrated how to control the stability of the emulsions within the microfluidic device. Hence, it is clear that the change in wettability, including heterogeneous surfaces (different hydrophilicity), improves droplet destabilization under flow conditions.

### 2.1.2 Confined Processes (CP)

We define as confined processes (CP) the conditions in which emulsion droplets are destabilized within a confined environment. Confined processes were developed primarily for three purposes: (i) to observe the behavior of the droplets over time in a packed system (Bremond et al., 2011), (ii) to evaluate the effect of adding external components to the colloidal system (Marze et al., 2014; Scheuble et al., 2017) and (iii) to observe the droplets while playing with their surface properties in order to have controlled fusion (Tullis et al., 2014). Herein, we divide the different approaches used in this type of destabilization (CP) in (1) droplets confinement, (2) reservoirs and (3) tailoring the wettability (Table 2). In the former case, either individual or a small number of droplets is captured within a structure in the devices (trap/anchors). Next, different components are added within the microchannel and the behavior of the droplets is monitored to provide information on the stability of the emulsions in contact with different compounds. Another strategy is the use of reservoirs, which collect hundreds or even thousands of droplets to allow the observation of their behavior when in contact with each other over time. Finally, in this same chamber, other approaches can be incorporated, such as modifying the wettability to also take into account the influence of this variable.

#### *Droplets confinement*

In a first scenario, *Marze et al* (Marze et al., 2014) developed a microfluidic device containing traps to confine oil droplets (O/W emulsions). Later, *Nguyen et al* (Nguyen et al., 2019ab) applied this same geometry, but instead of using plasma-treated PDMS, they modified

the surface wettability by applying a UV-based polymerization technique, to maintain channel hydrophilicity for longer periods of time than that typically offered by plasma treatment. Regardless of the case, they used the system to observe the behavior of immobilized droplets when facing the continuous injection of digestive fluids (simulating intestinal biochemical environments). Firstly, they produced the droplets and continuously injected them into the microfluidic traps. Therewith, they were able to evaluate the behavior of the emulsions by measuring the increase/decrease on droplets diameter over time. *Scheuble et al* (Scheuble et al., 2017) applied the same approach to study emulsion digestibility, but using glass channels fabricated by the wet-etching technique. These experiments were carried out after stabilizing the droplet interface overnight, while the studies mentioned previously (Marze et al., 2014; Nguyen et al., 2019ab) were performed immediately after emulsion formation. In fact, other technical details differ when comparing the two set of experiments, but it is beyond the scope of this review.

Similar to the traps, *Tullis et al* (Tulis et al., 2014) suggested another strategy for efficiently capturing and fusing pairs of water droplets under stationary conditions using anchors. On this platform, the coalescence of water-in-oil emulsions was achieved by injecting an external flow of surfactant-free oil into the device, leading to the dilution of the surfactant in the continuous phase. As expected, they also found that emulsions made with surfactant-free oil showed faster coalescence. However, this absence of surfactant resulted in an uncontrolled destabilization and, therefore, would not be indicated for processes that require controlled fusion. They also observed that, by manipulating the flow conditions, different patterns of coalescence and selective droplet fusion could be achieved, enlightening that this methodology can be considered an interesting tool to study surfactant absorption/desorption onto droplet surface.

### ***Reservoirs***

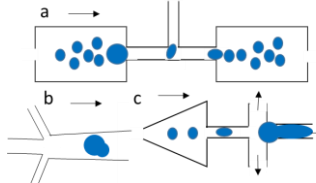
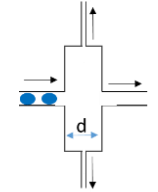
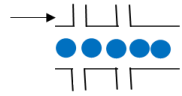
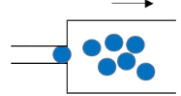
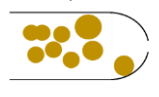
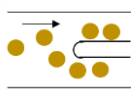
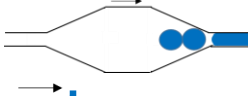

In the reservoir-based strategy, only the effect of droplet compaction is normally studied. In this context, *Bremond et al* (Bremond et al., 2011) investigated the coalescence propagation inside a microfluidic chamber and concluded that the phase inversion of the emulsion could be favored by the existence of a droplet size distribution (polydispersity). The authors also suggested that two main physico-chemical mechanisms may govern the destabilization of concentrated emulsion systems: the diffusion of the dispersed phase through the continuous phase and the coalescence of neighboring droplets. Taking advantage of this

geometry, they studied the propagation and the probability of coalescence for different sizes and organization of droplets.

### ***Tailoring the wettability***

The surface walls of a confined environment can be tailored to induce droplet destabilization. Studies typically use the same combination of emulsions and channel surface treatment, where the continuous phase perfectly wets the channel surface, i.e. O/W emulsions in hydrophilic channels and W/O emulsions in hydrophobic devices. A recent study (Santos et al., 2021), demonstrated the effect of opposite channel surface treatments on inducing emulsion instability, where O/W emulsions were destabilized in hydrophobic as well as in hydrophilic channels. This simple modification in the surface properties has been shown to generate other subtle destabilization mechanisms (in addition to coalescence) such as emulsion ‘bursts’, defined as the rupture of the droplet interfacial layer. Moreover, the role of surface charges (zeta potential) on both the channel walls and droplet interfaces proved to be equally important, depending on the nature of the surfactant used. For instance, emulsions stabilized by positively charged surfactants do not adhere to the positively charged surface walls due to inherent repulsion. By modifying the charge, destabilization can be induced by introducing non-negligible attractive forces between the emulsion droplets and the channel surface wall, thereby allowing the emulsion to break. Understanding the role of wettability is crucial to understand emulsion behavior during storage, because surface properties may change over time, depending on conditions, which can have adverse effects on emulsion stability.

Table 1. Strategies based on dynamic flow processes (DFP) that aim to promote droplet destabilization.

DFP	Ref.	Emulsion nature	Aqueous phase	Oil phase	Emulsifier	Channel strategy	Device characteristics	Scheme of the channel layout (based on the Reference)
Single direction of droplets approach	Tan et al. 2004	W/O	Water	Oleic acid	Span 80	<b>Geometry:</b> a) Straight expansion b) Tapered expansion c) Flow rectifying design	PDMS bonded to a glass slide	
	Tan et al. 2007	W/O	Water	Oleic acid	-	<b>Geometry:</b> Addition of a trifurcating junction with different (d) dimension	PDMS bonded to a glass slide	
	Gunes et al. 2013	W/O	Water	PDMS MCT	Tween 20 PGPR	<b>Geometry:</b> Lateral channels on both sides of the main channel to manage the amount of fluid between the droplets	TOPAS COC resin.	
	Baret et al., 2009	W/O	Buffered solution (10 mM Tris-HCl)	Fluorinated oil (FC40)	Amphiphilic molecule Krytox FHS + DMP	<b>Geometry:</b> Coalescence chamber - abrupt expansion of the channel	PDMS bonded to a glass slide and treated with aquapel	
	Krebs et al. 2012a	O/W	Water	Hexadecane	-	<b>Geometry:</b> Collision chamber	Glass	
	Dudek et al., 2020	O/W	Water Saline solution	Heptane Xylene Dodecane	Span 85	<b>Geometry:</b> Split channel + square chamber	Glass	
	Bremond et al. 2008	W/O	Water	Hexadecane	Span 80	<b>Geometry:</b> Expansion and contraction of the channel width	PDMS bonded to a spincoated-with-PDMS glass slide	
	Chokkalin gam et al. 2010	W/O	Water + different materials	Perfluoro-decalin	C <sub>8</sub> H <sub>3</sub> F <sub>15</sub> O	<b>Geometry:</b> Geometrical constriction	PDMS bonded to a glass slide	

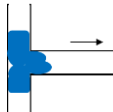
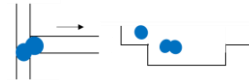
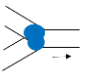

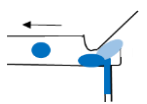
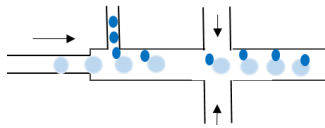
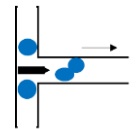
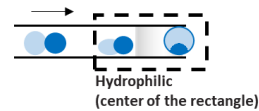
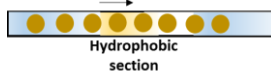


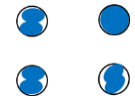
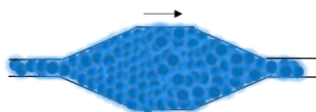
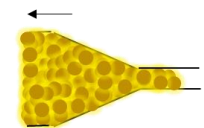
<i>Multiple directions of droplets approach</i>	Cristopher et al. 2009	W/O	Water Glycerol solution	Silicone oil	-	<b>Geometry::</b> Droplets collision at a T-junction	PDMS bonded to a spincoated-with-PDMS glass slide	
	Shen et al., 2017	W/O	Water Ethanol	Sunflower oil	-	<b>Geometry::</b> Droplets collision at a T-junction coupled with a rectangular microgroove	PDMS	
	Wang et al., 2013	W/O	Water	Pentanol Octanol Decanol	-	<b>Geometry::</b> Droplets collision at a Y-junction (60°, 120°, 180°)	Polymethyl methacrylate (PMMA)	
	Liu et al., 2015	W/O	Water	Liquid paraffin Silicon oil	-	<b>Geometry::</b> Droplets collision at a Y-junction and T-junction (30°, 60°, 90°, 120°, 150°, 180°)	-	
	Simone, 2015	W/O	Water Gelatin solution	Fluorinated oil	-	<b>Geometry::</b> Shuffling element	PDMS-glass composite	
	Mazutis et al. 2012	W/O	Water Sodium phosphate Tris-HCl NaCl sol.	FC-40 FC-77 Galden-HT135	EA-surfactant	<b>Geometry:</b> Droplets collision at a junction	PDMS bonded to glass and treated with aquapel	
<i>Insertion of other structures</i>	Deng et al. 2013	(1) W/O (2) O/W/O	Water	Silicone oil Soybean oil Benzyl benzoate	Dow Corning 749, PGPR nanoparticles, and SDS	<b>Structures:</b> Micro-lancets with different wettability and shapes (sharp and flat tips)	Micro-lancets (plastic, copper and aluminum wire) hydrophilic or hydrophobic	
<i>Tailoring the wettability</i>	Fidalgo et al. 2007	W/O	Water	Fluorous phase	-	<b>Surface wettability</b>	PDMS patterned with hydrophilic poly(acrylic acid)	
	Meng et al. 2016	O/W	Water + polyvinyl alcohol (PVA)	Paraffin oil	-	<b>Surface wettability</b>	Glass capillary patterned with octyltriethoxysilane (OTES) coating	



Table 2. Strategies based on confined processes (CP) that aim to promote droplet destabilization.

CP	Ref.	Emulsion nature	Aqueous phase	Oil phase	Emulsifier	Channel strategy	Device characteristics	Scheme of the simplified channel layout (based on the Reference)
<i>Droplets confinement (traps and anchors)</i>	Marze et al., 2014	O/W	Water	Tricaprylin Triolein Olive oil Fish oil	$\beta$ -lactoglobulin	Traps	PDMS used immediately after plasma treatment	
	Scheuble et al., 2017	O/W	Phosphate buffer solution	MCT oil	$\beta$ -lactoglobulin	Traps	Glass prepared by wet-etching	
	Tullis et al., 2014	W/O	Water with FeCl <sub>3</sub> and KSCN	Fluorinated oil Novec 7500	QX100 Pluronic F-68	Anchors	PDMS with a Novec 1720 coating	
<i>Reservoir</i>	Bremond et al., 2011	W/O	Water	Hexadecane	Span 80	Chamber with concentrated droplets	PDMS bonded to a spincoated-with-PDMS glass slide	
<i>Tailoring the wettability and reservoir</i>	Santos et al., 2021	O/W	Water	Light mineral oil Hexadecane	SDS, LDS, TTAB, DTAB, Tween 80	Microchamber with packed concentrated droplets	PDMS bonded to a spincoated-with-PDMS glass slide used after plasma treatment, after 5 hours or even chemically treated with APTES.	

## CONCLUSIONS AND PERSPECTIVES

This paper provides an overview of relevant studies in the field of droplet destabilization and coalescence in microfluidic channels, presenting their outcomes and highlighting their important aspects and specificities. Overall, one can observe that although recent studies have been published in the area, the facets that influence droplet destabilization are still being investigated, especially due to the complexity of the subject. In any case, in this paper we present fundamental insights and premises on how to induce droplet destabilization according to the application, in addition to showing the feasibility of implementation of each class of strategy. Furthermore, evaluating these studies, we were able to point out some challenges that still need to be overcome in order to properly promote emulsion coalescence within these microsystems. (i) In the case of droplets acting as micro-reactors, a more precise control of the process conditions must be implemented, as well as experiments with different compounds and multiple droplets. (ii) A wide range of materials must be tested and their efficiency compared, mainly because a direct correlation between the different techniques is hitherto not possible, since the materials used either to compose emulsions or to manufacture microfluidic devices are different. (iii) The influence of the wall material should be further exploited, especially for oil-in-water emulsions, in which surfactants can be highly charged and attraction to the surface can play a key role in promoting destabilization of the droplets. We believe that, by studying these different approaches, information of paramount importance can be obtained, improving the exploitation of microfluidics in the fields of emulsion development, droplets as micro-reactors or even separation of multiphase systems.

## Acknowledgements

This study is financed in part by the Coordenação de Aperfeiçoamento de Pessoal de Nível Superior – Brasil (CAPES) - Finance Code 001. Santos thanks grant number #2017/18109-0, São Paulo Research Foundation (FAPESP) and Conselho Nacional de Desenvolvimento Científico e Tecnológico - CNPq (Grant number 140700/2017-0) for the assistantship and Cunha thanks CNPq (307168/2016-6) for the productivity grant. The authors also thank São Paulo Research Foundation - FAPESP (Grant number #2019/07744-1).

## References

Atencia, J.; Beebe, D. J. (2005). Controlled microfluidic interfaces. *Nature*, v. 437, p. 648-655.  
Baret, J-C., Kleinschmidt, F., Harrak, A. E., Griffiths, A. D. (2009). Kinetic aspects of emulsion

- stabilization by surfactants: a microfluidic analysis. *Langmuir*, 25, 6088-6093.
- Baret, J-C. (2012). Surfactants in droplet-based microfluidics. *Lab on a Chip*, 12, 422-433.
- Bremond, N., Thiam, A. R., Bibette, J. (2008). Decompressing emulsion droplets favors coalescence. *Physical Review Letters*, 100, 024501-024501-4.
- Bremond, N., Doméjjean, H., Bibette, J. (2011). Propagation of drop coalescence in a two-dimensional emulsion: a route towards phase inversion. *Physical Review Letters*, 106, 214502-1-214502-4.
- Christopher, G. F., Bergstein, J., End, N. B., Poon, M., Nguyen, C., Anna, S. L. (2009). Coalescence and splitting of confined droplets at microfluidic junctions. *Lab on a Chip*, v. 9, p. 1102-1109.
- Chokkalingam, V., Weidenhof, B., Kramer, M., Maier, W. F., Herminghaus, S., Seemann, R. (2010). Optimized droplet-based microfluidics scheme for sol-gel reactions. *Lab on a chip*, v. 10, p. 1700-1705.
- Costa, A. L. R., Gomes, A., Cunha, R. L. (2017). Studies of droplets formation regime and actual flow rate of liquid-liquid flows in flow-focusing microfluidic devices. *Experimental Thermal and Fluid Science*, v. 85, p. 167–175.
- Deng, N-N., Sun, S-X., Wang, W., Ju, X-J., Xiea, R., Chu, L-Y. (2013). A novel surgery-like strategy for droplet coalescence in microchannels. *Lab on a Chip*, v. 13, p. 3653–3657.
- Dudek, M., Fernandes, D., Herø, E. H., Øye, G. (2020). Microfluidic method for determining drop-drop coalescence and contact times in flow. *Colloids and Surfaces A*, 586, 124265.
- Fang, A. Cathala, B. (2011). Smart swelling biopolymer microparticles by a microfluidic approach: synthesis, in situ encapsulation and controlled release. *Colloids and Surfaces B: Biointerfaces*, v. 82, p. 81-86.
- Fidalgo, L. M., Abellb, C., Huck, W. T. S. (2007). Surface-induced droplet fusion in microfluidic devices. *Lab on a Chip*, v. 7, p. 984-986.
- Gunes, D. Z., Bercy, M., Watzke, B., Breton, O., Burbidge, A. S. (2013). A study of extensional flow induced coalescence in microfluidic geometries with lateral channels. *Soft Matter*, 9, 7526.
- Heeres, A.S. (2016). Integration of product recovery in microbial advanced biofuel production: overcoming emulsification challenges, Thesis, Delft University of Technology.
- Hinderink E. B. A., Kaade, W., Sagis, L., Schroen, K., Berton-Carabin, C. C. (2020). Microfluidic investigation of the coalescence susceptibility of pea protein-stabilised emulsions: Effect of protein oxidation level. *Food Hydrocolloids*, 102, 105610.

- Krebs, T., Schroen, K., Boom, R. (2012a). A microfluidic method to study demulsification kinetics. *Lab on a chip*, 12, 1060-1070.
- Krebs, T., Schroen, K., Boom, R. (2012b). Coalescence dynamics of surfactant stabilized emulsions studied with microfluidics. *Soft Matter*, 8, 10650-10657.
- Krebs, T., Schroen, C.G.P.H., Boom, R. M. (2013). Coalescence kinetics of oil-in-water emulsions studied with microfluidics. *Fuel*, v. 106, p. 327–334.
- Lai, A., Bremond, N., Stone, H. A. (2009). Separation-driven coalescence of droplets: an analytical criterion for the approach to contact. *Journal of Fluid Mechanics*, 632, 97-107.
- Liu, L., Wu, F., Ju, X. J., Xie, R., Wang, W., Niu, C. H., Chu, L. Y. (2013). Preparation of monodispersion calcium alginate microcapsules via internal gelation in microfluidic-generated double emulsions. *Journal of Colloid and Interface Science*, v. 404, p. 85–90.
- Liu, Z., Cao, R., Pang, Y., Shen, F. (2015). The influence of channel intersection angle on droplets coalescence process. *Experiments in fluids*, 56.
- Marze, S., Algaba, H., Marquis, M. (2014). A microfluidic device to study the digestion of trapped lipid droplets. *Food & function*, 5, 1481-1488.
- Nguyen, H. T., Marquis, M., Anton, M., Marze, S. (2019a). Studying the real-time interplay between triglyceride digestion and lipophilic micronutrient bioaccessibility using droplet microfluidics. 1 lab on a chip method. *Food chemistry*, 275, 523-529.
- Nguyen, H. T., Marquis, M., Anton, M., Marze, S. (2019b). Studying the real-time interplay between triglyceride digestion and lipophilic micronutrient bioaccessibility using droplet microfluidics. 2 application to various oils and (pro)vitamins. *Food chemistry*, 275, 661-667.
- Mazutis, L., Griffiths, A. D. (2012). Selective droplet coalescence using microfluidic systems. *Lab on a Chip*, 12, 1800–1806.
- Meng, Q., Zhang, Y., Li, J., Lammertink, R. G. H., Chen, H., Tsai, P. A. (2016). Altering Emulsion Stability with Heterogeneous Surface Wettability. *Nature, Scientific reports*, 6:26953.
- Muijlwijk, K., Colijn, I., Harsono, H., Krebs, T., Berton-Carabin, C., Schroen, K. (2017). Coalescence of protein-stabilised emulsions studied with microfluidics. *Food Hydrocolloids*, 70, 96-104.
- Nisisako, T., Torii, T. (2008). Microfluidic large-scale integration on a chip for mass production monodisperse droplets and particles. *Lab on a Chip*, v. 8, p. 287–293.

- Ren, P. W., Ju, X. J., Xie, R., Chu, L. Y. (2010). Monodisperse alginate microcapsules with oil core generated from a microfluidic device. *Journal of Colloid and Interface Science*, v. 343, p. 392–3
- Roques-Carmes, T., Monnier, H., Portha., J-F., Marchal, P., Falk, L. (2014). Influence of the plate-type continuous micro-separator dimensions on the efficiency of demulsification of oil-in-water emulsion. *Chemical Engineering Research and Design*, v. 92, p. 2758–2769.
- Santos, T. P., Cejas, C. M., Cunha, R. L., Tabeling, P. (2021). Unraveling driving regimes for destabilizing concentrated emulsions within microchannels. *Soft Matter, Advanced Article*.
- Scheuble, N., Iles, A., Wootton, R. C. R., Windhab, E. J., Fischer, P., Elvira, K. S. (2017). Microfluidic Technique for the Simultaneous Quantification of Emulsion Instabilities and Lipid Digestion Kinetics. *Analytical chemistry*, 89, 9116-9123.
- Schroder, A., Sprakel, J., Schroen, K., Spaen, J. N., Berton-Carabin, C. C. (2018). Coalescence stability of Pickering emulsions produced with lipid particles: A microfluidic study. *Journal of food engineering*, 234, 63-72.
- Shen, F., Li, Yi., Liu, Z-M, Cao, R-T, Wang, G-R. (2015). Advances in micro-droplets coalescence using microfluidics. *Chinese Journal of analytical chemistry*, 43, 1942–1954.
- Shen, F., Li, Y., Liu, Z., Li, XJ. (2017). Study of flow behaviors of droplet merging and splitting in microchannels using Micro-PIV measurement. *Microfluid Nanofluidics*, 21:66.
- Simone, G. (2015). Demonstrating microdroplet coalescence for tailored and biodegradable microgel fabrication. *RSC Advances*, 5, 56848–56854.
- Simone, G., van de Donk, O. (2019). On demand coalescence in microchannel: Viscosity matters. *Chemical engineering science*, 208, 115173.
- Sugiura, S., Nakajima, M., Yamamoto, K., Iwamoto, S., Oda, T., Satake, M., Seki, M. (2004). Preparation characteristics of water-in-oil-in-water multiple emulsions using microchannel emulsification. *Journal of Colloid and Interface Science*, 270, 221–228.
- Tan, Y-C., Fisher, J. S., Lee, A. I., Cristini, V., Phillip. A. (2004). Design of microfluidic channel geometries for the control of droplet volume, chemical concentration, and sorting. *Lab on a Chip*, v. 4, p. 292-298.

- Tan, Y-C., Ho, Y. L., Lee, A. P., Cristini, V., Phillip. A. (2007). Droplet coalescence by geometrically mediated flow in microfluidic channels. *Microfluidics and Nanofluidics*, v. 3, p. 495-499.
- Tullis, J., Park, C. L., Abbyad, P. (2014). Selective fusion of anchored droplets via changes in surfactant concentration. *Lab on a chip*, 14, 3285-3289.
- Ushikubo, F. Y., Birribilli, F. S., Oliveira, D. R. B., Cunha, R. L. (2014). Y- and T-junction microfluidic devices: effect of fluids and interface properties and operating conditions. *Microfluidics and Nanofluidics*, v. 17, p. 711–720.
- Ushikubo, F.Y.; Oliveira, D.R.B.; Michelin, M.; Cunha, R.L. (2015). Designing food structure using microfluidics. *Food Engineering Reviews*, v. 7, p. 393-416.
- Wang, K., Lu, Y., Yang, L., Luo, G. (2013). Microdroplet Coalescences at Microchannel Junctions with Different Collision Angles. *American Institute of Chemical Engineers Journal*, 59, 643-649.
- Whitesides, G. M. (2006). The origins and the future of microfluidics. *Nature*, v. 442, p. 368-373.
- Xu, B., Nguyen, N-T., Wong, T. N. (2011). Droplet Coalescence in Microfluidic systems. *Micro and Nanosystems*, v.3, p. 131-136.
- Zhou, Q., Sun, Y., Yi, S., Wang, K., Luo, G. (2016). Investigation of droplet coalescence in nanoparticle suspensions by a microfluidic collision experiment. *Soft Matter*, 12, 1674-1682.

## CAPÍTULO 2

### **Designing biotechnological processes to reduce emulsions formation and improve oil recovery: Study of antifoams application**

Artigo publicado no periódico “Biochemical Engineering Journal”: Santos, T. P., Cunha, R. L. Designing biotechnological processes to reduce emulsions formation and improve oil recovery: Study of antifoams application. Biochemical Engineering Journal, 163, 107745, 2020. <https://doi.org/10.1016/j.bej.2020.107745>.



Contents lists available at ScienceDirect

# Biochemical Engineering Journal

journal homepage: [www.elsevier.com/locate/bej](http://www.elsevier.com/locate/bej)

## Regular article

# Designing biotechnological processes to reduce emulsions formation and improve oil recovery: Study of antifoams application



Tatiana Porto Santos, Rosiane Lopes Cunha\*

Department of Food Engineering, Faculty of Food Engineering, University of Campinas (UNICAMP), 13083-862, Campinas, SP, Brazil

## HIGHLIGHTS

- Energy density and antifoams features are major factors affecting emulsion stability.
- Yeast cells and antifoaming agents promoted formation of undesirable cream phase.
- Antifoams can interfere on physical properties of yeast cells.
- Emulsifier activity of antifoams depend on their physicochemical properties.
- The set of methodologies can be used as a tool to choose broth composition.

## ARTICLE INFO

### Keywords:

Antifoaming agents  
Yeast cells  
Emulsion stability  
Biotechnology  
Downstream processing  
Interfacial tension

## ABSTRACT

Fermentation aiming at oil production has emerged as an outstanding technique, but an undesirable emulsion can be formed preventing oil separation. There is still little knowledge about the mechanisms triggering the formation of such emulsions. Although this phenomenon is partly attributed to the cells presence, other essential compounds can contribute to the stability of emulsions, due to their surface properties. Thus, this study aimed at investigating the mechanisms of emulsions stabilization by *Saccharomyces cerevisiae* (a model microorganism) and two well-known antifoaming agents (Pluronic L81 and Antifoam C), since the surface properties of antifoams have hitherto gathered limited attention. This study also simulated conditions of energy density within the range used in similar bioprocesses. Emulsions were evaluated from droplet size, rheological properties, optical and confocal microscopy. Albeit all emulsions were stable, Pluronic L81 led to a greater reduction in interfacial tension and droplet size values, showing the drawback of its application for product recovery. It was also observed that the molecular characteristics of oils can contribute to hinder oil recovery. Therefore, the choice of an antifoam depends on the properties of the oil to be recovered. Moreover, it was demonstrated that the set of methodologies used in this study can be a tool to study the colloidal effects of fermentation components to gain insights on the development of more feasible bioprocesses.

## 1. Introduction

Biotechnological processes based on genetic engineering for the production of oils are classified as clean technologies, and farnesene ( $C_{15}H_{24}$ ) appears as a highly important compound, in addition to other substances, such as some flavors, food additives, pharmaceuticals, and chemicals [1]. They are produced by using an engineered yeast strain to which recombination of DNA (that codifies the enzymes to generate a particular substance from a specific source) is generally applied, allowing the yeast to secrete another type of component [2,3]. Therefore, this transformation in the yeast strain allows the microorganism to act differently in fermentation conditions. Especially for isoprenoids (that

can be commercialized for pharmaceutical, nutraceutical and biofuel industry), this strain was developed to not only produce the desired product, but also to increase the fermentation yield on an industrial scale [2]. In the biofuel industry (e.g. production of farnesene), genetically modified *Saccharomyces cerevisiae* is applied to convert sugarcane into farnesene, instead of standard ethanol, during the fermentation process. In addition, the production of alkanes has also been studied using modified *Escherichia coli* [4]. Despite this myriad of advantages, oil separation and recovery from these microbial-based processes are not simple tasks. More specifically, processes involving the mixture of polar and nonpolar compounds can generate undesirable stable emulsions depending on process conditions and composition

\* Corresponding author.

E-mail addresses: [tatiana.porto90@gmail.com](mailto:tatiana.porto90@gmail.com) (T.P. Santos), [rosiane@unicamp.br](mailto:rosiane@unicamp.br) (R.L. Cunha).<https://doi.org/10.1016/j.bej.2020.107745>

Received 25 June 2020; Accepted 27 July 2020

Available online 29 July 2020

1369-703X/ © 2020 Elsevier B.V. All rights reserved.



[3,5].

Changes in the broth composition simultaneously to oil formation, as well as the addition of other adjuvant compounds (such as anti-foams) during the biotechnological process, may also contribute to the formation of stable emulsions [6,7]. However, the addition of antifoams is essential during the fermentation process, as the production of the desired compounds is accompanied by foam generation. Apart from that, the introduction of gases into the culture broth is necessary depending on the process and, due to the broth composition, these gases are stabilized as foam [8]. Therefore, most commercial fermentation processes depend on the addition of antifoaming agents to prevent excessive foams build-up and accumulation [9]. Foams can not only influence the amount of oxygen dissolved within the fermentation broth, impairing yeast performance, but bubbles can also burst during the process, damaging proteins and yeast cells and leading to loss of sterility in bioreactors [10,11]. Thus, the type and concentration of antifoams should be balanced considering secondary effects within the broth culture [12] because, as mentioned earlier, antifoams not only reduce the foam formation but as surface-active agents, they may also have the ability to trigger emulsion stabilization, hampering the downstream process. Despite this, antifoams are usually applied within the fermentation broth with scant control about either the type or the concentration of the antifoam, and they have been vaguely studied regarding their action as surface agents. Moreover, cell concentration is also an important factor, since microorganisms themselves can act as stabilizing agents in emulsions, increasing the viscosity of the continuous phase [13,14] or acting as a *Pickering*-type stabilizer [14–17]. *Pickering* emulsion is based on stabilization promoted only by solid particles, which accumulate at the oil-water interface and physically stabilize emulsions droplets [18].

In general, the use of intense mechanical forces (centrifugation) combined with the addition of demulsifying agents is necessary to promote phase separation and oil recovery, which leads to high process costs and can be harmful to the environment [7,19,20]. Demulsifying agents are generally water-soluble chemicals, which are preferentially partitioned into the rejected aqueous phase during oil production. Thus, the discharge of demulsifying agents inevitably occurs, causing environmental contamination [21] and large volumes of non-ecofriendly effluent. In addition, the demulsification route based on centrifugation requires high capital costs for industrial implementation due to the high energy density associated with the process [19,22]. Costs will be even higher if information about products (physicochemical properties) and stabilization mechanisms during the process are little known, hindering the design of optimized process conditions for oil recovery. The knowledge of the interface properties as surface charge or interfacial tension may help to predict droplets formation and coalescence [23]. Therefore, emulsion composition and process conditions will have a direct impact on emulsions stability.

Within this context, we aimed to produce model emulsions containing *Saccharomyces cerevisiae* (as a model microorganism) and two widely used antifoams (Pluronic L81 and Antifoam C) to understand the role of these compounds on the formation of a stable emulsion during a biotechnological process. Furthermore, different oils were used with varied physicochemical properties as well as two strategies of energy input to emulsions formation simulating different products and energy conditions in fermentation processes, respectively. Our hypothesis is that, as distinct antifoaming agents act differently in the breaking of foams [12], they would also act differently in stabilizing emulsions. Therefore, we were able to understand the stabilization mechanisms of these antifoams and highlight the importance of studying each component of the fermentation broth. We could also confirm that antifoams should be critically chosen as their misapplication may imply on emulsion formation, hindering the oil recovery. Therefore, from this study, the knowledge of the effect of some components of the culture broth and process conditions on emulsions stability could be elucidated, allowing to overcome some drawbacks of the fermentation process from

the understanding of the most suitable composition to design more economical downstream techniques. Another approach of this paper was to demonstrate a set of methodologies that can be applied as a tool to evaluate colloidal interactions within the fermentation broth, in order to gain insights and predict emulsion formation to enable more efficient bioprocess design. This set of simple methodologies could be applied in lab-scale experiments in systems with more complex composition to predict potential problems that may arise during an actual biotechnological process.

## 2. Material and methods

### 2.1. Material

Fresh baker's yeast (*Saccharomyces cerevisiae* - moisture content of  $70.13 \pm 1.81$  % w/w) (Itaiquara, Tapiratiba, Brazil) and sunflower oil (Bunge Alimentos, Brazil) were purchased in the local market. Hexadecane (99 % v/v), antifoam C (a 30 % v/v aqueous emulsions of polydimethylsiloxane in which the active ingredient is a silicone-based polymer) and Pluronic L81 (poly(ethylene glycol)-block-poly(propylene glycol)-block-poly(ethylene glycol) with a molecular weight of 2800 Da) were obtained from Sigma-Aldrich (St. Louis, USA). The medium-chain-triacylglycerol (MCT) (NEOBEE®1053) was kindly donated by Stepan Lipid Nutrition (Northfield, USA). Ultrapure MilliQ water was used to prepare emulsions and all other chemicals were of analytical grade.

### 2.2. Preparation of oil-in-water emulsions

Two methodologies were applied to produce the emulsions using different agitation conditions (related to the energy density input) that were named as low- and high-energy processes. In the low-energy process, the oil and aqueous phase were mixed using a straight impeller agitator coupled to a mechanical impeller RW20 (IKA, Wilmington, USA) (900 rpm, 30 min and 25 °C). These conditions have been used in previous studies [3,14,17]. For the high-energy process, emulsions were prepared by mixing the phases using an Ultra Turrax T18 (IKA, Staufen, Germany) for 5 min at 15,000 rpm. Both process conditions (rotational speed and time) were chosen based on energy density values, because, using energy density of the same order of magnitude (regardless of the equipment), droplet disruption can be comparable, resulting in a similar droplet diameter [24]. Therefore, we used two orders of magnitude of energy density to simulate a wide range applied in biotechnological processes (considering usual specific power input and time). The energy density was around  $10^5$  J.m<sup>-3</sup> for the mechanical impeller and  $10^8$  J.m<sup>-3</sup> for the Ultra Turrax [25,26]. The calculations are shown in Supplementary Information (SI-1).

Oil-in-water emulsions were prepared by mixing aqueous phases containing yeast (Y), one of the antifoams (Antifoam C (AntC)/ Pluronic L81(P81)) or even a combination thereof to three different oils using the same volume phases ratio (90:10) as shown in Table 1. This concentration of oil was chosen according to previous studies [3], besides being approximately the maximum concentration of *farnesene* [27], in order to simulate specific conditions in which formation of stable emulsion occurs during the fermentation process. Oils with different characteristics (chain size, unsaturation degree, physicochemical properties, and polarity) were chosen to simulate a variety of potential products obtained from biotechnological processes, allowing a better understanding of the role of antifoams and yeast on emulsions stability. In this context, two triacylglycerols (TAGs) with different chain lengths and one hydrocarbon were evaluated. Sunflower oil (O) and MCT (M) were the TAGs, while hexadecane (H) was the selected hydrocarbon. Hexadecane (C<sub>16</sub>H<sub>34</sub>) has a straight saturated chain and presented viscosity of  $\sim 3.3$  mPa.s and density  $\sim 769$  kg/m<sup>3</sup>. Sunflower oil showed viscosity  $\sim 55$  mPa.s and density  $\sim 914$  kg/m<sup>3</sup> and a main fatty acid composition of 44.67 % of oleic acid (C18:1), 43.71 % of

**Table 1**  
Initial emulsions formulation.

Codification	Aqueous phase composition (90 % v/v)*			Oily phase composition (10 % v/v)*
	Yeast (%) w/v	Antifoam C (%) w/v	Pluronic L81 (%) w/v	
Y-H	7	–	–	Hexadecane (H)
AntC-H	–	0.3	–	
P81-H	–	–	0.3	
AntCY-H	7	0.3	–	
P81Y-H	7	–	0.3	
Y-O	7	–	–	Sunflower oil (O)
AntC-O	–	0.3	–	
P81-O	–	–	0.3	
AntCY-O	7	0.3	–	
P81Y-O	7	–	0.3	
Y-M	7	–	–	MCT (M)
AntC-M	–	0.3	–	
P81-M	–	–	0.3	
AntCY-M	7	0.3	–	
P81Y-M	7	–	0.3	

\* The percentage corresponds to the final concentration in the mixture. Y = yeast, AntC = Antifoam C, P81 = Pluronic L81, H = hexadecane, O = sunflower oil and M = medium-chain-triacylglycerol (MCT).

linoleic acid (C18:2), 5.76 % of palmitic acid (C16:0) and 3.57 % of stearic acid (C18:0). MCT is mainly comprised of 51.21 % of caprylic acid (C8:0), 44.39 % of capric acid (C10:0), 1.67 % of linoleic acid (C18:2), 1.16 % of oleic acid (C18:1) and presented viscosity ~ 24 mPa.s and density ~ 941 kg/m<sup>3</sup>.

Before emulsions production, aqueous phases were characterized according to scanning electron microscopy and zeta potential. In addition, the interfacial tension between phases was analyzed. After 24 h of emulsions preparation and gravity separation, the cream phases were quantified and characterized according to particle size distribution, rheological assays, confocal and optical microscopy. Emulsions cream phase was investigated in order to simulate the broth portion containing the product to be recovered.

### 2.3. Characterization of aqueous and oily phases

#### 2.3.1. Scanning electron microscopy

Before emulsions preparation, aqueous phases containing yeast and antifoams (Table 1) were freeze-dried (Lyophilizer LS 300 Terroni, São Carlos, Brazil) and coated with a thin layer of gold in a Sputter Coater Emitech K450 (Kent, United Kingdom). Afterward, yeast morphology was visualized using a scanning electron microscopy (Leo440i, LEO Electron Microscopy/Oxford, Cambridge, England) under 10 kV and 2000x of magnification. At least 10 pictures were taken for each sample.

#### 2.3.2. Zeta potential

Beforehand, three different aqueous solutions were prepared: yeast cells (0.005 % v/v), antifoam C (0.1 % v/v) and Pluronic L81 (0.1 % v/v) diluted in MilliQ water. Zeta potential (charge density) of these aqueous solutions was determined in a Nano-ZS Zetasizer (Malvern Instruments, Malvern, UK).

#### 2.3.3. Interfacial tension

Interfacial tension kinetics between aqueous phases containing yeast and/or antifoams (Antifoam C and Pluronic L81) and oily phases (hexadecane, sunflower oil or MCT) was measured using a Tracker-S tensiometer (Teclis, Longessaigne, France) at 25.0 ± 0.1 °C by the pendant drop method. Kinetics of interfacial tension was monitored for 90 min [17].

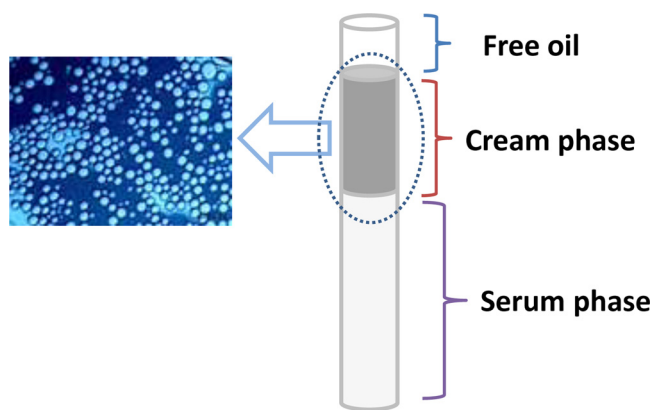


Fig. 1. Demonstrative design of the separated phases.

### 2.4. Characterization of emulsions cream phase

#### 2.4.1. Volume of oil, cream, and serum phases

After 24 h of emulsions preparation, the volumes of free oil, cream, and serum phases were measured (Eqs. (1), (2) and (3), respectively) to identify the volume fraction of emulsions separated phases. Free oil is the highest phase (on the top) that has occurred in some samples. The cream phase is the concentrated emulsion that is located at the top or in the middle of the sample (if free oil is present). This was the phase investigated, simulating the part of the fermentation broth that contains the product to be recovered (thus, it contains a dense distribution of oil droplets). The serum phase is the lower phase, composed mainly of free water, but it can also have some scattered droplets (Fig. 1).

$$\text{Volume of free oil (\%)} = 100 \times \left( \frac{HO}{HT} \right) \quad (1)$$

$$\text{Volume of cream phase (\%)} = 100 \times \left( \frac{HC}{HT} \right) \quad (2)$$

$$\text{Volume of serum phase (\%)} = 100 \times \left( \frac{HS}{HT} \right) \quad (3)$$

where HO is the height of the free oil, HC is the height of the cream phase (analyzed phase), HS is the height of the serum phase and HT is the height of the total mixture.

#### 2.4.2. Particle size distribution

Particle size distribution of cream phases and baker's yeast dispersed in water was analyzed by laser diffraction technique, which is based on static light scattering method using a Multi-Angle Static Light Scattering Mastersizer 2000 (Malvern Instruments, Malvern, UK) at a rotation speed of 1750 rpm. The mode was used as the mean size value of the droplets.

#### 2.4.3. Optical and confocal microscopy

Optical microscopy of cream phases was performed on a Carl Zeiss Axio Scope A1 microscope (Zeiss, Jena, Germany). Samples were placed directly on glass slides and visualized with a 10x objective for qualitative observation. In addition, confocal microscopy of cream phases produced under high-energy was performed in a Zeiss confocal microscope LSM 780 NLO on an Axio Examiner D1 (Zeiss, Jena, Germany) using a 40x objective. Oils were stained with Nile Red, while cream phases containing yeast were dyed with DAPI (4',6-Diamidino-2-Phenylindole, Dihydrochloride) [17,28] to perform confocal microscopy. Nile Red and DAPI were excited on a laser wavelength of 488 and 405 nm, while their emission wavelengths were 604 and 448 nm, respectively.

#### 2.4.4. Rheological properties

Rheological properties of the cream phases were carried out in a

stress-controlled rheometer AR1500ex (TA Instruments, New Castle, USA) attached to a parallel plate geometry (40 mm). The gap was fixed at 1000  $\mu\text{m}$ . Flow curves were obtained by up-down-up steps in order to eliminate thixotropy. Shear rate ranged from 0 to 1000  $\text{s}^{-1}$  and the third flow curve data were fitted to the power-law rheological model. Flow index ( $n$ ), consistency index ( $K$ ), and apparent viscosity at 75  $\text{s}^{-1}$  were evaluated. Shear rate of 75  $\text{s}^{-1}$  was chosen considering typical values found in biotechnological process based on the angular velocity [25] (see Supplementary Information SI-2). The degree of fit to the model was analyzed by the determination coefficient ( $R^2$ ).

## 2.5. Statistical analysis

Analysis of variance (ANOVA) was performed using the software Sisvar 5.6 [29] and significant differences between compositions were evaluated using Tukey test. The level of confidence was 95 %.

## 3. Results and discussion

### 3.1. Impact of emulsion composition on cream phase stability

Thermodynamically unfavorable contact between oily and aqueous phases may hinder their interactions, but the addition of components with surface activity can reduce the interfacial tension (IFT) between these two immiscible phases and potentially allow emulsion formation. Adsorption of surface-active compounds onto droplets interface can lead to the stabilization of droplets of either water or oil depending on their physicochemical properties [23,30]. However, some solid particles can also induce the physical stabilization of emulsions with no IFT reduction [18] in the *Pickering*-type stabilization, due to the formation of a strong mechanical barrier onto the interface.

Fig. 2 shows IFT kinetics for different aqueous phases (Y, AntC, P81, Y + AntC, Y + P81) and oils (H, O, or M) as well as the control using only water as the aqueous phase. Zeta potential (ZP) values of aqueous phases and corresponding pH values are shown in Fig. 3A, while yeast titration curve is presented in Fig. 3B. Electrostatic repulsion between droplets could have occurred mainly for emulsions with yeast and Pluronic L81 in the aqueous phase, since they presented zeta potential

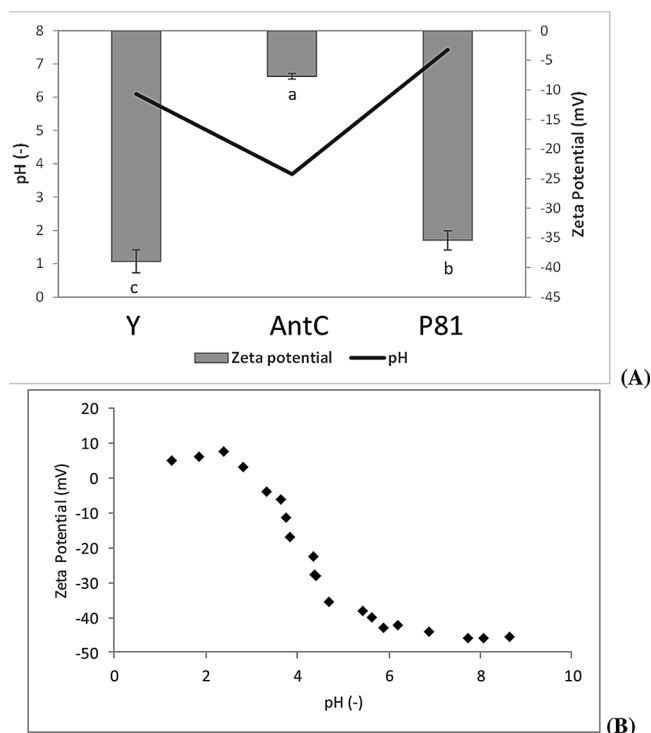


Fig. 3. (A) Zeta potential and corresponding pH values of aqueous phases containing Y (yeast), AntC (Antifoam C), and P81 (Pluronic L81). (B) Titration curve of yeast cells. Different letters in (A) indicate significant differences ( $p < 0.05$ ) comparing zeta potential data.

values of  $-38.97 \pm 1.95$  mV and  $-35.42 \pm 1.63$  mV, respectively. On the other hand, Antifoam C showed a reduced modulus value of  $-7.71 \pm 0.47$  mV. After preparing the emulsions (with Y), the natural pH of the cream phase was around 5.7. Therefore, it was expected that only Y and P81 would induce droplets electrostatic stability, as Antifoam C presented zeta potential of only  $-10.54 \pm 5.30$  mV at this pH.

In general, the use of hexadecane as oily phase presented the higher

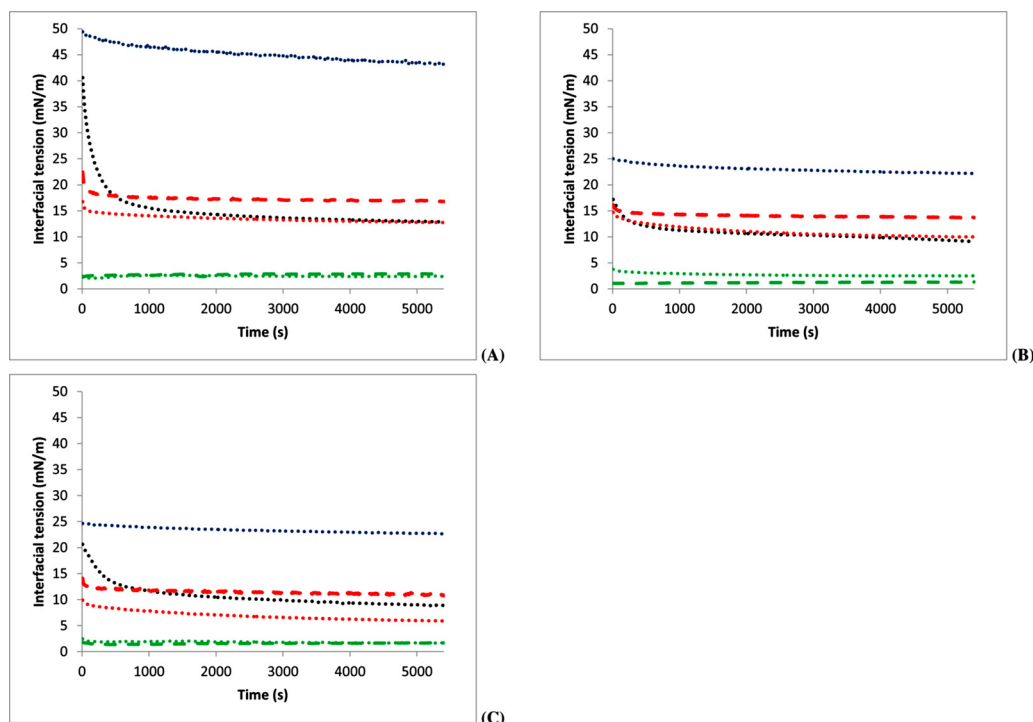


Fig. 2. Interfacial tension for different oils (A) hexadecane, (B) sunflower oil and (C) medium-chain-triacylglycerol (MCT) and aqueous phases containing: (blue dotted line) pure water, (black dotted line) Y (yeast), (red dashed line) AntC (Antifoam C), (green dashed line) P81 (Pluronic L81), (red dotted line) Y + AntC and (green dotted line) Y + P81. For interpretation of the references to colour in this figure legend, the reader is referred to the web version of this article.

decay of IFT regardless of the aqueous phase composition, comparing with the control aqueous phase (water) (Fig. 2A) and TAG-type oils (Fig. 2B-C). The decrease of IFT at the beginning of the process can allow the formation of reduced-size droplets in emulsions, whereas lower equilibrium IFT indicates greater stability over time [31]. Thus, although emulsions with hexadecane could be formed [32], they would probably present reduced long-term stability, as equilibrium IFT values with hexadecane were quite greater than with the other oils. The higher interfacial tension found for hexadecane systems can be associated with the highly non-polar character of this hydrocarbon. On the other hand, the lower values of IFT for TAG-type oils, including the control system (with water), can be related to the presence of hydrophilic portions in their chains [33]. Moreover, sunflower oil and MCT may have a small amount of mono- and diacylglycerols that show emulsifying properties [34] and may also contribute to the lower IFT of TAG-type oils.

In addition to oil properties, the formation and stability of emulsions could be related to antifoams affinity with both aqueous and oily phases in a similar way as an emulsifier [33]. Albeit yeast, Antifoam C, Pluronic L81, and a combination thereof have decreased IFT from the beginning of IFT measurement, P81 presented the shortest time required (Fig. 2A-B-C) to achieve the equilibrium IFT. Comparing pure compounds, AntC presented the second smallest initial IFT value, followed by Y. However, Y presented lower equilibrium IFT values (Fig. 2A-B-C) comparing to Antifoam C regardless of oil composition, indicating that the emulsion formed with AntC could be less stable than emulsions prepared with Pluronic L81 and Y. As a matter of fact, P81 as an amphiphilic block of copolymers drastically reduced IFT regardless of oil composition. The vanishingly small IFT values with P81 can be at least partly associated with the presence of charged groups (Fig. 3), promoting high mobility of P81 in water medium and allowing an easier encounter with the water-oil interface [33]. The presence of both hydrophilic (hydroxyl group) and hydrophobic (carbonic chain) portions in P81 molecule may also have improved emulsion stability, because hydroxyl groups in the chain can bind to water molecules by hydrogen bonds [33], meanwhile hydrophobic portions interact with oil molecules. On the other hand, AntC, a silicon-based agent comprised of non-ionic molecules (Fig. 3), seems to be a slower component that took longer time to decrease IFT values. Thus, the emulsion produced with this component may be more prone to loss of stability during storage due to the absence of repulsive electrostatic interactions between the droplets.

Stability conferred by yeast cells is not only explained by IFT values, as yeast can induce varied stabilizing mechanisms, such as *Pickering*-type, steric barrier, and electrostatic repulsion. The latter is associated with charged portions of products released by yeast, such as mannoproteins and bioemulsifiers, leading to IFT decay over time [13,14,16,35–37] as observed in our results (Fig. 2). Hydrophobic interactions of cell proteins could also lead to improved stabilization [13], which depends on the exposition of hydrophobic groups. Our results showed that the initial IFT of Y-based emulsions slightly changed comparing to pure water-oil IFT. Therefore, we assumed that stabilization was firstly associated with the physical barrier due to the presence of cells. However, other components with surface-activity can play a major role in keeping emulsions stability over time [14,17], displacing these cells from the interface and consequently reducing the IFT. Overall, association Y + AntC showed a synergistic effect on IFT reduction, while association Y + P81 exhibited the prevailed effect of the antifoam on IFT values. This could be associated with yeast displacement from the interface as P81 is the main responsible for stabilization in these emulsions.

Fig. 4 depicts the structure of pure yeast cells (Fig. 4A) and their combination with antifoaming agents (AntC and P81) (Fig. 4B-C). Although cell walls are known to be very strong and flexible [17], AntC seemed to induce cells adhesion and packing. In contrast, P81 caused a modification on cells interfaces, allowing them to be visually more defined (decreased cell adhesion). These results show that antifoams

not only play an important role in emulsions production but can also interfere with the properties of yeast cells. Particularly, there is a well-established literature highlighting the effect of antifoams on the biological pathway and the bioprocess productivity [12], especially considering their role in affecting growth [38,39] and inducing stress responses of yeast cells [40]. However, as far as we know, the physical-steric effect of antifoams on yeast cells has never been exposed.

### 3.2. Stability of emulsions cream phase

#### 3.2.1. Volume of free oil, cream, and serum phases

Visualization of phases' separation (into free oil, cream, and serum phases) (Fig. 5) provides important information to understand the effect of each component in triggering emulsion stability. Fig. 5 shows that P81 played a great role in emulsions stabilization, presenting no phase separation (considered 100 % of cream phase) when the system was subjected to the high-energy process. Unlike, in emulsions containing only AntC, the content of cream phase was reduced and more free oil was present (regardless of the oil properties), indicating the poor ability of AntC to entrap oil and generate a stabilized cream phase. AntC, as aforementioned, can achieve the interface more slowly resulting in non-completely covered droplets that favor coalescence and oil separation, especially employing the low-energy process. Corroborating with IFT results, AntC in combination with hexadecane produced even lower cream phase content (more free oil), also indicating the poor emulsifier ability of this antifoam. Moreover, hexadecane is the more hydrophobic oil and presented the highest density difference between the phases ( $\rho_{oil} - \rho_{aq}$ ), which according to Stokes law can increase phase separation. The subsequent section (section 3.2.2) entails this discussion elaborately.

Yeast seems to control the stabilization in Y + AntC. This may have occurred because, as AntC slowly goes to the surface, yeast initially dominates the stabilization phenomenon, mainly because it is highly charged, thereby with high mobility in the aqueous medium. Once on the surface, yeast can induce emulsion stabilization due to a combination of physical (due to the presence of "particles") and electrostatic (due to mannoproteins and bioemulsifiers) mechanisms. Moreover, exposure of hydrophobic groups of cellular protein can also improve emulsion stabilization [13]. On the other hand, it is clear the greater influence of P81 (especially under the high-energy process) in Y + P81 due to the faster deposition of P81 on the surface. Thus, P81 is the component that most easily induced the formation of an undesirable stable emulsion, while AntC presented favorable results (less emulsion stabilization). In general, increasing the energy density of the process enabled a higher content of cream phase and a reduction of free oil. This fact will be detailed in section 3.2.2.

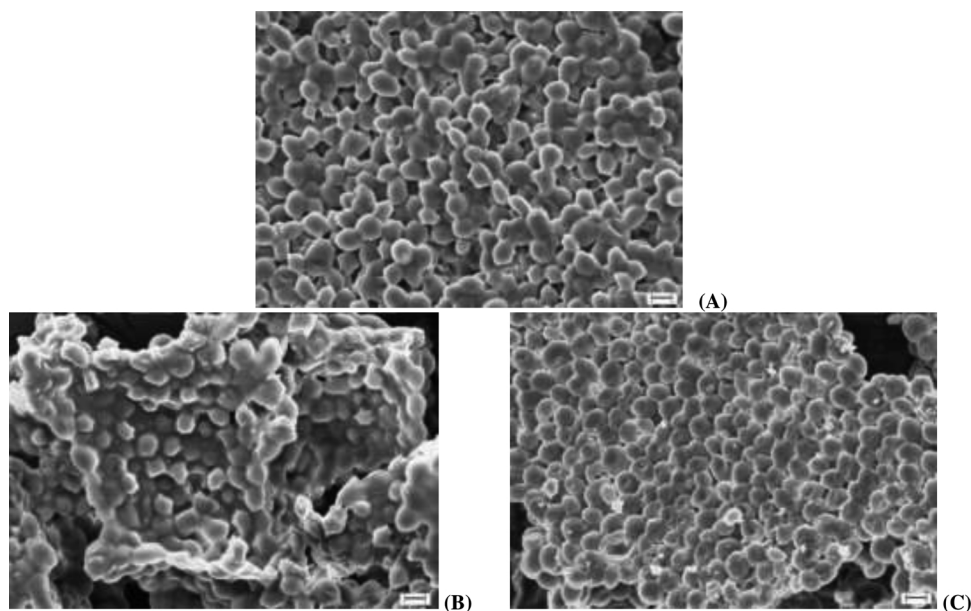
#### 3.2.2. Droplets size, rheological behavior, optical and confocal microscopy

Droplets size, optical and confocal microscopy as well as rheological behavior of cream phases were measured after 24 h of gravity separation. Droplet size determination and rheological behavior are essential analyzes to determine emulsion stability, allowing to obtain insights and even to predict emulsion stability over time.

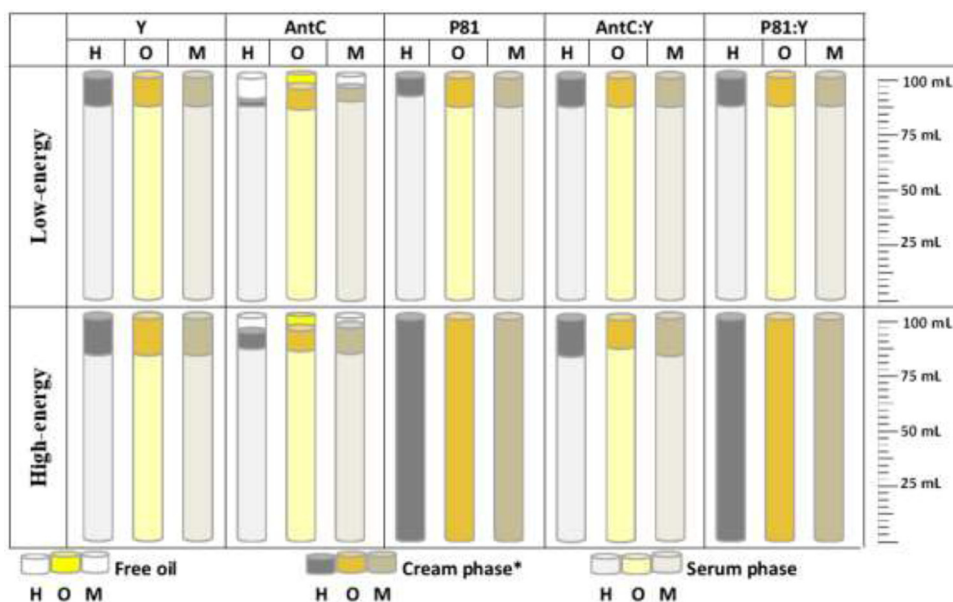
Confocal microscopy of MCT cream phases (M) was performed representing the different emulsion systems (Fig. 6). Oil droplets stained with Red Nile evidenced the formation of an oil-in-water cream phase. In addition, active yeasts stained with DAPI could be observed onto the droplets surface. Confocal (Fig. 6A) and transmittance microscopy of YM (Fig. 6B) show that only a small population of yeast cells had been dyed with DAPI as only cells with intact genetic material have this capacity [17]. Therefore, the high number of cells (active or not) visualized onto the droplets surface indicates a *Pickering*-type stabilization, as also observed by other authors [14–18]. Cream phases of emulsions stabilized with only antifoams also showed an oil-in-water type emulsion (Fig. 6C-D).

Droplet size distribution and viscosity were also measured to evaluate the stability mechanisms of these emulsions (cream phase).





**Fig. 4.** Scanning electron microscopy of aqueous phases containing (A) Y (yeast) (pH ~6.1), (B) Y + AntC (Antifoam C) (pH ~5.8), and (C) Y + P81 (Pluronic L81) (pH ~6.3). Scale bar = 3 μm.



**Fig. 5.** Volume of free oil, cream, and serum phases of emulsions after 24 h of preparation at 25 °C. \* Cream phase was the name given to the analyzed phase. Y: yeast, AntC: Antifoam C, P81: Pluronic L81, H: hexadecane, O: sunflower oil, and M: medium-chain-triacylglycerol.

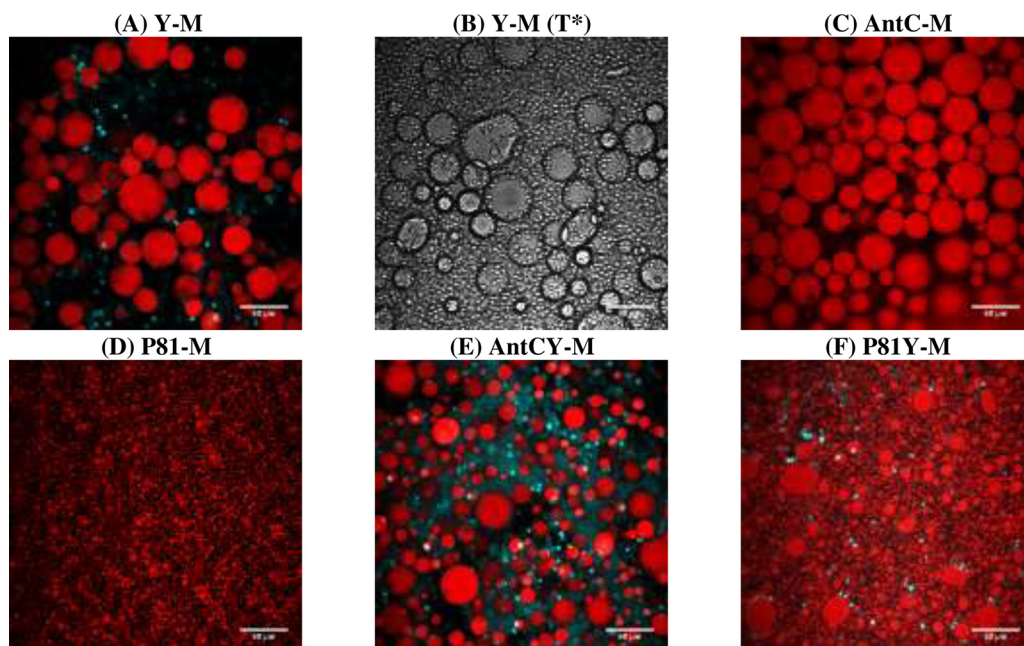
Droplet size ( $d_d$ ) and viscosity ( $\eta$ ) (related to rheological behavior) are associated with emulsions stability because, according to Stokes law (Eq. (4)), the increase of viscosity ( $\eta$ ) hinders emulsion destabilization. Moreover, droplets size is squared-proportional to creaming rate ( $v_c$ ) and, therefore, smaller droplets decrease phases separation. Density difference between oily ( $\rho_{oil}$ ) and aqueous ( $\rho_{aq}$ ) phases also exerts influence on the velocity of separation. Although Stokes law is valid for a single droplet, the influence of these parameters can also be extended to concentrated emulsion systems [7].

$$v_c = \frac{1}{18} \frac{(\rho_{oil} - \rho_{aq})}{\eta} g d_d^2 \quad (4)$$

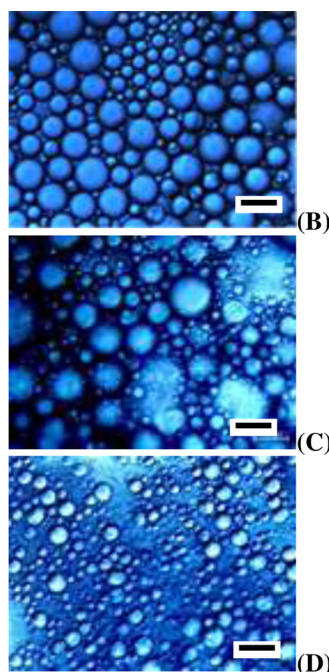
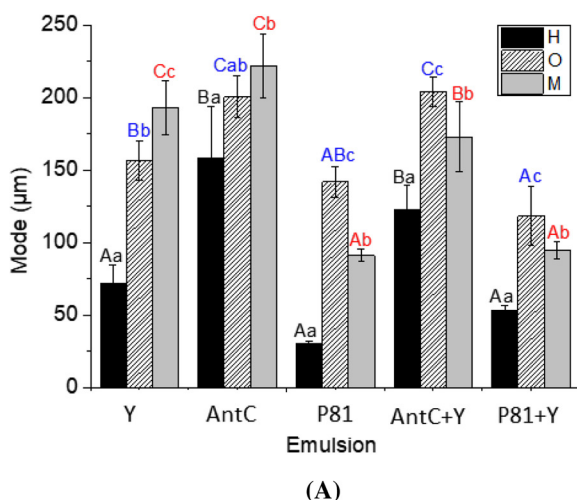
As previously demonstrated (Section 3.2.1), all emulsions presented a separated cream phase, except emulsions prepared under the high-energy process containing P81 (Fig. 5). Therefore, instead of the cream

phase, this entire emulsion was analyzed for size determination and rheological measurement. Although all cream phases have been observed from optical microscopy (data not shown), only samples with yeast (Figs. 7B-C-D and 8 B-C-D) were presented to represent the effect of processes with different energy densities on droplets size reduction. In general, droplet size distribution of samples containing yeast presented a bimodal distribution with a peak of around 5 μm representing yeast cells (data not shown) as observed by other authors [14,17]. A monomodal particle size distribution was observed for samples stabilized only by antifoams.

Droplets mode depended on cream phase composition and mainly on process conditions of emulsions production (associated with the amount of energy input (energy density)) (Figs. 7A and 8 A). Regarding the dispersed phase, hexadecane presented smaller droplets especially for emulsions prepared with P81 (Figs. 7 and 8), while for sunflower oil



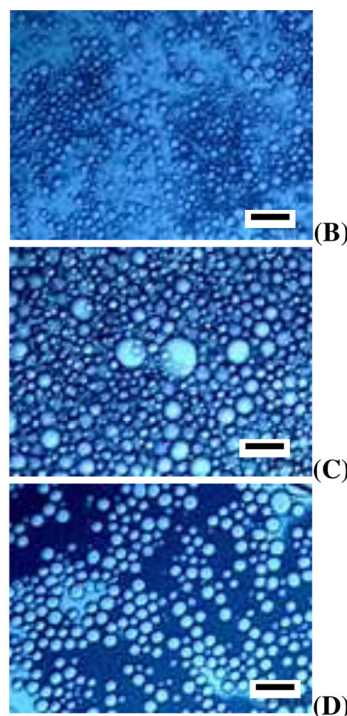
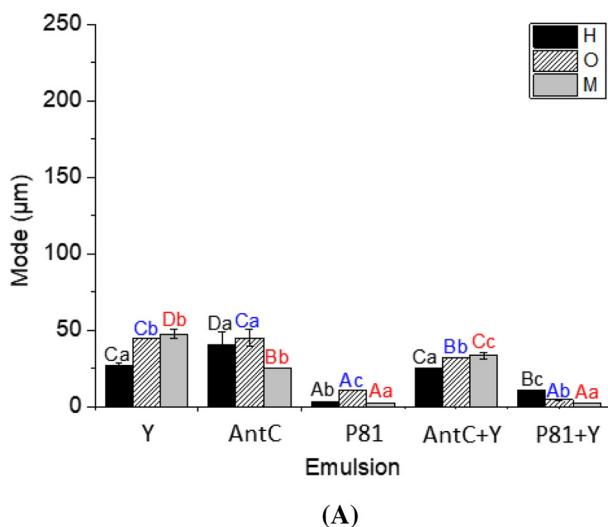
**Fig. 6.** Confocal laser microscopy of a representative emulsions cream phase produced under the high-energy process. T\* = Transmittance. Red droplets represent droplets of oil, while green particles are associated to active yeast cells. Scale bar = 50  $\mu\text{m}$ . Y: yeast, AntC: Antifoam C, P81: Pluronic L81, M: medium-chain-triacylglycerol (For interpretation of the references to colour in this figure legend, the reader is referred to the web version of this article).



**Fig. 7.** (A) Droplets mode of cream phases of hexadecane (H), sunflower oil (O), and medium-chain-triacylglycerol (M) -in-water emulsions prepared under the low-energy process after 24 h. Microscopy of (B) YH, (C) YO, and (D) YM. Y: yeast, AntC: Antifoam C, P81: Pluronic L81. Different letters indicate significant difference ( $p < 0.05$ ). Capital letters compare systems with the same oil, while lowercase letters are related to systems with the same stabilizing agent and different oil. Scale bar: 100  $\mu\text{m}$ .

and MCT results presented less disparity. These results can be partly correlated with IFT kinetics, but they are mostly driven by the lowest viscosity of hexadecane ( $\eta = 3.31 \text{ mPa}\cdot\text{s}$ ) compared to TAGs ( $\eta = 23.93 \text{ mPa}\cdot\text{s}$  for MCT and  $\eta = 55.03 \text{ mPa}\cdot\text{s}$  for sunflower oil), enabling an easier partition of the bulk oil into small droplets. Therefore, considering oil breakage into droplets, dispersed phase viscosity is an important factor in addition to IFT reduction effect [41]. Furthermore, the association of process energy input with these intrinsic properties of emulsions (viscosity of dispersed phase and IFT) are relevant to emulsion stability, since the high-energy process produced the smallest droplets size. However, emulsions produced with hexadecane presented lower stability in comparison to the other oils, showing that the interplay of characteristics -larger equilibrium interfacial tension and phases' density difference- prevailed in the long-term size of the droplets.

Droplets size was similar with addition of Y, AntC, or Y + AntC, while emulsions containing P81 showed the smallest size. Smaller droplets produced with P81 could be related to both faster IFT reduction between phases and equilibrium IFT, regardless of emulsions formation process. On the other hand, it is difficult to pinpoint the predominant mechanisms in Y or AntC analyzing only size measurements. AntC can be considered a slow surface-active component enabling formation of droplets with bigger diameter. The slow displacement of this antifoam to the surface of droplets can allow enough time for droplets to destabilize, recombine, and show increased size. This phenomenon might have occurred for both the low- and the high-energy processes, but the high mechanical energy produced smaller droplets with more available surface area (Fig. 8), allowing components to reach the surface easily. Such generation of smaller droplets is mainly regarding the applied torque, causing a faster and continuous disruption



**Fig. 8.** (A) Droplets mode of cream phases of hexadecane (H), sunflower oil (O), and medium-chain-triacylglycerol (M) -in-water emulsions prepared under the high-energy process after 24 h. Microscopy of (B) YH, (C) YO, and (D) YM. Y: yeast, AntC: Antifoam C, P81: Pluronic L81. Different letters indicate significant difference ( $p < 0.05$ ). Capital letters compare systems with the same oil, while lower-case letters are related to systems with the same stabilizing agent and different oil. Scale bar: 100  $\mu\text{m}$ .

of droplets. Thus, it is likely that the droplets present less coalescence when applied higher energy density and surfactants can easily cover droplets surface, also increasing the amount of cream phase as aforementioned in section 3.2.1. Although energy played a role in droplets breakage, in AntC-systems coalescence may have occurred (albeit in a lesser extent) even under the high-energy process, since AntC presumably did not cover the surface of the droplets at the end of the emulsification process.

Rheological properties of different cream phases containing hexadecane, sunflower oil, and MCT can be visualized in Tables 2 and 3, and Fig. 9. The behavior index ( $n$ ) from power-law fit is related to the degree of deviation from *Newtonian* rheological behavior (viscosity independent of shear rate and  $n$  equal to the unity). Pseudoplastic or shear-thinning behavior presents  $n < 1$ , whilst  $n > 1$  is related to

**Table 2**

Rheological properties (behavior index ( $n$ ) and consistency index ( $K$ )) of the cream phase of emulsions containing different aqueous and oily phases prepared under the low-energy process.

Emulsion	K (Pa.s <sup>n</sup> )	n (-)
Y-H	0.460 $\pm$ 0.109 <sup>A</sup>	0.565 $\pm$ 0.026 <sup>A</sup>
AntC-H*	–	–
P81-H	0.323 $\pm$ 0.002 <sup>A</sup>	0.590 $\pm$ 0.009 <sup>A</sup>
AntCY-H	0.161 $\pm$ 0.070 <sup>B</sup>	0.643 $\pm$ 0.088 <sup>A</sup>
P81Y-H	0.108 $\pm$ 0.029 <sup>C</sup>	0.671 $\pm$ 0.096 <sup>A</sup>
Y-O	0.100 $\pm$ 0.034 <sup>B</sup>	0.763 $\pm$ 0.048 <sup>A</sup>
AntC-O*	–	–
P81-O	0.078 $\pm$ 0.019 <sup>AB</sup>	0.802 $\pm$ 0.053 <sup>A</sup>
AntCY-O	0.050 $\pm$ 0.030 <sup>A</sup>	0.790 $\pm$ 0.009 <sup>A</sup>
P81Y-O	0.114 $\pm$ 0.011 <sup>B</sup>	0.802 $\pm$ 0.000 <sup>A</sup>
Y-M	0.093 $\pm$ 0.044 <sup>AB</sup>	0.751 $\pm$ 0.046 <sup>A</sup>
AntC-M*	–	–
P81-M	0.078 $\pm$ 0.025 <sup>A</sup>	0.781 $\pm$ 0.048 <sup>A</sup>
AntCY-M	0.075 $\pm$ 0.040 <sup>A</sup>	0.731 $\pm$ 0.070 <sup>A</sup>
P81Y-M	0.140 $\pm$ 0.009 <sup>B</sup>	0.730 $\pm$ 0.008 <sup>A</sup>

\* This cream phase volume was not enough to perform this analysis. Different capital letters in the same column indicate significant difference ( $p < 0.05$ ) between compositions for the same oil. Y = yeast, AntC = Antifoam C, P81 = Pluronic L81, H = hexadecane, O = sunflower oil and M = medium-chain-triacylglycerol (MCT).

**Table 3**

Rheological properties (behavior index ( $n$ ) and consistency index ( $K$ )) of the cream phase of emulsions containing different aqueous and oily phases prepared under the high-energy process.

Emulsion	K (Pa.s <sup>n</sup> )	n (-)
Y-H	0.055 $\pm$ 0.039 <sup>B</sup>	0.871 $\pm$ 0.041 <sup>A</sup>
AntC-H*	–	–
P81-H	0.001 $\pm$ 0.000 <sup>A</sup>	1.530 $\pm$ 0.134 <sup>B</sup>
AntCY-H	0.124 $\pm$ 0.018 <sup>C</sup>	0.847 $\pm$ 0.004 <sup>A</sup>
P81Y-H	0.003 $\pm$ 0.001 <sup>A</sup>	0.894 $\pm$ 0.157 <sup>A</sup>
Y-O	0.050 $\pm$ 0.033 <sup>A</sup>	1.102 $\pm$ 0.152 <sup>B</sup>
AntC-O*	–	–
P81-O	0.002 $\pm$ 0.002 <sup>B</sup>	1.266 $\pm$ 0.268 <sup>B</sup>
AntCY-O	0.077 $\pm$ 0.007 <sup>A</sup>	0.798 $\pm$ 0.039 <sup>A</sup>
P81Y-O	0.001 $\pm$ 0.000 <sup>B</sup>	1.693 $\pm$ 0.008 <sup>C</sup>
Y-M	0.028 $\pm$ 0.009 <sup>A</sup>	0.850 $\pm$ 0.030 <sup>A</sup>
AntC-M*	–	–
P81-M	0.001 $\pm$ 0.000 <sup>A</sup>	1.678 $\pm$ 0.007 <sup>B</sup>
AntCY-M	0.094 $\pm$ 0.080 <sup>B</sup>	0.816 $\pm$ 0.122 <sup>A</sup>
P81Y-M	0.001 $\pm$ 0.000 <sup>A</sup>	1.697 $\pm$ 0.024 <sup>B</sup>

\* This cream phase volume was not enough to perform this analysis. Different capital letters in the same column indicate significant difference ( $p < 0.05$ ) between compositions for the same oil. Y = yeast, AntC = Antifoam C, P81 = Pluronic L81, H = hexadecane, O = sunflower oil and M = medium-chain-triacylglycerol (MCT).

dilatant or shear-thickening behavior [23]. Viscosity and rheological behavior of the cream phase can change due to different factors such as interactions between droplets, the viscosity of the phases, droplet size, and charge [23], but in the case of this study, the amount of produced cream phase (phase volume) was also quite relevant to rheological properties.

All samples (cream phases) presented apparent viscosity depending on the shear rate. Shear-rate dependence changed according to emulsion composition and energy input since these conditions also influenced cream phases amount (Fig. 5). The behavior index ( $n$ ) increased for the high-energy process and, for samples with P81, the increase of energy also changed the fluid behavior from shear-thinning to shear-thickening (Tables 2 and 3). Moreover, the viscosity of the samples produced under the high-energy process and stabilized by P81 was also



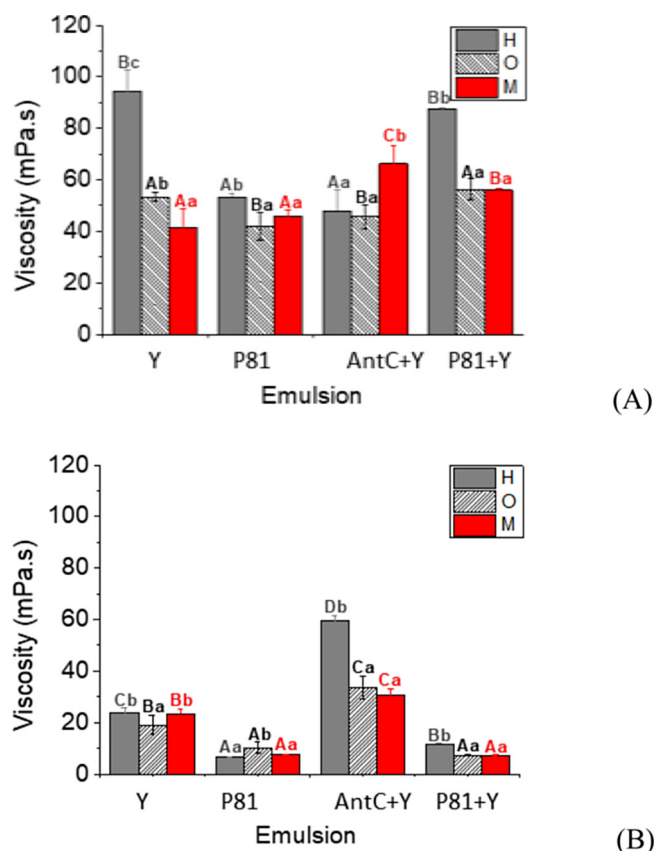


Fig. 9. Apparent viscosity at  $75 \text{ s}^{-1}$  of cream phases of emulsions prepared under the (A) low- and the (B) high- energy processes. Different letters indicate significant difference ( $p < 0.05$ ). Capital letters compare systems with the same oil, while lowercase letters are related to systems with the same stabilizing agent and different oil. The amount of cream phase of AntC-based system was not enough to perform this analysis. Y: yeast, AntC: Antifoam C, P81: Pluronic L81, H: hexadecane, O: sunflower oil, and M: medium-chain-triacylglycerol.

lower due to the great emulsion stability with no phase separation (Fig. 5). It should be highlighted that in this case (P81-based emulsion and the high-energy process) the entire emulsion was evaluated instead of concentrated emulsion (cream phase). In general, process with higher mechanical energy led to the production of smaller droplets and, considering that cream phase volume increased but the amount of entrapped oil was maintained constant, the formed droplets were less packed (less concentration of droplets), resulting in a lower viscosity (Fig. 9). However, for emulsions containing AntC, the energy process did not influence cream phases' viscosity. This might have occurred because AntC promoted adhesion of yeasts (as observed in microscopy (Fig. 4B)) indicating that this component can also improve droplets interaction acting as a glue between them, increasing the viscosity of these cream phases and showing a unique behavior.

Overall, cream phase of emulsions containing hexadecane as dispersed phase showed a viscosity two times higher compared to the pure oil (regardless of the process energy). However, for cream phase of MCT and sunflower oil systems, viscosity was less affected. These results indicate that smaller droplets of cream phase with hexadecane could induce greater interactions between droplets with a consequent higher viscosity. This could be assumed since cream phase of emulsions prepared with hexadecane presented almost the same or a reduced amount compared with the other dispersed phases (Fig. 5), showing less influence of droplets concentration. In general, larger droplets enhance oil separation over time, and it could also be associated with higher susceptibility to destabilization [42], however, it is noteworthy that most

of the cream phases demonstrated to be stable during seven days of observation. Despite droplet sizes found, these cream phases also presented high viscosity, explaining the increased stability. Thus, emulsions presented high viscosity and/or low droplet size, suggesting that different intrinsic features of these emulsions can hamper their destabilization. Our results also demonstrated that the nature of antifoams and the presence of yeast cells play a considerable role in emulsions properties and characteristics of stability. It is necessary to highlight that viscosity was extremely influenced by both the emulsion formation process and the amount of the formed cream phase. However, regardless of the amount of cream phase, these emulsions showed a high viscosity, inhibiting cream phase destabilization.

#### 4. Conclusion

Although the action of antifoams on emulsions stabilization is little known, they are not properly chosen and are added with a lack of control within the fermentation broth. Therefore, their side effect on processes aiming to produce oil was assessed to rationalize the choice of antifoams combined with the presence of yeast cells. In general, yeast, antifoam C, Pluronic L81 and their combinations promoted the formation of a stable cream phase, which was associated to intrinsic properties of both aqueous and oily phases (interfacial tension and surface charge), exerting an effect on droplet size values and/or viscosity of cream phases. Yeast cells could induce emulsion stabilization due to either physical (*Pickering*-type stabilization and high viscosity of the cream phase) and/or physicochemical (electrostatic repulsion between droplets) mechanisms. On the other hand, AntC showing reduced surface charge triggered the production of less-stable emulsions compared to yeast and P81. P81, as a block of copolymers, was the component that provided the undesirable highest stability to emulsions, showing a more pronounced reduction of interfacial tension values compared to the other components. Besides, P81 promoted the formation of the smallest droplets size, inducing the formation of a great amount of a stable cream phase with no free oil observation. In this sense, by comparing the undesirable ability of antifoams to stabilize emulsions, AntC would be more appropriated considering that in biotechnological processes the formation of a highly stable emulsion should be avoided. Thus, this study demonstrated that one of the keys to preventing emulsion formation during fermentation process might be to rationalize the choice of antifoams, which could be based on the evaluation of their emulsion stabilizing ability. We could clearly demonstrate that by combining different process conditions and components, emulsions (cream phase) with different degrees of stability could be formed. Furthermore, we were able to demonstrate that the set of methodologies present in this study can be used as a tool to obtain empirical data in order to maximize oil recovery. By applying these techniques, this study allowed the identification of mechanisms of stabilization promoted by important components of biotechnological processes. To summarize, studying the effects of compounds on bioprocesses is essential to design economically feasible techniques with reduced environmental damage and, in face of this, the techniques applied in this paper can be used to obtain insights on the effect of the components within the fermentation broth.

#### Declaration of Competing Interest

The authors declare that they have no known competing financial interests or personal relationships that could have appeared to influence the work reported in this paper.

#### Acknowledgements

This study was financed in part by the Coordenação de Aperfeiçoamento de Pessoal de Nível Superior – Brasil (CAPES) -



Finance Code 001. Santos thanks São Paulo Research Foundation - FAPESP (Grant number 2017/18109-0) and Conselho Nacional de Desenvolvimento Científico e Tecnológico (CNPq) (Grant number 140700/2017-0) for the assistantship and Cunha thanks CNPq (307168/2016-6) for the productivity grant. Authors also thank FAPESP (2019/07744-1; 2009/50591-0; 2011/06083-0; 2007/58017-5; 2004/08517-3, EMU 2009/54137-1) and Technology on Photonics Applied to Cell Biology (INFABIC) at University of Campinas co-funded by FAPESP (08/57906-3) and CNPq (573913/2008-0). We also appreciate Maria Cuellar's assistance in reading the manuscript, giving us valuable suggestions.

## Appendix A. Supplementary data

Supplementary material related to this article can be found, in the online version, at doi:<https://doi.org/10.1016/j.bej.2020.107745>.

## References

- [1] D. Julleson, F. David, B. Pfeleger, J. Nielsen, Impact of synthetic biology and metabolic engineering on industrial production of fine chemicals, *Biotechnol. Adv.* 33 (2015) 1395–1402.
- [2] Ubersax, D.M. Platt, US Patent No.: US 2010/0311065. (2010). Emeryville, CA (US), United States.
- [3] A.S. Heeres, J.J. Heijnen, L.A.M. van der Wielen, M.C. Cuellar, Gas bubble induced oil recovery from emulsions stabilized by yeast components, *Chem. Eng. Sci.* 145 (2016) 31–44.
- [4] P. Domínguez deMaría, Recent developments production of hydrocarbons: paving the way for bio-based platform chemicals, *Chem. Sus. Chem.* 4 (2011) 327–329.
- [5] A.S. Heeres, C.S.F. Picone, L.A.M. van der Wielen, R.L. Cunha, M.C. Cuellar, Microbial advanced biofuels production: overcoming emulsification challenges for large-scale operation, *Trends Biotechnol.* 32 (2014) 221–229.
- [6] J. Collins, M. Grund, C. Brandenbusch, G. Sadowski, A. Schmid, B. Buhler, The dynamic influence of cells on the formation of stable emulsions in organic-aqueous biotransformations, *J. Ind. Microbiol. Biotechnol.* 42 (2015) 1011–1026.
- [7] A.S. Heeres, K. Schroeën, J.J. Heijnen, L.A.M. van der Wielen, M.C. Cuellar, Fermentation broth components influence droplet coalescence and hinder advanced biofuel recovery during fermentation, *Biotechnol. J.* 10 (2015) 1206–1215.
- [8] A. Eroc, F. Delvigne, J.P. Lecomte, P. Thonart, Foam control in fermentation bioprocess: from simple aeration tests to bioreactor, *Appl. Biochem. Biotechnol.* 130 (2006) 392–404.
- [9] R. Pelton, A review of antifoam mechanisms in fermentation, *J. Ind. Microbiol. Biotech.* 29 (2002) 149–154.
- [10] W. Holmes, R. Smith, R. Bill, Evaluation of antifoams in the expression of a recombinant FC fusion protein in shake flask cultures of *Saccharomyces cerevisiae*, *Microb. Cell Fact.* 5 (2006) 30.
- [11] J. Varley, A. Brown, R. Boyd, P. Dodd, S. Gallagher, Dynamic multipoint measurement of foam behaviour for a continuous fermentation over a range of key process variables, *Biochem. Eng. J.* 20 (2004) 61–72.
- [12] S.J. Routledge, Beyond de-foaming: the effects of antifoams on bioprocess productivity, *Comput. Struct. Biotechnol. J.* 3 (2012) e201210014.
- [13] H. Firoozmand, D. Rousseau, Microbial cells as colloidal particles: pickering oil-in-water emulsions stabilized by bacteria and yeast, *Food Res. Int.* 81 (2016) 66–73.
- [14] G.F. Furtado, C.S.F. Picone, M.C. Cuellar, R.L. Cunha, Breaking oil-in-water emulsions stabilized by yeast, *Colloids Surf. B Biointerfaces* 128 (2015) 568–576.
- [15] S.U. Dickinson, Use of nanoparticles and microparticles in the formation and stabilization of food emulsions, *Trends Food Sci. Technol.* 24 (2012) 4–12.
- [16] L.S. Dorobantu, A.K.C. Yeung, J.M. Foght, M.R. Gray, Stabilization of oil-water emulsions by hydrophobic bacteria, *Appl. Environ. Microbiol.* 70 (2004) 6333–6336.
- [17] T.C.P. Moreira, V.M. Silva, A.K. Gombert, R.L. Cunha, Stabilization mechanisms of oil-in-water emulsions by *Saccharomyces cerevisiae*, *Colloids Surf. B Biointerfaces* 143 (2016) 399–405.
- [18] S.U. Pickering, J. Emulsions, *Chem. Soc. Trans. Home.* 91 (1907) 2001–2021.
- [19] S. Glonke, G. Sadowski, C. Brandenbusch, Applied catastrophic phase inversion: a continuous non-centrifugal phase separation step in biphasic whole-cell biocatalysis, *J. Ind. Microbiol. Biotechnol.* 43 (2016) 1527–1535.
- [20] P. Tabur, G. Dorin, Methods for Purifying Bio-organic Compounds, US2012/0040396 A1 (2012).
- [21] Y. Wen, H. Cheng, L.-J. Lu, J. Liu, Y. Feng, W. Guan, Q. Zhou, X.-F. Huang, Analysis of biological demulsification process of water-in-oil emulsion by *Alcaligenes sp. S-XJ-1*, *Bioresour. Technol.* 101 (2010) 8315–8322.
- [22] S.A. Issaka, A.H. Nour, R.M. Yunus, Review on the fundamental aspects of petroleum oil emulsions and techniques of demulsification, *J. Pet. Environ. Biotechnol.* 6 (2015) 1–15.
- [23] D.J. McClements, *Food Emulsions: Principles, Practices, and Techniques*, 2nd ed., CRC Press, FL, Boca Raton, 2005.
- [24] H. Karbstein, H. Schubert, Developments in the continuous mechanical production of oil-in-water macro-emulsions, *Chem. Eng. Process.* 34 (1995) 205–211.
- [25] Y. Chisti, U.J. Jauregui-Haza, Oxygen transfer and mixing in mechanically agitated airlift bioreactors, *Biochem. Eng. J.* 10 (2002) 143–153.
- [26] R.A. Sheikh, O.A. Al-Bar, Y.M.A. Soliman, Biochemical studies on the production of biofuel (bioethanol) from potato peels wastes by *Saccharomyces cerevisiae*: effects of fermentation periods and nitrogen source concentration, *Biotechnol. Biotechnol. Equip.* 30 (2016) 497–505.
- [27] K.W. George, J. Alonso-Gutierrez, J.D. Keasling, T.S. Lee, Isoprenoid drugs, bio-fuels, and chemicals-artemisinin, farnesene, and beyond, in: J. Schrader, J. Bohlmann (Eds.), *Biotechnology of Isoprenoids*, Springer International, Heidelberg, 2015, pp. 355–390.
- [28] M.H. Ly, M. Naïtali-Bouchez, T. Meylheuc, M.-N. Bellon-Fontaine, T.M. Le, J.-M. Belin, Y. Waché, Importance of bacterial surface properties to control the stability of emulsions, *Int. J. Food Microbiol.* 112 (2006) 26–34.
- [29] D.F. Ferreira, Sisvar: a computer statistical analysis system, *Ciência e agrotecnologia (UFPA)* 35 (2011) 1039–1042.
- [30] I. Gülsereen, M. Corredig, Interactions of chitin nanocrystals with lactoglobulin at the oil-water interface, studied by drop shape tensiometry, *Colloids Surf. B Biointerfaces* 111 (2013) 672–679.
- [31] J. Weiss, J.N. Coupland, D. Brathwaite, D.J. McClements, Influence of molecular structure of hydrocarbon emulsion droplets on their solubilization in nonionic surfactant micelles, *Colloids Surf. A Physicochem. Eng. Asp.* 121 (1997) 53–60.
- [32] P.J. Wilde, Interfaces: their role in foam and emulsion behavior, *Curr. Opin. Colloid Interface Sci.* 5 (2000) 176–181.
- [33] F.Y. Ushikubo, R.L. Cunha, Stability mechanisms of liquid water-in-oil emulsions, *Food Hydrocoll.* 34 (2014) 145–153.
- [34] H. Moonen, H. Bas, Mono- and diglycerides, in: V. Norn (Ed.), *Emulsifiers in Food Technology*, John Wiley & Sons, Ltd, Chichester, 2015, pp. 73–91.
- [35] J.A.T. Barriga, D.G. Cooper, E.S. Idziak, D.R. Cameron, Components of the bio-emulsifier from *S. Cerevisiae*, *Enzyme Microb. Technol.* 25 (1999) 96–102.
- [36] D.R. Cameron, D.G. Cooper, R.J. Neufeld, The mannoprotein of *Saccharomyces cerevisiae* is an effective bioemulsifier, *Appl. Environ. Microbiol.* 54 (1988) 1420–1425.
- [37] D.J. McClements, Lipid-based emulsions and emulsifiers, in: C.C. Akoh, D.B. Min (Eds.), *Food Lipids: Chemistry, Nutrition and Biotechnology*, CRC Press, New York, 2002chapter 3.
- [38] V. Koch, H. Rüffer, K. Schügerl, E. Innertsberger, H. Menzel, et al., Effect of anti-foam agents on the medium and microbial cell properties and process performance in small and large reactors, *Process. Biochem.* 30 (1995) 435–446.
- [39] W. Holmes, R. Smith, R. Bill, Evaluation of antifoams in the expression of a recombinant FC fusion protein in shake flask cultures of *Saccharomyces cerevisiae*, *Microb. Cell Fact.* 5 (2006) 30.
- [40] J.C. Nielsen, F.S.O. Lino, T.G. Rasmussen, J. Thykæ, C.T. Workman, T.O. Basso, Industrial antifoam agents impair ethanol fermentation and induce stress responses in yeast cells, *Appl. Microbiol. Biotechnol.* 101 (2017) 8237–8248.
- [41] A. Gomes, A.L.R. Costa, R.L. Cunha, Impact of oil type and WPI/Tween 80 ration at the oil-water interface: adsorption, interfacial rheology and emulsion features, *Colloids Surf. B Biointerfaces* 164 (2018) 272–280.
- [42] G. Gutiérrez, A. Lobo, D. Allende, A. Cambiella, C. Pazos, J. Coca, J.M. Benito, Influence of coagulant salt addition on the treatment of oil-in-water emulsions by centrifugation, ultrafiltration, and vacuum evaporation, *Sep. Sci. Technol.* 43 (2008) 1884–1895.

## SUPPLEMENTARY INFORMATION

### DESIGNING BIOTECHNOLOGICAL PROCESSES TO REDUCE EMULSIONS FORMATION AND IMPROVE OIL RECOVERY: STUDY OF *ANTI*FOAMS APPLICATION

Tatiana Porto Santos<sup>a</sup>, Rosiane Lopes Cunha<sup>a\*</sup>

<sup>a</sup> Department of Food Engineering, Faculty of Food Engineering, University of Campinas (UNICAMP), 13083-862 – Campinas, SP, Brazil

\*Corresponding author. Tel.: +55 19 3521 4047; fax: +55 19 3521 4027

E-mail address: rosiane@unicamp.br (Rosiane L. Cunha)\*

tatiana.porto90@gmail.com (Tatiana P. Santos)

#### **Supplementary Information (SI-1):**

Generally, in fermentation, the relation power/volume varies from 1 to 1400 W/m<sup>3</sup>, while the duration is typically 5 days (120h) (Chisti and Jauregui-Haza, 2002; Sheikh et al., 2016) and, therefore, mechanical energy density ranges from 4.3.10<sup>5</sup> to 6.1.10<sup>8</sup> J/m<sup>3</sup>.

According to Karbstein and Schubert (1995), emulsification performed in different devices can be compared using the energy density. This means that droplet breakage (and consequently the average droplet size) would be similar when the bulk phase is subjected to the same order of magnitude of energy density, regardless of the equipment. In this sense, we used two equipment -**mechanical impeller** and **Ultra Turrax**- to simulate the mechanical energy density during the fermentation processes. Next, the calculation of the energy density of both processes is demonstrated.

- **Mechanical impeller:**

Equation 1 defines the Reynolds number in an agitation process (Geankoplis, 1993), making possible to evaluate flow regime in a mechanical impeller.

$$Re = \frac{\rho ND^2}{\mu} \quad (1)$$

where  $\rho$  is the density of the fluid (kg/m<sup>3</sup>),  $N$  is the rotational speed (rps),  $D$  is the diameter of the impeller (m), and  $\mu$  is the viscosity of the fluid (Pa.s). The flow is laminar when  $Re < 10$ , turbulent when  $Re > 10^4$ , and it is in the transition region when  $Re$  is between 10 and  $10^4$ .

Properties of water and the different oils used to calculate Reynolds numbers are presented in Table 1, as well as the corresponding Reynolds numbers of the emulsion phases and the calculated energy density ( $De$ ). In order to calculate Reynolds number the following conditions were used:  $N=900$  rpm (15 rps) and  $D=5$  cm.

Table 1. Viscosity ( $\eta$ ) and density ( $\rho$ ) of the phases, and Reynolds number.

Phase	Density $\rho$ (kg/m <sup>3</sup> )*	Viscosity $\mu$ (mPa.s)*	Re	De (J/m <sup>3</sup> )
Hexadecane	769.80 $\pm$ 0.01	3.3 $\pm$ 0.1	9613	1.9 $\times$ 10 <sup>5</sup>
Sunflower oil	914.41 $\pm$ 0.02	55.0 $\pm$ 0.3	623	2.4 $\times$ 10 <sup>5</sup>
MCT	940.91 $\pm$ 0.01	23.9 $\pm$ 0.1	1411	2.3 $\times$ 10 <sup>5</sup>
Water	997.10 $\pm$ 0.00	1.1 $\pm$ 0.01	37400	2.5 $\times$ 10 <sup>5</sup>
Emulsion Y-H	999.00 $\pm$ 0.02	94.5 $\pm$ 8.00	399	2.5 $\times$ 10 <sup>5</sup>

\* Viscosity of the phases was determined using a stress-controlled rheometer AR1500ex (TA Instruments, New Castle, USA) within the shear rate from 0 to 1000 s<sup>-1</sup>. Density of the phases was measured using a digital densimeter (DMA 4200M, Anton Paar, Austria). All measurements were performed at 25 °C. Y= yeast; H=hexadecane.

The diagram relating the power number (Npo) and Reynolds number (Geankoplis, 1993) was used to obtain Npo of a straight impeller (similar to that used to produce our emulsions). Power number (Npo) was close to 3 over a wide range of Reynolds number, from water (close to the initial process condition) to the emulsion with the highest viscosity (produced with hexadecane and 7% w/v of yeast in the aqueous phase Y-H).

From that point, the power of the system was calculated using Equation 2 and, consequently, the energy density (De) (Table 1) from Equation 3 (Geankoplis, 1993).

$$Npo = \frac{P}{\rho N D^5} \quad (2)$$

where Npo is the power number, P is the power (J/s),  $\rho$  is the density of the fluid (kg/m<sup>3</sup>), N is the rotational speed (rpm) and, D is the diameter of the impeller (m).

$$De = \frac{P \times t}{V} \quad (3)$$

where P is the power (J/s), t is the duration of the process (s) and V is the volume of sample (m<sup>3</sup>). In our experiments, t was 30 min (1800 s) and V was 100 mL (10<sup>-4</sup> m<sup>3</sup>).

Therefore, we used this set of parameters (N=900 rpm; t=30 min; V=100 mL; D<sub>impeller</sub>=0.05m) in order to simulate the smallest value of energy density in the fermentation process (order of magnitude~10<sup>5</sup> J/m<sup>3</sup>).

- **Ultra Turrax:**

A different approach was applied to calculate energy density using Ultra Turrax, as it is not a mechanical impeller-based agitation. Therefore, we had to evaluate the actual power applied to the system. For this, the electric current that was supplied to the system was measured using a multimeter pliers. We measured the current when water or sunflower oil was stirred, as they were the least and most viscous systems in this process, respectively. Using Equation 4, the power of both the oil and the water system could be calculated (Table 2).

$$P = U \times I, \quad (4)$$

where P is the power (J/s), U is the voltage (U=220V), and I is the measured current (A).

Table 2. Angular velocity set on the equipment, measured current (I) and calculated power (W).

Angular velocity (rpm)	I <sub>water</sub> (A)	I <sub>sunfloweroil</sub> (A)	Power <sub>water</sub> (W)	Power <sub>sunfloweroil</sub> (W)
4,000	1.07	1.1	235.4	242
5,000	1.13	1.16	248.6	255.2
6,000	1.18	1.22	259.6	268.4
7,000	1.21	1.28	266.2	281.6
8,000	1.24	1.31	272.8	288.2
9,000	1.27	1.34	279.4	294.8
10,000	1.31	1.37	288.2	301.4
11,000	1.34	1.40	294.8	308.0
12,000	1.37	1.46	301.4	321.2
13,000	1.41	1.47	310.2	323.4
14,000	1.43	1.47	314.6	323.4
<b>15,000</b>	<b>1.46</b>	<b>1.48</b>	<b>321.2</b>	<b>325.6</b>
16,000	1.5	1.52	330	334.4

We applied an angular velocity of 15,000 rpm for 5 min and, therefore, the energy density (Equation 3) was:  $De_{\text{SunflowerOil}}=9.7 \times 10^8 \text{ J/m}^3$ ;  $De_{\text{water}}=9.6 \times 10^8 \text{ J/m}^3$ .

Thus, we used this set of parameters (N=15,000 rpm; t=5 min; V=100 mL) in order to simulate the greatest value of energy density in the fermentation process (order of magnitude of  $10^8 \text{ J/m}^3$ ).

### **Supplementary Information (SI-2):**

The shear rate used to determine the rheological properties of emulsions was chosen according to typical values found in biotechnological processes (based on the angular velocity between 250 and 400 rpm (Srivastava et al., 2019; Chisti and Jauregui-Haza, 2002)).

In a typical agitation-based process, the shear rate is defined from Equation 5 (Metzner and Otto, 1957):

$$\dot{\gamma} = K_s \times N_i \quad (5)$$

where  $N_i$  is the shaft angular velocity (rps) and  $K_s$  is a non-dimensional constant dependent on the impeller type. We assumed  $N=350 \text{ rpm}$  ( $\sim 5.8 \text{ rps}$ ) (Srivastava et al., 2019; Chisti and Jauregui-Haza, 2002) and  $k \sim 13$  (Wu et al., 2006) to calculate shear rate, which was  $\dot{\gamma} \sim 75 \text{ s}^{-1}$ .

### **References**

- A.B. Metzner, R.E. Otto, Agitation of non-Newtonian fluids, *AIChE J.* 3 (1957) 3-10.  
J. Wu, L.J. Graham, N.N. Mehidi, Estimation of Agitator Flow Shear Rate, *AIChE J.* 52 (2006) 2323-2332.  
N. Srivastava, M. Srivastava, P.K. Mishra, P.W. Ramteke, R.L. Singh, *New and Future Developments in Microbial Biotechnology and Bioengineering: From Cellulose to Cellulase: Strategies to Improve Biofuel Production*, Elsevier (2019), chapter 6.  
Y. Chisti, U.J. Jauregui-Haza, Oxygen transfer and mixing in mechanically agitated airlift bioreactors, *Biochem. Eng. J.* 10 (2002) 143–153.

- H. Karbstein, H. Schubert, Developments in the continuous mechanical production of oil-in-water macro-emulsions, *Chem. Eng. Process* 34 (1995) 205-211.
- Y. Chisti, U.J. Jauregui-Haza, Oxygen transfer and mixing in mechanically agitated airlift bioreactors, *Biochem. Eng. J.* 10 (2002) 143–153.
- R.A. Sheikh, O.A. Al-Bar, Y.M.A. Soliman, Biochemical studies on the production of biofuel (bioethanol) from potato peels wastes by *Saccharomyces cerevisiae*: effects of fermentation periods and nitrogen source concentration, *Biotechnol. Biotechnol. Equip.* 30 (2016) 497-505.
- C.J. Geankoplis, *Transport processes and Unit operations*, Prentice-Hall, Englewood Cliffs, New Jersey. (1993), third edition.

### **CAPÍTULO 3**

#### **Microfluidic tools to observe (de)stabilization mechanisms of water-in-oil emulsions**

Artigo a ser submetido no periódico “Microfluidics and Nanofluidics”: Santos, T. P., Cunha, R. L. Microfluidic tools to observe (de)stabilization mechanisms of water-in-oil emulsions.

## Microfluidic tools to observe (de)stabilization mechanisms of water-in-oil emulsions

Tatiana Porto Santos<sup>a</sup>, Rosiane Lopes Cunha<sup>a\*</sup>

<sup>a</sup>Department of Food Engineering and Technology, School of Food Engineering, University of Campinas (UNICAMP), 13083-862 – Campinas, SP, Brazil

\*Corresponding author: rosiane@unicamp.br; tatiana.porto90@gmail.com (Tatiana P. Santos)

### ABSTRACT

Although emulsions can have different physical properties depending on the composition, the kinetic stability of these colloidal systems is usually the most relevant for technological applications. In this light, microfluidics emerges as a remarkable and cost-effective technique that allows not only the production of emulsions with monodisperse droplet size distribution, but also the systematic observation of their stability from the real-time visualization. Therewith, this technology can be useful in choosing the composition of emulsions, improving and expanding their application. Nonetheless, some care should be taken to define the properties of microfluidic devices to form droplets and determine their stability. As a proof of concept, we produced water-in-oil (W/O) emulsions composed by different continuous phases (hexadecane or sunflower oil combined with PGPR or Span 80) in a T-junction of *glass-* or *PDMS-* based microfluidic devices. Afterwards, emulsions were exposed to an expansion (triangle-like) chamber to observe the droplets and correlate the data obtained with emulsions stability. The nature of the fluids, interfacial features, flow conditions and channel surfaces were evaluated and correlations between these properties and droplets formation/coalescence were established. Droplets size decreased mainly due to the increase in the viscosity of the continuous phase, which is related to the higher shear stress favoring droplets detachment. However, the channel surface was the main driver inducing droplets production. Regarding the observation of coalescence, albeit the flow rate of the phases was very relevant to promote the encounter of the droplets, oil composition and surfactant nature as well as their potential affinity with channel surface also affected the fusion of the droplets. Such results indicate that different microchips can be used to produce and evaluate the stability of W/O emulsions, but an adequate microfluidic strategy must be designed depending on the properties of the emulsion phases. Ultimately, microfluidic devices can be considered as a window of opportunity to define the most appropriate composition of emulsions, considering the complexity of their (de)stabilization mechanisms.

**Keywords:** microdevice, fusion, destabilization, emulsions, passive strategies.

## 1. Introduction

Water-in-oil (W/O) emulsions are present in several food, pharmaceutical and cosmetic products. Although most of these emulsions are in solid or semi-solid state and are stabilized by a three-dimensional network (McClements, 2005), there is also a range of fluid emulsions that have low stability (Ushikubo and Cunha, 2014). Such low stability is due to the fact that droplets stabilization is triggered only by steric forces and also to the inherent high mobility of water droplets (Claesson et al., 2004; Ushikubo and Cunha, 2014). Hence, these properties can induce different phenomena related to emulsions destabilization such as sedimentation, flocculation and mainly coalescence.

In this sense, the stability of W/O emulsions could be eventually improved if a better understanding of their features and the interactions between water, oil and surfactants was achieved (Ushikubo and Cunha, 2014), especially since the choice of the emulsion composition is substantial to obtain stability. The properties of the oil phase such as density, interfacial tension with the aqueous phase, polarity and viscosity exert influence on emulsions stability. Furthermore, the behavior of emulsifiers is extremely relevant in modifying the stabilizing capacity of the colloidal structure. In general, emulsifiers that exhibit oil solubility and low hydrophilic-lipophilic balance (HLB) are applied in W/O emulsions. In this vein, two non-ionic emulsifiers can be highlighted for the stabilization of W/O emulsions: polyglycerol polyricinoleate (PGPR) and sorbitan monooleate (Span 80). PGPR is typically generated by the esterification of polymerized glycerol and castor oil fatty acids, while Span 80 is derived from a reaction between sorbitol and fatty acids (Cottrel and van Peij, 2006; Gulseren and Corredig, 2012; Tadros, 2008; Weyland and Hartel, 2008; Wilson et al., 1998). Nevertheless, the choice of these surfactants and their appropriate concentration are quite difficult to be established, implying numerous trials to determine the most suitable condition (Politova et al., 2017).

Generally, assessing emulsion stability to ensure adequate quality criteria is based on the droplet size distribution combined with gravitational methods (e.g. visual observation and/or turbidity measurements) (McClements, 2007). However, these techniques do not provide means to explain some phenomena such as phase inversion and re-coalescence (Baret et al., 2009; Bremond et al., 2008). In addition, these techniques do not allow the evaluation of emulsions during the development of droplets and, especially, the high-throughput screening under different conditions. In this context, emulsification can be evaluated instantly within microfluidic devices right after droplets production, providing information about droplets behavior in the early stages of emulsification, which ultimately determines droplets final size (Zhou et al., 2016). Moreover, studies during dynamic flow in microchannels are more



appropriate for this assessment than a static process, because droplets collide in conventional processes of emulsion formation. Not only that, microfluidic-based analyses can also be applied after droplet interfacial stabilization to evaluate emulsion stability over time. Therefore, in view of their outstanding characteristics, microfluidic devices can be an interesting tool to study (d)emulsification mechanisms in order to choose an improved composition depending on the emulsion final application. Notwithstanding, the conditions for droplets formation and determination of stability within microfluidic devices must be carefully chosen since not only emulsion properties are responsible for these phenomena, but also the characteristics of the channels (such as geometry and wall surface wettability). Finally, the assessment of droplet coalescence is typically performed using an abrupt expansion of the channel (Baret et al., 2009; Krebs et al., 2012b) that induces a less-controlled destabilization of the droplets. Herein, we applied another type of expansion chamber that consists in a triangle-like geometry. Such geometry was tested in order to allow a gradual decrease of the droplet velocity and thus, the better visualization of the coalescence phenomenon.

Given the above, this study aimed to understand the formation and stability of water droplets by applying a T-junction geometry coupled to an expansion triangle-like chamber presenting different surface properties. As aforementioned, such a chamber was implemented in order to induce a reduction of droplets velocity and a consequent collision between them. Phases of emulsions were characterized (viscosity, density and interfacial properties) for a better evaluation of the colloidal systems. These data were correlated with the droplets formation and mainly with their coalescence using the well-known Capillary number. Finally, we demonstrate alternatives to modulate the stabilization of emulsions, mainly by incorporating different surfactants and aqueous/oily phases, but also emphasizing the relevance of choosing an appropriate channel (design and surface wettability).

## **2. Material and methods**

### **2.1. Material**

#### *2.1.1 Microfluidic devices (PDMS- and glass- based)*

Microfluidic devices were produced using glass slides (Perfecta, Brazil) and poly(dimethylsiloxane) (PDMS) (Dow Corning, USA). PDMS was prepared by mixing Sylgard 184 silicon elastomer base and curing agent at the ratio of 10:1 (w/w), respectively.

### 2.1.2 Emulsions

N-hexadecane (Sigma-Aldrich, USA) or sunflower oil (Bunge Alimentos, Brazil) was used to prepare the continuous phase. Sunflower oil had a main fatty acid composition of 44.67 % oleic acid (C18:1), 43.71 % linoleic acid (C18:2), 5.76 % palmitic acid (C16:0) and 3.57 % stearic acid (C18:0). Sorbitan monooleate (Span 80, Sigma Aldrich) and polyglycerol polyricinoleate (PGPR, Danisco) were selected as the surfactants to produce the W/O emulsions. Physical properties of the oily phases and interfacial tension between the different oily and aqueous phases are presented in Table 1. Density was measured with a pycnometer previously calibrated with deionized water, whilst viscosity was obtained using a stress-controlled rheometer AR1500ex (TA Instruments, New Castle, USA). Flow curves were evaluated within the shear rate from 0 to 1000 s<sup>-1</sup> and viscosity was obtained. All oily phases presented Newtonian behavior. The interfacial tension was carried out by the pendant droplet method with a Tracker-S tensiometer (Teclis, France). Finally, the contact angle between the different oily phases and surfaces of the channels (PDMS or glass) was performed by the sessile drop goniometric method (Table 2) with the same tensiometer. All measurements were carried out at 25 °C. Surfactants concentration was chosen based on the contact angle with the PDMS surface, aiming to achieve the same value of contact angle for a direct comparison related to their “affinity” with the surface.

Table 1. Viscosity ( $\eta$ ) and density ( $\rho$ ) of different oily phases. Interfacial tension ( $\gamma$ ) of oily phase-water interfaces.

Oily phase	$\eta_{oil}$ (mPa.s)	$\rho_{oil}$ (kg/m <sup>3</sup> )	$\gamma$ (mN/m)
Hexadecane (H)	3.31 ± 0.02	766.6 ± 0.3	49.89 ± 0.42
Sunflower oil (S)	55.02 ± 0.00	915.9 ± 0.3	26.57 ± 2.02
Sunflower oil + Span 80 (0.1 % w/w) (S_Span)	55.85 ± 0.00	916.0 ± 0.1	17.65 ± 0.33
Sunflower oil + PGPR (1 % w/w) (S_PGPR)	61.26 ± 0.00	915.8 ± 0.4	4.76 ± 0.20

Table 2. Contact angle (°) between oily phases and PDMS-based surfaces.

Oily phase	Contact angle (°)*
Hexadecane	26.71 ± 0.66
Sunflower oil	61.91 ± 1.70
Sunflower oil + Span 80 (0.1 % w/w)	50.70 ± 2.75
Sunflower oil + PGPR (1 % w/w)	50.20 ± 4.13
Sunflower oil + PGPR (0.1 % w/w)	57.08 ± 0.81

\* The contact angle with the glass slides was not measured due to the oil sliding on the surface.

## 2.2. Methods

### 2.2.1 Microfluidic devices fabrication (PDMS-based)

Firstly, the microfluidic device (Figure 1A) was designed using AutoCAD 2012 software (Autodesk Inc., San Rafael, CA, USA) and plotted in photomasks (high resolution). PDMS chips were then manufactured using the soft lithography technique at Brazilian Center for Research in Energy and Materials (CNPEM, Campinas, Brazil). The microfluidic molds were produced using a SU-8 photoresist-coated silicon wafer, where the design of the photomasks was transferred using a mask aligner model MJB-3 UV300 (KarlSuss, Garching, Germany). After mold production, the casting of PDMS was performed and the produced PDMS channels were sealed on glass slides using oxygen plasma (PLAB SE80, Plasma Technology, Wrington, England) at 100 W and 70 mTorr ( $\sim 9.3$  Pa) for 20 seconds. Thus, the channel was constituted of three PDMS surfaces and one glass surface, presenting 50  $\mu\text{m}$  of depth and 100  $\mu\text{m}$  of width.

### 2.2.2 Microfluidic devices fabrication (glass-based)

After microchannel design (Figure 1B) and photomasks production (as in PDMS-based devices), glass slides were metallized with chrome followed by the application of an adhesion promoter (HMDS hexamethyldisilozane) and the photoresist (AZ-4620 Clariant) on their surfaces. Then, standard photolithography was applied to transfer the geometry of the mask to the photoresist using a mask aligner model MJB-3 UV300 (KarlSuss, Garching, Germany). Revelation was then performed with AZ 400K (Clariant) and corrosion of chrome with ETCH1 (Chromium mask etchant) (Technic, France) was initiated. The corrosion of glass was accomplished with a solution composed of  $\text{HF}:\text{NH}_4\text{F}:\text{HCl}$  (hydrofluoric acid: ammonium fluoride: hydrochloric acid) in the ratio of 1:41:1 v / v / v, respectively (HF 49 %, 1.38 M  $\text{NH}_4\text{F}$  and 38 % HCl) by exposing the slides for 6 minutes under magnetic stirring. Finally, the slides were treated with HF 20 % v/v solution during the same time and conditions. Simultaneously, PDMS was prepared at 100 °C for 50 minutes. Glass and PDMS were sealed using oxygen plasma at 100 W and 70 mTorr ( $\sim 9.3$  Pa) for 20 seconds. Thus, the channel was formed of three surfaces of glass and one surface of PDMS. Glass-based devices presented a higher space between the channels in the serpentine region due to the process of corrosion that is not precisely controlled (Figure 1). Therefore, the serpentine was designed with a higher space between them, but their total length and thus the dimension of channel before the chamber was the same, which means that the adsorption time was not changed comparing PDMS- and glass-

based devices. The width and depth of glass-based channels were around 150  $\mu\text{m}$  and 45  $\mu\text{m}$ , respectively, although being designed with 100  $\mu\text{m}$  of width.

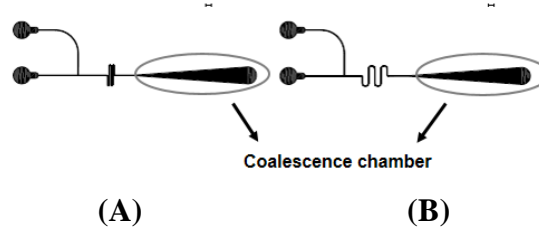


Figure 1. Design of (A) *PDMS*- and (B) *glass*- based microchips. Scale bar: 1000  $\mu\text{m}$ .

### 2.2.3 Emulsion production in microchannels

Sunflower oil, hexadecane or sunflower oil with the addition of surfactants (0.1 % w/w Span 80 or 1 % w/w PGPR) was used to compose the oily phase. Aqueous (deionized water) and oily phases were fed to the microfluidic chips using two syringe pumps (PHD22/2000, Harvard Apparatus, USA). During the injection, water droplets were formed after contact with the oily phase, passing through a serpentine to increase the adsorption time and establish the formation of a more stable interface. Droplets formation and coalescence were observed using a Multizoom AZ100 optical microscope (Nikon, Japan). Images and videos were recorded by a DS-Ri1 camera (Nikon, Japan) and analyzed using the NIS-Elements Documentation software (Nikon, Japan). Spherical and individual droplets were observed and their diameter values (named “initial diameter”) were evaluated immediately after entering the triangle-like chamber (before collisions). Moreover, the coefficient of variation (CV) was calculated to analyze droplets polydispersity (Equation 1) as the ratio between the standard deviation (SD) of the diameter values and the mean droplet diameter.

$$CV (\%) = \frac{SD}{mean\ diameter} \times 100 \quad \text{Equation 1}$$

The flow rates of the continuous ( $Q_c$ ) and dispersed ( $Q_d$ ) phases applied to produce the droplets were 2, 3 or 4  $\mu\text{L}/\text{min}$  and 0.5, 0.7, 1 or 2  $\mu\text{L}/\text{min}$ , respectively. Flow rate ratio ( $q$ ) (Equation 2), viscosity ratio between continuous ( $\eta_c$ ) and dispersed ( $\eta_d$ ) phases ( $\lambda$ ) (Equation 3) and Capillary number (Equation 4) were correlated with the results obtained under different process conditions. Furthermore, the Capillary number ( $Ca$ ) was also used to judiciously describe droplets generation and coalescence. This dimensionless number represents the

relationship between viscous and interfacial forces, having been calculated based on the properties of the phase with the highest viscosity (continuous phase) (Ushikubo et al., 2014).

$$q = \frac{Qc}{Qd} \quad \text{Equation 2}$$

$$\lambda = \frac{\eta c}{\eta d} \quad \text{Equation 3}$$

$$Ca_c = \frac{\eta_c U_c}{\gamma} \quad \text{Equation 4}$$

where Q is the flow rate and  $\eta$  is the viscosity (the subscript “c” indicates the continuous phase, while “d” refers to the dispersed phase).  $\gamma$  is the interfacial tension between the oily phase and water and  $U_c$  is the velocity of the continuous phase calculated considering the average flow rate of the continuous phase and the cross-sectional area of the channels (width and depth).

#### 2.2.4 Emulsion coalescence in microchannels

Emulsion coalescence within the microchannels was evaluated in two sections named initial and final. The first (initial) section corresponded from the chamber entrance to the length of 600  $\mu\text{m}$ , while the second (final) section was between 600 and 1000  $\mu\text{m}$ . To obtain the number of coalescence events (Equation 5) (Muijlwijk et al., 2017), the initial area of a hundred droplets ( $A_i$ ) was calculated based on the initial diameter of the droplets described in Section 2.2.3 ( $A_i = \pi(\text{diameter})^2/4$ ). Then, the average area of the initial droplets ( $A_{i-av}$ ) was obtained considering the same composition and flow conditions. The final area ( $A_f$ ) of a hundred droplets (regardless of their morphology and size) after (potential) coalescence was calculated for each condition using the software NIS-Elements Documentation (Nikon, Japan). Thus, for each final area a different number of coalescence events ( $N_{\text{coalescence}}$ ) was measured. Then, results were converted into a percentage (%) of droplets that presented a specific  $N_{\text{coalescence}}$ .

$$N_{\text{coalescence}} = \frac{A_f}{A_{i-av}} - 1 \quad \text{Equation 5}$$

### 3. Results and discussion

#### 3.1. Droplets generation

Mean diameter and CV of the droplets formed at a T-junction within either a PDMS- or a glass- based microchannel are shown in Figure 2 and Table 3, respectively. Process conditions and emulsion composition are discussed separately to better elucidate their influence on droplets generation.

##### *3.1.1 Effect of the oily phase on droplets size (fixed condition: PDMS-based channels)*

Mean diameter of droplets produced with different oily phases is shown in Figure 2. Smaller values of diameter were obtained in systems containing sunflower oil (70-154  $\mu\text{m}$ ) compared to hexadecane (107-184  $\mu\text{m}$ ). However, polydispersity (evaluated by CV) did not seem to be affected by the nature of the oil. Both sunflower oil and hexadecane exhibited Newtonian fluid behavior, but the former had a much higher viscosity ( $\eta \sim 55 \text{ mPa.s}$  -  $\lambda \sim 55$ ) compared to hexadecane ( $\eta \sim 3 \text{ mPa.s}$  -  $\lambda \sim 3$ ). Furthermore, the sunflower oil-water interface exhibited a lower initial tension ( $\gamma \sim 26 \text{ mN/m}$ ) than the hexadecane-water interface ( $\gamma \sim 50 \text{ mN/m}$ ). As a matter of fact, a higher viscosity ratio ( $\lambda$ ) indicates a more pronounced shear stress, allowing for easier droplets detachment (Ushikubo et al., 2014), while a reduction in interfacial tension between phases promotes easier droplets generation, since it is associated with the decrease in the energy needed to form/break the droplets in the continuous phase (Gulseren and Corredig, 2013; McClements, 2005). Therewith, sunflower oil properties may have implied in the improvement of droplets formation, generating droplets with smaller sizes.

Faced with such a scenario, the effect of viscosity and interfacial tension on emulsions formation in microfluidic systems is generally assessed by means of the Capillary number (Figure 2). This dimensionless number represents the balance between two opposing forces that govern droplets generation: viscous and interfacial (Steggmans et al., 2009). High viscous forces related to friction enable droplets breakage (implying a higher Capillary number), whilst high interfacial forces can hinder their formation (which leads to a decrease in the Capillary number). Therefore, the interfacial tension must be the minimum possible for droplets generation, otherwise, if the interfacial tension is high, droplets breakup could not occur. Hence, the balance between these two forces is necessary for droplets generation and further stabilization within the devices. Despite this, the reduction of interfacial tension (increase of Ca number), triggered by the addition of surfactants, had little effect on the diameter of droplets in systems with a higher  $\lambda$  (sunflower oil). This result can be explained by

the fact that the viscous forces are prevailing over the interfacial forces, which means that the effect of the latter could be considered negligible in these cases (Garstecki, 2010; Ushikubo et al., 2014). On the other hand, due to the low viscosity and high interfacial tension with water provided by hexadecane, the Capillary number was very low for this system (ranging between 0.0004 and 0.0009) (Figure 2).

Apart from these intrinsic properties of the oily phases (viscosity and interfacial tension), the process can also be modulated to improve and even increase the throughput of droplets production, which will be discussed in the next topic (3.1.2).

### *3.1.2 Effect of the flow rate ratio ( $q$ ) on droplets size (fixed condition: PDMS-based channels)*

As observed in the numerator of the Capillary number equation (that encompasses  $U_c$ ), a  $Q_c$  greater than  $Q_d$  (or  $>q$ ) would provide more shear between the emulsion phases (Equation 4), inducing the formation of smaller droplets (Ushikubo et al., 2014). The increase of  $Q_c$ , however, presented a limit within the (expansion) chamber-like devices, since the continuous phase either invaded the inlet channel of the dispersed phase or increased the backpressure phenomenon. Such backflow may be mainly associated with an increase of area in the chamber region, reducing droplets velocity. Despite the limitation of flow conditions, droplets were in general formed, even in systems presenting higher interfacial tension (e.g. pure oil and water) that typically require additional energy for the formation of droplets (Abedi et al., 2019). One can assume that this energy was provided by both emulsion phases (viscosity and interfacial features) and process conditions (channel properties and flow rates) regardless of the emulsion system.

Overall, the effect of operating flow conditions for most systems ( $S$ ,  $H$  and  $S\_Span$ ) (Figure 2) was reflected by the flow rate ratio ( $q$ ). In general, flow rate ratio close to 1 ( $Q_c \sim Q_d$ ) produced droplets with higher diameter values, whilst the increased difference between  $Q_c$  and  $Q_d$  ( $>q$ ) allowed the formation of smaller droplets (Figure 2). As aforementioned, a higher flow rate ratio improves the shearing process and droplets breakup. However, the addition of 1 % (w/w) PGPR to the oily phase reduced the influence of the flow rate ratio ( $q$ ) on droplets size. Indeed, regardless of the applied  $Q_d$  (over a fixed  $Q_c$ ), droplets showed almost the same diameter values in PGPR-based systems (Figure 2). This could be explained based on the fast surfactant adsorption on the water-oil interface (proved by initial interfacial tension values in Table 1) that unleashes a reduction of interfacial forces, allowing easy droplet development and minimizing the effect of the flow rate ratio.

### *3.1.3 Effect of microchannels surface on droplets size (PDMS- versus glass- based channels)*

Since the objective of this study was to analyze not only the emulsion production, but also the behavior of the droplets under collision (and potential coalescence), specific flow rates had to be defined to induce droplets encounter (Mazutis and Griffiths, 2012; Shen et al., 2015). Such head-on encounter is required because the fusion of droplets within microfluidic devices is based on previous important steps - droplets contact, interfacial film drainage and film rupture (Gunes et al., 2010; Tadros and Vicent, 1983).

In general, in PDMS-based channels, a higher flow rate of the continuous phase ( $Q_c = 4 \mu\text{L}/\text{min}$ ) allowed a faster displacement of the droplets throughout the chamber, almost hindering the clash among them. In contrast, lower flow rate values ( $Q_c = 2 \mu\text{L}/\text{min}$ ) favored droplets contact, but in some cases the collision did not seem to be enough to remove the fluid between them, hampering droplets merge. Therefore, among the results exposed in Figure 2,  $Q_c = 3 \mu\text{L}/\text{min}$  and  $Q_d = 0.7 \mu\text{L}/\text{min}$  were chosen to analyze the coalescence, especially since this condition enabled the droplets to have sufficient contact that could potentially allow droplets fusion. Due to such a scenario, these same flow rates were applied to perform the experiments using glass-based channels, in order to compare the effect of different surfaces. In this sense, Table 3 shows the diameter values of droplets formed within glass-based microchannels (S\_PGPR and S\_Span). S\_PGPR and S\_Span systems were chosen to compare the different surfaces, since these emulsions were easily developed in glass-based devices. Overall, the droplets generated in glass-based microchannels showed diameter values greater than channel width ( $>150 \mu\text{m}$ ) (Table 3), while in the PDMS-based counterpart, the droplets were formed with diameter values smaller than microchannel width dimension ( $<100 \mu\text{m}$ ) (Figure 2).

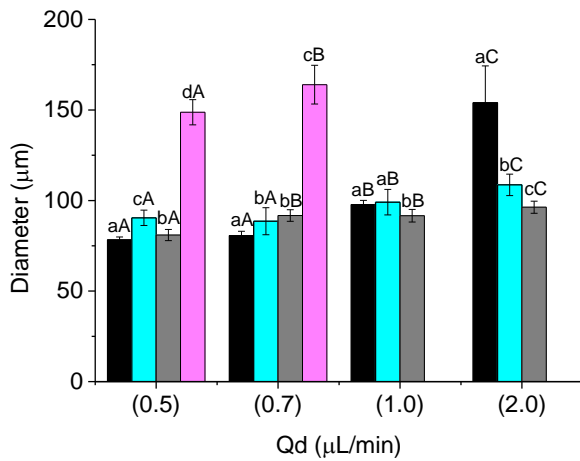
Such results may be associated not only with the channel dimensions, influencing the motion of the droplets inside the microfluidic devices, but also with the differences in their surface wettability. The latter can be inferred especially considering that the continuous phase of the emulsions was oil-based, showing greater affinity with hydrophobic surfaces (PDMS) that would facilitate the generation of water droplets. In addition, during the experimental analysis of the contact angle, it was observed that the different oils presented a pronounced slippage on the surface of the glass slides, which could also decrease the shearing induction. Another important outcome supporting the role of the channels surface in droplets production is that the glass-based devices did not allow the production of emulsions with hexadecane. Instead, a double layer of fluids and pronounced instabilities were observed, which can be



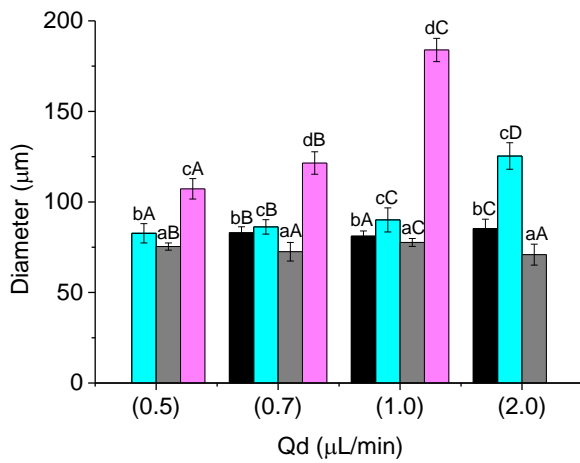
associated not only with the low shear and high interfacial tension provided by this oil, but also with the surface properties. Therefore, it is clear that surface nature is partly responsible for droplets production.

Table 3. Droplets diameter, coefficient of variation (CV) and Capillary number (Ca) of droplets generated in a *glass-based* microfluidic chip using sunflower oil with Span 80 (S\_Span) or sunflower oil with PGPR (S\_PGPR) as continuous phase.

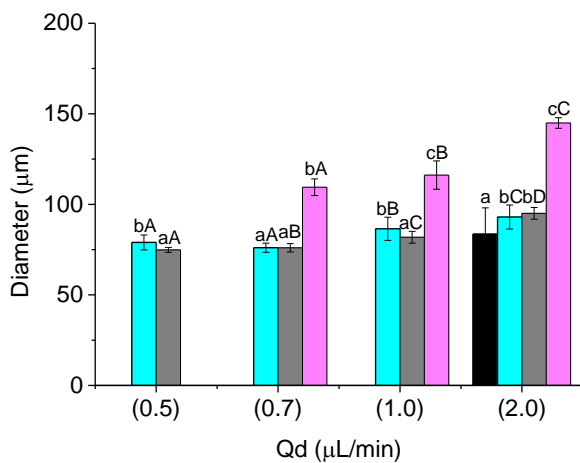
	Qc ( $\mu\text{L}/\text{min}$ )	Qd ( $\mu\text{L}/\text{min}$ )	q (-)	Diameter ( $\mu\text{m}$ )	CV (%)	Ca (-)
S_Span_Glass	3	0.7	4.3	$153.45 \pm 7.39$	4.82	0.0235
S_PGPR_Glass	3	0.7	4.3	$159.08 \pm 5.73$	3.61	0.0953



(A)



(B)



(C)

Figure 2. Diameter, coefficient of variation (CV) and Capillary number of droplets generated in a PDMS-based microchannel at (A)  $Q_c = 2 \mu\text{L/min}$ , (B)  $Q_c = 3 \mu\text{L/min}$  and (C)  $Q_c = 4 \mu\text{L/min}$  using different continuous phases: (■) S, (■) S\_Span, (■) S\_PGPR and (■) H. Different letters indicate a significant difference at  $p < 0.05$ . Lowercase letters are related to comparison between different systems at the same  $Q_d$ , while capital letters are related to the effect of different  $Q_d$  in the same emulsion.

CV (%)					
Qd (μL/min)	q	S	S_Span	S_PGPR	H
0.5	4.0	2.04	4.69	3.83	4.68
0.7	2.9	2.90	8.43	3.50	6.51
1.0	2.0	2.38	7.14	3.80	*
2.0	1.0	13.18	5.44	3.50	*

\* Not possible to be evaluated – backflow/invasion of the dispersed phase; q = flow rate ratio.

Capillary number			
S	S_Span	S_PGPR	H
0.0138	0.0211	0.0857	0.0004

CV (%)					
Qd (μL/min)	q	S	S_Span	S_PGPR	H
0.5	6.0	*	6.44	2.62	5.26
0.7	4.3	3.99	4.62	7.07	5.11
1.0	3.0	3.52	7.36	2.81	3.50
2.0	1.5	6.17	5.84	8.12	*

\* Not possible to be evaluated – backflow/invasion of the dispersed phase; q = flow rate ratio.

Capillary number			
S	S_Span	S_PGPR	H
0.0207	0.0317	0.1286	0.0007

CV (%)					
Qd (μL/min)	q	S	S_Span	S_PGPR	H
0.5	8.0	*	5.22	1.81	*
0.7	5.7	*	3.32	3.02	4.21
1.0	4.0	*	7.42	3.98	6.73
2.0	2.0	17.38	7.11	3.41	2.02

\* Not possible to be evaluated – backflow/invasion of the dispersed phase; q = flow rate ratio.

Capillary number			
S	S_Span	S_PGPR	H
0.0276	0.0422	0.1715	0.0009

### 3.2. Evaluation of droplets stability

Droplet coalescence was continuously observed in the triangle-like chamber (Figure 1) after emulsion production. As afore discussed in Section 3.1.3, the flow rates chosen for this experiment were  $Q_c = 3 \mu\text{L}/\text{min}$  and  $Q_d = 0.7 \mu\text{L}/\text{min}$ . However, to further justify such a choice, a brief discussion on the subject will be given, especially since the flow rate can directly affect coalescence within microfluidic devices (Muijwijk et al., 2017). Lower flow rates are supposed to increase both the residence time and contact time of colliding droplets, and if the collision time is longer than the time for film drainage, droplet fusion can potentially occur (Krebs et al., 2012a; Zhou et al., 2016). Nonetheless, as noted in this study, a very small flow rate of the continuous phase did not provide sufficient “force” to remove the oil phase between the droplets and, thus, no fusion could be observed. Therefore, flow rates must be balanced in order to induce droplets coalescence within the microfluidic chamber.

#### *3.2.1 Effect of Capillary number (fixed condition: PDMS-based channels) and correlation with Stokes Law*

The effect of the Capillary number on droplets fusion was evaluated by comparing three different continuous phases: hexadecane (H), sunflower oil (S) and sunflower oil with PGPR (S\_PGPR). Figure 3 shows the number of coalescence events in two different sections of the channel (initial and final), as described in section 2.2.4. Figure 4, on the other hand, exhibits qualitative information comparing the different emulsions observed throughout the chamber. Such specific emulsions (H, S and S\_PGPR) were chosen because they did not seem to influence PDMS surface during destabilization (which will be discussed in section 3.2.2). In this sense, only the increase in the area that leads to the decrease in velocity was the operating condition considered here, since flow rates ( $Q_c$  and  $Q_d$ ) were kept constant. Due to these facts, Capillary number was mainly affected by the physicochemical properties of the phases (viscosity and interfacial tension).

Regarding sunflower oil based-system (S), the number of intact droplets was around 85 % in the initial section of the chamber, while the final section presented ~60 % of unfused droplets. Nevertheless, S\_PGPR system did not show signs of coalescence until the final section of the channel (100 % of unfused droplets) (Figure 3A-B) despite numerous collisions (Figure 4). Therefore, one can assume that the phenomenon of re-coalescence is not supposed to occur with this system. As previously described, S\_PGPR emulsion also had the largest Capillary number (0.1286) in relation to the other systems (H and S). This higher Capillary number is associated to both the highest viscosity of the oily phase and the lowest interfacial tension

compared to surfactant-free emulsions. Indeed, the highly-viscous continuous phase decreases droplets mobility, therefore, a longer contact time is usually necessary to drain the oil film (Gunes et al., 2013). In addition, the lower interfacial tension represents an improved steric barrier against droplets merge, which can also be corroborated by other studies that showed that the steric barrier between surfactant layers of two colliding droplets prevented coalescence (Baret et al., 2009). This assumption can also be confirmed by the fact that surfactant-free systems (S) easily reached coalescence. In addition to steric barriers, emulsions stabilized by surfactants also experience the Marangoni effect (Dai and Leal, 2008). Such phenomenon usually occurs simultaneously with the drainage process of the continuous phase placed between the droplets. During the drainage mechanism, the concentration of surfactants on the droplets surface is continuously changed, leading to gradients of surface tension. Consequently, the Marangoni convection is triggered from the border towards the center of the liquid film (between the droplets), which in turn reduces film drainage and hinders coalescence (Dai and Leal, 2008; Shen et al., 2015). In this sense, both the substances that increase the viscosity of the continuous phase and the components that are adsorbed on droplets surface can retard or even inhibit the process of droplets merge (Heeres et al., 2015).

On the other hand, hexadecane based-system showed a greater number of coalescence events at the beginning (6-10) and at the end ( $>21$ ) of the collision chamber. These results reflect that almost 80 % of the droplets did not merge in the initial process, although this number decreased to about 45 % at the end of the section (Figure 3A-B), representing the lowest amount of intact droplets. Such outcome can be related to the low value of Capillary number (reflected by hexadecane lower viscosity and higher interfacial tension), improving droplets merge. Moreover, it is clear that coalescence events also increased during the passage throughout the channel.

Although these experiments were carried out under dynamic flow conditions, a correlation between the Capillary number and static approaches contemplated by Stokes law (Equation 6) can be established. According to Stokes Law, the sedimentation of droplets in a W/O emulsion is directly related to the difference of density ( $\rho_{aq}-\rho_{oil}$ ) between the continuous and dispersed phases, as well as to the droplet diameter ( $d_d$ ). On the contrary, an increase in the viscosity ( $\eta$ ) of the continuous phase hinders separation of the droplets, providing resistance to coalescence (Heeres et al., 2015) or even a decrease of the sedimentation velocity ( $v_s$ ). In this sense, when stablishing a correlation between Stokes law and destabilization within microfluidic channels, some aspects can be pointed out. Regarding droplets formation, greater Capillary numbers (higher viscosity and lower initial interfacial tension) could provide the

production of smaller droplets ( $d_d$ ) (Figure 2) and, consequently, more stable colloidal systems. These emulsion droplets also separate gently (more slowly) according to Stokes law. Furthermore, the more unstable emulsion that presents the lowest Capillary number (hexadecane-based), in addition to its lower viscosity and higher interfacial tension with water, also presents a more pronounced density difference ( $\rho_{aq}-\rho_{oil}$ ), which also could increase the velocity of droplet sedimentation.

$$v_s = \frac{1}{18} \frac{(\rho_{aq} - \rho_{oil})}{\eta} g d_d^2$$

Equation 6

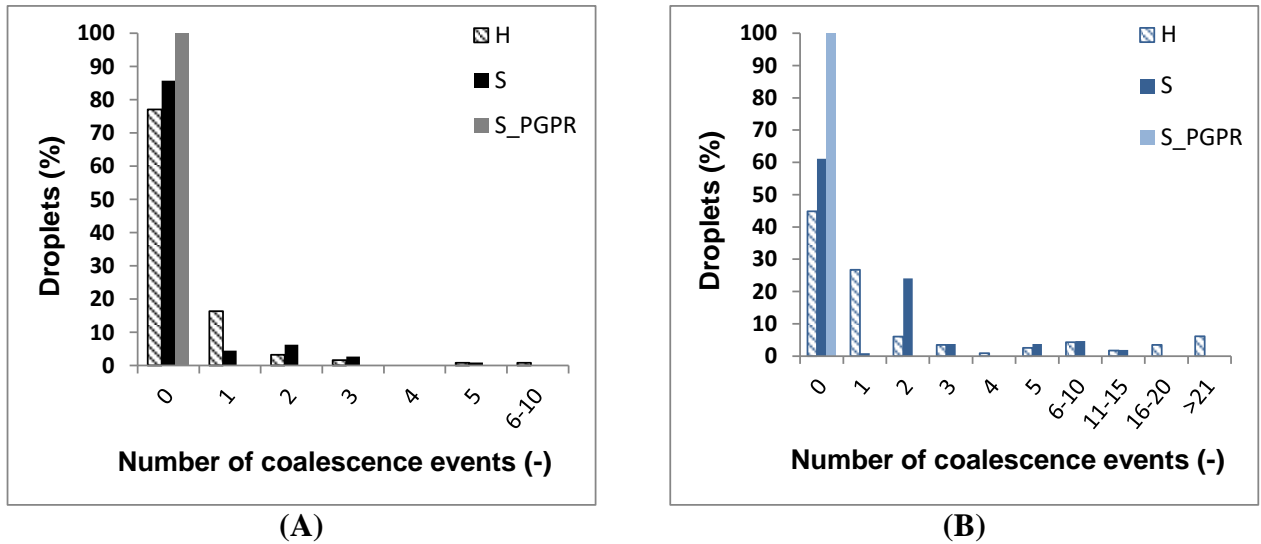


Figure 3. Number of coalescence events of water droplets using hexadecane (H), sunflower oil (S) or sunflower oil with PGPR (S\_PGPR) as continuous phase. (A) Initial (0-600 μm) and (B) final (600-1000 μm) sections of the chamber (*PDMS-based* channel).

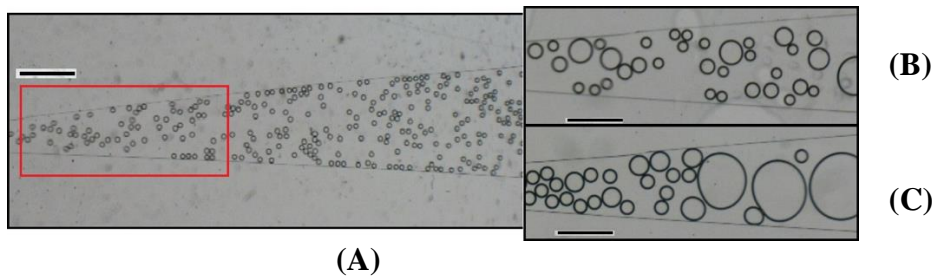


Figure 4. Microfluidic chamber of systems prepared with different continuous phases: (A) S\_PGPR, (B) S and (C) H. (*PDMS-based* channel). Scale bar denotes (A) 1000 μm and (B) (C) 500 μm.

### 3.2.2 Effect of the affinity of surfactants and PDMS surface (fixed condition: PDMS-based channels)

Emulsions containing different surfactants with sunflower oil (S, S\_PGPR and S\_Span) (and consequently different degree of stability) were studied to reveal the role of the affinity of surfactants and PDMS surface in modulating droplet coalescence. Figure 5A-B shows that in the presence of 0.1 % w/w of Span 80 (S\_Span) a greater number of coalescence events was observed, mainly in the final section of the chamber. Unexpectedly, the number of coalescence events was even greater than those of samples with no surfactant.

We assume that the increase in droplets merge in the S\_Span system occurred due to the adherence of water droplets to the surface of the PDMS channels (Figure 5C). In contrast, emulsions containing PGPR (Figure 4A) or surfactant-free droplets (Figure 4B) collided with the channel wall, but left the surface immediately. After the adhesion of the ‘Span\_80 systems’ droplets to the channel surface, they acquired a tendency to flow in a preferential path, which consequently decreased the flow area (but with the same flow rate), providing more collisions and coalescence between the droplets. Such adhesion of droplets containing Span 80 was a surprising outcome, which may have been unleashed due to a combination of mechanisms. Firstly, the (expansion) triangle-like geometry of the channel induced the emulsion droplets to flow towards the wall, which may have triggered the droplet adhesion in Span\_80 systems. Conversely, some studies that applied Span 80-stabilized emulsions in microfluidic channels showed that droplets did not adhere to the surface (Bremond et al., 2008; Bremond et al., 2011; Ushikubo et al., 2014), therefore, suggesting that such outcome may have a direct relationship not only with the emulsion composition (different oils and surfactant concentration) but also with the channel geometry. Secondly, once on the walls, shear stresses are induced by the non-slip boundary conditions (Kovalchuk et al., 2018) and, with the aid of Marangoni effect, they may have led to the rearrangement of surfactants on the droplets surface. These rearrangements can give surfactants the opportunity to attach preferentially to the PDMS surface rather than interact with the oil, depending on the triad “surfactant-oil-channel surface”. Of course, if there is an excess of surfactants, some molecules will likely interact with the channel walls while others will remain in contact with the oil, stabilizing the droplets (which do not adhere to the PDMS surface – *data not shown*). However, at low surfactant concentration, preferential interactions (with the PDMS surface or the oil) may dictate the occurrence of adhesion, as this phenomenon seems to be governed by the molecular affinity of the surfactant with the nonpolar molecule, mainly because the associated interactions are due to hydrophobic domains. This means that surfactant hydrophobic moieties may preferentially interact with either the oil or the

hydrophobic surface, depending on their greater chemical affinity (Ushikubo and Cunha, 2014). Such attachment on hydrophobic solid surfaces has also been observed with other components presenting surface properties (Nakanishi et al., 2001). Finally, it is extremely important to note that this attachment was observed only within a time interval after the beginning of the experiments. This means that after a while, the interactions seemed to disappear, which may be associated with the saturation of the channel wall surface with the surfactant molecules.

In order to prove this interaction, the contact angle between sunflower oil (pure or with surfactants) and a PDMS surface (Table 2) was evaluated, showing that both surfactants (PGPR and Span 80) decreased the measured value, which indicates that these components have affinity with the PDMS surface. However, by comparing the same concentration, Span 80 decreased the contact angle by 12°, while PGPR addition allowed a reduction of only 5°, indicating that Span 80 showed a more pronounced affinity with the PDMS surface and, therefore, a more hydrophobic character. Such outcome can be associated with the chemical composition of both surfactants, since Span 80 has a longer hydrocarbon chain length, as well as a heterocyclic ring. Another hypothesis is that the PGPR could have a higher molecular weight (since it can contain polymers with >1 molecule) (O'Brien, 2008), which can impair its physical approach to the PDMS surface. Therefore, these characteristics combined with the low concentration of surfactant (the attachment occurred only when the surfactant concentration was low or before the saturation of the PDMS surface) may have induced the preferential adhesion of Span 80-based droplets at the channel surface, mainly due to the more pronounced hydrophobic character of PDMS (Ushikubo and Cunha, 2014).

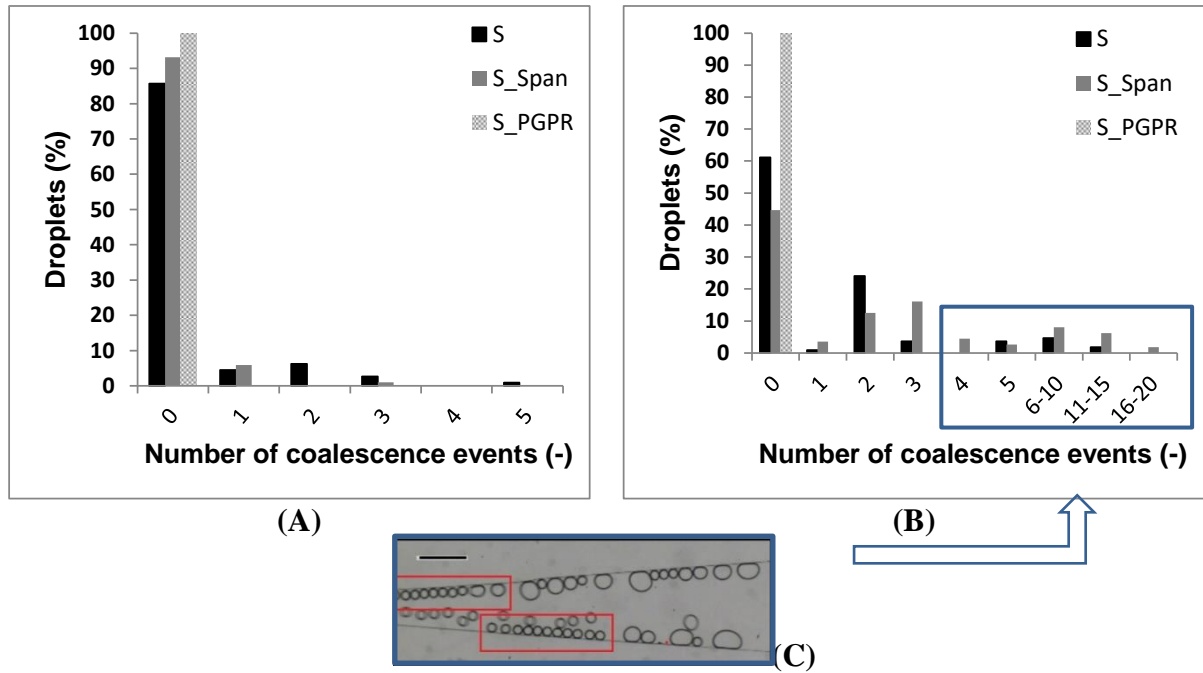


Figure 5. Number of coalescence events of water droplets using sunflower oil (S), sunflower oil with Span 80 (S\_Span) or sunflower oil with PGPR (S\_PGPR) as continuous phase. (A) Initial (0-600 μm) and (B) final (600-1000 μm) sections of the chamber. (C) Detail of the droplets at the PDMS surface in S\_Span system. (PDMS-based channel). Scale bar = 500 μm.

### 3.2.3 Effect of the different microchannel surfaces (PDMS- and glass- based channels)

In order to confirm the effect of the PDMS walls on the droplets stabilized by Span 80, glass-based channels were also applied to assess the destabilization of this emulsion. In addition to the reduction of coalescence events (Figure 6), the droplets did not adhere to the glass walls (detail in Figure 6), which means that only “natural” collisions were responsible for droplets fusion. However, as the droplets flowed in a straight line inside the microchannels, instead of flowing towards the walls, they could have attached to the only PDMS-based surface presented at the bottom of the microfluidic device.



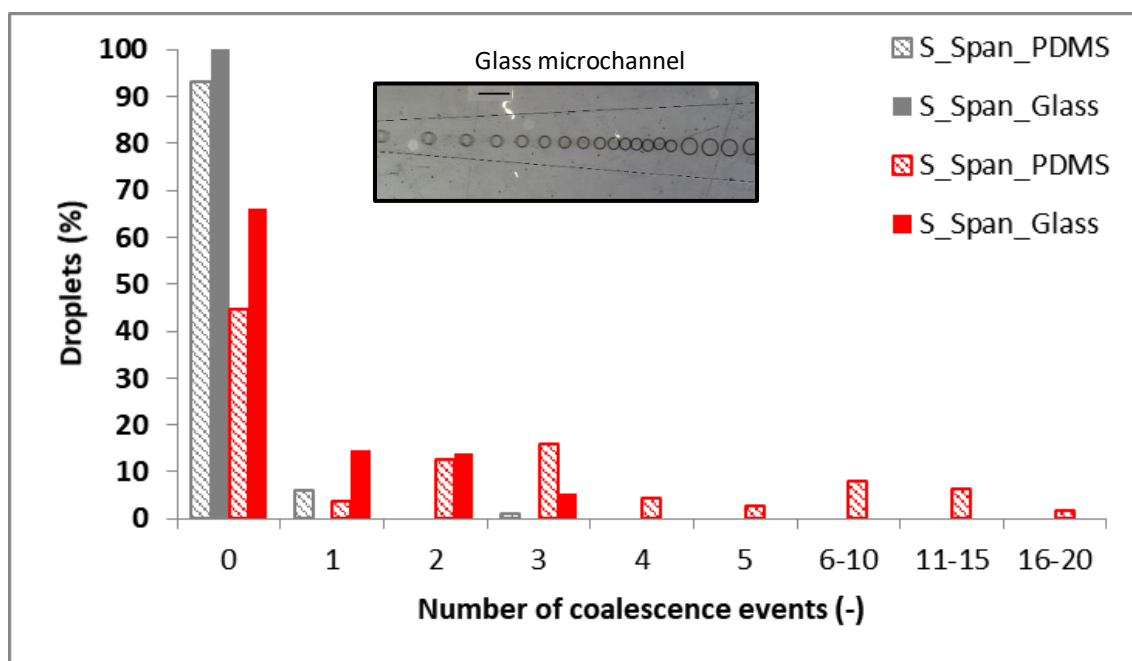


Figure 6. Number of coalescence events of water droplets using sunflower oil with Span 80 (S\_Span) as continuous phase. Initial (grey columns) and final (red columns) sections of the chamber. In detail: *S\_Span* system within *glass-based* microchips. Scale bar = 500  $\mu\text{m}$ .

## Conclusion

This work demonstrated that the de(stabilization) of droplets within microfluidic channels can be governed not only by the intrinsic features of the emulsions (such as oil viscosity and the presence/concentration of surfactants), but also by the process variables (e.g., channel design, surface properties and flow conditions). Overall, these characteristics can be associated using the Capillary number ( $Ca$ ), which represents the balance between viscous and interfacial forces. Regarding emulsion formation, the detachment of the droplets occurred more easily under a greater Capillary number dictated mainly by the high viscosity of the continuous phase, but also imposed by the reduction of the interfacial tension promoted by the surfactants. However, the shear stress induced by the channel surface has also been shown to play a considerable role in droplets generation. In the same vein, systems with higher  $Ca$  numbers presented a lower degree of coalescence due to the higher oil viscosity and lower tension at the oil-water interface. In fact, the surface of the channels was also responsible for destabilizing the droplets, especially in systems with a lower concentration of surfactants, although all surfactant-based systems (under the concentration applied in this study) showed a similar contact angle with solid PDMS. All things considered, it is clear that the choice of an appropriate microfluidic channel (geometry and wall material) is essential to improve droplet development. Not only that, a refined microfluidic device would also enable an efficient determination of emulsion stability,

allowing to understand the effect of the chosen composition on emulsion properties, susceptibility to re-coalescence and kinetic stability.

### Acknowledgements

This study was financed in part by the Coordenação de Aperfeiçoamento de Pessoal de Nível Superior – Brasil (CAPES) - Finance Code 001. Santos thanks grant #2017/18109-0, São Paulo Research Foundation (FAPESP) and Conselho Nacional de Desenvolvimento Científico e Tecnológico (CNPq, grant number 140700/2017-0) for the scholarship and Cunha thanks CNPq (307168/2016-6) for the productivity grant. The authors also thank grant numbers #2019/07744-1, #2011/06083-0 and #2004/08517-3 São Paulo Research Foundation (FAPESP) and CNPq (Universal Project 423960/2016-4). The authors also appreciate the assistance provided by Maria Helena de Oliveira Piazzeto and Angelo Gobbi of the Microfabrication Laboratory at the LNNano/CNPEM (Brazilian Center for Research in Energy and Materials).

### References

- Abedi, S., Suteria, N. S., Chen, C-C, Vanapalli, S. A. (2019). Microfluidic production of size-tunable hexadecane-in-water emulsion: Effect of droplet size on destabilization of two-dimensional emulsions due to partial coalescence. *Journal of Colloid and Interface Science*, 533, 59-70.
- Baret, J-C., Kleinschmidt, F., Harrak, A. E., Griffiths, A. D. (2009). Kinetics aspects of emulsion stabilization by surfactants: a microfluidic analysis. *Langmuir*, 25, 6088-6093.
- Bremond, N., Thiam, A. R., Bibette, J. (2008). Decompressing emulsion droplets favors coalescence. *Physical Review Letters*, 100, 024501-024501-4.
- Bremond, N., Doméjjean, H., Bibette, J. (2011). Propagation of drop coalescence in a two-dimensional emulsion: a route towards phase inversion. *Physical Review Letters*, 106, 214502-1-214502-4.
- Claesson, P. M., Blomberg, E., Poptoshev, E. (2004). Surfaces forces and emulsion stability. In S. E. Friberg, K. Larsson, J. Sjöblom (Eds.), *Food emulsions* (4th ed.). New York: Marcel Dekker, (chapter 7) (e-book version).
- Gulserrell, T., van Peij, J. (2006). Sorbitan esters and polysorbates. In R. J. Whitehurst (Ed.), *Emulsifiers in food technology* (pp. 162-185). Oxford: Blackwell Publishing.
- Dai, B., Leal L. G. (2008). The mechanism of surfactant effects on drop coalescence. *Physics of Fluid*, 20, 040802-1 – 040802-13.

- Garstecki, P. (2010). Formation of droplets and bubbles in microfluidic systems. In: Kakac, S., Kosoy B, Pramuanjaroenkij A (eds). *Microfluidics based microsystems: fundamentals and applications*. Springer, The Netherlands, pp 163–181.
- Gulseren, I. Corredig, M. (2012). Interactions at the interface between hydrophobic and hydrophilic emulsifiers: Polyglycerol polyricinoleate (PGPR) and milk proteins, studied by drop shape tensiometry. *Food Hydrocolloids*, 29, 193-198.
- Gulseren, I. Corredig, M. (2013). Interactions of chitin nanocrystals with lactoglobulin at the oil–water interface, studied by drop shape tensiometry. *Colloids and Surfaces B*, 111, 672–679.
- Gunes, D. Z., Clain, X., Breton, O., Mayor, G., Burbidge, A. S. (2010). Avalanches of coalescence events and local extensional flows – Stabilisation or destabilization due to surfactant. *Journal of Colloid and Interface Science*, 343, 79-86.
- Heeres, A. S., Schroën, K., Heijnen, J. J., van der Wielen, L. A. M., Cuellar, M. C. (2015). Fermentation broth components influence droplet coalescence and hinder advanced biofuel recovery during fermentation. *Biotechnology Journal*, 10, 1206-1215.
- Krebs, T., Schroen, K., Boom, R. (2012a). Coalescence dynamics of surfactant stabilized emulsions studied with microfluidics. *Soft Matter*, 8, 10650-10657.
- Krebs, T., Schroen, K., Boom, R. (2012b). A microfluidic method to study demulsification kinetics. *Lab on a chip*, 12, 1060-1070.
- Mazutis, L., Griffiths, A. D. (2012). Selective droplet coalescence using microfluidic systems. *Lab on a Chip*, 12, 1800–1806.
- McClements, D. J. (2005). *Food emulsions: principles, practices, and techniques* (2nd ed.). Boca Raton: CRC Press (e-book version).
- McClements, D. J. (2007). Critical review of techniques and methodologies for characterization of emulsion stability. *Critical Reviews in Food Science and Nutrition*, 47, 611-649.
- Muijlwijk, K., Colijn, I., Harsono, H., Krebs, T., Berton-Carabin, C., Schroen, K. (2017). Coalescence of protein-stabilised emulsions studied with microfluidics. *Food Hydrocolloids*, 70, 96-104.
- Nakanishi, K., Sakiyama, T., Imamura, K. (2001). On the adsorption of proteins on solid surfaces, a common but very complicated phenomenon. *Journal of Bioscience and Bioengineering*, 91, 233-244.
- O'Brien R. D. (2008). *Fats and oils – formulating and processing for applications*. CRC Press, New York.

- Politova, N., Tcholakova, S., Denkov, N. D. (2017). Factors affecting the stability of water-oil-water emulsion films. *Colloids and Surfaces A: Physicochemical and Engineering Aspects*, 522, 608-620.
- Shen, F., Li, Yi., Liu, Z-M, Cao, R-T, Wang, G-R. (2015). Advances in micro-droplets coalescence using microfluidics. *Chinese Journal of analytical chemistry*, 43, 1942–1954.
- Steggmans M. L. J., Schroen C. G. P. H., Boom, R. M. (2009). Generalised insights in droplet formation at T-junctions through statistical analysis. *Chemical Engineering Science*, 64, 3042–3050.
- Tadros, T. F., Vincent, B. (1983). Emulsion stability, in: Becher, P. (Ed.), *Encyclopedia of Emulsion Technology*, Marcel Dekker, New York, pp. 269–272.
- Tadros, T. F. (2008). *Applied surfactants: Principles and applications* (2nd ed.). Weinheim: Wiley-VCH.
- Ushikubo, F. Y., Cunha, R. L. (2014). Stability mechanisms of liquid water-in-oil emulsions. *Food Hydrocolloids*, 34, 145-153.
- Ushikubo, F. Y., Birribilli, F. S., Oliveira, D. R. B., Cunha, R. L. (2014). Y- and T- junction microfluidic devices: effect of fluids and interface properties and operating conditions. *Microfluidics Nanofluidics*, 17, 711-720.
- Weyland, M., Hartel, R. (2008). Emulsifiers in confectionery. In G. L. Hasenhuettl, R. W. Hartel (Eds.), *Food emulsifiers and their applications* (2nd ed.). (pp. 285-305) New York: Springer.
- Wilson, R., Van Schie, B. J. Howes, D. (1998). Overview of the preparation, use and biological studies on polyglycerol polyricinoleate (PGPR). *Food and Chemical Toxicology*, 36, 711-718.
- Zhou, Q., Sun, Y., Yi, S., Wang, K., Luo, G. (2016). Investigation of droplet coalescence in nanoparticle suspensions by a microfluidic collision experiment. *Soft Matter*, 12, 1674-1682.

## **CAPÍTULO 4**

### **Microfluidics for assessing the formation and stability of oil-in-water emulsions based on components of bioprocesses**

Artigo submetido no periódico “Colloids and Surfaces A: Physicochemical and Engineering Aspects”: Santos, T. P., Michelon, M., Carvalho, M. S., Cunha, R. L. Microfluidics for assessing the formation and stability of oil-in-water emulsions based on components of bioprocesses.

## Microfluidics for assessing the formation and stability of oil-in-water emulsions based on components of bioprocesses

Tatiana Porto Santos<sup>a</sup>, Mariano Michelin<sup>bc</sup>, Marcio Silveira Carvalho<sup>c</sup>, Rosiane Lopes Cunha<sup>a\*</sup>

<sup>a</sup> Department of Food Engineering, Faculty of Food Engineering, University of Campinas (UNICAMP), 13083-862 – Campinas, SP, Brazil.

<sup>b</sup> School of Chemistry and Food, Federal University of Rio Grande (FURG), 96203-900, Rio Grande, RS, Brazil.

<sup>c</sup> Department of Mechanical Engineering, Pontifical Catholic University of Rio de Janeiro (PUC-Rio), 22451-900 – Rio de Janeiro, RJ, Brazil.

\*Corresponding author. Tel.: +55 19 3521 4047; fax: +55 19 3521 4027

E-mail address: rosiane@unicamp.br (Rosiane L. Cunha); tatiana.porto90@gmail.com (Tatiana P. Santos); michelonmariano@gmail.com (Mariano Michelin); msc@puc-rio.br (Marcio S. Carvalho)

### Abstract

Production of stable oil-in-water (O/W) emulsions is generally desired in food, pharmaceutical and chemical industries. Nonetheless, undesired emulsions can be developed during bioprocesses, hampering the recovery of bioproducts. Regardless of the process, high-throughput test of the formation and stability of the emulsion is paramount to establish an appropriate composition, which can potentially be achieved by applying microfluidic approaches. To address the concept, we analyzed O/W emulsions stabilized by yeast cells and antifoams (Pluronic L81 and Antifoam C) within glass microcapillaries. Both antifoams and yeast cells enabled droplets formation depending on the characteristics of the oily phase, but marked differences were observed on the stability of the formed emulsions. Such results indicate that a particular choice of the pair antifoam-oily phase can facilitate the (de)stabilization process. Moreover, the assessment of the mechanisms of droplets formation and coalescence within microchannels demonstrated to be a valuable tool to adjust emulsion properties depending on the sought-after stability.

**Keywords:** oil recovery, antifoams, yeast cells, capillary number, microcapillaries.

### 1. Introduction

Biotechnological processes have demonstrated an outstanding performance for the generation of products with high-added value, because depending on the process conditions and formulation, different oils can be generated to be applied in varied fields such as biofuels, food, cosmetics and pharmaceutical industries (Julleson et al., 2015). Notwithstanding, the oil produced in these fermentative bioprocesses tends to form an undesirable oil-in-water emulsion

due to the action of surface-active compounds present in the culture broth (aqueous phase) (Heeres et al., 2014). Such surface-active substances can be either added or formed over the fermentation time (Collins et al., 2015; Heeres et al. 2015), hampering the product (oil) recovery. Yeast cell is the most important compound in the fermentation process, enabling the synthesis of the desired product, but other components such as antifoams are also relevant for controlling the formation of air-bubbles during the process. Although both yeast cells and antifoams are essential components for fermentation, they can stabilize emulsions (Santos and Cunha, 2020), reducing the process yield. However, unlike yeast cells, which are generally well-established and specific for each process, concentration and type of antifoams are important factors to be defined in order to balance their contribution to the process with their undesirable effects, assessing whether the antifoam will increase or hinder the process yield (Routledge, 2012). Despite enormous importance of antifoams, their contribution to the formation of emulsions has been little studied (Santos and Cunha, 2020).

Typically, antifoams can be divided into two main categories (denominated as fast and slow antifoams) related to the foam rupture mechanism. Slow antifoams are usually oil-based, destroying the foam over a long period of time by surface adsorption, whilst fast antifoams can easily breakdown the foam film (Denkov et al., 2000; Routledge, 2012). In such categories, specific behaviors can also be found. Therefore, as each antifoaming agent acts in a unique way in the foam rupture, we hypothesized that they would also act singularly in relation to the emulsion formation during the process. Hence, the study of both yeast cells and antifoams effect on emulsions formation, when combined with different oily phases, is relevant to infer the appropriate broth composition depending on the product generated (Firoozmand and Rousseau, 2016; Furtado et al. 2015; Routledge, 2012). In this light, an adequate choice of the fermentation components would allow an improved process, reducing not only the need for demulsifiers but also the application of high-energy for the separation of emulsion phases, which, consequently, would reduce costs and environmental damage. In an ideal scenario, the evaluation of the ability of different surface-active compounds to form and stabilize emulsions should be done quickly and efficiently. For this, microfluidics emerges as a remarkable technique to enable the understanding of interfacial phenomena and to speed up the screening of components.

Within microfluidic devices, it is possible to study the formation and stability of emulsions by inducing contact between the droplets (Feng et al., 2015). Therewith, microfluidics can allow the understanding of the mechanisms involved in the droplets generation, since they are produced individually during the encounter of emulsion phases

(Ushikubo et al., 2014), while the susceptibility to (re)coalescence can be observed with the induced contact between the droplets. In this way, the (re)coalescence can be evaluated either immediately or after a period of time has elapsed from droplet formation, depending on the process to be simulated. To make a parallel with an actual fermentation, the droplets need to be developed and destabilized within the same system, in order to understand the recoalescence during a real biotechnological process. Ultimately, the observation of droplets within microfluidic devices can be relevant to assess surfactant kinetics. Indeed, the study of emulsifiers inducing stability of different dispersed (oily) phases within the devices is of great interest, since both the surface-active compound and the emulsion phases can affect droplet formation. The flow behavior is observed as a function of Capillary number ( $Ca$ ), as conventional emulsifiers generally decrease interfacial tension of the system, whilst different phases (oily and aqueous) can modify the viscous forces applied to droplets detachment (Kovalchuk et al., 2018). In general, for the production of droplets, different types of devices may be used depending on the application and composition. However, inert glass-capillary microfluidic devices not only have the advantage of being easily produced but also the benefit of having chemical resistance, allowing droplets formation for use in a wide range of products (Li et al., 2018).

In this context, this study aimed to evaluate droplets generation and potential recoalescence by contact-induction in order to determine the effect of process parameters and composition (flow rate ratio, viscosity of the phases, interfacial tension) on emulsion formation and stability (the latter being evaluated by events of coalescence). The influence of individual compounds on emulsions formation allowed to understand the stabilization mechanisms provided by different biotechnological components. These outcomes can provide interesting information to increase the efficiency of oil recovery, reducing environmental damage and increasing the profits associated with the product synthesis. Finally, this work showed that microfluidic tools can speed up the evaluation of the technological properties of oil-in-water emulsions, allowing the establishment of an appropriate composition to either stabilize or destabilize an emulsion.

## **2. Material and methods**

### **2.1. Material**

#### *2.1.1. Microfluidic devices*

Microfluidic devices were obtained using cylindrical (inner and outer diameters 0.58 mm and 1 mm, respectively) and square (inner dimension 1.05 mm) glass capillaries,



purchased from World Precision Instruments Inc. (USA) and Atlantic International Technology Inc. (USA), respectively. Polyethylene tubing of inner diameter of 0.86 mm (Scientific Commodities, Inc., USA), stainless steel dispensing needles (McMaster-Carr, USA) and Epoxy® (Devcon Corp., USA) were also used. Glass capillaries were treated using both poly(acrylamide-co-diallyldimethyl-ammonium chloride) (Sigma-Aldrich, USA) and a commercial water repellent named Glass Shield (Inove Pack do Brasil, Brazil).

### 2.1.2. Emulsions

Oil-in-water (O/W) emulsions were produced using three different oils: (i) sunflower oil (S) (Liza, Cargill Agricola S.A., Brazil); (ii) hexadecane 99 % (H) (Sigma-Aldrich, USA) and (iii) medium-chain-triacylglycerol (M) (MCT, NEOBEE®1053, kindly donated by Stepan Lipid Nutrition, Northfield, USA). The surface-active components, polyoxyethylene sorbitan monooleate (Tween® 80) (T), antifoam C (AntC) and Pluronic L81 poly(ethylene glycol)-block-poly(propylene glycol)-block-poly(ethylene glycol) (P81) were supplied by Sigma-Aldrich (St. Louis, USA). Fresh baker's yeast *Saccharomyces cerevisiae* (Y) from Itaiquara (Tapiratiba, Brazil) with a moisture content of  $70.13 \pm 1.81$  % (w/w) was purchased in the local market.

## 2.2. Methods

### 2.2.1. Physical properties of the phases

The concentration of components in the aqueous phase is shown in Table 1. Viscosity of the phases was determined using a stress-controlled rheometer AR1500ex (TA Instruments, New Castle, USA) within the shear rate from 0 to  $1000 \text{ s}^{-1}$ . Flow curves were obtained in a sequential three flow steps (up-down-up) and viscosity was obtained from the third curve in order to ensure rheological behavior at steady state. In addition, the density of the phases was measured using a digital densimeter (DMA 4200M, Anton Paar, Austria). Interfacial tension measurements were carried out by the pendant droplet method using a Tracker-S tensiometer (Teclis, France) to observe the initial interfacial tension. Initial interfacial tension was used for Capillary number calculation because droplets were immediately formed after the junction of the phases (short time) in the microchannels and the coalescence was evaluated subsequently. Zeta potential of aqueous phases dispersions/solutions was determined in a Nano-ZS Zetasizer (Malver Instruments, Malvern, UK) with a previous dilution of yeast cells (0.005 % v/v), antifoam C (0.1 % v/v), Pluronic L81 (0.1 % v/v) and Tween 80 (0.02 % v/v) in MilliQ water. All measurements were performed at 25 °C.

### 2.2.2. *Microfluidic devices fabrication*

The three-dimensional microfluidic devices were built on a glass slide and consisted of two cylindrical glass capillaries inserted at the opposite ends of a square capillary, as previously reported by Utada et al. (2005). The cylindrical glass capillaries were tapered to an inner diameter of approximately 20  $\mu\text{m}$  with a micropipette puller (model P-1000, Sutter Instrument Co., USA). Then, the tips were carefully sanded to desired final inner diameter. The collection capillary tubes - which have a larger inner tip diameter ( $\phi_c = 250 \mu\text{m}$ ) (Figure 1b, right) - were treated with a polyelectrolyte solution composed of 1 wt.% poly(acrylamide-co-diallyldimethyl-ammonium chloride) in 2M NaCl to render a hydrophilic surface. On the other hand, the injection capillary tubes - which have a smaller inner tip diameter ( $\phi_i = 80 \mu\text{m}$ ) (Figure 1b, right) - were treated with water repellent to obtain a hydrophobic surface. Both treatments were performed over 60 min. For the assembly of the microfluidic device, the square capillary was fixed to the slide with Epoxy® resin. Afterwards, the treated capillaries with sanded tips were inserted into the square capillary at both ends, which enabled the alignment of the axes of the capillaries, maintaining the desired separation distance ( $l = 120 \mu\text{m}$ ) (Figure 1b, right) between them. Finally, the dispensing needles were placed at the junctions (between capillaries or at their ends), and fixed to the slide with Epoxy® resin. Channel dimensions were based on a previous study reported by Michelon et al. (2020).

### 2.2.3. *Emulsion production in microchannels*

O/W emulsions were generated within the capillary channels using three different oils as dispersed phase combined with five aqueous phases (Table 1). The concentration of components in the aqueous phase was chosen based on systematic preliminary experiments, in which the determination of the minimum amount to produce emulsion droplets was assessed (only one emulsion could not be formed or presented several instability-related phenomena, regardless of the process conditions, which will be detailed in Section 3.2). The yeast cell concentration was also increased from 0.1 to 1 % w/w to evaluate possible effects of its concentration on emulsion formation and stability. Phases of the emulsions were injected into the device using three syringe pumps (Pump 11, Harvard Apparatus, USA) connected to the inlets shown in Figure 1a (detailed as A, B and C). These inlets can also be visualized in the schematic configuration in Figure 1b. The oil (dispersed phase) was injected into the cylindrical tube of smaller inner diameter with a flow rate  $Q_d$ , while the continuous phase flowed in opposite directions through the gap between the cylindrical and square capillary tubes. Thus, the flow rate of the continuous phase ( $Q_c$ ) was the sum of the flow rate of the two entrances of

the continuous phase. Events of emulsion formation and coalescence were visualized using an optical inverted microscope (DMi8, Leica Microsystem, Germany) equipped with a high-speed camera (Fastcam SA-3, Photron, USA). The Photron FASTCAM software (PFV) was used to analyze the videos recorded at 1,000 frames per second for a total of 10,000 frames. Diameter values were evaluated immediately after droplet formation (before any coalescence event), as well as their coefficient of variation (CV), by observing the droplets in the collection capillary (Figure 1b, detail). CV (Equation 1) was associated to polydispersity and calculated as the ratio between the standard deviation (SD) of the diameter values and the mean droplet diameter.

Table 1. Emulsion composition.

Codification	Aqueous phase (% w/w)				Oily phase
	Yeast (Y)	Tween 80 (T)	AntC	P81	
S-Y1%	1	-	-	-	Sunflower oil (S)
S-Y0.1%	0.1	-	-	-	
S-T	-	0.1	-	-	
S-AntC	-	-	0.03	-	
S-P81	-	-	-	0.03	
H-Y1%	1	-	-	-	Hexadecane (H)
H-Y0.1%	0.1	-	-	-	
H-T	-	0.1	-	-	
H-AntC	-	-	0.03	-	
H-P81	-	-	-	0.03	
M-Y1%	1	-	-	-	MCT (M)
M-Y0.1%	0.1	-	-	-	
M-T	-	0.1	-	-	
M-AntC	-	-	0.03	-	
M-P81	-	-	-	0.03	

S = sunflower oil, H = hexadecane, M = medium-chain-triacylglycerol (MCT). Yeast (Y), Tween 80 (T), antifoam C (AntC) and Pluronic L81 (P81).

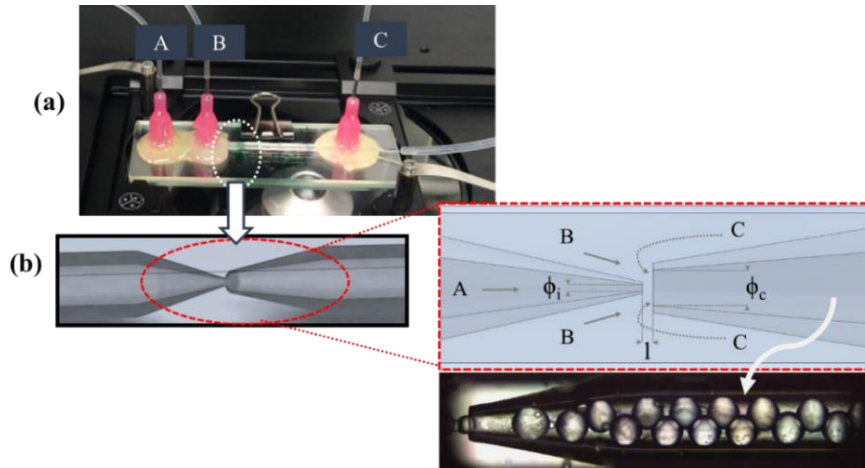


Figure 1. (a) Microfluidic device used to the analyses, where: (A) oil inlet and (B) and (C) inlet of the aqueous phase; (b) perspective view of the coaxial glass-capillary device (left) and a schematic configuration with geometric parameters of the design (right), where:  $\phi_i = 80 \mu\text{m}$  and  $\phi_c = 250 \mu\text{m}$  are the inner diameter of the injection and collection capillary tubes, respectively.  $l = 120 \mu\text{m}$  denotes the separation distance between injection and collection tubes. In detail: visualization of droplets passing through the channel.

$$\text{CV (\%)} = \frac{\text{SD}}{\text{mean diameter}} \times 100 \quad \text{Equation 1}$$

For the production of emulsions, the flow rate of the continuous aqueous phase was kept constant ( $Q_c = 2300 \mu\text{L/h}$ , being  $1500 \mu\text{L/h}$  at the inlet B and  $800 \mu\text{L/h}$  at the inlet C of Figure 1), while the flow rate of the dispersed oil phase was varied ( $Q_d = 500, 2000, 2600, 3200 \mu\text{L/h}$ ). The flow rate ratio of the phases ( $q$ ) was calculated according to Equation 2 and the values used are shown in Table 2. These flow rates were chosen with the aim of allowing droplets contact and *in situ* assessing their stability.

$$q = \frac{Q_c}{Q_d} \quad \text{Equation 2}$$

Table 2. Flow rate ratio ( $q$ ) of the phases and corresponding flow rate of the continuous ( $Q_c$ ) and dispersed ( $Q_d$ ) phases.

$Q_c (\mu\text{L/h})$	$Q_d (\mu\text{L/h})$	$q (-)$
2300	500	4.60
2300	2000	1.15
2300	2600	0.89
2300	3200	0.72

Moreover, another important dimensionless number, the ratio between the viscosity of the continuous ( $\eta_c$ ) and the dispersed ( $\eta_d$ ) phases ( $\lambda$ ) was determined according to Equation

3. Viscosity ratio ( $\lambda$ ) depended mainly on the oily phase and  $\lambda$  values were around 0.02 for sunflower oil, 0.04 for MCT and 0.33 for hexadecane.

$$\lambda = \frac{\eta_c}{\eta_d} \quad \text{Equation 3}$$

The Capillary number was also determined (Equation 4) from the ratio between viscous and interfacial forces, having been calculated based on the properties of the continuous or dispersed phase (Nabavi et al., 2017).

$$Ca = \frac{\eta U}{\gamma} \quad \text{Equation 4}$$

where,  $\eta$  is the viscosity of the respective analyzed phase,  $\gamma$  is the initial interfacial tension between oil-aqueous phase and  $U$  (Equation 5 or 6) is the velocity of the analyzed phase, which is calculated considering the flow rate of the phase and the cross-section area of the channel. Sub-indexes c and d refer to the continuous and dispersed phases, respectively.

$$U_c = \frac{Q_c}{\left[ L^2 - \pi \left( \frac{\phi_e}{2} \right)^2 \right]} \quad \text{Equation 5}$$

where  $L = 1050 \mu\text{m}$  (external square) and  $\phi_e = 1000 \mu\text{m}$  (internal cylinder).

$$U_d = \frac{Q_d}{\pi \left( \frac{\phi_i}{2} \right)^2} \quad \text{Equation 6}$$

where  $\phi_i = 80 \mu\text{m}$ .

#### 2.2.4. Emulsion coalescence in microchannels

During emulsion passage through the collecting capillary, the droplets came into contact and coalesced, these events being correlated with emulsion stability. The number of coalescence events was determined visually by analyzing 2,500 frames of the videos. After determining the total number of droplets and coalescence events, the results were converted into a percentage (%) of droplets that presented a specific number of coalescence events. This was calculated from the ratio between the number of droplets that underwent this specific

number of coalescence events and the total number of droplets analyzed. It should be highlighted that to maintain the same flow conditions (flow rates), the size of the droplets was inevitably different as it may vary depending on the emulsion phases (different surface-active compounds and oils).

### 3. Results and discussion

#### 3.1. Physical properties of the phases

Properties of the aqueous and oily phases were characterized to evaluate their influence on the emulsion formation and stability. Sunflower oil presented viscosity of  $55.03 \pm 0.01$  mPa.s and density of  $914.36 \pm 0.01$  kg.m<sup>-3</sup>. MCT, on the other hand, exhibited similar density ( $940.92 \pm 0.01$  kg.m<sup>-3</sup>) but the viscosity was about 2-fold lower ( $23.93 \pm 0.01$  mPa.s). Finally, hexadecane showed low viscosity ( $3.31 \pm 0.02$  mPa.s) and density ( $769.83 \pm 0.01$  kg.m<sup>-3</sup>). Only the viscosity value is presented (as rheological property), since all oils showed behavior of Newtonian fluid. The high viscosity of sunflower oil can be attributed not only to its long chain of triacylglycerol but also to chain unsaturation (Carreau et al., 2002). Moreover, hexadecane presented both the lowest viscosity and density amongst the oils tested. On the other hand, the different aqueous phases showed viscosity and density values similar to those of pure water (viscosity  $\sim 1$  mPa.s and density  $\sim 997$  kg.m<sup>-3</sup>). Table 3 shows the tension values at the oil-aqueous phase interfaces, while zeta potential of the aqueous solutions/dispersions in their natural pH is shown in Table 4. Tween 80 (T) and Pluronic L81 (P81) were the components that most affected the results of interfacial tension, regardless of the composition of the oily phase. Moreover, the results of zeta potential show that yeast cells (Y) and P81 had more pronounced surface negative charges, while Antifoam C (AntC) and Tween 80 presented reduced modulus value. Although the natural pH of AntC solution was  $\sim 3.7$ , previous studies showed that when the emulsion is formed with the combination of AntC and yeast cells, the pH of the latter component prevails and, at this pH, AntC still presents a reduced zeta potential compared to P81 (of  $\sim -10$  mV) (Santos and Cunha, 2020). All properties will be discussed later (sections 3.2 and 3.3) correlating the data with emulsion formation and coalescence visualized within the microdevices.

Table 3. Initial tension at oily-aqueous phases interfaces ( $\gamma_{\text{initial}}$ ).

Oily-aqueous interface	$\gamma_{\text{initial}}$ (mN.m <sup>-1</sup> )
S-water	25.64 ± 0.43
H-water	49.83 ± 0.57
M-water	24.96 ± 0.47
S-Y1%	24.24 ± 0.03
H-Y1%	47.49 ± 6.59
M-Y1%	25.97 ± 0.61
S-Y0.1%	24.76 ± 0.18
H-Y0.1%	50.88 ± 0.63
M-Y0.1%	25.51 ± 0.50
S-T	9.47 ± 0.39
H-T	12.25 ± 0.36
M-T	10.23 ± 0.14
S-AntC	18.27 ± 0.20
H-AntC	31.28 ± 1.37
M-AntC	22.35 ± 0.23
S-P81	7.88 ± 0.22
H-P81	8.74 ± 0.12
M-P81	7.42 ± 0.52

S = sunflower oil, H = hexadecane, M = medium-chain-triacylglycerol (MCT). Aqueous phase composed by yeast (Y), Tween 80 (T), antifoam C (AntC) and Pluronic L81 (P81).

Table 4. Zeta potential values of different components in the aqueous phases.

Samples	Zeta Potential (mV)	pH (-)
Y	-38.97 ± 1.95	6.45 ± 0.21
T	-8.05 ± 1.18	5.79 ± 0.07
AntC	-7.71 ± 0.47	3.69 ± 0.03
P81	-35.42 ± 1.63	7.42 ± 0.01

Aqueous phase composed by Yeast (Y), Tween 80 (T), antifoam C (AntC) and Pluronic L81 (P81).

### 3.2. Emulsion droplets generation

In a study covering the evaluation of both droplets formation and coalescence, special attention should be given to the droplet generation process, especially because high frequency is required for droplets encounter in order to visualize emulsion coalescence (Wang et al., 2020). It means that the first step is to screen different flow rate ratio conditions in order to find a droplet formation frequency capable of inducing droplets contact and (potential) coalescence. In this vein, Figure 2 shows the frequency screening based on the flow rate ratio for the different emulsion systems and process conditions. It can be observed that to achieve “droplets encounter”, they were not formed under a typical process of oil droplets generation, in which  $Q_c \gg Q_d$ . Instead, the flow rate of the dispersed phase was increased (higher volume fraction of oil), which may impair droplets formation depending on the  $q$  values. Furthermore, it was possible to verify that by increasing the flow rate of the dispersed phase, there was an

increase in the frequency of droplets formation up to a “threshold” where the frequency no longer changed or even reduced (Figure 2). In addition to the frequency, some valuable dimensionless numbers can be applied for assessing droplets formation in microfluidic systems, such as the ratio of the phases viscosity ( $\lambda$ ) and the Capillary number ( $Ca$ ) of both continuous ( $Ca_c$ ) and dispersed ( $Ca_d$ ) phases, which are reported in Table 5. Ultimately, once droplets are formed under specific conditions, the evaluation of their diameter (Figure 3) is primordial to determine and differentiate emulsion properties.

In relation to the frequency screening, Figure 2 shows that for emulsions with the same composition (constant  $\lambda$  and  $\gamma$ ), a lower flow rate of the dispersed phase ( $q = 4.60$ ) decreased the frequency of droplets generation regardless of the type of oil (Figure 2A). In general, as the force provided by the aqueous phase in the shear plane was constant ( $Q_c$  and  $\eta_c$  almost did not change), more droplets could be formed by increasing  $Q_d$  ( $<q$ ), although for  $q$  close to or less than 1 (Figure 2B-C-D) (or  $Q_d \sim Q_c$  and  $Q_d > Q_c$ ) the frequency values were quite similar. According to these results, it can be inferred that the process reached the maximum limit (saturation) of  $Q_d$  for droplets production (since the fluid dynamics, limited by  $Q_c$ , was constant) and, therefore, a further increase in  $Q_d$  did not change (or even reduced) the frequency of droplets formation. Indeed, it is clear that the “threshold” or the limit to increase the frequency of droplets formation occurred when  $q$  was around 1. Overall, no clear trend was observed for the diameter of the droplets, although it typically showed an upward trend with decreasing  $q$  (Figure 3). In addition to the flow rate conditions, emulsion phases are especially important on the droplet formation (frequency and diameter) and, therefore, the outcomes can be explained based on the Capillary number that encompasses the interfacial and viscous forces of a two phase system. Therefore, before explaining the results and making correlations, we must first understand the Capillary number in detail. In this sense, the next few paragraphs will address the Capillary number concept, focusing on specificities of our samples. After such explanation, results will be discussed.

The Capillary number is typically assessed for droplets breakup, as it reflects the viscous and interfacial forces that are the main forces driving droplets detachment within microfluidic devices. Indeed, the regime of droplets generation in microfluidic systems is the result of absolute instability, balanced by a combination of viscous and capillary forces. Hence, to enable droplets formation, the interfacial tension between the phases must be low enough that the viscous force of the two-phase system (which is triggered by the increase of the projected area of the droplet) is predominant, exceeding the interfacial tension that maintains the droplet on the capillary tip (Deng et al., 2017; Steegmans et al., 2009). Therefore, greater



tension between the phases may impair droplets detachment.

However, albeit the Capillary number is highly used to access microfluidic conditions for droplets formation, it is possible to visualize in our set of results that this dimensionless number has limited application. Capillary number does not consider stabilization mechanisms that do not trigger interfacial tension reduction (such as *Pickering*). This means that this property does not always reflect emulsion formation, since there are compounds that can form/stabilize emulsions without affecting the interfacial tension (Dorobantu et al., 2004). For instance, yeast cells have barely decreased the interfacial tension (Table 3), thus, their stabilization mechanisms may be associated with *Pickering*, although it is also influenced by steric and electrostatic hindrance (Firoozmand and Rousseau, 2016; Furtado et al., 2015), the latter also demonstrated by zeta potential values (Table 4). This complexity of mechanisms occurs mainly due not only to the presence of yeast cells, but also to bioemulsifiers and cell wall proteins (Furtado et al., 2015), which can modify the prevailing mechanism depending on their concentration. Therefore, we consider that the Capillary number was not representative for our two-phase systems with yeast cells.

Furthermore, a point of discussion is the effective role of the interfacial tension values (measured using a tensiometer) in the assessment of this dimensionless number. For instance, tensiometer-based measurements are not suitable for evaluating events that occur at millisecond time-scales (Schroen et al., 2020), such as those visualized in droplets formation within microchannels. Moreover, tensiometer measurements do not take into account the migration of surface-agents during droplets formation. However, the development of droplets in microfluidic systems depends to a large extent on the surface-agent ability to migrate towards the interface, which can dictate droplet size. This phenomenon is especially important in this study, since the dispersed phase presents higher viscosity and achieves higher flow rates compared to the continuous phase, thus the migration of the emulsifier facilitating droplets formation may emerge as a factor of outmost relevance. This diffusion may contribute to establish the mean droplet size, which can be more evident in a process that occurs under laminar flow conditions.

Bearing in mind the limitations of the Capillary number, the properties of both the continuous and dispersed phases can be applied to obtain specific insights. Capillary number of the continuous phase ( $Ca_c$ ) represents the balance of forces applied to break the dispersed phase (Kovalchuk et al., 2018) and, in this study, depends mainly on the interfacial tension, as the viscosity of the different continuous phases was similar to that of water. In addition, the flow rate of the continuous phase was kept constant, thus the force generated by the continuous phase

did not change for the different samples (Cobos et al., 2009). Overall,  $Ca_c$  values were similar in relation to triacylglycerol oils (MCT and sunflower oil), while this dimensionless number was lower with hexadecane (Table 5). Moreover, P81 and Tween 80 increased  $Ca_c$  by a factor of 2.5 to 5.5, which was caused by the lower values of interfacial tension. Although two opposite forces are analyzed in  $Ca_c$  (Ushikubo et al., 2014) (viscous forces improving the break of oil droplets and interfacial forces that hinder this formation), the viscosity of the dispersed phase in O/W emulsions is more important, because it represents the most viscous liquid of the system (Kovalchuk et al., 2018). In fact, different studies forming W/O emulsions used  $Ca_c$  to represent the system, taking into account the phase with the highest viscosity (Belkadi et al., 2015). Thus,  $Ca_d$  will be the main focus of this paper because, unlike  $Ca_c$ , it was calculated using the different viscosity values of the dispersed phase (oil), although, depending on the process and emulsion composition, either  $Ca_c$  or  $Ca_d$  can better reflect the mechanisms of the formation of emulsions.

After this detailed understanding of the Capillary number and its implications for droplets formation, the previously exposed outcomes of formation frequency (Figure 2) and droplet diameters (Figure 3) can be related to the viscosity ratio ( $\lambda$ ) and the Capillary number of the dispersed phase ( $Ca_d$ ). Comparing the emulsions formed with different oily phases, sunflower oil-based systems presented the lowest value of  $\lambda$  (0.02) and the highest value of  $Ca_d$  (Table 5) mainly due to the viscosity of the dispersed phase that affects the shear forces. MCT presented intermediate viscosity values and, consequently,  $\lambda$  (0.04), but  $Ca_d$  values were of the same order of magnitude as the sunflower oil systems, since both oils showed similar values of interfacial tension with the different aqueous phases (Table 3). However, breakage and droplets formation were more difficult with sunflower oil compared to MCT, mainly due to its high viscosity. This difficulty in droplets breakage reflected in a larger diameter of the droplets (Figure 3) and a lower frequency of formation (Figure 2).

In general, if sufficient viscous forces are present in the system, droplets formation with low viscosity oils can be achieved more easily (for systems with similar interfacial tension values). The low viscosity value of hexadecane (used as a dispersed phase) resulted in the highest  $\lambda$  (0.33) and lowest  $Ca_d$  ( $<0.1$ ), albeit the high interfacial tension promoted by this oil also contributed to this low value of  $Ca_d$ . Thus, despite the low viscosity (high  $\lambda$ ), the interfacial tension may hamper the detachment of hexadecane-based emulsions, resulting in increased size and reduced frequency of droplets formation when compared to MCT. In fact, emulsions using MCT as dispersed phase were easily produced regardless of the stabilizing agent, generating

droplets with smaller diameters (Figure 3) at a higher frequency of formation (Figure 2) compared to the other oils.

Although suitable conditions have been applied with different surface-agents, with the objective of producing droplets as often as possible, in some samples the encounter between the droplets was not visualized (frequency was very low). For instance, for S-P81, S-T and H-Y1% emulsions, the increase in the frequency of droplets formation (up to the upper limit value) was not sufficient for the droplets to touch and, therefore, to observe coalescence events, which will be further entailed in Section 3.3. As afore-mentioned, the interfacial tension must be low enough to allow droplets breakup. Therefore, considering the interfacial tension generated by P81, T and AntC (the surface-agent components), it would be expected an easier formation using T and mainly P81, which was not visualized when sunflower oil was applied as the dispersed phase.

Our hypothesis is that, for S-T and S-P81 the low interfacial tension, instead of improving droplets formation, impaired its occurrence. Such episode can be explained by the fact that small interfacial forces tend to generate reduced adhesive forces (smaller than the shedding forces produced by inertial and viscous forces), impairing the adherence of the droplets at the channel tip and inducing the formation of an oil stream that further breaks into droplets (Deng et al., 2017). Such phenomenon mainly affected the emulsions produced with the most viscous oil (sunflower oil) that, besides generating a great drag force between the phases, requires additional effort to flow and break into droplets, resulting in the observation of a lower formation frequency (Figure 2) due to the consequent growth of droplets (Figure 3). In particular, S-P81 showed a smaller frequency of droplets formation and an extremely high diameter of sunflower oil droplets. Moreover, the size of S-P81-based droplets was even more affected by  $q$ , since the high amount of dispersed phase ( $>Q_d$ ) must have further contributed to droplet growth. Interestingly, in S-T emulsions, although the frequency was reduced, droplet growth has not been pronounced. Anyway, both S-P81 and S-T showed higher  $Ca_d$  values compared to the other surface agent-oil combinations (due to lower interfacial tension and higher viscosity), highlighting the need to understand the balance of forces acting in droplets formation within microfluidic systems.

In addition to sunflower oil-based emulsions, H-Y1% exhibited similar behavior, as the droplets formed under low frequency presented high diameter values. However, it is difficult to pinpoint the reason why this phenomenon happened in this case, mainly because yeast did not affect the values of interfacial tension. Therefore, this outcome could be associated with the conventional fact that the viscous forces could not exceed the “interfacial forces”.

However, in this case, even more difficulty would be expected for the formation of H-Y0.1% emulsions, which was not observed. Thus, our hypothesis is that the same phenomenon (reduced adhesive forces) occurring in S-T and S-P81 emulsions would be responsible for such outcome. It is necessary to comment that very small  $Ca_d$  values were found for H-Y(0.1 and 1%) emulsions, which further highlights the limitation of the Capillary number to explain droplets breakup and stabilization in systems that do not present a reduction in interfacial tension. Another interesting result was found for H-AntC, in which droplets did not even form or was produced with extreme instability (generating uncontrolled droplets triggering flow instability and clogging), indicating that very low  $Ca_d$  values did not allow proper droplets formation. In fact, since AntC slightly reduced the tension at the hexadecane-water interface ( $31.28 \text{ mN.m}^{-1}$ ) (Table 3), the interfacial forces were probably predominant, not allowing the system to achieve the balance of forces for droplets generation. This non-droplet formation is an important outcome, which can be useful for managing bioprocess conditions.

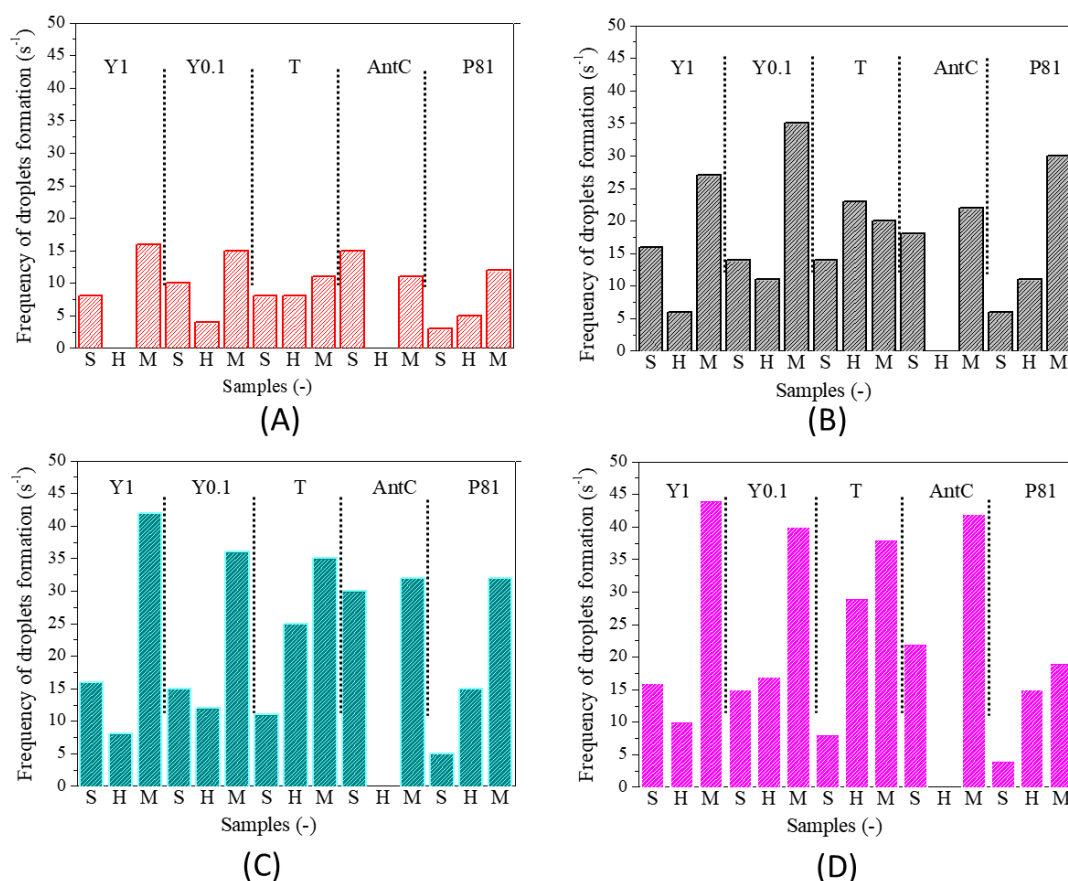


Figure 2. Frequency of droplets formation for different aqueous and oily phases. Flow rate ratio (q): (A) 4.60, (B) 1.15, (C) 0.89 and (D) 0.72. S= sunflower oil, H= hexadecane, M= MCT, Y = yeast, T= Tween 80, AntC= Antifoam C and P81 = Pluronic L81.

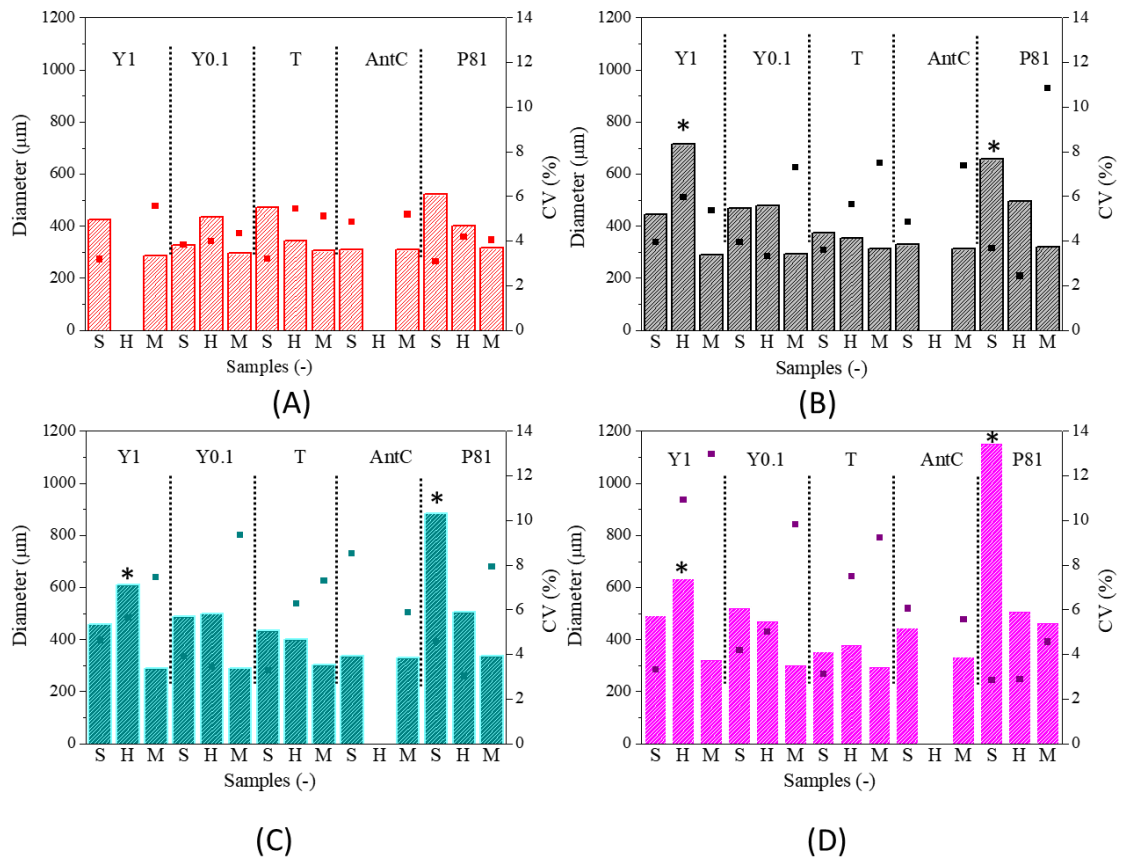


Figure 3. Mean droplet diameter (columns) and coefficient of variation (CV) (■). Flow rate ratio (q): (A) 4.60, (B) 1.15, (C) 0.89 and (D) 0.72. S= sunflower oil, H= hexadecane, M= MCT, Y = yeast, T= Tween 80, AntC= Antifoam C and P81 = Pluronic L81. \* The mean diameter of these droplets was the horizontal axis measurement, since droplets were flattened and the vertical axial measurement represents the channel dimension (580 μm).

Based on the afore-discussed results, some conclusions can be drawn regarding the Capillary number of samples produced with T, P81 and AntC (components that affect the interfacial tension). Firstly, a critical Capillary number ( $Ca_{d,critical}$ ) or a maximum Capillary number (Table 5), above which no marked change in the frequency of oil droplets formation was observed, was identified for each oily phase. For sunflower oil, the  $Ca_{d,critical}$  was between 0.43 and 0.84, while for MCT this range was about 2 times smaller (between 0.20 and 0.47). For hexadecane, the  $Ca_{d,critical}$  was more difficult to establish, but it was clearly around 0.05. Identification of this transition point ( $Ca_{d,critical}$ ) that allows droplet formation as often as possible is paramount to establish the conditions that induce droplets fusion. Furthermore, the mechanisms of droplets formation and detachment can also be inferred by the Capillary number. For a constant q, higher  $Ca_d$  values ( $\ll$  interfacial tension and  $\gg$  viscosity of the dispersed phase) induced the difficulty of the droplets to adhere to the channel tip and, as a consequence, the frequency of droplets formation was reduced. On the other hand, at extremely low  $Ca_d$

values, not even droplets were formed. Therewith, it is between these extremes that an improved formation was achieved.

Furthermore, we could affirm that the numbers  $\lambda$  and  $q$  associated with the values of interfacial tension (in cases where this property is important) can also adequately represent the process of droplets detachment. In general, low  $\lambda$  prevents droplets formation; however,  $\lambda$  must be analyzed together with the kinetics of interfacial tension to understand the influence of all these properties. Finally, we demonstrate that droplets generation could either occur or not, depending on the stabilizing compound-oily phase combination. In addition, the association of the process conditions (flow rate ratio of the phases) with the characteristics of the oil and aqueous phases (viscosity of the phases and interfacial tension between them) are important to study the formation and stabilization of droplets within microfluidic devices.

Table 5. Capillary number of the continuous (aqueous) ( $Ca_c$ ) and dispersed (oily) ( $Ca_d$ ) phases of the systems.

Emulsion	$Ca_c (-) * 10^{-5}$		$Ca_d (-)$			
	$Q_c (\mu L/h) =$	$2300$	$Q_d (\mu L/h)$			
			<b>500</b>	<b>2000</b>	<b>2600</b>	<b>3200</b>
			<b>(q=4.6)</b>	<b>(q=1.15)</b>	<b>(q=0.89)</b>	<b>(q=0.72)</b>
S-Y1%	5.41		0.063	0.251	0.326	0.402
H-Y1%	2.76		0.002	0.008	0.010	0.012
M-Y1%	5.05		0.026	0.103	0.133	0.164
S-Y0.1%	5.30		0.061	0.246	0.319	0.393
H-Y0.1%	2.58		0.002	0.007	0.009	0.012
M-Y0.1%	5.15		0.026	0.104	0.136	0.167
S-T	13.85		0.161	0.642	0.835	1.028
H-T	10.72		0.007	0.030	0.039	0.048
M-T	12.83		0.065	0.260	0.338	0.416
S-AntC	7.18		0.083	0.333	0.433	0.533
H-AntC	4.20		0.003	0.012	0.015	0.019
M-AntC	5.87		0.030	0.119	0.155	0.191
S-P81	16.68		0.193	0.773	1.005	1.237
H-P81	15.01		0.010	0.042	0.055	0.067
M-P81	17.68		0.090	0.359	0.466	0.574

S = sunflower oil, H = hexadecane, M = medium-chain-triacylglycerol (MCT). Aqueous phase composed by yeast (Y), Tween 80 (T), antifoam C (AntC) and Pluronic L81 (P81).

### 3.3. Evaluation of droplets stability

Coalescence has been highly investigated in microfluidic channels, being this phenomenon typically described by the liquid film drainage model. This model includes particular steps associated to - the approximation of two droplets, collision and deformation; drainage of the continuous film between the droplets; and rupture of the interfacial film

allowing droplets fusion (Bremond et al., 2008; Christopher et al., 2009; Shen et al., 2015). In the present paper, the coalescence (as illustrated in Figure 4) was studied by evaluating the number of coalescence events for sunflower oil (Figure 5A), hexadecane (Figure 5B) and MCT (Figure 5C) droplets. It is of paramount importance to highlight that although it was qualitatively possible to observe the degree of coalescence events, from a quantitative point of view it was difficult to express the exact number of coalescence events occurring within the capillary microchannels. It means that, since the capillaries are 3D geometries, it is sometimes difficult to analyze the coalescence related to the increase of the area of the droplets. Therefore, as these events were visually monitored and inferred, some errors are associated with the measurements. Moreover, when a large number of droplets is generated within the microchannels (to induce droplets contact), the coalescence observation is even more difficult to be performed due to the droplets overlap.

In spite of these limitations, the experiments were performed and, as previously mentioned, droplets were produced in order to induce contact between them (whenever possible) and, in these induced-contacts, coalescence seemed to be directly influenced by the droplets formation conditions, which also highlights the importance of a systematic study of the conditions to allow both droplets formation and contact. Frequencies greater than  $\sim 11$  droplets per second led to collisions between droplets, whereas at lower frequencies of droplets formation, their encounter and consequent (potential) coalescence did not take place (Figure 2). This corroborates the importance of finding the highest possible frequency triggered by the increase of  $Q_d$  ( $< q$ ), which, as previously discussed in Section 3.2, was achieved with specific Capillary numbers ( $Ca_d$ ) for the different dispersed phases.

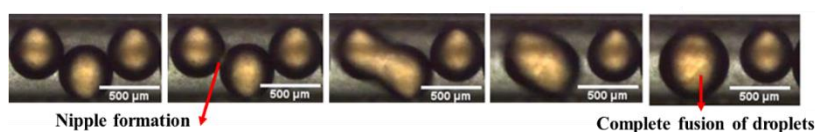


Figure 4. Demonstration of a coalescence event.

Overall, coalescence did not occur for emulsions using P81 and Tween 80 in the aqueous phase due to: i) production of highly stable droplets of MCT and hexadecane or because ii) P81 and Tween 80 generated droplets of sunflower oil that did not collide (as discussed in section 3.2). Thus, these samples were omitted from Figure 5 because they did not present coalescence events. These results indicate that P81 and Tween 80 provided high stability to oil droplets, corroborating our previous study that applied high mechanical forces

to the production of droplets using P81 in the aqueous phase (Santos and Cunha, 2020). On the other hand, when the oil droplets were stabilized by AntC or yeast cells (Y1% and Y0.1%), droplets interacted with each other and showed pronounced coalescence. In general, a greater number of coalescence events was observed for droplets of sunflower oil using AntC as a stabilizer compared to yeast-based emulsions (Figure 5A). However, the hexadecane-AntC combination did not form droplets (instability/non-formation) and stabilization with yeast showed coalescence events with only Y0.1% (given that with Y1% droplets did not touch each other) (Figure 5B). For H-Y0.1%, as expected, higher frequencies of droplets formation led to more events of coalescence (Figure 5B). Therefore, for these emulsions susceptible to destabilization, a correlation between these results and frequency of droplets generation could be established. Higher frequencies (generated by low  $q$  or high fraction of dispersed phase) led to greater droplets detachment and, consequently, to a higher concentration of droplets in a same volume. Hence, a higher concentration of droplets can promote more interactions and collisions between them, increasing coalescence events (Figure 5).

In general, droplet coalescence of sunflower oil and hexadecane was more difficult to be analyzed considering different aqueous solutions/dispersions, since the droplets of these oils were less prone to detach, hampering the formation of a higher concentration of droplets and consequently their fusion. However, it is noticeable that for the same aqueous phase, hexadecane droplets were more easily destabilized, a fact that can be attributed to the lower viscosity and greater interfacial tension with the aqueous phases. This result suggests that  $Ca_d$  can be used to evaluate coalescence, since the higher viscosity reduces droplets fusion, while the lower interfacial tension improves droplets stability (both resulting in an increased  $Ca_d$ ). Therefore, once again, it is clear that the process conditions and composition must be carefully established for the evaluation of the droplets stability.

On the other hand, MCT droplets were produced at higher frequency, mainly because of the lower viscosity of MCT (compared to sunflower oil) that improves droplets formation. Thereby, it was possible to study the formation and stability of MCT droplets stabilized by each surface-active agent individually. In general, MCT droplets did not present coalescence with P81 and Tween 80, which was mainly attributed to the reduction of the interfacial tension provided by these surface-active compounds. However, the interfacial tension was higher for the AntC-based systems and the coalescence of the droplets occurred more easily. P81 features ionic chains that lead to charged droplets (Table 4) that improve stability due to electrostatic repulsion between them. On the other hand, AntC seems to present a less efficient surface coverage, leading to emulsions more susceptible to destabilization



(Santos and Cunha, 2020), which may be related, at least in part, to the low zeta potential values (Table 4). As previously stated, a comparison with yeast dispersions, based on interfacial tension, could not be carried out since yeast presents a combination of stabilization mechanisms, which do not seem to be influenced by the kinetics of interfacial tension. Nevertheless, the presence of charged groups (Table 4), as well as the exposure of the hydrophobic domains of the cells contribute to the stability of the droplets (Firoozmand and Rousseau, 2016; Furtado et al., 2015). Another important point to be highlighted is that when observing the videos, the coalescence of the previously fused droplets occurred more easily. This means that droplets that have undergone a coalescence process were more susceptible to showing (new) extra fusions with other droplets (Sugiura et al., 2004; Taylor, 1998). Therefore, it is clear that polydispersity decreased the droplets stability.

Ultimately, as a suggestion for future studies, an increase in the cross-section area of the microchannel (Baret et al., 2009; Tan et al., 2004) may allow a better collision of droplets due to the velocity reduction. Moreover, 2D channels would probably be more appropriate. However, these techniques need to be judiciously studied, since these collision chambers are not produced using inert glass microcapillaries (capillary channels do not allow this flexibility of geometry design), which can induce different interactions with the channel surface, affecting the interpretation of the results. Manipulating the channels where the droplets are produced can also be a reasonable approach to inducing the formation of droplets at a higher frequency. For instance, flow focusing can induce different shear forces by modifying conditions of droplets formation and, consequently, their stability (Lashkaripour et al., 2019). Nevertheless, the application of microcapillaries seems to be an interesting strategy to study different phenomena associated with the droplets formation.

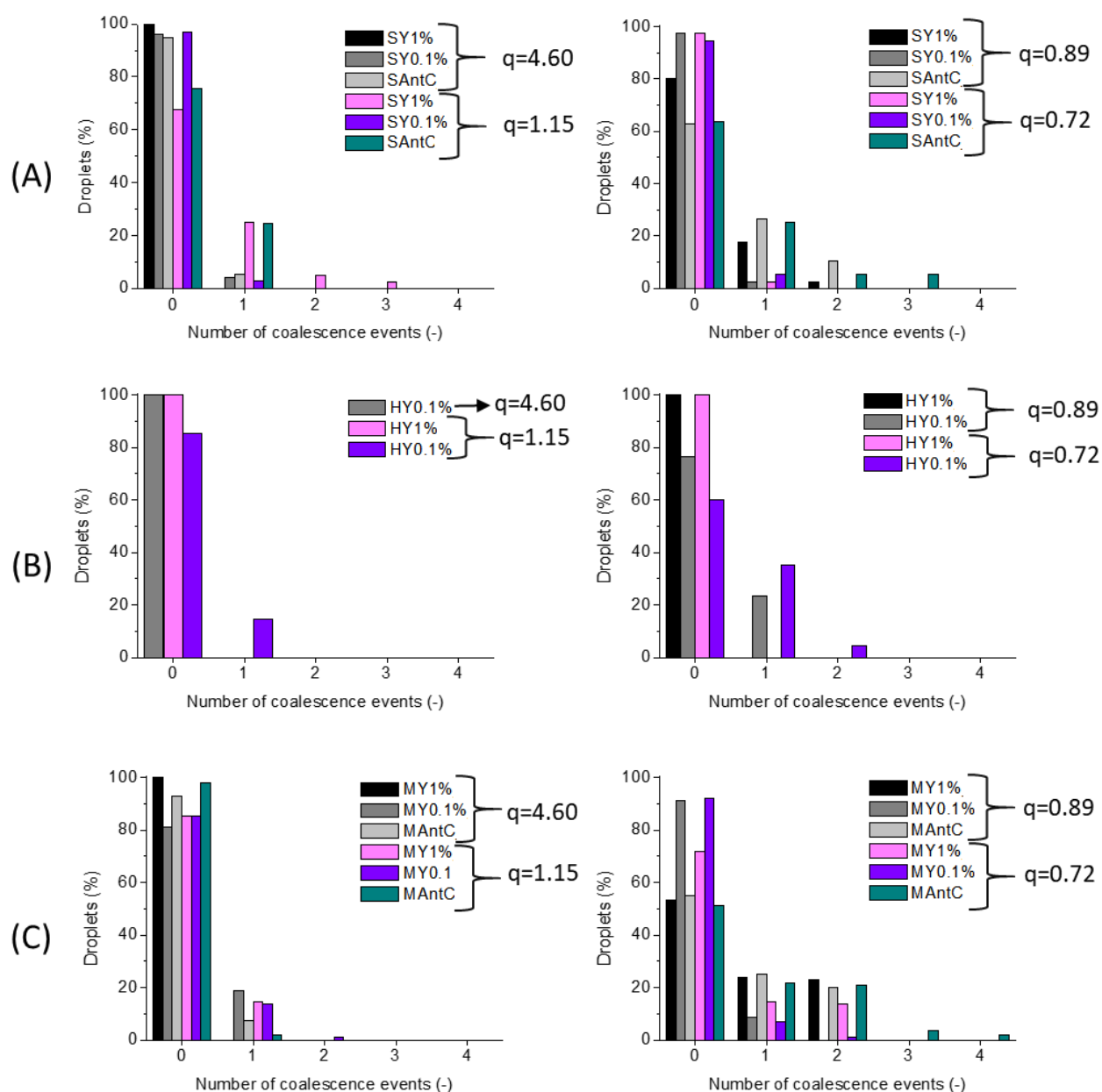


Figure 5. Number of coalescence events of (A) sunflower oil (S), (B) hexadecane (H), and (C) medium-chain-triacylglycerol (M) droplets in different aqueous continuous phase: Y = yeast, and AntC= Antifoam C.

Finally, in order to encompass the outcomes of this study and better visualize the appropriate conditions for emulsion formulation, Table 6 summarizes droplet generation and coalescence.

Table 6. Overview of the results.

Emulsion	Formation of droplets	Encounter of droplets	Was coalescence observed?	Mechanisms associated with the formation/non-formation or the coalescence/non-coalescence (when there is contact) of droplets
S-Y1%	Yes	Yes	Yes	<b>Coalescence:</b> combination of mechanisms was not enough to stabilize the droplets
H-Y1%	Yes (big droplet)	No	No	<b>Formation:</b> low adhesive forces with hexadecane
M-Y1%	Yes	Yes	Yes	<b>Coalescence:</b> combination of mechanisms was not enough to stabilize the droplets
S-Y0.1%	Yes	Yes	Yes	<b>Coalescence:</b> combination of mechanisms was not enough to stabilize the droplets, lower concentration of yeast cells
H-Y0.1%	Yes	Yes	Yes	
M-Y0.1%	Yes	Yes	Yes	
S-T	Yes	No*	No	<b>Formation:</b> low interfacial tension (low adhesive forces), high-viscous oil
H-T	Yes	Yes	No	<b>Non-coalescence:</b> low interfacial tension
M-T	Yes	Yes	No	
S-AntC	Yes	Yes	Yes	<b>Coalescence:</b> high interfacial tension
H-AntC	No	-	-	<b>Non-formation:</b> even higher interfacial tension
M-AntC	Yes	Yes	Yes	<b>Coalescence:</b> high interfacial tension
S-P81	Yes (big droplet)	No	No	<b>Formation:</b> low interfacial tension (low adhesive forces), high-viscous oil
H-P81	Yes	Yes	No	<b>Non-coalescence:</b> low interfacial tension, charged surface-agent
M-P81	Yes	Yes	No	

S = sunflower oil, H = hexadecane, M = medium-chain-triacylglycerol (MCT). Aqueous phase composed by Yeast (Y), Tween 80 (T), antifoam C (AntC) and Pluronic L81 (P81). \* Limited contact was observed in only one condition ( $Q_d = 2000 \mu\text{L/h}$ ).

#### 4. Conclusion

This study allowed to conclude that both formation of droplets and stability based on their coalescence can be studied within microchannels and, therefore, microfluidics is an efficient tool to obtain information about emulsion features. However, for an adequate evaluation of emulsion stability, the process variables must be adjusted, especially considering that the droplets must encounter each other and collide to induce coalescence. Moreover, we can infer that although microfluidic channels can be a solid strategy to induce and observe droplets fusion, 3D microcapillaries have limited application in the observation of droplet coalescence. However, in our study it was possible to assess remarkable differences between the surface-

active agents. Both coalescence and formation of oil-in-water emulsions could be characterized by the Capillary number of the dispersed phase, making it possible to establish correlations and understand these phenomena. Nevertheless, one must keep in mind that  $Ca_d$  has limitations associated to surface-active agents that do not trigger the reduction of interfacial tension. Overall, it was possible to understand some mechanisms of emulsion stability and to determine under which conditions within the microchannels the emulsions can be formed and evaluated. The effect of each antifoaming agent on emulsion formation and stabilization could be identified, showing that these relevant components in the fermentation processes must be selected according to the nature of the product (oil). According to our results, AntC would be more suitable to induce the formation of a less stable emulsion, while P81 produced highly stable colloidal structures. Thus, AntC would be suggested for biotechnological process aiming at the generation of emulsions with low stability. Finally, it was also demonstrated that yeast present in bioprocesses can improve the formation of droplets, but the mechanisms that provide such stabilization must be better elucidated, since yeast cells may present a combination of mechanisms that induce the formation of droplets.

### **Conflicts of interest**

There are no conflicts to declare.

### **Acknowledgements**

This study was financed in part by the Coordenação de Aperfeiçoamento de Pessoal de Nível Superior – Brasil (CAPES) - Finance Code 001. Santos thanks grant number #2017/18109-0, São Paulo Research Foundation – FAPESP and Conselho Nacional de Desenvolvimento Científico e Tecnológico – CNPq (Grant number 140700/2017-0) for the scholarship. Michelin thanks CNPq (140283/2013-7) for the graduate assistantship grant and Universal Call MCTIC/CNPq 28/2018 (435803/2018-2). Cunha thanks CNPq (307168/2016-6) for the productivity grant. This work was also supported by grant number #2019/07744-1, São Paulo Research Foundation - FAPESP. The authors also thank FAPESP (2011/06083-0; 2004/08517-3; EMU 2009/54137-1) and CNPq (Universal Project 423960/2016-4).

### **References**

Abedi, S., Suteria, N. S., Chen, C-C, Vanapalli, S. A. (2019). Microfluidic production of size-tunable hexadecane-in-water emulsion: Effect of droplet size on destabilization of two-

- dimensional emulsions due to partial coalescence. *Journal of Colloid and Interface Science*, 533, 59-70.
- Baret, J-C., Kleinschmidt, F., Harrak, A. E., Griffiths, A. D. (2009). Kinetics aspects of emulsion stabilization by surfactants: a microfluidic analysis. *Langmuir*, 25, 6088-6093.
- Belkadi, A., Tarlet, D., Montillet, A., Bellettre, J., Massoli, P. (2015). Water-in-oil emulsification in a microfluidic impinging flow at high capillary numbers. *International Journal of Multiphase Flow*, 72, 11-23.
- Bremond, N., Doméjjean, H., Bibette, J. (2011). Propagation of drop coalescence in a two-dimensional emulsion: a route towards phase inversion. *Physical Review Letters*, 106, 214502-1-214502-4.
- Carreau, P. J., Cotton, F., Citerne, G. P., Moan, M. (2002). *Rheological Properties of Concentrated Suspensions. Engineering and Food for the 21st Century. Food Preservation Technology*, CRC Press.
- Christopher, G. F., Bergstein, J., End, N. B., Poon, M., Nguyen, C., Anna, S. L. (2009). Coalescence and splitting of confined droplets at microfluidic junctions. *Lab on a Chip*, v. 9, p. 1102-1109.
- Cobos, S., Carvalho, M.S., Alvarado, V. (2009). Flow of oil–water emulsions through a constricted capillary. *International Journal of Multiphase Flow*, 35, 507-515.
- Collins, J., Grund, M., Brandenbusch, C., Sadowski, G., Schmid, A., Buhler, B. (2015). The dynamic influence of cells on the formation of stable emulsions in organic-aqueous biotransformations. *Journal of Industrial Microbiology Biotechnology*, 42, 1011-26.
- Deng, C., Wang, H., Huang, W., Cheng, S. (2017). Numerical and experimental study of oil-in-water (O/W) droplet formation in a co-flowing capillary device. *Colloids and Surfaces A*, 533, 1-8.
- Denkov, N. D., Krastanka, M., Christova, C., Hadjiiski, A., Cooper, P. (2000). Mechanisms of action of mixed solid-liquid antifoams: 3. Exhaustion and reactivation. *Langmuir*, 21, 8163-8619.
- Dorobantu, L. S., Yeung, A. K., Foght, J. M., Gray, M. R. (2004). Stabilization of oil–water emulsions by hydrophobic bacteria, *Applied and Environmental Microbiology*, 70, 6333–6336.
- Firoozmand, H.; Rousseau, D. (2016). Microbial cells as colloidal particles: Pickering oil-in-water emulsions stabilized by bacteria and yeast. *Food Research International*, 81, 66-73.
- Furtado, G. F, Picone, C. S. F., Cuellar, M. C., Cunha, R. L. (2015). Breaking oil-in-water emulsions stabilized by yeast *Colloids and Surfaces B: Biointerfaces*, 128, 568-576.

- Heeres, A. S., Picone, C. S. F., van der Wielen L. A. M., Cunha, R. L., Cuellar, M. C. (2014). Microbial advanced biofuels production: overcoming emulsification challenges for large-scale operation. *Trends Biotechnology*, 32, 221–229.
- Heeres, A. S., Schroën, K., Heijnen, J. J., van der Wielen, L. A. M., Cuellar, M. C. (2015). Fermentation broth components influence droplet coalescence and hinder advanced biofuel recovery during fermentation. *Biotechnology Journal*, 10, 1206-1215.
- Julleson, D., David, F., Pflieger, B., Nielsen, J. (2015). Impact of synthetic biology and metabolic engineering on industrial production of fine chemicals. *Biotechnology Advances*, 33, 1395–1402.
- Kovalchuk, N. M., Roumpea, E., Nowak, E., Chinaud, M., Angeli, P., Simmons, M. J. H. (2018). Effect of surfactant on emulsification in microchannels. *Chemical Engineering Science*, 176, 139-152.
- Krebs, T., Schroen, K., Boom, R. (2012). A microfluidic method to study demulsification kinetics. *Lab on a chip*, 12, 1060-1070.
- Lashkaripour, A., Rodriguez, C., Ortiz, L., Densmore, D. (2019). Performance tuning of microfluidic flow-focusing droplet generators. *Lab on a Chip*, 19, 1041-1053.
- Li, W., Zhang, L., Ge, X., Xu, B., Zhang, W., Qu, L., Choi, C-H., Xu, J., Zhang, A., Lee, H., Weitz, D. A. (2018). Microfluidic fabrication of microparticles for biomedical applications. *Chemical Society Reviews*, 47, 5646-5683.
- Michelon, M., Leopércio, B. C., Carvalho, M. S. Microfluidic production of aqueous suspensions of gellan-based microcapsules containing hydrophobic compounds. *Chemical Engineering Science*, 211, 115314, 2020.
- Nabavi, S. L., Vladisavljevic, G. T., Manovic, V. (2017). Mechanisms and control of single-step microfluidic generation of multi-core double emulsion droplets. *Chemical and Engineering Journal*, 322, 140-148.
- Routledge, S. J. (2012). Beyond de-foaming: the effects of antifoams on bioprocess. *Productivity. Computational and structural biotechnology journal*, 3, e201210014.
- Santos, T. P., Cunha, R. L. (2020). Designing biotechnological processes to reduce emulsions formation and improve oil recovery: Study of antifoams application. *Biochemical Engineering Journal*, 163, 107745.
- Schroën, K., de Ruiter, J., Berton-Carabin, C. (2020). The Importance of Interfacial Tension in Emulsification: Connecting Scaling Relations Used in Large Scale Preparation with Microfluidic Measurement Methods. *ChemEngineering*, 4, 63.

- Shen, F., Li, Yi., Liu, Z-M, Cao, R-T, Wang, G-R. (2015). Advances in micro-droplets coalescence using microfluidics. *Chinese Journal of analytical chemistry*, 43, 1942–1954.
- Steegmans, M. L. J., Warmerdam, A., Schroen, K. G. P. H., Boom, R. M. (2009). Dynamic interfacial tension measurements with microfluidic Y-junctions. *Langmuir*, 25, 9751-9758.
- Sugiura, S., Nakajima, M., Yamamoto, K., Iwamoto, S., Oda, T., Satake, M., Seki, M. (2004). Preparation characteristics of water-in-oil-in-water multiple emulsions using microchannel emulsification. *Journal of Colloid and Interface Science*, 270, 221-228.
- Tan, Y-C., Fisher, J. S., Lee, A. I., Cristini, V., Phillip. A. (2004). Design of microfluidic channel geometries for the control of droplet volume, chemical concentration, and sorting. *Lab on a Chip*, v. 4, p. 292-298.
- Taylor, P. Ostwald ripening in emulsions. (1998). *Advances in Colloid Interface Science*. 75, 107–163.
- Ushikubo, F. Y., Cunha, R. L. (2014). Stability mechanisms of liquid water-in-oil emulsions. *Food Hydrocolloids*, 34, 145-153.
- Ushikubo, F. Y., Birribilli, F. S., Oliveira, D. R. B., Cunha, R. L. (2014). Y- and T- junction microfluidic devices: effect of fluids and interface properties and operating conditions. *Microfluidics Nanofluidics*, 17, 711-720.
- Utada, A.S., Lorenceau, E., Link, D.R., Kaplan, P.D., Stone, H.A., Weitz, D.A. (2005). Monodisperse double emulsions generated from a microcapillary device. *Science*, 308, 537-541.
- van Dijke, K., Veldhuis, G., Schroen, K., Boom, R. (2010). Simultaneous Formation of Many Droplets in a Single Microfluidic Droplet Formation Unit. *AIChE*, 56, 833-836.
- Wang, T., Andersen, S.I., Shapiro, A. (2020). Coalescence of oil droplets in microchannels under brine flow. *Colloids and Surfaces A: Physicochemical and Engineering Aspects*, 598, 124864.

## CAPÍTULO 5

### **Unraveling driving regimes for destabilizing concentrated emulsions within microchannels**

Artigo publicado no periódico “Soft Matter”



*Reproduced from the Ref. Santos, T. P., Cejas, C. M., Cunha, R. L., Tabeling, P. Unraveling driving regimes for destabilizing concentrated emulsions within microchannels. Soft Matter, 17, 1821-1833, 2021. <https://doi.org/10.1039/D0SM01674H> with permission from the Royal Society of Chemistry.*





Cite this: *Soft Matter*, 2021,  
17, 1821

## Unraveling driving regimes for destabilizing concentrated emulsions within microchannels†

Tatiana Porto Santos, <sup>‡\*ab</sup> Cesare M. Cejas, <sup>‡\*b</sup> Rosiane Lopes Cunha<sup>a</sup> and Patrick Tabeling<sup>b</sup>

Coalescence is the most widely demonstrated mechanism for destabilizing emulsion droplets in microfluidic chambers. However, we find that depending on the channel wall surface functionalization, surface zeta potential, type of surfactant, characteristics of the oil as a dispersed phase, or even the presence of externally-induced stress, other different destabilization mechanisms can occur in subtle ways. In general, we observe four regimes leading to destabilization of concentrated emulsions: (i) coalescence, (ii) emulsion bursts, (iii) a combination of the two first mechanisms, attributed to the simultaneous occurrence of coalescence and emulsion bursts; and (iv) compaction of the droplet network that eventually destabilizes to fracture-like behavior. We correlate various physico-chemical properties (zeta potential, contact angle, interfacial tension) to understand their respective influence on the destabilization mechanisms. This work provides insights into possible ways to control or inflict emulsion droplet destabilization for different applications.

Received 16th September 2020,  
Accepted 21st December 2020

DOI: 10.1039/d0sm01674h

rsc.li/soft-matter-journal

## 1 Introduction

Microfluidics offers exceptional conditions for droplet production with low polydispersity and controlled size, as well as tools to observe the droplets behavior subjected to various process conditions. Several microfluidic devices have been designed to observe the droplets behavior by using a wide range of materials,<sup>1–4</sup> but the most common devices are manufactured with polydimethylsiloxane (PDMS) due to its non-toxicity, optical transparency, flexibility and easy sealing.<sup>5</sup> In addition, a unique property that deserves attention is the ability of PDMS to change its hydrophobicity using plasma oxidation,<sup>6</sup> which can also serve as a precursor to surface functionalization. These changes in the properties of the microchannel surface cater to different applications. For instance, this approach can be used to understand the behavior of surfactants in stabilizing emulsions or to induce emulsion phases separation for oil recovery.<sup>7–10</sup>

Microchannels have been developed to observe the behavior of droplets in emulsion destabilization under flow conditions

using either active or passive strategies.<sup>7,11–16</sup> Passive strategies concern modifications on both surface walls and design of microchannels, and are frequently applied to induce the destabilization of emulsions. However, due to the high stability promoted by surfactants, it remains a great challenge to trigger emulsion destabilization. Moreover, in either diluted or concentrated emulsions, only coalescence could be observed in PDMS microchannels as a mechanism for destabilizing emulsion.<sup>11,17,18</sup> Our assumption is that this may have occurred because these studies generally applied similar process conditions, which did not allow for the observation of different destabilization phenomena. Furthermore, they generally use the same combination of emulsions and channels surface (oil-in-water emulsions with hydrophilic channels and water-in-oil emulsions with hydrophobic channels). This restrictive condition can delay the destabilization process and even impair the occurrence of other destabilization mechanisms during the residence time within the channels. Thus, a study of emulsions on different channel surfaces would be beneficial in assessing droplet stability and observing emulsion destabilization. In addition, this study could be relevant in determining the effect of surface properties on emulsion behavior during storage.

In this paper, we aim to understand the mechanisms of destabilization of packed oil-in-water emulsions inside microchambers when different surfactants (cationic, anionic, and non-ionic) are used to stabilize these emulsions. We also evaluate the effect of different treatments on the PDMS walls (native, plasma-treated and APTES (aminopropyltriethoxysilane)-treated PDMS) to induce the destabilization of droplets.

<sup>a</sup> Department of Food Engineering, Faculty of Food Engineering, University of Campinas, Rua Monteiro Lobato, 80-CEP 13083-862 Campinas, Brazil. E-mail: tatiana.porto90@gmail.com

<sup>b</sup> Microfluidics, MEMS, Nanostructures Laboratory, CNRS Chimie Biologie Innovation (CBI) UMR 8231, Institut Pierre Gilles de Gennes (IPGG), ESPCI Paris, PSL Research University, 6 rue Jean Calvin 75005, Paris, France. E-mail: cesare.cejas@gmail.com

† Electronic supplementary information (ESI) available. See DOI: 10.1039/d0sm01674h

‡ These authors contributed equally to this work.

In addition, we inject different components (deionized water or saline solution) inside the channels using two pressure values (20 or 200 mbar) in order to determine the influence of pressure-induced stress on emulsion destabilization. From careful control of the aforementioned experimental conditions, we demonstrate the existence of other subtle regimes (in addition to coalescence) triggering emulsion destabilization, and properly define the influence of these experimental conditions on the type of regime. In fact, we observe three regimes after the injection of deionized water: coalescence (due to the attraction between droplets), emulsion bursts (redistributed to the attraction between the droplet and the channel surface – defined as a rupture of the emulsions, *i.e.* they split open and the dispersed phase wets the surface wall) and a combination of both regimes occurring simultaneously. We additionally investigate the influence of the increase of ionic strength and, interestingly, we observe a fourth regime (fracture) that is triggered by an increase in emulsion stability promoted by the saline solution addition. This regime is replaced by other regimes over time, when emulsion stability decreases due to the continuous addition of salt to the system. Due to the complexity of both emulsion composition and channel surfaces, it is still a challenge to provide a unified view of all parameters affecting the destabilization. However, a clear correlation between emulsion features, surface of the channels, and type/pressure of the fluid injected inside the chamber could be established. Therefore, this work could indicate possible ways to either control or induce destabilization mechanisms, since the role of the most important properties modulating the regimes (surfaces properties of the channels, as well as interfacial tension and zeta potential of emulsions) has been properly elucidated.

## 2 Materials and methods

### 2.1 Microfluidic channel fabrication

We fabricate microfluidic devices using standard soft lithography. For this, we prepare chips made of poly(dimethylsiloxane) (PDMS) (Dow Corning, USA) by mixing Sylgard 184 silicone elastomer base and curing agent at a ratio of 10:1 (w/w), respectively, and use PDMS-spin coated glass slides (Spincoater Polos, SPS Europe) as a basis for PDMS chips. We produce two types of microchips with different applications: (1) the standard flow-focusing design (width = 50  $\mu\text{m}$   $\times$  height = 50  $\mu\text{m}$ ) for emulsion production and (2) microchambers for visualization of emulsion destabilization (Fig. 1). The latter has two different configurations depending on the applied pressure. In both chamber configurations, the height of the main channel and chamber are both 55  $\mu\text{m}$ , but the dimension of the small outlet channels varies according to the pressure applied (20 or 200 mbar) to allow a more controlled retention of droplets within the chamber limits. Fig. 1a shows the design observed on an optical profilometer NT9100 (Veeco, USA), representing the configuration we use for high-pressure experiments (200 mbar), in which the outlet channels have 20  $\mu\text{m}$  of height and 20  $\mu\text{m}$  of width (Fig. 1a – detail). In low-pressure studies

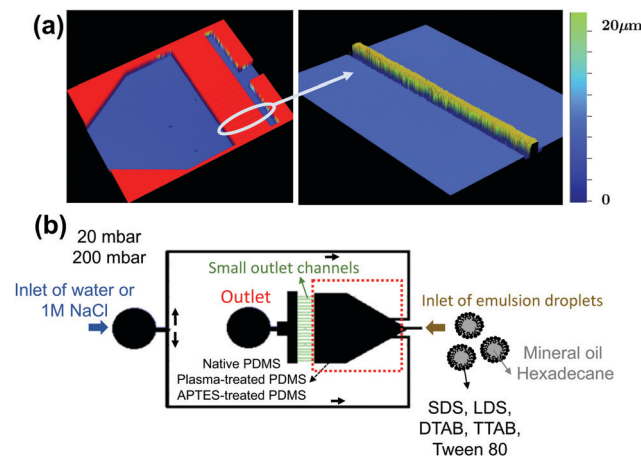


Fig. 1 (a) Profilometer image of the device highlighting the outlet channels used for high-pressure experiments (channel 20  $\mu\text{m}$   $\times$  20  $\mu\text{m}$ ). (b) Sketch of the microfluidic device used for emulsion destabilization studies and the controlled experimental conditions. Emulsions were injected and concentrated into the chamber (red dotted square) to achieve droplet close packing. The outlet refers to the outlet of the entire system, where emulsion droplets and either water or saline solution flow. The thin channels prior to the outlet contribute to maintaining the emulsions inside the chamber during destabilization experiments and ensure that the fluid passes through.




(20 mbar), on the other hand, we use bigger outlet channels (width = 20  $\mu\text{m}$   $\times$  height = 55  $\mu\text{m}$ ).

We apply different surface treatments to the flow-focusing devices for the production of emulsions with varied properties. For example, emulsions stabilized by positively charged surfactants should flow on positively charged surfaces to prevent droplet adhesion onto the wall and clogging. In addition, application of different treatments is essential to understand the role of surface properties on emulsion destabilization. Regardless of the treatment, we first submit the PDMS-chips and glass-coated slides to a plasma oxidation step in a plasma machine (Femto Science, Hwaseong-Si, South Korea) and immediately test some of these hydrophilic PDMS-chips (HI) after sealing onto glass-coated slides. In addition, some of these chips sealed with glass-coated slides are left in the oven at 95  $^{\circ}\text{C}$  for at least 5 hours (HO) so that the PDMS reverts back to its original hydrophobicity. Both hydrophobic (HO) and hydrophilic (HI) channels present negatively charged surfaces.<sup>19,20</sup> To render microchannels with positive charges, the chips are treated with 1% w/w aminopropyltriethoxysilane (APTES) in ethanol (98–99% purity) immediately after plasma oxidation for at least 15 min.<sup>21</sup> Then, we perform measurements of contact angle between water and the different surfaces (Table 1) by the sessile drop goniometric method using the Kruss DSA30 tensiometer (Kruss, France). Also,  $\zeta$ -potential of the walls ( $\zeta_w$ ) is estimated from literature (HI  $\sim$  –160 mV, HO  $\sim$  –70 mV, APTES  $\sim$  +80 mV and with saline solution (1 M NaCl) addition –20, –5 and +10 mV, respectively).<sup>19,20,22–25</sup>

### 2.2 Emulsion production and characterization

Oil-in-water emulsions are produced with a mean droplet diameter of approximately 40  $\mu\text{m}$  using a flow-focusing device.

**Table 1** Contact angle between water and microchannel surfaces

Microchannel surface	Contact angle (°)	
PDMS (HO) <sup>a</sup>	102.7 ± 2.1	
Plasma-treated PDMS (HI) <sup>b</sup>	42.9 ± 4.2	
APTES-treated PDMS (APTES)	81.4 ± 0.6	

<sup>a</sup> HO – hydrophobic. <sup>b</sup> HI – hydrophilic.

Droplets generation in an intermittent dripping flow regime is controlled by a pressure controller (model MFCS-EZ, Fluigent, Le Kremlin-Bicetre, France) and monitored within the microfluidic device using an optical microscope (model Eclipse, Nikon, Japan).

*n*-Hexadecane or light mineral oil (Sigma-Aldrich, USA) is used as dispersed phase, while aqueous phase is composed of deionized water and a surfactant. We use five different surfactants for this study: two anionic (sodium dodecyl sulfate (SDS) and lithium dodecyl sulfate (LDS)), two cationic (dodecyltrimethylammonium bromide (DTAB) and trimethyl(tetra-decyl) ammonium bromide (TTAB)) and a non-ionic (Polysorbate 80 (Tween 80)). All surfactants have a concentration of 1% w/w in the aqueous phase, but we also test SDS at a concentration of 0.1% w/w to demonstrate the effect of a reduced concentration (<critical micellar concentration (CMC)), in which the emulsions are not stable regardless of the microchannels properties. The physical properties of the oils (viscosity and density) are shown in Table 2. Density is measured with a pycnometer previously calibrated with deionized water, whilst viscosity is obtained using a stress-controlled rheometer AR1500ex (TA Instruments, New Castle, DE, USA). Steady state rheological properties of the oils are evaluated within shear rates from 0 to 300 s<sup>-1</sup>, observing Newtonian behavior within the evaluated range. We measure interfacial tension ( $\gamma$ ) between oil and aqueous phase using the pendant droplet method with a Kruss DSA30 tensiometer (Kruss, France). We determine the  $\zeta$ -potential of the emulsions ( $\zeta_e$ ) applying the Helmholtz–Smoluchowski model in a ZetaSizer Nano Series (Malvern Instruments, Worcestershire, UK) at 25 °C. Beforehand, emulsions were diluted (2 : 1 emulsion : dilution solution) in either deionized water or saline solution (1 M NaCl) and, just before the analysis, these solutions were further diluted in deionized water (1 : 1000). At least six measurements from each process were performed to obtain the results.

### 2.3 Microfluidic process destabilization

After production of the emulsions, we carefully introduce them inside the main chamber (Fig. 1b) with different surface treatments (native, plasma-treated and APTES-treated PDMS). After

packing the emulsions close to a random-close packing, we introduce deionized water or saline solution (1 M NaCl) in the chamber using a pressure-driven flow of either 20 or 200 mbar and the corresponding flow rate of the fluid is calculated based on the Poiseuille's law<sup>26</sup> considering laminar flow. The flow rate is determined based on the pressure difference between the inlet and outlet of the chamber and the resistances found along the passage of the fluid within the microchannels (SI-A and SI-B, ESI†). The resistances are related to both the channel and the emulsions themselves acting as a porous system (Wu *et al.*, 2008). To demonstrate the rapid introduction of the fluid injected into the chamber, we stain the fluid with fluorescein in different experiments (data not shown) and verify the fast flow using a video microscope Leica DMI8 (Leica, Germany) coupled to a camera C11440 (Hamamatsu, Japan) with time-lapse on the order of milliseconds.

Fig. 1b summarizes the different parameters that we analyze during the destabilization of emulsions within the microfluidic chamber. We combine different permutations of these parameters, resulting in 64 experimental conditions, each condition being tested at least twice. We evaluate the emulsion destabilization using a standard optical microscope and images are acquired at different intervals, whose frame rates depend on the applied pressure. After data acquisition, we perform image analysis using ImageJ and Matlab 2019 (Mathworks, MA, US). We analyze the destabilization events based on a motion tracking discrimination of the droplets in the chamber. We observe the regimes leading to emulsion destabilization during early times (first change-event) because, after extended periods of time, most of the droplets undergo fusion or coalescence (with or without surface wetting). However, the mechanisms of destabilization are explained by covering the entire observation time (later times: ~2 min for high-pressure studies and until 3 hours for low-pressure studies). In addition, to verify the formation of a double layer of droplets caused by compression in studies using high pressure, we employ confocal microscopy using a microscope Leica DMI8 (Leica, Germany).

## 3 Results and discussion

### 3.1 Emulsion characterization

Emulsion characteristics and the combination of different oil/aqueous phases are evaluated to establish relationships between these properties and the phenomena observed within the chambers. This section shows results of interfacial tension between the phases ( $\gamma$ ) and zeta potential of the emulsions ( $\zeta_e$ ). The interfacial tension is an indispensable property to be studied since thermodynamically unfavorable contact between the phases favors the destabilization of emulsion droplets. Therefore, emulsion stabilization can be modulated depending on the surface-active compound that is adsorbed onto the interfaces of the droplets.<sup>27,28</sup> In addition to interfacial tension, zeta potential of the emulsions should be quantified, as it is one of the most important parameters for determining the behavior of surfactants at the oil–water interface.<sup>29,30</sup>

**Table 2** Viscosity ( $\eta$ ) and density ( $\rho$ ) of the different oils

Oil (dispersed phase)	$\eta_{\text{oil}}$ (mPa s)	$\rho_{\text{oil}}$ (kg m <sup>-3</sup> )
Light mineral oil (M)	30.17 ± 0.12	846.6 ± 0.3
<i>n</i> -Hexadecane (H)	3.31 ± 0.02	771.9 ± 0.2

Tables 3 and 4 show that surfactants reduce the interfacial tension between the aqueous phase and the two tested oils (hexadecane and mineral oil) in the same way, because the difference between interfacial tension with pure water and that with aqueous phase containing surfactant is comparable. In addition, cationic surfactants provide the lowest  $\gamma$  values, especially the TTAB. However, in all cases a trend could be observed considering either water or salt addition. For instance, the addition of water increases  $\gamma$  due to the decrease of surfactant concentration, as predicted by the CMC theory. CMC is the critical micelle concentration, above which surfactants spontaneously form micelles.<sup>27</sup> But even under diluted conditions, interfacial tension values were quite lower as compared to that of pure water. On the other hand, the increase of ionic strength in the aqueous phase allows the reduction of  $\gamma$ . However, the increase of ionic strength presents a major effect on ionic surfactants, while Tween 80 (non-ionic) is only slightly affected.<sup>31,32</sup> Dehydration triggered by salt reduces the size of the surfactant head groups, improving their accommodation at the water–oil interface,<sup>33</sup> although an extreme size reduction may cause surfactant collapse.<sup>32,33</sup>

Moreover,  $\zeta_e$  (Table 5) decreases (in modulus) with the addition of saline solution. Indeed, salt screens surface charges,<sup>22,34–36</sup> which can facilitate interactions between the droplets themselves or between the droplets and the channel surface (when both have the same charge signal). An adequate reduction in the screening length may allow the destabilization of emulsions.<sup>37</sup> However, upon evaluating  $|\zeta_e|$ , we observe a major difference for SDS (an anionic surfactant), while LDS (also anionic) is the most salt-resistant surfactant, as the value

**Table 5** Zeta potential of emulsions ( $\zeta_e$ ) in different oil/surfactant experimental conditions

Emulsion: oil/ surfactant in aqueous phase	$\zeta_e$ (mV)	$\zeta_e$ (mV) in saline solution (ratio 1 : 1 aq. phase: 1 M NaCl solution) <sup>a</sup>	$ \Delta\zeta_e $ <sup>b</sup>
Mineral oil/SDS	$-51.2 \pm 0.6$	$-14.7 \pm 1.4$	36.5
Hexadecane/SDS	$-63.6 \pm 3.7$	$-16.2 \pm 0.5$	47.4
Mineral oil/LDS	$-56.5 \pm 3.5$	$-41.3 \pm 1.7$	15.2
Hexadecane/LDS	$-64.9 \pm 1.5$	$-50.5 \pm 0.7$	14.4
Mineral oil/DTAB	$+23.1 \pm 0.6$	$+1.1 \pm 1.1$	22.0
Hexadecane/DTAB	$+23.1 \pm 0.1$	$+1.4 \pm 0.1$	21.7
Mineral oil/TTAB	$+51.5 \pm 1.6$	$+32.6 \pm 0.8$	18.9
Hexadecane/TTAB	$+79.0 \pm 0.9$	$+19.6 \pm 0.7$	59.4
Mineral oil/Tween 80	$-42.9 \pm 2.2$	$-21.6 \pm 0.5$	21.3
Hexadecane/Tween 80	$-48.6 \pm 1.2$	$-26.7 \pm 1.3$	21.9

<sup>a</sup> This approximation was made based on the ratio emulsion : dilution solution applied to perform the analysis (2 : 1) and the fact that the emulsions have  $\sim 50\%$  v/v of aqueous phase. <sup>b</sup>  $|\Delta\zeta_e|$  represents the variation of zeta potential values after saline solution addition.

of  $\zeta_e$  is not much changed with salt addition. This enables the LDS surfactant to be used as a model in saline systems (*e.g.* in seawater). Furthermore, comparing  $\zeta_e$  of the cationic surfactants, DTAB provides the smallest value.<sup>38</sup> Despite both surfactants having the same polar head, the  $\zeta_e$  differences can be related to their binding tendencies to the droplet interface, which may be governed by the length of the hydrocarbon chain.<sup>38</sup> An important data to be highlighted is the negative  $\zeta_e$  value of Tween 80-stabilized emulsions. These negative charges may arise from either the residual molecules adsorbed onto the surface (*e.g.* OH<sup>−</sup> from aqueous phase) or surface-active impurities or contaminants present in surfactant composition.<sup>27,39,40</sup> Indeed,

**Table 3** Interfacial tension ( $\gamma$ , mN m<sup>−1</sup>) between hexadecane and aqueous solutions (containing different surfactants and diluted with water or saline solution)

Hexadecane					
Water	$28.65 \pm 0.06$				
Aqueous (aq.) phase surfactant	1% w/w surfactant	0.5% w/w surfactant	0.1% w/w surfactant	0.5% w/w surfactant in NaCl solution	0.1% w/w surfactant in NaCl solution
SDS	$2.30 \pm 0.05$	$3.83 \pm 0.02$	$20.58 \pm 0.39$	$0.50 \pm 0.00$	$1.50 \pm 0.00$
LDS	$6.48 \pm 0.26$	$7.48 \pm 0.06$	$10.22 \pm 0.10$	$1.00 \pm 0.00$	$1.11 \pm 0.00$
DTAB	$0.52 \pm 0.00$	$1.65 \pm 0.12$	$14.45 \pm 0.11$	$0.01 \pm 0.00$	$0.32 \pm 0.00$
TTAB	$0.50 \pm 0.00$	$1.60 \pm 0.02$	$3.58 \pm 0.09$	$0.01 \pm 0.00$	$0.02 \pm 0.00$
Tween 80	$6.69 \pm 0.06$	$7.31 \pm 0.02$	$7.35 \pm 0.04$	$5.58 \pm 0.03$	$5.11 \pm 0.01$

**Table 4** Interfacial tension ( $\gamma$ , mN m<sup>−1</sup>) between mineral oil and aqueous solutions (containing different surfactants and diluted with water or saline solution)

Mineral oil					
Water	$33.15 \pm 0.62$				
Aqueous (aq.) phase surfactant	1% w/w surfactant	0.5% w/w surfactant	0.1% w/w surfactant	0.5% w/w surfactant in NaCl solution	0.1% w/w surfactant in NaCl solution
SDS	$4.36 \pm 0.05$	$5.38 \pm 0.16$	$14.31 \pm 0.51$	$1.00 \pm 0.01$	$2.00 \pm 0.04$
LDS	$7.04 \pm 0.02$	$7.25 \pm 0.03$	$7.25 \pm 0.07$	$1.02 \pm 0.01$	$1.83 \pm 0.09$
DTAB	$2.22 \pm 0.04$	$2.52 \pm 0.13$	$14.48 \pm 0.18$	$0.30 \pm 0.00$	$1.95 \pm 0.05$
TTAB	$0.50 \pm 0.00$	$1.15 \pm 0.03$	$2.16 \pm 0.02$	$0.01 \pm 0.00$	$0.02 \pm 0.00$
Tween 80	$7.08 \pm 0.06$	$6.65 \pm 0.06$	$6.73 \pm 0.04$	$4.09 \pm 0.01$	$4.27 \pm 0.01$



several surfactants, such as Tween-80, may present free fatty acids in its composition, contributing to the negative charge of emulsions. Another possibility raised by other authors is that the counterions present within the medium can also adsorb at the droplet interface influencing the zeta potential of the emulsions.<sup>41</sup>

### 3.2 Diagrams of regimes leading to destabilization

After production of the emulsions, we pack or concentrate the emulsion droplets in the chamber shown in Fig. 1a and b. We inject a liquid stream into this chamber (saline solution or water), in order to allow the observation of different regimes of emulsion destabilization over time. The behavior of the emulsions within the chamber and an image showing each regime occurring during early and later times are shown in Fig. 2. During the experiments, we distinctly identify four regimes, namely: fracture, coalescence, emulsion bursts (defined as a rupture of emulsion, *i.e.* they split open and the dispersed phase wets the channel wall surface) and a combination of the latter two regimes (coalescence and emulsion bursts). Fracture is described by emulsions that have aggregated or adhered to each other due to packing compression and thus, as a result, move globally as a solid. Low energy sites within the compressed emulsion are points of local strain that eventually lead to displacement.<sup>42</sup>

Then, we plot diagrams relating the properties (interfacial tension between emulsion phases), contact angle and zeta potential of emulsions ( $\zeta_e$ ) and walls ( $\zeta_w$ ) in order to establish a correlation for these regimes. However, a single diagram could not be generated due to the complexity of the problem and the large number of parameters influencing the emulsion

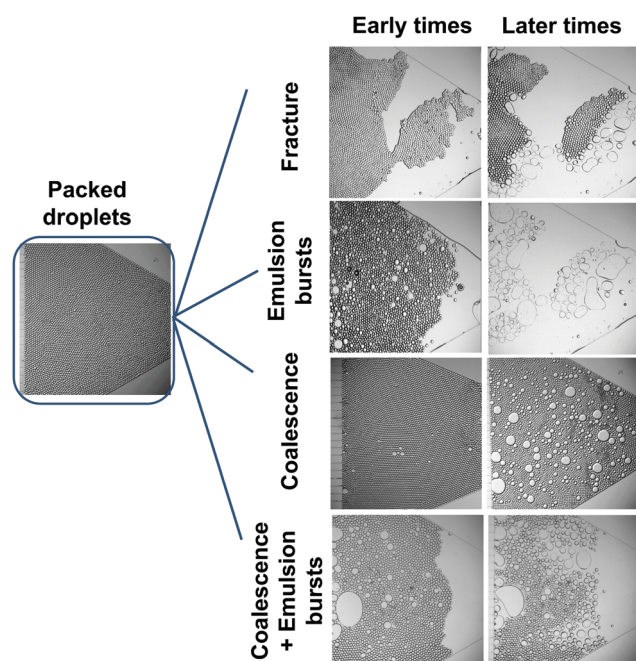


Fig. 2 Representative images of the different regimes leading to emulsion destabilization. Early times refer to the first change-event, while later times are  $\sim 2$  min for the high-pressure experiments demonstrated in this figure.

behavior. In order to plot the diagrams (Fig. 3), we focus only on the first change-event, because over long periods of time, a combination of regimes can occur that further complicates the problem. Initially, different mechanisms may occur and the regimes can be easily distinguished (coalescence, emulsion bursts, coalescence + emulsion bursts and fracture). However, in later time events, fracture may be overcome and other combination of regimes and mechanisms of destabilization may arise. In addition, all later time events would converge in coalescence (either with or without surface wetting) due to the “washing” and compression of droplet surfaces. The results suggest that the control of some parameters such as channel surface properties and emulsion composition can induce different regimes leading to destabilization. Next, the role of each variable will be discussed accordingly.

**3.2.1 Role of interfacial tension, ( $\gamma$ ).** Fig. 3(a and c) shows the role of interfacial tension on the kind of regime that triggers emulsion destabilization. Fracture (Fig. 3a and c (left)) is observed only with salt presence and within a determined range of interfacial tension (between  $0.5\text{--}1\text{ mN m}^{-1}$ ). However, destabilization mechanisms seem to depend mainly on the surface properties if the interfacial tension is not within this range ( $\ll 1$  or  $> 1\text{ mN m}^{-1}$ ). An extremely small  $\gamma$  value ( $\ll 1\text{ mN m}^{-1}$ ) leads to an association of phenomena (coalescence and emulsion bursts) regardless of the ionic strength of the medium (Fig. 3a (right and left)). In addition, when the product of  $\zeta_w\zeta_e$  is negative (meaning that emulsion and surface have opposite charged signs), emulsion bursts regime is always triggered regardless of interfacial tension values. On the other hand, emulsions with higher interfacial tension ( $\gamma > 1\text{ mN m}^{-1}$ ) show different regimes depending on the  $\zeta_w\zeta_e$ . A combination of the highest values of interfacial tension and  $\zeta_w\zeta_e$  (both emulsion and wall with the same charge) may induce greater repulsion between the surface and the droplets, leading to the coalescence regime. However, lower values of  $\zeta_w\zeta_e$ , or less repulsive charges (closer to zero, but positive) trigger emulsion bursts and surface wetting. Also, Fig. 3b shows that, when  $\zeta_w\zeta_e$  is positive (there are repulsive charges between emulsion droplets and channel surfaces), the regimes are highly influenced by the contact angle of the channels (except the fracture), which will be further detailed.

**3.2.2 Role of contact angle, ( $\theta$ ).** As aforementioned, when  $\zeta_w\zeta_e$  is positive, the regimes leading to destabilization seem to be mainly governed by the contact angle (hydrophilicity of the channel) and well-defined regions are observed in Fig. 3b and c. At high values of contact angle (HO surfaces), emulsion bursts regime occurs easily, while at low contact angle values (HI surfaces) coalescence takes place. In fact, a contact angle between HI ( $\sim 43^\circ$ ) and HO ( $\sim 103^\circ$ ), of around  $82^\circ$  (APTES-treated wall), leads to a combination of the two regimes (emulsion bursts and coalescence). The relationship between  $\zeta_w\zeta_e$  and the destabilization regimes will be detailed in the next topic.

**3.2.3 Role of  $\zeta_w\zeta_e$ .** Fig. 3a and b shows that when the product  $\zeta_w\zeta_e$  value is negative, *i.e.* droplets and channel surfaces have opposite signs, emulsion bursts always take place. In addition, when  $\zeta_w\zeta_e$  values are positive, emulsion bursts regime

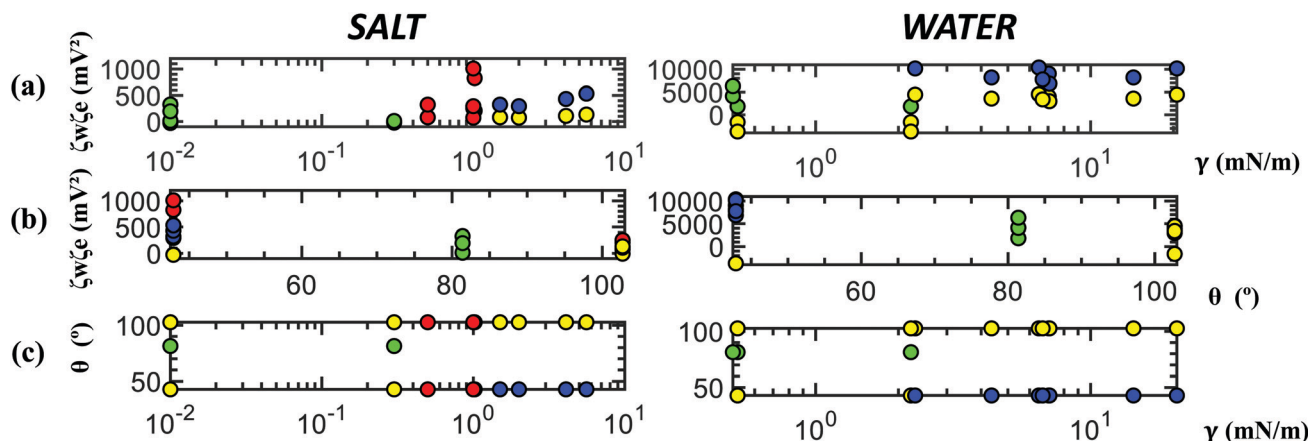


Fig. 3 Diagrams of the regimes leading to destabilization (coalescence (blue), emulsion bursts (yellow), coalescence + emulsion bursts (green) and fracture (red)) observed from different process conditions and emulsions properties. The regimes were evaluated as a function of interfacial tension ( $\gamma$ ), contact angle ( $\theta$ ) and  $\zeta_w \zeta_e$  (obtained by multiplying the values of zeta potential of both wall and emulsion).

occurs only at the lowest  $\zeta_w \zeta_e$  values, which means that repulsion between channel walls and droplets must be reduced for this type of destabilization mechanism to occur. Emulsion droplets must be close enough to the surface (less repulsive forces) to allow and favor the contact between the hydrophobic interfaces (oil and PDMS).<sup>20</sup> On the other hand, at the highest  $\zeta_w \zeta_e$  values, coalescence occurs due to the elevated repulsion between the droplets and the channel walls. Fig. 3b supports this fact, also considering the relationship with hydrophilicity/hydrophobicity of the channel (for positive  $\zeta_w \zeta_e$  values). Clearly, in addition to low  $\zeta_w \zeta_e$  values, HO surface is required to trigger emulsion bursts and surface wetting. On the other hand, the coalescence regime prevails in HI channels instead of emulsion bursts, due to the high repulsion and a thick hydration layer on the surface,<sup>34,43,44</sup> which disfavors the droplet attraction to the surface. Although the behavior is the same for either the addition of a saline solution or deionized water (Fig. 3a), the  $\zeta_w \zeta_e$  increase for water. In the latter, coalescence only occurs when  $\zeta_w \zeta_e > 5000$  mV<sup>2</sup>, whereas for saline solution, coalescence occurs with only  $\zeta_w \zeta_e \sim 300$  mV<sup>2</sup>. In the latter, it is probable that the hydration layer formed with ions from strong electrolytes (“strong ions” in saline solution) plays a more important role in hindering surface wetting because, at high electrolyte concentrations, hydrated cations can strongly bind to oxidized surfaces (e.g. HI surfaces after plasma-oxidation), generating a repulsive hydration energy (further details in Section 3.5).

The phenomenon of fracture depends on the hydrophobicity/hydrophilicity of the channel, but the range of  $\zeta_w \zeta_e$  changes with the wall surface properties (Fig. 3b – left). For instance, salt presence reduces both  $\zeta_w$  and  $\zeta_e$ , but for a certain surface, e.g. hydrophilic (HI),  $\zeta_w$  reduction is the same for all systems. Therefore, the parameter  $\zeta_w \zeta_e$  is mainly governed by the presence of salt in the emulsions ( $\zeta_e$ ), because  $\zeta_e$  changes as a function of the different applied surfactants. As a result, we also observe that the salt seems to behave distinctively in each type of emulsion (Table 5). In this sense, in HI surfaces, higher values of  $\zeta_w \zeta_e$  (meaning higher  $\zeta_e$  value, i.e. higher repulsion between the droplets, since  $\zeta_w$  is fixed for the HI surface) are

required to induce fracture, whereas in lower values of  $\zeta_w \zeta_e$  (or lower  $\zeta_e$  value) coalescence is favored. For HO, a low value of  $\zeta_w \zeta_e$  induces fracture, also strongly suggesting that  $\zeta_e$  is the principal factor that drives the mechanism, whether emulsion bursts or fracture. However, as very low  $\zeta_w \zeta_e$  values are needed for surface wetting (otherwise hydrophobic forces do not take place), a lower value (compared to HI surfaces) of this property allows the close-packed droplet structure to induce fracture-like behavior, thereby disfavoring the emulsion bursts regime.

### 3.3 Determination of time for the first emulsion change-event

The time it takes for the first change-event to occur in the emulsion droplets (Fig. 4) is quantified and we assess its impact by correlating this data with the process parameters and emulsion features. The most relevant parameter that affects the destabilization time is the magnitude of the pressure applied into the systems. Under high-pressure conditions, we use smaller outlet channels (greater resistance) to keep the droplets inside the chamber for longer periods. Thus, in such systems, despite having a pressure of one order of magnitude higher than the lower pressure systems, the flow rate remained in the same order of magnitude ( $\sim 1 \mu\text{L s}^{-1}$ ) for both systems. In this sense, the effect of pressure can be properly assessed. Evidently, application of higher pressure induces greater compression of the emulsions, leading to the formation of a compact bilayer of droplets and a rapid destabilization. The formation of the bilayer is confirmed by confocal microscopy images of the channel “slices” (Fig. 5a). Therefore, high-pressure systems induce destabilization not only by the addition of an external phase (saline solution/water), but also due to droplet compression. On the other hand, the destabilization of emulsions in low-pressure systems is more associated with either the “washing” of the droplet interface or the dissolution of the dispersed phase in the aqueous phase (triggered mainly by high ionic strengths). In this sense, a larger amount of fluid had to be flushed in low-pressure systems to reach the first change-event.

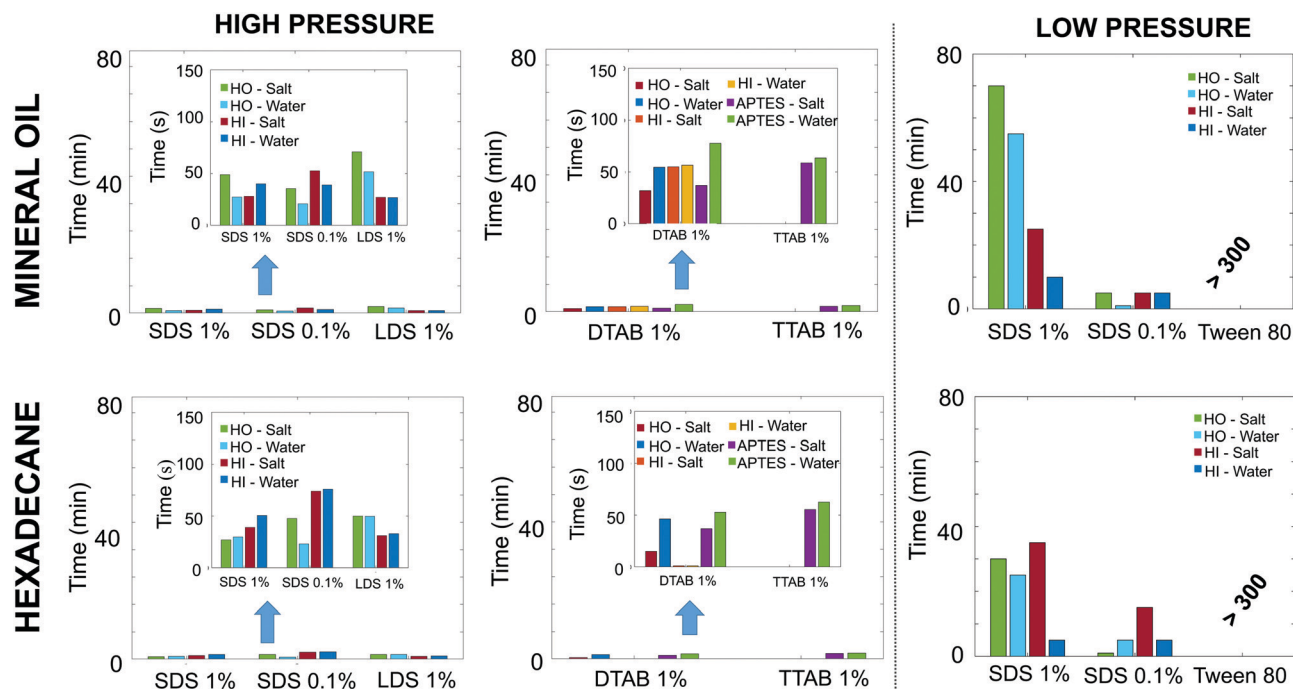


Fig. 4 Time for the first emulsion change-event to occur. \* Tween 80-based emulsions is subjected to high pressure but the same behavior as low pressure (no destabilization) is visualized.

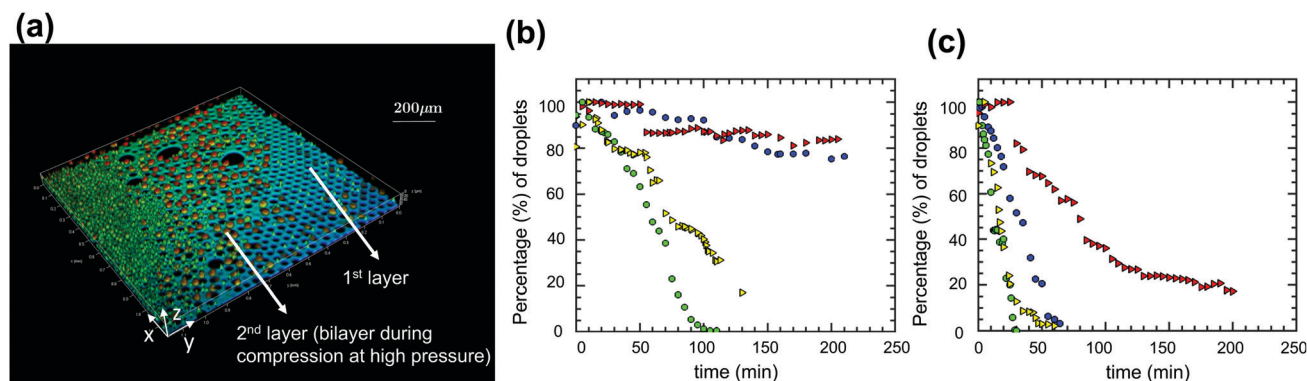


Fig. 5 (a) Confocal microscopy slice of a high-pressure experiment. Blue region indicates the 1st layer observed in both low- and high-pressure experiments, while orange and green regions correspond to the 2nd layer visualized only in high-pressure systems. (b) Percentage (%) of droplets visualized in a HO channel over time in SDS 1% (w/w). (c) Percentage (%) of droplets visualized in a HO channel over time in SDS 0.1% (w/w). In both cases, emulsions were prepared with mineral oil (red and blue) or hexadecane (green and yellow) and flushed with either saline solution (triangles) or water (circles).

In addition to the pressure, the type of fluid injected into the channels (saline solution/deionized water) also determines the first event (time and regime). However, as the destabilization time is delicate to interpret, the effect of the fluid can only be more precisely evaluated in low-pressure systems, because under high pressure a trend could not be properly observed due to the effect of droplet packing. In general, when comparing the same emulsion and process conditions (wall surface and low-pressure systems), water induces destabilization faster than saline solution. This can be explained mainly based on the decrease in the values of interfacial tension when salt is added

(Tables 3 and 4),<sup>45,46</sup> reinforcing the structure stability. However, further continuous injection of saline solution can promote more intense destabilization, since salt ions increase the likelihood of flocculation, dehydrate the surfactant head<sup>33</sup> and also increase the surface tension (water-air). Such effects may have triggered the “mixing” of the phases, detailed in Section 3.5. Also, values for  $\zeta_e$  (Table 5) and  $\zeta_w$  both decrease (in modulus) as ionic strength increases, indicating a reduction of repulsion between droplets and wall surface. In general, salt decreases the strength of electrostatic double layer forces (DLVO theory), reducing the energy barrier between the droplets, which

can lead to their aggregation and further disintegration.<sup>47</sup> In addition to the fluid injected into the system, another parameter inherent to the process is the nature of the channel surface (hydrophilic or hydrophobic). Although this parameter affects the behavior of the emulsions and the regimes leading to destabilization (Section 3.5), surface treatment ultimately does not significantly influence the time for the first event to occur (Fig. 4).

Comparing the two different oils used as dispersed phase (mineral oil and hexadecane), we could not distinguish their effect on emulsion stability. However, a data to be highlighted is regarding hexadecane droplets stabilized with cationic surfactants, as in these systems, destabilization occurs immediately after fluid injection (even when droplets are still entering inside the chamber), especially when the surface and the surfactants have opposite charges (attraction forces).<sup>20</sup> In fact, Tween 80 is the surfactant that provides the highest emulsion stability, and not even a single event was observed in 300 min at low (Fig. 4) and high pressure (data not shown). The high stability conferred by Tween 80 may be associated with the steric effect on stabilization, because DLVO theory suggests that non-ionic surfactants do not have enough repulsive barriers to avoid droplets agglomeration. However, the impurities and residues of Tween molecules that increase the charges on the systems (Table 5) can also improve the droplet stability. Emulsions with ionic surfactants, on the other hand, are stabilized mainly by electrostatic forces.<sup>37</sup> In addition, Tween 80, a non-ionic surfactant, presents a hydrophilic-lipophilic balance (HLB) value of 15, while SDS HLB value is 40.<sup>48</sup> A lower HLB value means that the surfactant molecule presents more hydrophobic sites. Therefore, Tween 80 has the ability to strongly adsorb on the oil/water interface because the driving force to leave the bulk phase and move towards the interface is high.<sup>37</sup> Indeed, previous studies have shown that the stability conferred by Tween 80 is higher compared to CTAB<sup>49</sup> and SDS.<sup>49,50</sup> Also, the physical barrier created by Tween 80 surfactants cannot simply be overcome with saline solution addition, therefore, even with salt addition, these droplets would not come close enough for van der Waals (vdW) forces to occur.<sup>37</sup> Moreover, it is confirmed that the increase of salinity also increases the stabilization capacity of non-ionic surfactants,<sup>51</sup> preventing adhesion between the droplets.<sup>52</sup> In this sense, the use of non-ionic surfactants can be advantageous in comparison to the application of charged molecules, because the stability of the former is not sensitive to high ionic strength. Supporting these results, the interfacial tension values between Tween 80 dispersions and different oils decrease with salt addition, but not as drastically as with ionic surfactants. Thus, this reduction may not be enough for the droplets to destabilize at short periods of time.

#### 3.4 Later time events: comparison between emulsions with different surfactant concentrations in low-pressure HO-system

As stated in Section 3.3, the effect of the fluid in the early stages (first change-event) could be only judiciously evaluated using low-pressure systems. Therefore, we also assess later events under the same conditions (low pressure). An advantage of the low-pressure system is that it allows the droplets to remain

within the chamber limits for the entire observation time. To assess the evolution of destabilization over time, one model system is chosen (SDS as surfactant and HO surface) where the number of droplets therein is counted. We chose this model system to observe the behavior of droplets over time as it presents repulsive charges and, therefore, the rate of droplets destabilization when either saline solution or water was added could be evaluated. The same test would be difficult to perform with systems containing attractive charges, as the rate of destabilization is very high.

Fig. 5b and c shows that, regardless of the concentration of surfactant, emulsions made with mineral oil are more stable than those prepared using hexadecane as dispersed phase, which was also observed visually during all experimental procedures. Furthermore, we could make a direct comparison between surfactant concentrations (similar to early times). Clearly, a lower surfactant concentration ( $C_{\text{surf}} = 0.1\% \text{ w/w} < C_{\text{CMC}}$ ) improves droplet destabilization, whilst  $C_{\text{surf}} = 1\% \text{ w/w} > C_{\text{CMC}}$  reduces its occurrence. CMC is the critical micelle concentration and, it is determined using interfacial tension analysis for SDS. We find that, using either mineral oil or hexadecane as dispersed phase, the calculated CMC of SDS is approximately 0.3% (w/w), corroborating the literature.<sup>53</sup> Comparing the injection of saline solution and deionized water, the increase of ionic strength triggers a slower destabilization, also agreeing with the results obtained in the early times. In early events, it is not possible to observe the influence of the oil on the destabilization phenomenon, mainly using a concentration of surfactant below CMC. By evaluating later events, this influence is revealed and clearly hexadecane reduces the stability of the emulsion droplets. This result is mainly associated with the intrinsic characteristics of this non-polar compound. Hexadecane not only has a viscosity ( $\sim 3 \text{ mPa s}$ ) ten times less than mineral oil ( $\sim 30 \text{ mPa s}$ ), but also a lower density, which can improve the separation process (Table 2). Observing a combination of data for both early and later times, it can be concluded that the determination of the time for events to occur is better evaluated under low-pressure conditions.

#### 3.5 Mechanisms of destabilization

The regimes leading to emulsion destabilization can be explained by the correlation between different surface (hydrophilicity/hydrophobicity and surface charge) and emulsion (surfactant charge and nature) properties, as well as the ionic strength of the injected fluid within the channel. Firstly, the injection of either deionized water or saline solution may have induced a rearrangement and a gradient of surfactant concentration on the surface of the droplets, triggering the drainage of the continuous phase and the Marangoni stress, which occurs in the interstitial space between emulsion droplets.<sup>54,55</sup> From this point on, different mechanisms could be observed and are shown in Fig. 6 and 7.

Fig. 6 shows the proposed mechanisms for channel surfaces and emulsion droplets showing repulsive charges and using anionic surfactants. When saline solution is added inside the microchannels with HO surfaces (Fig. 6a), the strong salt ions screen the repulsive electrostatic double layer on the droplets



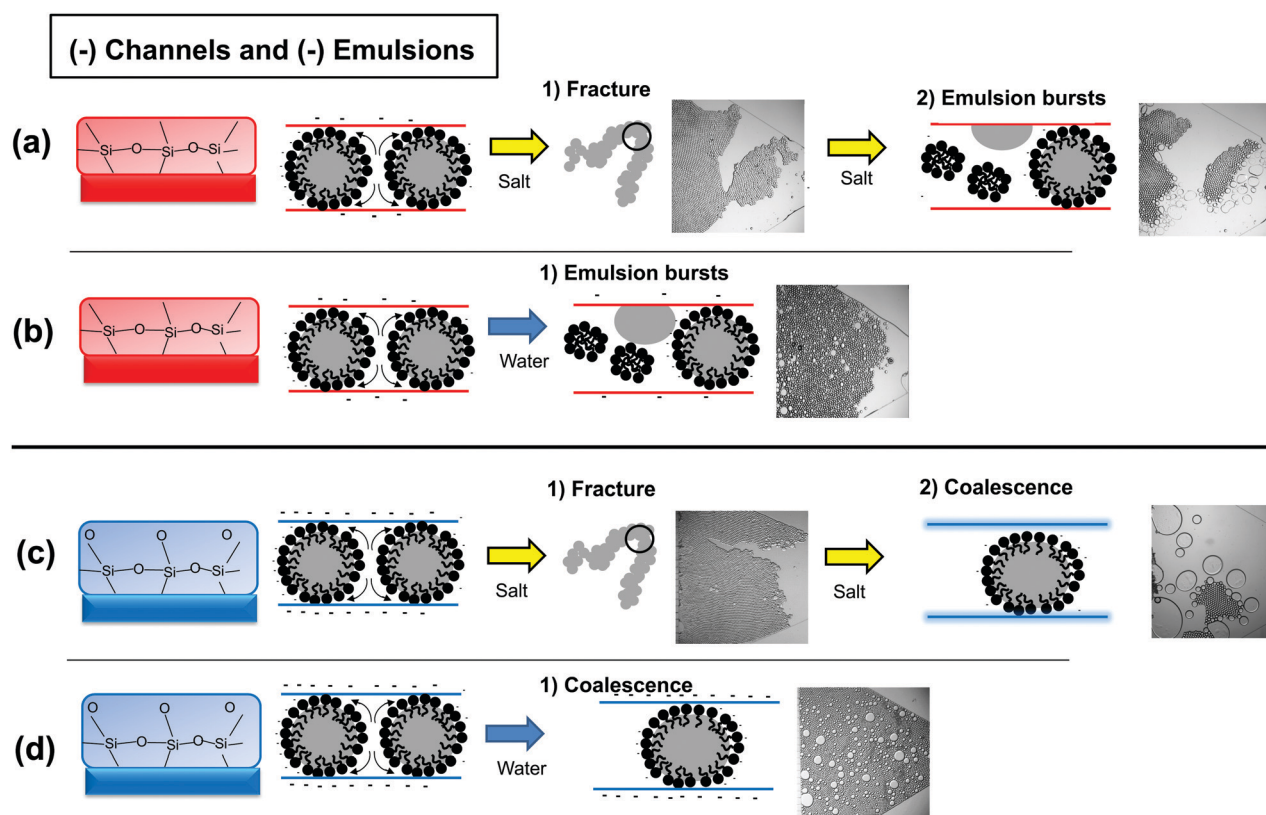


Fig. 6 Destabilization mechanisms of anionic surfactants in contact with different surfaces: (a and b) native PDMS (HO-red) and (c and d) plasma-oxidized PDMS (HI-blue) with the addition of saline solution or deionized water.

surfaces, allowing the attractive van der Waals forces between droplets to become more dominant.<sup>35</sup>

As the ionic strength in the medium increases, strong ions present in the aqueous solution decreases the available free water molecules, leading to disruption of the water structure around the polar head of the surfactant and, therefore, to depletion/dehydration of the hydration layer and contraction of the hydrophilic domains.<sup>33,56</sup> Such phenomena enable droplets to be in close contact, allowing the prevalence of van der Waals adhesion forces. If droplets are not close enough, despite the existence of attractive vdW forces, the repulsive forces generated by the electrostatic double layer remain predominant.<sup>20</sup> The vdW forces coupled with a close-packing of droplets (even to a small degree as in low-pressure systems) lead to an adhesion condition, forming droplet networks that can contract and result in increased droplet deformation.<sup>57</sup> These phenomena can, therefore, induce the appearance of low energy sites, giving rise to the fracture regime<sup>57</sup> during early times. Furthermore, NaCl has the capacity to reduce the polarity of the aqueous medium, allowing the decrease of the tension between the water–oil interface (as also seen in the interfacial results of Tables 3 and 4) and resulting in a non-zero contact angle between the droplets.<sup>56–58</sup> But, over time, the fracture regime is overcome and different phenomena contribute to the predominance of the emulsion bursts regime (when the oil wets the surface). Indeed, by further injecting salt into the aqueous medium, the head groups of surfactants become less

water-soluble and even more dehydrated. Thus, although first contributing to the vdW forces and fracture regime, continuous salt injection can subsequently lead to a collapse of surfactant head<sup>33,59,60</sup> and, consequently, to burst regime. In this case, surface wetting may have been induced by factors associated with a lesser repulsion between the channel walls and the droplets (salt also reduces channel surface charges), in addition to hydrophobic forces playing an important role in attracting the oil towards the surface wall. A mechanism similar to that observed for the HO surface is observed in HI surface (Fig. 6c). However, instead of emulsion bursts, coalescence occurs over time. Coalescence can be explained due to the use of oxidized PDMS surface. In this case, the surface is extremely negatively charged and, when saline solution is added, a strong hydration layer is formed.<sup>34,43,44</sup> This hydration layer is highly repulsive and surface wetting with oil should not occur, favoring instead the droplet interactions and, consequently, the coalescence. On the other hand, when water is added, an increase in interfacial tension between emulsion phases should occur due to dilution of the surfactant (as seen in the results of Tables 3 and 4). The same phenomenon occurs in HO (Fig. 6b) and HI surfaces (Fig. 6d), but emulsion bursts is clearly observed in HO surfaces, while coalescence rather takes place in HI surfaces. Emulsion bursts regime is probably induced by the increase of hydrophobic forces associated with the reduced intrinsic charges already present in HO surfaces. Coalescence, on the other hand, may have had the same origin attributed to the

presence of a strong hydration layer on the surface resulting from the introduction of the saline solution. At low ionic strength, the electrostatic double layer forces are even greater and the length of the Debye layer is as thick as possible.<sup>20,22,34,35</sup> The addition of another component, *i.e.* the highly-oxidized surface wall, further intensifies the repulsion forces between wall and droplets. As a result, these phenomena hinder the attraction of the droplets towards the surface wall of the microchamber and, therefore, they preferentially compress with each other.

Explaining it in greater detail, the fracture behavior can occur due to the continuous addition of saline solution. The increase in ionic strength makes the droplet packing denser and more concentrated owing to the screening of the repulsive EDL around the droplets, thereby making the van der Waals adhesion forces more dominant. As the overall droplet network becomes more

and more compact, it globally acts as a bulk soft material<sup>42,57</sup> that restructures and contracts as the adhesion forces continue to become stronger. This contraction is a result of the strong ions attracting water molecules and disrupting the water structure around the polar head of the surfactants. As previously mentioned, this phenomenon decreases the polarity of the aqueous medium<sup>33,56,58</sup> and, as a result leads to a non-zero contact angle between the droplets,<sup>57</sup> which ultimately contributes to the droplet deformation that accompanies the contraction of the droplet network. It is difficult to pinpoint where exactly in the droplet packing will the fracture begin to propagate but the rate of disruption caused by the strong salt ions may not be homogeneous across the bulk material, so locally water molecules in certain areas might be disrupted at a faster rate. This evidently induces local points of strain, which leads to deformation.<sup>42</sup>

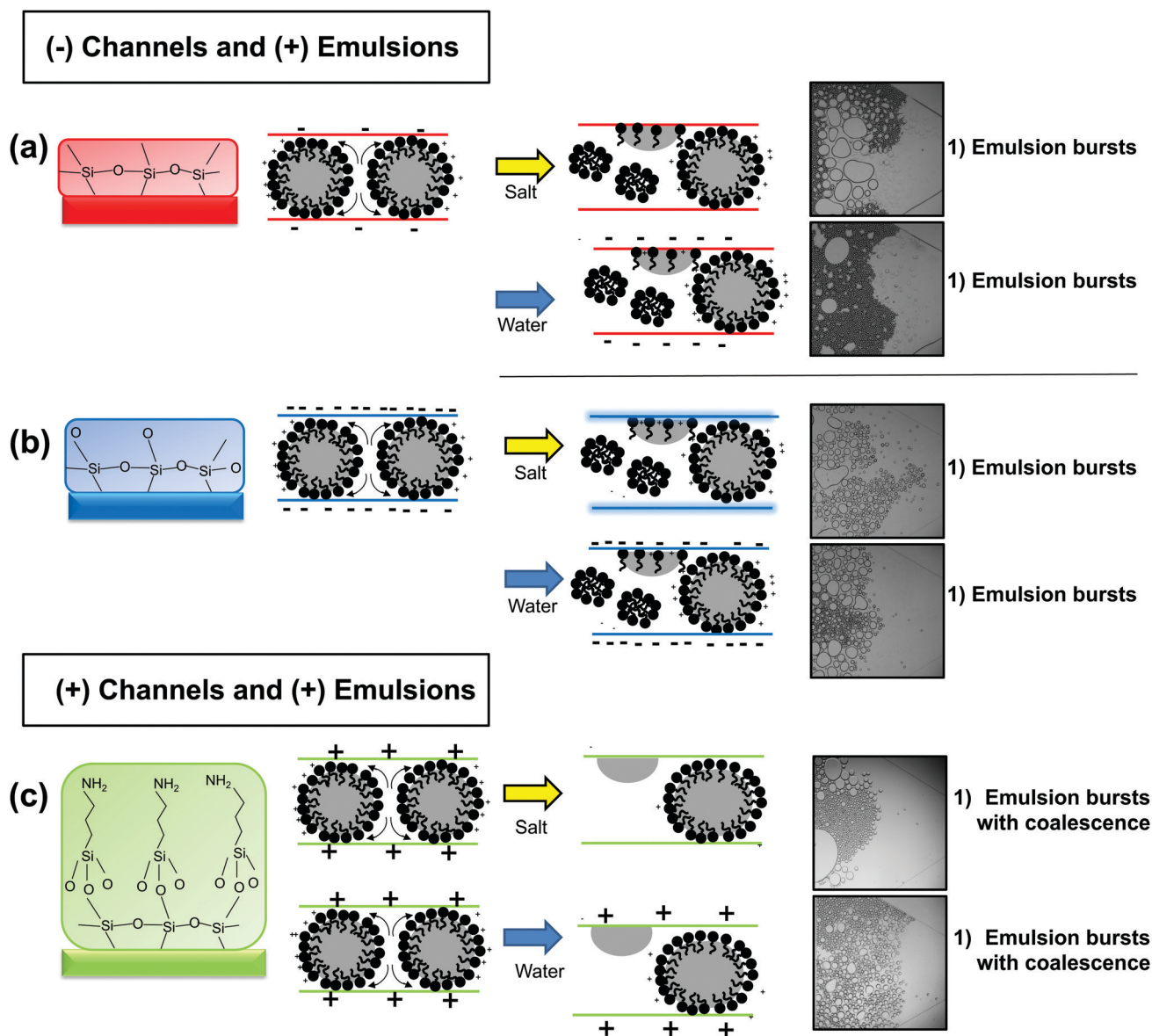


Fig. 7 Destabilization mechanisms of cationic surfactants in contact with different surfaces: (a) native PDMS (HO-red), (b) plasma-oxidized PDMS (HI-blue) and (c) APTES-treated PDMS (APTES-green) with the addition of saline solution or deionized water.

Ultimately, the emulsions bursts phenomenon is attributed to the attraction between the emulsion and channel surface, resulting in the adhesion of emulsion to the surface (through the rupture of the interfacial layer) and the spreading or wetting of the dispersed phase over the channel wall.<sup>61</sup> As more and more aqueous solution (whether saline/non-saline) is injected into the medium, this gradually washes or dilutes the surfactant surrounding the emulsion. However, as aforementioned, in the presence of salt, there is an additional phenomenon. As more saline solution is added, the salt dehydrates the surfactant head. For both cases, the continuous injection of aqueous solution (saline/non-saline solution) eventually reaches a critical moment when the interfacial layer ruptures, thereby allowing the dispersed phase to spread on the surface wall. The precise mechanisms may vary, *e.g.* depending on the type of surfactant or presence of salt, since it has been shown in earlier studies that emulsion rupture is a complex phenomenon resulting from a combination of reduced electrostatic, steric, or hydrophobic interactions.<sup>61,62</sup>

Fig. 7a and b shows the mechanisms of emulsion destabilization proposed for channel surfaces and droplets with attractive charges. After the addition of saline solution in systems with HO surfaces, we observe the same mechanism at later times (Fig. 7a) for anionic surfactants; however, no fracture regime is observed in early times. This may be due to the attraction of the droplets towards the surface, with reduced ability to aggregate to each other. On the other hand, attractive HI surfaces (Fig. 7b), in contrast to the HI repulsive systems (Fig. 6c), show emulsion bursts regime (and surface wetting) instead of coalescence after adding saline solution. Clearly, charges play a key role, and, despite the formation of a hydration layer, charges are sufficiently high enough to overcome this barrier.<sup>20</sup> The addition of deionized water leads to emulsion bursts regime and wetted channel walls (by oil) in both HO and HI surfaces (Fig. 7a and b). In both cases, the surfaces are negatively charged and, therefore, the opposite charges of both the surface and the emulsion droplets may have induced the faster wetting of the surface. For droplets (containing cationic surfactants) and channels with repulsive charges (using APTES as a hydrophobic and positively charged wall material) (Fig. 7c), we observe the same mechanism as the system with HO channel and negatively-charged surfactants, although no fracture occurs. Additionally, coalescence could also be observed simultaneously with emulsion bursts. This is possibly due to the nature of the surfactant (cationic) under salt exposure.<sup>52,57</sup> Although some cationic surfactants exhibit adhesion under very specific conditions (high viscosity of oil droplets combined with specific salts depending on the surfactant), they are most affected when salt is added, easily reducing the emulsion stability.<sup>52</sup>

## 4 Conclusion

In this paper, we demonstrate experimentally the ability of concentrated emulsions to undergo different destabilization

mechanisms through different regimes (coalescence, emulsion bursts, fracture or a combination of coalescence and emulsion bursts) in a confined microfluidic system. We also define the influence of the different experimental parameters on the type of regime. By adding deionized water to the system, only three regimes are observed: (i) coalescence, which is identified by the fusion of two or more contacting droplets or the attraction between emulsion droplets (ii) emulsion bursts, attributed to the attraction between the emulsion droplets and the channel surface, when the emulsions “split open” and the dispersed phase wets the surface wall, (iii) a combination of the two first mechanisms, which is attributed to the regime when coalescence and emulsion bursts occur at the same time. However, when saline solution is injected, a fourth regime emerges: fracture, which is described by emulsions that have aggregated or adhered to each other due to droplets packing and thus, as a result, move globally as a solid. These regimes are mainly governed by the properties of channels surface and emulsions. By controlling these properties, we can make the transition from one regime to another. However, the change in the ionic strength and pressure-induced stress of the fluids injected inside the channel also play an important role. The relationship between these parameters could be established using well-known surface wall characterization (such as contact angle between water and the different surfaces and zeta potential), as well as emulsion properties (interfacial tension and zeta potential). These relationships are translated in different diagrams that permit explanation of the different regimes using an interdisciplinary approach based on physical and chemical principles. To our knowledge, these four regimes have not yet been demonstrated experimentally in microfluidic systems, especially for emulsion destabilization. Nevertheless, because emulsions are extremely complex systems, it is still a challenge to provide a unified view of all properties affecting the destabilization in one single universal diagram. But since the role of each property has been revealed and properly explained, this work could provide insights into possible ways to control these regimes with respect to applications associated with stabilization or destabilization of emulsions.

## Conflicts of interest

There are no conflicts of interest to declare.

## Acknowledgements

This work is supported by ESPCI Paris, Institut Pierre Gilles de Gennes (laboratoire d'excellence, “investissements d'avenir” program ANR-10-IDEX-0001-02 PSL and ANR-10-LABX-31 and équipement d'excellence program ANR-10-EQPX-34). We also appreciate the support of CNRS Chimie Biologie Innovation (CBI) UMR8231 as well as CNRS Gulliver UMR7083 and the Microfluidics, MEMS, Nanostructures (MMN) group. We also thank the Sao Paulo Research Foundation – FAPESP (Grant numbers: #2017/18109-0 and #2018/18103-4) from Brazil that

supported Tatiana Porto Santos to do a PhD exchange program in Paris, France. Sao Paulo Research Foundation – FAPESP (Research aid – Regular project Grant number: #2019/07744-1) has also supported this work.

## References

- 1 X. H. Ge, J. P. Huang, J. H. Xu, J. Chen and G. S. Luo, *Soft Matter*, 2016, **12**, 3425–3430.
- 2 N. Purwanti, S. Ichikawa, M. A. Neves, K. Uemura, M. Nakajima and I. Kobayashi, *Food Hydrocolloids*, 2016, **60**, 98–108.
- 3 T. P. Santos, A. L. R. Costa, M. Michelo, L. P. Costa and R. L. Cunha, *J. Food Eng.*, 2020, **276**, 109884.
- 4 F. Y. Ushikubo, D. R. B. Oliveira, M. Michelin and R. L. Cunha, *Food Eng. Rev.*, 2015, **7**, 393–416.
- 5 J. C. McDonald and G. M. Whitesides, *Acc. Chem. Res.*, 2002, **35**, 491–499.
- 6 S. H. Tan, N. T. Nguyen, Y. C. Chua and T. G. Kang, *Biomechanics*, 2010, **4**, 032204.
- 7 N. N. Deng, S. X. Sun, W. Wang, X. J. Ju, R. Xie and L. Y. Chu, *Lab Chip*, 2013, **13**, 3653–3657.
- 8 L. M. Fidalgo, C. Abellb and W. T. S. Huck, *Lab Chip*, 2007, **7**, 984–986.
- 9 S. Marze, H. Algaba and M. Marquis, *Food Funct.*, 2014, **5**, 1481–1488.
- 10 Q. Meng, Y. Zhang, J. Li, R. G. H. Lammertink, H. Chen and P. A. Tsai, *Sci. Rep.*, 2016, **6**, 26953.
- 11 N. Bremond, A. R. Thiam and J. Bibette, *Phys. Rev. Lett.*, 2008, **100**, 024501.
- 12 G. F. Christopher, J. Bergstein, N. B. End, M. Poon, C. Nguyen and S. L. Anna, *Lab Chip*, 2009, **9**, 1102–1109.
- 13 D. Z. Gunes, M. Bercy, B. Watzke, O. Breton and A. S. Burbridge, *Soft Matter*, 2013, **9**, 7526–7537.
- 14 T. Krebs, K. Schroen and R. Boom, *Lab Chip*, 2012, **12**, 1060–1070.
- 15 Y. C. Tan, J. S. Fisher, A. I. Lee, V. Cristini and A. Phillip, *Lab Chip*, 2004, **4**, 292–298.
- 16 Y. C. Tan, Y. Ho, A. P. Lee, V. Cristini and A. Phillip, *Microfluid. Nanofluid.*, 2007, **3**, 495–499.
- 17 S. Abedi, N. S. Suteria, C.-C. Chen and S. Vanapalli, *J. Colloid Interface Sci.*, 2019, **533**, 59–70.
- 18 N. Bremond, H. Domejean and J. Bibette, *Phys. Rev. Lett.*, 2011, **106**, 244502.
- 19 B. J. Kirby and E. F. Hasselbrink, *Electrophoresis*, 2004, **25**, 187–202.
- 20 T. P. Santos, R. L. Cunha, P. Tabeling and C. M. Cejas, *Phys. Chem. Chem. Phys.*, 2020, **22**, 17236–17246.
- 21 J. H. L. Beal, A. Bubendorfer, T. Kemmitt, I. Hoek and W. M. Arnold, *Biomechanics*, 2012, **6**, 036503.
- 22 B. Mustin and B. Stoeber, *Langmuir*, 2016, **32**, 88–101.
- 23 C. Pick, C. Argento, G. Drazer and J. Frechette, *Langmuir*, 2015, **31**, 10725–10733.
- 24 A. Sze, D. Erickson, L. Ren and D. Li, *J. Colloid Interface Sci.*, 2003, **261**, 402–410.
- 25 D. Yan, C. Yang, N. T. Nguyen and X. Huang, *Electrophoresis*, 2006, **27**, 620–627.
- 26 J. Pfitzner, *Anaesthesia*, 1976, **31**, 273–275.
- 27 D. J. McClements, *Food emulsions: principles, practices, and techniques*, CRC Press, Boca Raton, FL, 2nd edn, 2005.
- 28 I. Gulseren and M. Corredig, *Colloids Surf., B*, 2013, **111**, 672–679.
- 29 N. Garti, Y. Slavin and A. Aserin, *Food Hydrocolloids*, 1999, **13**, 145–155.
- 30 M. Jayme, D. Dunstan and M. Gee, *Food Hydrocolloids*, 1999, **13**, 459–465.
- 31 M. J. Qazi, R. W. Liefferink, S. J. Schlegel, E. H. G. Backus, D. Bonn and N. Shahidzadeh, *Langmuir*, 2017, **17**, 4260–4268.
- 32 H. Schott, *J. Am. Oil Chem. Soc.*, 1988, **65**, 1658.
- 33 J. A. Molina-Bolivar, J. Aguiar and C. Carnero Ruiz, *J. Phys. Chem. B*, 2002, **106**, 870–877.
- 34 C. M. Cejas, F. Monti, M. Truchet, J. Burnouf and P. Tabeling, *Langmuir*, 2017, **33**, 6471–6480.
- 35 C. M. Cejas, F. Monti, M. Truchet, J. Burnouf and P. Tabeling, *Phys. Rev. E*, 2018, **98**, 062606.
- 36 C. M. Cejas, L. Maini, F. Monti and P. Tabeling, *Soft Matter*, 2019, **15**, 7438.
- 37 B. J. Palla and D. O. Shah, *J. Colloid Interface Sci.*, 2002, **256**, 143–152.
- 38 S. K. Mehta, S. Kumar and M. Gradzielski, *J. Colloid Interface Sci.*, 2011, **360**, 497–507.
- 39 S. Mun, E. A. Decker and D. J. McClements, *Food Res. Int.*, 2007, **40**, 770–781.
- 40 A. Gomes, A. L. R. Costa and R. L. Cunha, *Colloids Surf., B*, 2018, **164**, 272–280.
- 41 M. M. Sakuno, S. Matsumoto, S. Kawai, K. Taihei and Y. Matsumura, *Langmuir*, 2008, **21**, 11483–11488.
- 42 G. E. Gimenes and E. Bouchaud, *Soft Matter*, 2018, **14**, 8036–8043.
- 43 M. Dishon, O. Zohar and U. Sivan, *Langmuir*, 2009, **25**, 2831–2836.
- 44 Y. Wang, L. Wang, M. Hampton and A. Nguyen, *J. Phys. Chem. C*, 2013, **117**, 2113–2120.
- 45 J. J. Jasper, M. Nakonecznyj, C. S. Swingley and H. K. Livingston, *J. Phys. Chem.*, 1970, **74**, 1535.
- 46 A. G. Gaonkar, *J. Colloid Interface Sci.*, 1992, **149**, 256–260.
- 47 K. Abdolmeki, M. A. Mohammadifar, R. Mohammadi, G. Fadavi and N. M. Meybod, *Carbohydr. Polym.*, 2016, **140**, 342–348.
- 48 X. Zhu, Y. Liu, Z. Li and W. Wang, *Sci. Rep.*, 2018, **8**, 4015.
- 49 H. Esmaeili, F. Esmaeilzadeh and D. Mowla, *J. Chem. Eng. Data*, 2014, **59**, 1461–1467.
- 50 G. Stalidis, A. Avranas and D. Jannakoudakis, *J. Colloid Interface Sci.*, 1990, **135**, 313–324.
- 51 H. Esmaeili, F. Esmaeilzadeh and D. Mowla, *Iran. J. Chem. Chem. Eng.*, 2019, **38**, 151–166.
- 52 J. Bibette, F. Leal-Calderon, V. Schmitt and P. Poulin, *Emulsion Science: Basic Principles. An Overview*, Springer, 2002, vol. 181, ch. Surface forces, pp. 5–45.



- 53 Z. Sun, V. Nicolosi, D. Rickard, S. D. Bergin, D. Aherne and J. N. Coleman, *J. Phys. Chem. C*, 2008, **112**, 10692–10699.
- 54 B. Dai and L. G. Leal, *Phys. Fluids*, 2008, **20**, 040802.
- 55 S. Feng, L. Yi, L. Zhao-Miao, C. Ren-Tuo and W. Gui-Ren, *Chin. J. Anal. Chem.*, 2015, **43**, 1942–1954.
- 56 A. Pawlik, P. W. Cox and I. T. Norton, *J. Colloid Interface Sci.*, 2010, **352**, 59–67.
- 57 J. Bibette, T. G. Mason, H. Gang, D. A. Weitz and P. Poulin, *Langmuir*, 1993, 3352–3356.
- 58 M. P. Aronson and M. F. Petko, *J. Colloid Interface Sci.*, 1993, **159**, 134–149.
- 59 P. Versluis and J. C. van de Pas, *Langmuir*, 2001, **17**, 4825–4835.
- 60 T. Jiao, X. Liu and J. Niu, *RSC Adv.*, 2016, **6**, 13881.
- 61 D. M. Dresselhuis, G. A. van Aken, E. H. A. de Hoog and M. A. Cohen Stuart, *Soft Matter*, 2008, **4**, 1079–1085.
- 62 J. M. Dickhout, J. M. Kleijn, R. G. H. Lammertink and W. M. de Vos, *Soft Matter*, 2018, **14**, 5452–5460.

## Supplementary Information

# Unraveling Driving Regimes for Destabilizing Concentrated Emulsions within Microchannels

T. Porto Santos,<sup>\*,†,‡</sup> C. M. Cejas,<sup>\*,‡</sup> R. Lopes Cunha,<sup>†</sup> and P. Tabeling<sup>‡</sup>

<sup>†</sup>*Department of Food Engineering, Faculty of Food Engineering, University of Campinas,  
Rua Monteiro Lobato, 80-CEP 13083-862 Campinas, Brazil*

<sup>‡</sup>*Microfluidics, MEMS, Nanostructures Laboratory, CNRS Chimie Biologie Innovation (CBI)  
UMR 8231, Institut Pierre Gilles de Gennes (IPGG), ESPCI Paris, PSL Research University,  
6 rue Jean Calvin 75005, Paris, France*

E-mail: tatiana.porto90@gmail.com; cesare.cejas@gmail.com

### A: Resistance and flow rate calculations

A schematic of the microchamber is shown in Fig. 1. This microchamber houses the packed emulsion droplets. Pressure-induced stress occurs by injecting fluid (deionized water/saline solution) from the input. The fluid interacts with the emulsion packing and then exits at the output.

The resistance,  $R$ , of microchannels is calculated from the following equations.<sup>1,2</sup>

$$R = \frac{12\mu L}{WH^3} \left\{ 1 - \left[ \left( \frac{192W}{W\pi^5} \right) \tan \left( \frac{\pi W}{2H} \right) \right] \right\}^{-1} \quad (1)$$

where  $\mu = 10^{-3}$  Pa·s,  $L$  is the length,  $W$  is the width and  $H$  is the height of the microchannel chamber. The parameters  $L$ ,  $H$ , and  $W$  refer to different parts of the location in the chamber as explained below.

**For the triangular part of the chamber:**

$$L_{tri} = 2800\mu\text{m}; W_{tri} = 1650\mu\text{m}; H_{tri} = 55\mu\text{m}$$

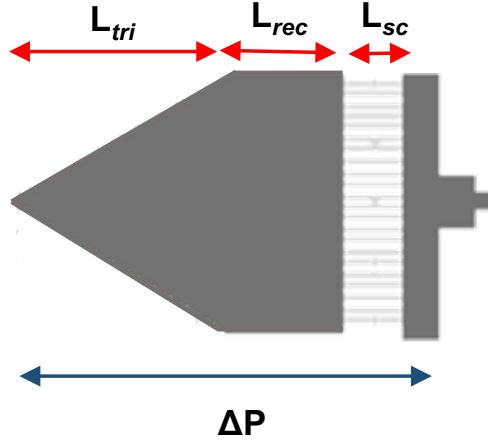


Figure 1: Sketch of the principal microchamber with its component parts. The entire microchamber can be subdivided into a triangular section (where  $L_{tri}$  is the length of this subsection), a rectangular section (where  $L_{rec}$  is the length of this subsection), and the section with the small channels at the outlet (where  $L_{sc}$  is the length of the small outlet channels). The pressure difference,  $\Delta P$ , is calculated across the entire total length of the microchamber.

Using Eq.1, we can calculate the resistance of the triangular chamber,  $R_{tri}$ .

**For the rectangular part of the chamber:**

$$L_{rec} = 1400\mu\text{m}; W_{rec} = 3300\mu\text{m}; H_{rec} = 55\mu\text{m}$$

Using Eq.1, we can calculate the resistance of the rectangular chamber,  $R_{rec}$ .

**For the small channels in the outlet:**

$L_{sc} = 1020\mu\text{m}; W_{sc} = 20\mu\text{m}; H_{sc} = 55\mu\text{m}$  or  $H_{sc} = 20\mu\text{m}$  (for  $P=20\text{mbar}$  and  $P=200\text{mbar}$  respectively).

Because the small channels are in parallel:

$$\frac{1}{R_{sc-total}} = \frac{1}{R_1} + \frac{1}{R_2} + \frac{1}{R_3} + \dots \frac{1}{R_N} \quad (2)$$

where  $N$  is the number of channels in the outlet,  $N = 22$ .

Since all resistances are equal ( $R_1 = R_2 = \dots = R_{sc}$ ), we can calculate the resistance of each individual outlet channel using the general Eq.1. The total resistance of all the small outlet channels combined is then:

$$R_{sc-total} = \frac{R_{sc}}{N} \quad (3)$$

**Total resistance of the entire microfluidic chip:**

From the aforementioned parameters, the total resistance of the entire chip is a series of its individual components:

$$R_T = R_{tri} + R_{rec} + R_{sc-total} \quad (4)$$

And the flow rate can be calculated from:

$$Q = \frac{\Delta P}{R_T} \quad (5)$$

where  $\Delta P$  is either 20 or 200 mbar (converted to Pa) and  $R_T$  is the total resistance from Eq.4.



## B: Permeability and flow rate calculations

When the interior of the microchannel chamber is packed with emulsion droplets, the system can be considered as a porous medium. Since we are injecting an external phase (saline solution/water) into the chamber, then the permeability of both emulsion droplet packing as well as the small channels should also be considered.

**Permeability of the small channels ( $k_{sc}$ ):**

$$\frac{dP_{sc}}{dL} = \frac{\Delta P}{L_{sc}} \quad (6)$$

where  $\frac{dP_{sc}}{dL}$  is the change in pressure per unit length of the small channels,  $L_{sc}$  is the length of the small channels and  $\Delta P$  is the pressure difference applied in the system. Thus, the permeability of the small channels,  $k_{sc}$ , can be calculated according to Eq.7.

$$k_{sc} = \frac{\mu Q}{WHN} \frac{dL}{dP_{sc}} \quad (7)$$

where  $W$ ,  $H$  and  $N$  are the width, height and number of the small channels, respectively:  $H = 55\mu\text{m}$  or  $20\mu\text{m}$  and  $N = 22$ ;  $Q$  is the flow rate obtained from Eq.5 and  $\mu = 10^{-3}$  Pa.s.

**Permeability of the the emulsion droplet packing ( $k_{drop}$ ):**

$$\frac{dP_{total}}{dL} = \frac{\Delta P}{L_{tri} + L_{rec} + L_{sc}} \quad (8)$$

where  $\frac{dP_{total}}{dL}$  is the change in pressure per unit length of the entire system,  $L_{sc}$ ,  $L_{tri}$ , and  $L_{rec}$  are the length of the small channels, the triangle chamber, and the rectangle chamber respectively.  $\Delta P$  is the pressure applied in the system.

$$\frac{\sigma}{\sigma_0} = \left[ \frac{\varphi - \varphi_c}{1 - \varphi_c} \right]^u \quad (9)$$

where  $\frac{\sigma}{\sigma_0}$  is the conductivity of the fluid phase within the porous material with respect to the fluid's bulk conductivity.<sup>3</sup>  $\varphi = 0.64$  is the porosity of the emulsion packing in quasi-2D cases assuming random close packing,  $\varphi_c = 0.32$  is the percolation threshold of overlapping droplets in quasi-2D

and  $u = 1.3$  is the critical exponent.

The permeability of the porous medium (emulsion droplet packing),  $k_{drop}$ , is:

$$k_{drop} = C(l_c)^2 \frac{\sigma}{\sigma_0} \quad (10)$$

where  $C=1/12$  is a constant for 2D systems;  $l_c = 40\mu\text{m}$  is the local pore geometry (usually the same order of magnitude of droplet size).

Therefore, total permeability is:

$$k_{total} = k_{sc} + k_{drop} \quad (11)$$

And the actual flow rate is:

$$Q_{final} = \left( \frac{k_{total}}{\mu} \right) \cdot P_{total} \cdot W \cdot H \cdot N \quad (12)$$

where  $W$ ,  $H$ , and  $N$  are the width, height, and number of small channels respectively. In Eq.12, the area considered is  $W \cdot H \cdot N$  and  $\mu = 10^{-3}\text{Pa}\cdot\text{s}$ .

## References

- (1) Tabeling, P. *Introduction to Microfluidics*; Oxford University Press: Oxford, UK, 2005.
- (2) Fuerstman, M. J.; Lai, A.; Thurlow, M. E.; Shevkoplyas, S. S.; Stone, H. A.; Whitesides, G. M.  
The pressure drop along rectangular microchannels containing bubbles. *Lab Chip* **2007**, *7*,  
1479–1489.
- (3) Scholz, C.; Wirner, F.; Gotz, J.; Rude, U.; Schroder-Turk, G. E.; Mecke, K.; Bechinger, C.  
Permeability of Porous Materials Determined from the Euler Characteristic. *Phys. Rev. Lett.*  
**2012**, *109*, 264504.

## CAPÍTULO 6

### **Colloidal particle deposition on microchannel walls, for attractive and repulsive surface potentials**


Artigo publicado no periódico “Physical Chemistry Chemical Physics”

*Reproduced from the Ref. Santos, T. P., Cunha, R. L., Tabeling, P., Cejas, C. M. Colloidal particle deposition on microchannel walls, for attractive and repulsive surface potentials. Physical Chemistry Chemical Physics, 22, 17236-17246, 2020. <https://doi.org/10.1039/D0CP01999B> with permission from the PCCP Owner Societies.*



Cite this: *Phys. Chem. Chem. Phys.*,  
2020, 22, 17236

# Colloidal particle deposition on microchannel walls, for attractive and repulsive surface potentials†

Tatiana Porto Santos, <sup>‡\*ab</sup> Rosiane Lopes Cunha,<sup>a</sup> Patrick Tabeling<sup>b</sup> and Cesare M. Cejas <sup>‡\*b</sup>

Surface interactions are an interplay of van der Waals adhesion forces with electrostatic charges. In colloidal deposition, at low ionic strengths, the Debye layer is sufficiently large to prevent particles from approaching the surface. It is only with the addition of higher salt concentrations, typically above 0.1 M, that surface charges are screened for interactions to take place *via* van der Waals-adhesion forces. This is true for repulsive charges, when both surfaces have similar charges and signs of the zeta potential are the same. However, with attractive charges, where zeta potential signs are opposite, the result is also opposite. By combining microfluidic experiments, theory, and numerical simulations, results show that when charges are attractive, particle deposition instead increases at low ionic strengths (at greater Debye lengths), at rates controlled by van der Waals forces but assisted by electrostatic forces. We propose a mechanism where particles approach the wall, mobilized by electrostatic attraction, up to a distance where van der Waals forces come into play, collecting the particles at the wall, which electrostatic forces alone are unable to achieve, owing to hindered diffusion. The present work thus allows us to understand the different mechanisms that govern deposition in the case where surface charges are opposite.

Received 13th April 2020,  
Accepted 9th July 2020

DOI: 10.1039/d0cp01999b

rsc.li/pccp

## 1 Introduction

Colloidal deposition on channel surfaces is a delicate interplay of adhesion, electrostatic, and longitudinal and transverse diffusion forces.<sup>1–10</sup> Recent literature<sup>2,5,8,11</sup> has demonstrated the existence of different deposition regimes, each dominated by a certain force such as van der Waals forces (van der Waals regime) and electrostatic forces (Debye regime), as well as the conditions that define their transitions. Thus, as also suggested by the DLVO theory,<sup>3,12–16</sup> by playing with parameters that permit one force to supercede the other, we can move from adhesion-dominated van der Waals (defined by the Hamaker constant,  $A$ ) to electrostatic-dominated (defined by the  $\zeta$  potential) interaction.

Zeta potentials,  $\zeta$ , play a non-negligible role in electrokinetic phenomena of colloidal dispersions,<sup>17</sup> especially in particle mobility, colloidal stability, surface interactions<sup>18</sup> and consequently in the design of microfluidic channels.<sup>19</sup> The  $\zeta$  potential describes the strength of the surface charges<sup>14</sup> within the electrostatic double layer (EDL) or Debye layer,<sup>20</sup> shown in Fig. 1, defined by the Debye length,  $\lambda_D$  or  $\kappa^{-1}$ . For a monovalent salt,  $\lambda_D$  typically decreases with increasing salt concentration. The  $\zeta$  potentials are determined using electrokinetic techniques<sup>21</sup> (usually with a Zetasizer) *via* electrophoresis<sup>22–24</sup> or streaming potentials<sup>25,26</sup> or electroosmosis.<sup>18,27–29</sup>

Signs of  $\zeta$  potentials determine whether surface charges are attractive or repulsive. In particular for microfluidics, microchannel walls are usually made of polymers and exposed to water molecules that interact onto the surface. As a result, charges on the channel wall are often negative. Most colloidal particles in aqueous suspensions are also negatively-charged to prevent agglomeration and aggregation.<sup>14</sup> Thus, the most common surface interaction behavior under aqueous conditions reported in literature<sup>2,5–8</sup> involves straightforward repulsion<sup>30</sup> (similar charges) and that at low salt concentrations, the magnitude of the  $\zeta$  potential is high such that insipid aggregation is observed.<sup>16</sup> DLVO theory, along with experiments and numerics<sup>2,5</sup> predicts that at low ionic strengths, especially for

<sup>a</sup> Department of Food Engineering, Faculty of Food Engineering, University of Campinas, Rua Monteiro Lobato, 80-CEP 13083-862 Campinas, Brazil.  
E-mail: tatiana.porto90@gmail.com

<sup>b</sup> Microfluidics, MEMS, Nanostructures Laboratory, CNRS Chimie Biologie Innovation (CBI), UMR 8231, Institut Pierre Gilles de Gennes (IPGG), ESPCI Paris, PSL Research University, 6 rue Jean Calvin 75005, Paris, France.  
E-mail: cesare.cejas@gmail.com

† Electronic supplementary information (ESI) available: SI: A–D. See DOI: 10.1039/d0cp01999b

‡ These authors contributed equally to this work.

highly-charged particles,<sup>16</sup> the Debye layer is sufficiently large to exert repulsion between surfaces and deposition is almost (if not) zero. It is only with increasing salt concentrations, typically at  $\geq 0.1$  M salt, where surface charges are screened and particle-surface interactions take place *via* van der Waals-adhesion forces.

When two surface charges are opposite,  $\zeta$  potential signs are opposite, attraction naturally takes place as in the case of oppositely-charged colloids,<sup>31–33</sup> where there is an increasing heteroaggregation rate at decreasing monovalent salt levels.<sup>32,34</sup> This is also described by DLVO theory due to a decrease in stability when double layer forces are attractive.<sup>30,32,35</sup> Repulsion has also been observed between oppositely-charged surfaces but only in the presence of multivalent electrolytes,<sup>36,37</sup> which induces charge reversal or inversion caused by the presence of complex ions.<sup>16,36</sup> Classically, for monovalent salts, it has been demonstrated that when charged colloids approach a charged collector surface, interaction forces are developed causing enhanced deposition rates in the presence of attractive EDL interactions.<sup>30,38</sup> However, most of these studies have been limited to theory and numerics.<sup>38</sup> To our knowledge, most experimental studies focus on colloids and collectors of similar charges and there are only a limited number of experiments<sup>30</sup> that investigate particle deposition on surface collectors with opposite charges.

With the advent of microfluidics and its many applications involving particle flow and deposition in constrictions such as microchannels, we believe it is important to revisit the phenomenon experimentally by understanding the role of the ionic strength and surface treatments. More importantly, we aim to understand at which point do the van der Waals forces, which are universal, play a role when surface charges are opposite.

In this paper, we demonstrate experimentally that at high ionic strengths, the salt ions screen surface charges, permitting a high quantity of colloidal deposition on the surface *via* van der Waals forces. However, at lower ionic strengths,  $< 0.1$  M salt, we find an even higher quantity of deposited particles on the microchannel surface. Classic literature<sup>30</sup> points out that even with attractive EDL forces, van der Waals forces have no effect and deposition is purely controlled by EDL interactions. On the contrary, we find that particle deposition at low ionic strengths instead increases at rates controlled by van der Waals forces, independently of the salt concentration. We experimentally demonstrate this behavior using flow visualization in microfluidics and characterization of particle hydrodynamics (mobility) and deposition behavior (particle-surface interactions) across multiple magnitudes of aqueous salt concentrations,  $C_{\text{salt}}$ , and different surface charge treatments. We support experimental results with theoretical analysis and numerical simulations based on Langevin equations.

## 2 Materials and methods

### Microfluidic channel fabrication

Microfluidic channel fabrication is performed using standard soft lithographic techniques and chip preparation using

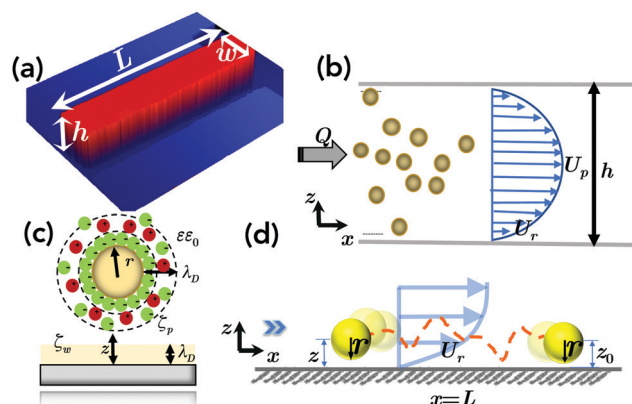


Fig. 1 (a) Microfluidic chip of a single rectangular channel with dimensions,  $h$  (height),  $w$  (width),  $L$  (length). Total dimension is  $h \times w \times L$ , where  $h \ll w$ . (b) Scheme of the model with a particle concentration injected at flow rate,  $Q$ . Average particle flow speed,  $U_p$ , follows Poiseuille fluid velocity profile with near-wall velocity,  $U_r$ , which is the velocity at a distance  $z \approx r$ , where  $z$  is the distance between particle center and wall. (c) Scheme of particle of radius,  $r$ , interacting close to wall with the following parameters: electrostatic Debye layer,  $\lambda_D$ ; dielectric constant,  $\epsilon$ ; permittivity of free space,  $\epsilon_0$ ; zeta potential of particle surface,  $\zeta_p$ ; and zeta potential of surface walls,  $\zeta_w$ . (d) Trajectory of a particle close to the wall, initially at position  $z$  and then at final position  $z_0$ .

polydimethylsiloxane, PDMS (Sylgard 187, Dow Corning, France).<sup>1,2,10</sup> The motif presented six parallel rectangular channels connected to an entrance and exit reservoir. The channels have a distance of  $150 \mu\text{m}$  apart to limit cake formation<sup>1,2,10</sup> and that each channel could act independently. Fig. 1(a) shows one of these channels taken using a profilometer (Veeco Instruments, NY, USA), which have the following dimensions: height  $h = 20 \mu\text{m}$ , width  $w = 100 \mu\text{m}$ , and length,  $L = 400 \mu\text{m}$ . We also prepare glass slides coated with a  $30 \mu\text{m}$ -layer of PDMS using a spin coater (SPS Europe, Germany). The PDMS-coated glass slides served as the base of the PDMS chips.

### Different surface treatments

Different surface treatments are chosen in order to characterize various particle-wall interactions. In all cases, chip bonding on glass slides requires an oxidation step with a plasma machine (Femto Science, South Korea). For hydrophobic native PDMS, chips are left in the oven at  $95^\circ\text{C}$  for at least 1 hour to be reverted back to its original state. For hydrophilic PDMS, the chips are used immediately after oxygen plasma-treatment. To introduce covalent positive charges on the PDMS surface walls, the chips are treated with aminopropyltriethoxysilane (APTES) after plasma treatment<sup>39</sup> for at least 15 min.

Schemes of the surfaces are shown in Fig. 2. Native PDMS surfaces mainly consists of siloxane groups,  $(\text{CH}_3)_2\text{Si}-\text{O}$ , which do not readily dissociate. The methyl groups render the surface hydrophobic. In the presence of water, PDMS chains are collapsed and water molecules interact with PDMS *via* water- $\text{CH}_3$ , water-Si, and water-O hydrogen-bonding interactions, although this H-bonding is not expected to be significant.<sup>40</sup> The highly-negative oxygen atom in water, forming a layer

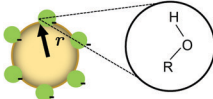
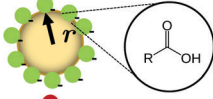
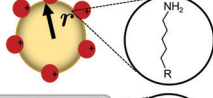
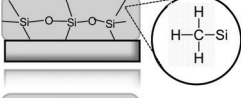
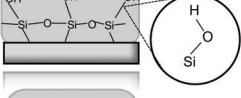
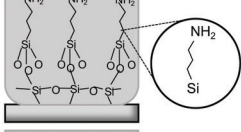
		Surface Group Ionization	Origin of Zeta potential	Zeta potential $\zeta$	Acidic/Basic Strength of Surface Groups
PS-plain		$\text{ROH} + \text{H}_2\text{O} \rightleftharpoons \text{RO}^- + \text{H}_3\text{O}^+$	Negatively-charged hydroxyl anions	$-15.0 \pm 1.1 \text{ mV}^*$	ROH group: weak acid
PS-fluo		$\text{RCOOH} + \text{H}_2\text{O} \rightleftharpoons \text{RCOO}^- + \text{H}_3\text{O}^+$	Negatively-charged carboxylate anions	$-57.0 \pm 3.1 \text{ mV}^*$	RCOOH group: moderately weak acid
PS-amine		$\text{RNH}_2 + \text{H}_2\text{O} \rightleftharpoons \text{RNH}_3^+ + \text{OH}^-$	Positively-charged ammonium ions	$+15.0 \pm 0.9 \text{ mV}^*$	RNH <sub>2</sub> group: moderately weak base
Native PDMS		$\text{SiOH} + \text{H}_2\text{O} \rightleftharpoons \text{SiO}^- + \text{H}_3\text{O}^+$	Negatively-charged oxygen atoms from water	-10 to -60 mV†	H <sub>2</sub> O: weak acid
Plasma-treated PDMS		$\text{SiOH} + \text{H}_2\text{O} \rightleftharpoons \text{SiO}^- + \text{H}_3\text{O}^+$	Negatively-charged oxide anion	-20 to -100 mV†	SiOH group: weak acid
APTES-treated PDMS		$\text{RNH}_2 + \text{H}_2\text{O} \rightleftharpoons \text{RNH}_3^+ + \text{OH}^-$	Positively-charged ammonium ions	+18 to +100 mV†	RNH <sub>2</sub> group: moderately weak base

Fig. 2 Different surface groups on PS particles and PDMS surfaces, their ionization mechanism, information on zeta potential, and their acidic/basic strength. Non-functionalized PS-plain particles have less negative charges than PS-fluo. PS-amine particles, on the other hand, have positive surface charges. \* Measured experimentally using ZetaSizer with deionized water (no salt) at  $T = 22.6^\circ\text{C}$  and  $\text{pH} = 5.78 \pm 0.02$  (PS-fluo),  $\text{pH} = 6.05 \pm 0.07$  (PS-plain), and  $\text{pH} = 6.74 \pm 0.18$  (PS-amine). The pH values are also measured using deionized water. † Determined numerically from simulations at low ionic strengths. Adsorption results do not significantly change within this given range.

above the PDMS surface, provides the negative  $\zeta$  of native PDMS in aqueous solution.

For plasma-treated PDMS, the surface mainly consists of silanol groups,  $\text{R}_2\text{Si}-\text{OH}$ , which readily dissociates into  $\text{R}_2\text{Si}-\text{O}^-$ , thereby providing a negative zeta potential. Silanol groups also provide the hydrophilic nature of plasma-treated PDMS.

For APTES-treated PDMS, the surface mainly consists of an aliphatic amine groups (aminopropyl). In aqueous suspensions, the  $\text{RNH}_2$  group is protonated to yield positively-charged ammonium ion,  $\text{RNH}_3^+$ .

### Aqueous particle suspensions

Aqueous particle suspensions are prepared using a commercial fluorescent polystyrene (PS) latex aqueous suspensions, (PS-fluo, Thermo-Fisher, France). The PS-fluo particles are functionalized with carboxylate surface groups with yellow/green fluorophore and most of the fluorophore is expected to be buried in the particle core.<sup>41</sup> In aqueous suspensions, carboxylic acids slightly ionize to form moderately acidic solutions. The H from the carboxylate group dissociates to yield a highly negative carboxylate anion  $\text{COO}^-$ .

In contrast, natural latex particles (PS-plain, Sigma-Aldrich, France) are not specifically functionalized but may be slightly negative due to trace amounts of initiator during polymerization.<sup>41</sup> In some particles, this initiator is potassium persulfate, however in our particles, hydrogen peroxide was used according to the manufacturer, resulting to a hydroxyl surface.

We also use amine-modified latex particles (PS-amine, Invitrogen, France), which contains a high density of amine groups attached to the terminus of an aliphatic six-carbon spacer arm. In aqueous suspensions, the  $\text{RNH}_2$  group is protonated to yield positively-charged ammonium,  $\text{RNH}_3^+$ .

For all particle suspensions, we prepare different concentrations by varying  $C_{\text{salt}}$  spanning  $10^{-5}$  to 1 M NaCl. Samples are extensively sonicated (Branson 2800, France) for one hour before deposition experiments to break any aggregates, especially at higher  $C_{\text{salt}}$ . The  $\zeta_p$  of these particles is determined using the Zetasizer (Malvern Instruments, UK) and also compared with literature.<sup>5,29</sup> All of the particles have diameters  $d \approx 5 \mu\text{m}$ .

### Zeta potentials

Zeta potentials of all colloidal particles used in the experiments are measured using a Zetasizer at different  $C_{\text{salt}}$  and are reported in SI-A (ESI†) exhibiting a sigmoidal pattern, where there is no significant change at low ionic strengths, followed by a transition, and a plateau at higher ionic strengths. This is the case for PS-fluo and PS-plain particles, where they exhibit negative  $\zeta_p$ . For PS-amine particles, which exhibit positive  $\zeta_p$ , the pattern is still sigmoidal but only the trends are reversed. PS-fluo particles have higher surface charges due to the highly negative carboxylate anions and thus the  $\zeta_p$  curve is more negative than that of PS-plain (SI-A) (ESI†). The  $\zeta_p$  values in Fig. 2 are measured with no salt in deionized water.

The zeta potentials for the microfluidic walls,  $\zeta_w$ , could not be measured directly with the Zetasizer and thus values are

determined from numerical simulations based on Langevin equations (see also in SI-C and D, ESI†) and also cross-referenced from literature.<sup>5</sup> The simulations show that the adsorption results ultimately do not significantly change within a range of two orders of magnitude of  $\zeta_w$  values (see simulations in SI-C and D, ESI†).

The origin of a surface's  $\zeta$  potential depends on the ionization of their surface groups in aqueous solution, shown in Fig. 2.

### Hydrodynamic flow experiments

Hydrodynamic flow experiments are performed using pressure-driven flow of the particle suspensions inside the microfluidic chip connected to a pressure controller (Fluigent, France). We observe the flow and deposition behavior using a microscope and acquire images at various time intervals. We perform image analyses using ImageJ and Matlab 2019. We apply a threshold on the images for binarization. Using image detection and subtraction, we discriminate between the particles that deposited onto the surface and those that flowed across the channel without sticking in the same manner as ref. 1, 2 and 10. The number of particles in each image is counted using Matlab techniques (*e.g.* circle detection).

## 3 Theory

We attempt a theoretical analysis, taking into account van der Waals adhesion forces and electrostatic forces (repulsive or attractive charges), based on the advection-diffusion equation:<sup>2,10,42</sup>

$$U_p \frac{\partial C}{\partial x} = \frac{\partial}{\partial x} \left( D \beta_x(z) \frac{\partial C}{\partial x} \right) + \frac{\partial}{\partial z} \left( D \beta_z(z) \frac{\partial C}{\partial z} \right) - \frac{\partial}{\partial z} \left( \frac{D \beta_z(z)}{kT} \left( -\frac{Ar}{6(z-r)^2} + \frac{\chi}{\lambda_D} \exp\left(-\frac{z-r}{\lambda_D}\right) \right) C \right) \quad (1)$$

where  $U_p$  is the average particle flow speed that follows Poiseuille profile,  $r$  is particle radius,  $k$  is the Boltzmann constant,  $T$  is the temperature. We suppose that at the channel entry, the particle concentration is homogeneous,  $x = 0$  ( $C = 1$ ), and that the particles irreversibly adsorb on the walls when  $z \approx r$ , where  $z$  is the distance between the particle center and the wall. Since particles cannot physically cross the walls and also using plane symmetry at  $z = \frac{h}{2}$ , the boundary conditions (B.C.)<sup>1,2,10</sup> are:

$$x = 0, \quad C = 1; \quad z = r, \quad C = 0; \quad z = \frac{h}{2}, \quad \frac{\partial C}{\partial z} = 0 \quad (2)$$

We also impose that if the particles are below a certain distance away from the wall, they irreversibly stick on the wall (we perform additional calculations in the range 0.1–1 nm, the result is that this distance is not critical). We consider channel symmetry at  $z = h/2$  and  $y = w/2$  and only count the individual particles adsorbed on the floor and ceiling, at  $z = \pm h/2$ .

There is another approach to solving eqn (1) by using the Lagrangian approach,<sup>43,44</sup> *i.e.* determining particle trajectory by writing that particle speed is equal to the force applied on it times its mobility.<sup>2,45</sup> This Lagrangian approach provides

equations easier to solve analytically. By applying these general equations to shallow rectangular channels where  $h \gg w$ , we find that geometry is invariant in the  $y$  direction and we obtain the following equations:

$$\dot{x}(t) = \gamma(z)U(z) + \beta_x(z)\delta(t) \quad (3)$$

$$\dot{z}(t) = \beta_z(z)\delta(t) + \frac{d\beta_z}{dz}D + \beta_z \frac{D}{kT}(F_{vdWz} + F_{elz}) \quad (4)$$

where  $\gamma(z) = \frac{U_p(z)}{U(z)}$ , where  $U(z)$  is the near-wall velocity, *i.e.* the particle flow speed at  $z \approx r$  and thus equivalent to  $U_r$ , and  $\gamma(z)$  is given in SI-B (ESI†). The parameter  $U_r = \frac{6Qr}{wh^2} \left(1 - \frac{r}{h}\right)$ . The parameter  $D$  is the bulk diffusion coefficient of the particles,  $\beta_x(z)$  and  $\beta_z(z)$  are dimensionless functions expressing the dependence of the longitudinal and transverse particle diffusion coefficients with  $z$ , the initial position of the particle w.r.t the wall. From literature,  $\beta_x(z) = 1 - 9/16z + 1/8z^3 - 45/256z^4 - 1/16z^5$  and  $\beta_z(z) = \frac{6(z-r)^2 + 2r(z-r)}{6(z-r)^2 + 9r(z-r) + 2r^2}$ <sup>46,47</sup> The parameter  $\delta(t)$  is a zero mean step random function with amplitude  $\sqrt{2D\tau}$ , where  $\tau$  is a (supposedly infinitesimal) incremental step. This parameter is well-established<sup>48</sup> to take the Brownian movement into account. This makes the equation stochastic and as a result very difficult to solve, except in the case where this term can be neglected.

In eqn (4),

$$F_{vdWz} = -\frac{Ar}{6(z-r)^2} \text{ and } F_{elz} = \frac{\chi}{\lambda_D} \exp\left(-\frac{z-r}{\lambda_D}\right) \quad (5)$$

where  $F_{vdWz}$  is the contribution of the van der Waals forces and  $F_{elz}$  is the contribution of the electrostatic force. The Hamaker constant,  $A$ , defines the strength of the surface interactions and can vary with significant surface roughness.<sup>49</sup> In this theoretical analysis, however, we do not introduce a roughness term but instead consider that any change in the effective value of  $A$  already takes into account effects of surface roughness.<sup>50</sup> Furthermore, we restrict ourselves to  $A > 0$ .

For electrostatic forces,  $F_{elz}$  can either be negative or positive, depending on the sign of the  $\zeta$  potential of both particle and channel wall surface, present in the definition of  $\chi$ :

$$\chi = 4\pi\epsilon\epsilon_0\zeta_w\zeta_p r \quad (6)$$

where  $\epsilon$  is the dielectric constant of the fluid,  $\epsilon_0$  is the permittivity of free space,  $\zeta_w$  is the zeta potential of the wall (with varying surface treatments),  $\zeta_p$  is the zeta potential of the colloidal particles, and  $r$  is particle radius. The parameter  $\chi$  is dimensionless.

The parameter  $\lambda_D$  is the Debye length (also expressed as  $\kappa^{-1}$ ), which for a monovalent electrolyte solution, is defined as:<sup>20</sup>

$$\lambda_D = \kappa^{-1} = \sqrt{\frac{\epsilon\epsilon_0 kT}{2(N_{Av})e^2 I}} \quad (7)$$

where  $N_{Av}$  is Avogadro's number,  $e$  is the elementary charge, and  $I$  is the ionic strength ( $\text{mol m}^{-3}$ ) and can be converted to  $C_{\text{salt}}$  (in molar units).



We now assume that diffusion contribution in the aforementioned equations is minimal because the particle sizes are a few micrometers, and thereby can be considered as non-Brownian. Consistently, we assume that the particles that contribute to the deposition, and which we are interested in, remains close to the wall in the sense that  $z - r \ll r$  at all times. In such a case, eqn (3) and (4) respectively become:

$$\dot{x}(t) = \gamma U(z) \quad (8)$$

$$\dot{z}(t) = \frac{z-r}{r} \frac{D}{kT} \left( -\frac{Ar}{6(z-r)^2} + \frac{\chi}{\lambda_D} \exp\left(-\frac{z-r}{\lambda_D}\right) \right) \quad (9)$$

It is interesting to transform these dynamical equations into a dimensionless form, as was done in ref. 1 and 2, in order to calculate directly the exit trajectory, *i.e.* the trajectory followed by a particle injected at the entry  $x = 0$  and collected at the wall at the end of the channel, at  $x = L$ . The knowledge of this exit trajectory, *i.e.* the position  $z_0$  of the particle that will be eventually collected at the outlet (Fig. 1(d)), determines the collection factor  $S$  by:

$$S = \frac{2z_0}{h} \quad (10)$$

After some rearrangements, we find the following dimensionless equation, which governs the particle trajectories:

$$\dot{\eta}(t') = -\frac{P}{\eta} + \eta \exp(-\eta) \quad (11)$$

here we introduce the dimensionless altitude  $\eta = \frac{(z-r)}{\lambda_D}$ , the corresponding ultimate particle position  $\eta_0 = \frac{(z_0-r)}{\lambda_D}$ , the dimensionless time  $t' = t \frac{D}{kT \lambda_D^2}$ , the parameters  $P = \frac{Ar}{6\chi \lambda_D}$  and  $\sigma_L = \frac{D\chi L}{\gamma_0 U_r \lambda_D r kT}$  for which we assumed, as in ref. 1, 2 and 10, that  $\gamma$  is constant, its value being approximately 2.1. The parameter  $P$  was introduced before, in ref. 2, and it is a dimensionless parameter that takes into account the strength of the van der Waals forces with respect to the electrostatic forces.

In term of these dimensionless quantities the exit trajectory defined by  $\eta_0 = \frac{z_0-r}{r}$  is related to  $S$  by the following expression, from the solution to eqn (11):

$$S = \eta_0 \frac{\lambda_D}{r} \quad (12)$$

When the charges have the same sign, the equation has been exactly solved in ref. 2, in two limiting cases: the van der Waals and Debye regimes. When the charges have opposite sign, *i.e.*  $\chi, P, \sigma < 0$ , the case we study herein, eqn (11) needs to be reconsidered.

In the case where  $|P|$  is large, then the van der Waals forces dominate and, obviously, eqn (11) provides the same

expression as in the case where charges have the same side. We find in this case:

$$S = S_{\text{vdW}} \approx \left( \frac{A}{2.1 kT \zeta_L} \right)^{1/2} \quad (13)$$

as in ref. 1, 2 and 10, where  $\zeta_L$  is an effective Peclet number:

$$\zeta_L = \frac{LD}{U_r r^2} \quad (14)$$

where  $L$  is channel length,  $D$  is the Stokes–Einstein diffusion coefficient,  $U_r$  is the near-wall velocity, at a distance  $z \approx r$  calculated from  $U_r = \frac{6Qr}{wh^2} \left(1 - \frac{r}{h}\right)^{1,2,10}$  where  $Q$  is flow rate,  $r$  is particle radius,  $w$  is channel width,  $h$  is channel height.

The opposite limit is the case where electrostatic forces dominate, *i.e.*  $|P|$  is small. One difficulty is that one cannot put directly  $P = 0$  in the equation (eqn (11)) because, in this limit, one can show that no particle is collected to the wall. All particles flow downstream. This result is obtained by noting that, as the particle approaches the wall,  $\eta$  becomes vanishingly small,  $\exp(-\eta)$  can be replaced by 1, the equation can be solved, and we find that its distance to the wall decreases exponentially with time. Consequently, it takes an infinite time to reach the altitude  $\eta = 0$ , *i.e.* to be collected by the wall. Therefore, however small  $|P|$  can be, we need the action of van der Waals force to collect the particle on the walls.

With the addition of van der Waals forces, collection becomes possible. Formally, it is possible to develop a perturbative scheme for the resolution of the equation at small  $|P|$ , and obtain analytical formula for the ultimate trajectory and consequently the collection factor. The formula are unfortunately complicated, and does not help much visualizing the structure of the result. In this calculation the exponential integral function ( $E_i$ ) is involved, preventing to obtain simple expressions. All what we can say here, qualitatively, is that the rate of deposition is enhanced in comparison with the van der Waals regime (because an attractive electrostatic force adds to it), but still controlled by van der Waals forces.

## 4 Simulations

We also perform numerical simulations by expressing the advection-diffusion equation in terms of Langevin equations<sup>6–8,42</sup> of the form:

$$\dot{\mathbf{r}}_i(t) = \frac{\mathbf{D}_i \mathbf{F}_i}{kT} + \nabla \cdot \mathbf{D}_i + U(\mathbf{r}_i) + \Delta(t) \quad (15)$$

where  $\mathbf{r}_i$  is the vector position of the  $i$ th particle with respect to time,  $\Delta(t)$  is the random Brownian displacement (analogue to  $\delta(t)$  in eqn (3)),  $\mathbf{D}_i$  is the anisotropic diffusion,  $\mathbf{F}_i$  is the total force acting on the particle,  $\mathbf{U}$  is the contribution of the flow to the particle speed. In non-complex geometries, such as a straight rectangular channel, these quantities are documented in literature. The time derivatives are replaced by a first order discretization. Ideally,  $\tau$  (simulation time step) should be as small as possible. However, using an even smaller value of  $\tau$

greatly increases computing times. In practice, the values we use for  $\tau$  range between  $0.5 \times 10^{-6}$  s and  $1.5 \times 10^{-5}$  s, which are well below the characteristic times of the problem. We verify that the results are insensitive to the value of  $\tau$  within this range.

Similar to the solution of eqn (1), the Lagrangian approach also makes it easier to compute Langevin equation. In eqn (15), this physically means that the particle trajectory depends on the total external forces acting upon it, its diffusion, and its velocity. Thus, by applying these general equations to the particular geometry we consider, *i.e.* long shallow channels with rectangular cross-sections, we also obtain the eqn (3) and (4). Additional information on simulations is presented in SI-B (ESI†).

## 5 Experiments: repulsive charges

### Description of surface treatments

In this section, we analyze the interaction between PS-fluo and PS-plain (both negative  $\zeta_p$ ) on both native PDMS and plasma PDMS. Native PDMS is hydrophobic and thus, when charges are screened at high ionic strengths, PS latex particles should adsorb naturally onto its surface.<sup>1,2,5</sup> Plasma-treated PDMS, on the other hand, is heavily negatively-charged due to the oxidation of the siloxane bonds. Even at high  $C_{\text{salt}}$ , all of the charges may not be fully screened. At low  $C_{\text{salt}}$ , both  $\zeta_p$  and  $\zeta_w$  are highly negative, resulting in repulsive interaction charges. In Fig. 3 (qualitatively) and Fig. 4 (quantitatively), there are significantly less particles collected on plasma-treated PDMS than on native PDMS.

### Determination of Hamaker constants

We first measure the Hamaker constant,  $A$ , between the PS-fluo and the PDMS wall of certain surface treatment using micro-fluidics, as described in ref. 1, 2 and 10, by performing a

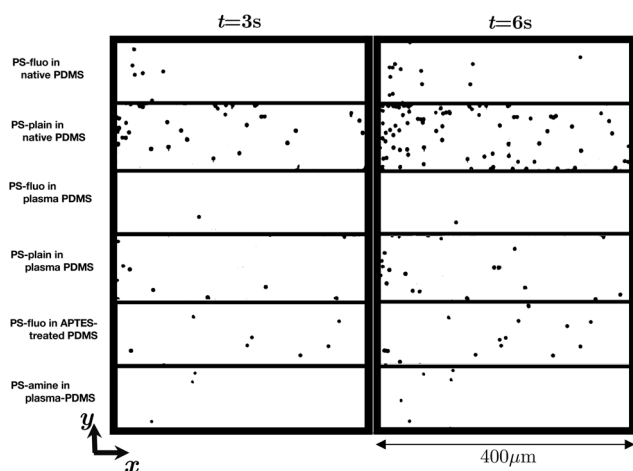


Fig. 3 Experimental treated images show the number of adsorbed or collected particles at different time intervals and also at various combinations of particle and surfaces. Data for non-functionalized PS latex (PS-plain) reproduced from ref. 1 and 2.

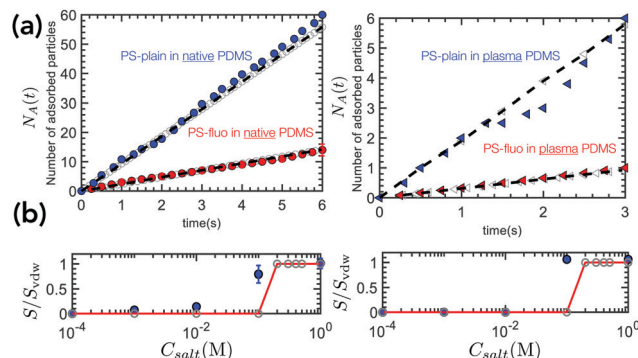


Fig. 4 (a, left) Plot of  $N_A(t)$  for PS-fluo and PS-plain<sup>1,2,10</sup> in native PDMS (hydrophobic). (a, right) Plot of  $N_A(t)$  for PS-fluo and PS-plain<sup>1</sup> in plasma-treated PDMS (hydrophilic). For all experimental runs,  $d \approx 5 \mu\text{m}$  and average velocity range is  $U_p \sim 8\text{--}10 \text{ mm s}^{-1}$  ( $U_r = 5.1\text{--}6.4 \text{ mm s}^{-1}$ ). In (a), solid points are experiments, broken black lines are theory (eqn (13)), and hollow points are simulations. Experiments and simulations both performed at 1 M NaCl. (b, left) Plot of  $S/S_{\text{vdw}}$  as function of  $C_{\text{salt}}$  for PS-fluo on native PDMS. (b, right) Plot of  $S/S_{\text{vdw}}$  as function of  $C_{\text{salt}}$  for PS-plain on plasma PDMS. In (b), solid points are experiments, solid red line is theory ( $\frac{S}{S_{\text{vdw}}} = \text{eqn (16)}/\text{eqn (13)}$ ), and hollow points are simulations. For PS-plain and native/plasma-PDMS,  $P \approx 0.541$ . For PS-fluo in native/plasma-PDMS,  $P \approx 0.074$ . The latter has a lower  $P$  because of a lower  $A$  value.

deposition experiment at 1 M NaCl, *i.e.* in the vdW regime. This is because electrostatic surface charges are generally screened at high ionic strengths<sup>1,10,15</sup> and thus  $\lambda_D$  decreases with increasing  $C_{\text{salt}}$ . At this point, surface interactions are dominated primarily by van der Waals forces. We count the number of particles adsorbed as function of time,  $N_A(t)$ . The results are shown in Fig. 4(a) for two particle-surface conditions all obtained at 1 M NaCl. We perform at least six deposition experiments for each case, where we experimentally measure the equivalent deposition function,  $S$ :<sup>1,2,10</sup>

$$S = \left( \frac{h-r}{2} \right) \frac{v_p}{\phi Q t} N_A(t) \quad (16)$$

in which  $N_A(t)$  is the number of particles collected by the walls  $z = \pm \frac{h}{2}$  as a function of time,  $h$  is channel height,  $r$  is particle radius,  $v_p$  is the volume of the spherical particle,  $\phi$  is particle concentration in the suspension, and  $Q$  is flow rate. The function  $\frac{r}{\frac{h}{2} - r} S$  is the collector efficiency.<sup>1,51,52</sup>

From eqn (16), we calculate the experimental value of  $S$  during the initial seconds of deposition and then equate it with eqn (13) to determine  $A$ . For PS-fluo on native PDMS (Fig. 4(a)),  $A = 1.1 \times 10^{-21}$  J. We show the deposition results for PS-fluo on both native PDMS and plasma-PDMS in Fig. 4 (a, left), and also plot data for PS-plain on the same surface treatment at comparable velocities from ref. 1 and 2. We then compare with the theoretical expression for  $S$  in the vdW regime, derived from ref. 1, 2 and 10 and is shown in eqn (13). We also compare it with simulation results, using the obtained  $A$  value. Results in

Fig. 4(a) show comparison between experiments,  $S$  (eqn (16)), and theory,  $S_{\text{vdW}}$  as well as simulations based on Langevin equations showing excellent agreement. To perform the simulations in repulsive cases, we use a known equation for  $\zeta_{\text{w}}$  of microfluidic PDMS walls from ref. 5 and 19. In all cases regarding repulsive charges, at high ionic strengths, the  $\zeta_{\text{w}}$  is insignificant due to charge screening and at low ionic strengths,  $\zeta_{\text{w}}$  value may have a large magnitude but regardless, deposition is also close to if not zero.

Surface roughness is not introduced in the theoretical analysis but can be gauged numerically in the simulations (see SI-B, ESI†). Any change in the effective Hamaker constant determined from experiments as a function of the different particle-surface combinations already takes roughness into account. For example, PS-plain is generally considered smooth because it lacks surface functionalization. On one hand, we expect PS-fluo surface to have a coarser surface due to the additional surface functionalization thereby decreasing the overall effective Hamaker constant when compared to PS-plain. In literature,<sup>49,50</sup> it has been demonstrated further through atomic force microscopy measurements (AFM) that effective Hamaker constants generally decrease with increasing surface roughness.

The results for the Hamaker constants strongly suggest that this microfluidics-based deposition measurement, as initially suggested in ref. 1, is able to provide insights into the size of the surface layer based on the value of  $A$ .<sup>1</sup>

We also measure  $A$  for PS-plain and PS-fluo on plasma-treated PDMS in Fig. 4 (a, right) and find a much lower value than that of their interactions with native PDMS. In particular, based on the images of Fig. 3, almost no interaction is observed between PS-fluo and plasma-PDMS. This strong negative charge for plasma-PDMS, coupled with even stronger (–)–charges for PS-fluo (as confirmed by  $\zeta_{\text{p}}$  in SI-A, ESI†) causes even greater repulsion, thereby preventing particle deposition. Even at 1 M NaCl, there is still minimal deposition. This suggests that the high ionic strength is not sufficient enough to screen all of the surface charges on both particles and channel surface.

Limited interaction is also observed between PS-plain and plasma-PDMS, as also reported in ref. 1. AFM measurements<sup>53</sup> attribute this weak interaction to the existence of hydration forces between silicon-based surfaces and inorganic electrolytes,<sup>1,53,54</sup> arguing that at high electrolyte concentrations, hydrated cations bind strongly to the oxidized surfaces, which are heavily negatively charged, giving rise to a repulsive hydration energy.

When salt (electrolyte ions) is added to the solution, the origin of the repulsive force is entropic (osmotic) instead of electrostatic.<sup>15</sup> The overall system remains electrically neutral. In repulsive cases where deposition is more evident at high salt concentration, van der Waals (vdW) forces dominate the system (entropy < vdW forces). In repulsive cases and low/intermediate concentrations of salt, the electrostatic forces remain neutral and vdW forces are insignificant, thus entropy plays a role in the repulsion between the particle and the surface. In any case, studies<sup>55</sup> have observed that for larger particles (> 100 nm), entropic effects can be considered negligible and osmotic pressure only results from the electrostatic

interaction effect. Therefore, for our particles having  $d \sim 5 \mu\text{m}$ , entropic effects can be neglected.

### Determination of $S/S_{\text{vdW}}$ as function of $C_{\text{salt}}$

Within four orders of magnitude of  $C_{\text{salt}}$ , we perform deposition experiments and similarly measure  $N_{\text{A}}(t)$  to determine  $S$  in eqn (16) as well as the deposition ratio with respect to vdW regime,  $S/S_{\text{vdW}}$ . We plot the results for both native PDMS and plasma-PDMS in Fig. 4(b). Both native PDMS (left) and plasma PDMS (right) exhibit negative surface charges in aqueous solutions, with the latter presumably having a greater quantity of (–)–charges due to oxidation. With both PS-fluo and PS-plain particles also having (–)–surface charges, their interaction with the PDMS surface at low  $C_{\text{salt}}$  (large Debye lengths) is mainly governed by repulsion. This explains why the deposition is nearly (if not) zero below 0.1 M NaCl.

We also equally plot the theoretical and simulation results, which have been shown to agree with the results based from DLVO.<sup>2,5</sup> The graph generally exhibits a sigmoidal behavior, where there is minimal change (and low deposition) at low  $C_{\text{salt}}$ , followed by a sharp transition at orders of magnitude of  $\sim 0.1$  M NaCl, and a plateau at high ionic strengths. In Fig. 4 (b, left), results are for PS-fluo on native PDMS. Similar results have also been obtained for PS-plain on native PDMS as reported in literature.<sup>1,2,10</sup> In Fig. 4 (b, right), results are for PS-plain on plasma-PDMS. Based on Fig. 3, the deposition signal for PS-fluo on plasma-PDMS is weak, which is attributed to the higher quantity of negative charges on the surface of PS-fluo that may not have been fully screened at 1 M NaCl.

For additional information on simulations of repulsive charges, we generate a phase diagram of  $\zeta_{\text{p}}$  and  $\zeta_{\text{w}}$  combinations having charges of the same sign (see SI-C, ESI†). We show that for a wide range of values, the deposition result does not change significantly, *i.e.* the particles are either attracted to or repelled from the surface.

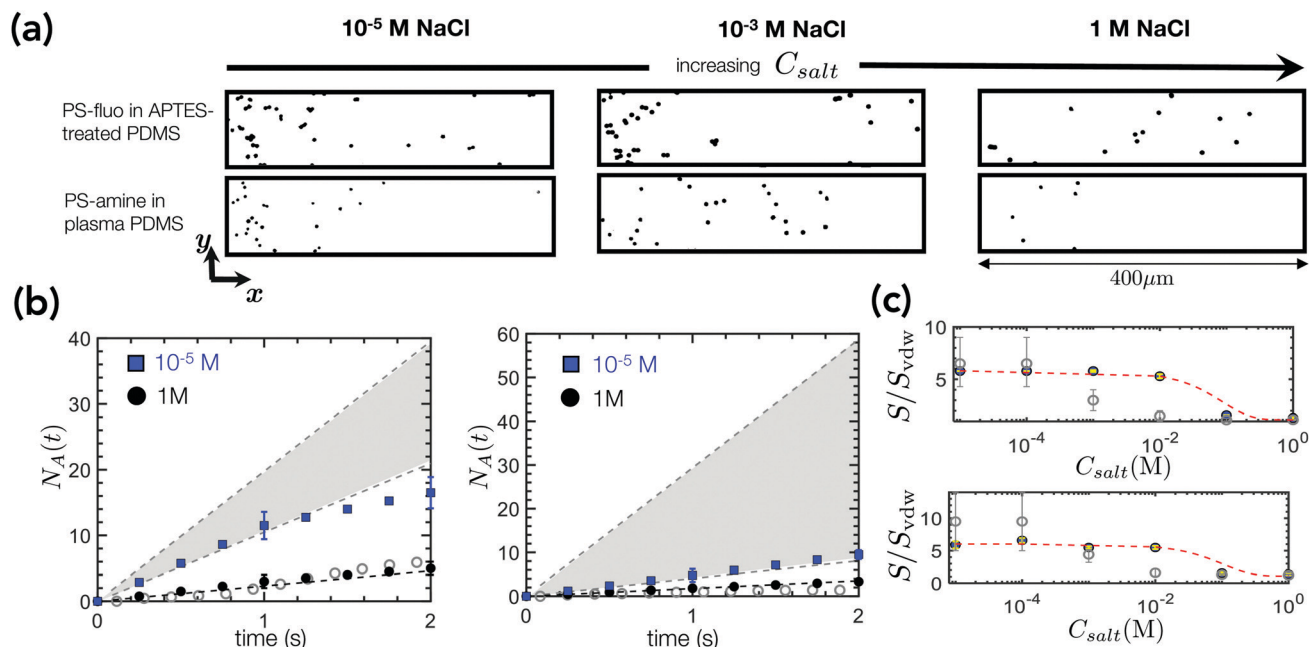
## 6 Experiments: attractive charges

### Description of surface treatment

Aminopropyltriethoxysilane (APTES) is a molecule that covalently binds to plasma-oxidized PDMS, incorporating an amine functionality and therefore a positive surface charge.<sup>39</sup> The protocol for grafting APTES is based on ref. 39. PS-fluo particles inherently have negative charges, which leads to an attractive potential with respect to APTES-modified PDMS. Similarly, we can also demonstrate an attractive potential by using plasma-treated PDMS and amine-coated polystyrene latex particles, PS-amine. In both situations, one of the  $\zeta$  potentials is (+) while the other is (–).

### Determination of Hamaker constants

Similarly to the previous section, the  $A$  value characterizing the interaction between PS-fluo and APTES-treated PDMS is determined in the vdW regime, *i.e.* at 1 M NaCl to screen surface charges. Moreover, the  $A$  value for the other attractive potential case, PS-amine and plasma PDMS is also measured. The  $A$  is



**Fig. 5** (a) Typical experimental treated images showing collected particles in the channel at different  $C_{salt}$  and for two conditions: PS-fluo on APTES-treated PDMS (at  $t = 6$  s) and PS-amine on plasma-treated PDMS (at  $t = 3$  s). All experimental runs performed at  $U_p \sim 8\text{--}10\text{ mm s}^{-1}$  ( $U_t = 5.1\text{--}6.4\text{ mm s}^{-1}$ ) at different  $C_{salt}$ . Particle diameters are  $d \approx 5\text{ }\mu\text{m}$ , although PS-amine particles that we use have slightly smaller diameters than PS-fluo. (b, left) Plot of  $N_A(t)$  for PS-fluo in APTES-treated PDMS. (b, right) Plot of  $N_A(t)$  for PS-amine on plasma-PDMS (more results shown in SI-E, ESI†). In both cases, solid points are experiments, broken line is theory ( $S_{vdw}$  in eqn (13)) and corresponding hollow gray points are simulations at high ionic strengths. At low ionic strengths, we perform simulations for a range of  $\zeta_w$  values, shown by the gray shaded region bound by minimum and maximum values (gray broken lines). (c, top) Plot of  $S/S_{vdw}$  as function of  $C_{salt}$  for PS-fluo on APTES-treated PDMS. (c, bottom) Plot of  $S/S_{vdw}$  as function of  $C_{salt}$  for PS-amine on plasma-treated PDMS. In (c), solid points are experiments, broken red line is a guide, and hollow gray points are numerical simulations, where error bars designate minimum-maximum range (see SI-D, ESI†). For PS-fluo and APTES-treated PDMS,  $P \approx -0.0012\zeta_w^{-1}$ . For PS-amine in plasma-PDMS,  $P \approx -0.0016\zeta_w^{-1}$ . The exact value of  $P$  depends on the  $\zeta_w$ .

determined from the slope of the linear regime during initial seconds of deposition by calculating  $S$  in eqn (16) and equating with eqn (13). Experimental images of these behaviors are shown in Fig. 5(a). For PS-fluo and APTES-treated PDMS (and taking into account surface roughness) we determine the effective Hamaker constant to be  $A = 1.1 \times 10^{-21}$  J, while for PS-amine and plasma-PDMS,  $A = 0.4 \times 10^{-21}$  J.

The plots of  $N_A(t)$  in Fig. 5(b) for PS-fluo on APTES-treated PDMS as well as PS-amine on plasma-treated PDMS, where both surfaces have opposite charges, consistently demonstrate much higher deposition at low  $C_{salt}$  (results for additional salt concentrations are also shown in SI-E, ESI†). To perform the simulations with attractive charges (see SI-D, ESI†), we use a range of probable  $\zeta_w$ . In all cases at high ionic strengths, the  $\zeta_w$  is insignificant due to charge screening. However, at low ionic strengths, the simulation results largely depend on the  $\zeta_w$  value. Hence, in Fig. 5(b), we depict that as a range based on minimum and maximum values. Our experiments fall within the lower part of the shaded region. Part of this discrepancy might be due to the fact that the simulation does not take into account interparticle interactions once the experiment saturates (too many particles that results to aggregation).

#### Determination of $S/S_{vdw}$ as function of $C_{salt}$

By varying the magnitude of  $C_{salt}$ , we also determine  $S/S_{vdw}$ . The Debye length,  $\lambda_D$ , increases with decreasing  $C_{salt}$ . Thus, for

repulsive potentials, deposition decreases with decreasing  $C_{salt}$  owing to larger Debye lengths. However, for attractive potentials, we find that the opposite behavior is true where deposition increases with decreasing  $C_{salt}$ . Plotting  $S/S_{vdw}$  as a function of salt in Fig. 5(c) shows a sigmoidal pattern but in reverse, i.e. the plateau begins at low  $C_{salt}$ , followed by a transition value around the order of magnitude of  $\sim 0.1$  M NaCl, then followed by constant value at higher salt concentrations for both cases.

As previously discussed in Section 3, we have not found a simple theoretical formula that establishes this behavior so the broken red line in Fig. 5(c) serves as guide.

In terms of numerical simulations, we also generate a diagram of  $\zeta_p$  and  $\zeta_w$  combinations having opposite charges (see SI-D, ESI†). Results show at a constant  $\zeta_p$  value and varying  $\zeta_w$  over two orders of magnitude, the deposition result does not change significantly. At ionic strengths  $\geq 0.1$  M, the simulations agree with experiments and thus  $S/S_{vdw} \approx 1$ . At lower ionic strengths  $< 0.1$  M, quantitatively there is greater disparity between simulations and experiments in quantitative terms. The experiments reveal that particle deposition is independent of salt concentration and qualitatively the behavior or trend obtained from simulations agree with experiments. We equally find that, when surface charges are of the opposite sign, there is greater deposition at lower ionic strengths (larger Debye lengths) than at higher ionic strengths (smaller Debye lengths).



In attractive cases, van der Waals (vdW) forces dominate the system (entropy < vdW forces). Therefore, entropy still does not play a considerable role as long as vdW forces are predominant especially at high salt concentrations. However, at low/intermediate concentrations of salt, attraction is improved due to an increase in electrostatic attraction that allows van der Waals forces to occur.<sup>15</sup>

## 7 Additional discussion

We summarize the results in Table 1.

At high  $C_{\text{salt}}$ , regardless of  $\zeta$  sign, surface charges are screened and therefore attraction is mainly driven by van der Waals adhesion forces, which act within sub-nanometric levels (angstroms). However, when surface charges are sufficiently strong, such as in the case of plasma-treated PDMS, it is possible that all of the surface charges may not be fully screened and thus residual charges may play a role during interaction. This is for example the case for PS-fluo on plasma-treated PDMS where the deposition signal remains low. At high  $C_{\text{salt}}$ , there is also a risk of ion pairing and reduction of apparent ionic strength. However, numerical studies<sup>56</sup> have shown that this would not affect the current result because for monovalent salts the amount of ion pairing does not seem to be significant. Additional simulations<sup>57</sup> show that there is minimal ion pairing at high salt concentrations due to the strength of effective solvent-mediated interaction between ions in the solution (1–5 M salt) and this is associated with high osmotic pressures. Solvation pushes the ions further apart from one another, which decreases favorable association between ions. Experimentally, excessive ion pairing is accompanied by poor solubility,<sup>58</sup> which we have not observed at 1 M NaCl. Instead, we still observe classical electrolyte behavior, *i.e.* greater amount of collected particles with increasing salt concentration in repulsive cases, thereby implying the reduction of the screening length. This is also corroborated by Debye–Huckel law predictions for ideal solutions, *i.e.* decreasing screening length at high ionic strengths.<sup>59</sup> It is only at much higher electrolyte concentrations ( $\gg 1$  M) where the electrolyte behavior becomes non-ideal and the screening length increases due to a combination of steric or volume exclusion and ion correlations.

At low  $C_{\text{salt}}$ , the Debye length increases (nm order of magnitude). When signs of both  $\zeta$  are the same, the particles far from the wall are unable to come closer to the wall due to repulsion generated by the Debye layer. But when signs of both  $\zeta$  are different, the particles far from the wall can further approach much closer to the wall mobilized by electrostatic

attraction. The magnitude of the attractive EDL forces, at low ionic strengths, are large, whose range extend far from the surface.<sup>30,38</sup> This suggests that due to the attractive potential, the particles far from the wall can cross the Debye threshold and approach the wall up to a distance where van der Waals forces come into play, collecting the particles at the wall, which electrostatic forces alone are unable to achieve, owing to hindered diffusion. This mechanism agrees with a typical deposition process where the particle is first transported close to the surface mainly *via* convection but also enhanced by electrostatic attractive forces, then followed by particle attachment *via* adhesion interactions.<sup>3,31</sup> As a result, this effect is an electrostatic-assisted van der Waals force, which is more pronounced at low  $C_{\text{salt}}$ .

Because the mechanism is controlled by the strength of the surface charges in the electrostatic double layer or Debye layer, the colloidal deposition with attractive charges under these conditions still fall within the so-called “Debye” regime.<sup>2</sup> Such a regime has also been reported in ref. 2, but instead with repulsive charges. Thus, we extend the definition of the “Debye regime”<sup>2</sup> by demonstrating that this regime is governed by the Debye layer but with either repulsive or attractive charges.

## 8 Conclusion

Colloidal particle-surface interactions are a delicate interplay of adhesion, electrostatic, and diffusion forces. Depending on the nature of the surface, the electrostatic potential could be repulsive (*i.e.* both  $\zeta$  values have the same sign) or attractive (*i.e.* both  $\zeta$  values have the opposite sign). The former case has also been typically reported in literature<sup>2,5–7</sup> with deposition at a minimum (almost close to zero) at low salt concentrations and maximum at high ionic strengths. To our knowledge, there has only been limited experiments involving the deposition with attractive charges. Here, we show that in such cases of attractive charges, deposition occurs at salt concentrations of several orders of magnitude due to van der Waals adhesion forces but with greater number of collected particles at lower ionic strengths than at higher ionic strengths.

In the van der Waals regime,<sup>1,2,10</sup> only particles injected at a position  $z \approx r$  will have the opportunity to approach closer to the wall. In the Debye regime,<sup>1,2,10</sup> when potential is repulsive, particles far from the wall cannot cross the barrier erected by the Debye layer and therefore they cannot approach the wall further. However, in the Debye regime when potential is attractive, such as the case herein, particles at  $z > r$  can still cross the Debye layer barrier mobilized by attractive electrostatic charges, permitting them to approach even much closer towards the wall so that adhesion can take place *via* van der Waals forces. In such cases, this is van der Waals interactions assisted by attractive electrostatic potentials.

## Conflicts of interest

There are no conflicts to declare.

**Table 1** Values for Hamaker constant,  $A$ , for the different interaction conditions

Particle	Surface Wall	Charge	$A (\times 10^{-21} \text{ J})$
PS-fluo	Native PDMS	Repulsive	1.10
PS-plain	Native PDMS	Repulsive	8.00
PS-fluo	Plasma PDMS	Repulsive	0.02
PS-plain	Plasma PDMS	Repulsive	0.29
PS-fluo	APTES-treated PDMS	Attractive	1.10
PS-amine	Plasma PDMS	Attractive	0.40

## Acknowledgements

This work has been supported by ESPCI Paris, Institut Pierre Gilles de Gennes (laboratoire d'excellence, "investissements d'avenir" program ANR-10-IDEX-0001-02 PSL and ANR-10-LABX-31 and équipement d'excellence program ANR-10-EQPX-34). We also thank the support of CNRS Chimie Biologie Innovation (CBI) UMR8231 as well as CNRS Gulliver UMR7083 and the Microfluidics, MEMS, Nanostructures (MMN) group. We also thank the Sao Paulo Research Foundation - FAPESP (Grant numbers: 2017/18109-0, 2018/18103-4, and 2019/07744-1) from Brazil that has permitted Tatiana Porto Santos to do a PhD exchange program in Paris, France.

## References

- 1 C. M. Cejas, F. Monti, M. Truchet, J. Burnouf and P. Tabeling, *Langmuir*, 2017, **33**, 6471–6480.
- 2 C. M. Cejas, F. Monti, M. Truchet, J. Burnouf and P. Tabeling, *Phys. Rev. E: Stat., Nonlinear, Soft Matter Phys.*, 2018, **98**, 062606.
- 3 M. Elimelech, J. Gregory, X. Jia and R. Williams, *Particle deposition and aggregation-measurement in modelling and simulation*, Elsevier, Amsterdam, 1995.
- 4 Z. Adamczyk, *Particles and Interfaces, Interactions, Deposition, and Structure*, Academic Press, New York, 2006.
- 5 B. Mustin and B. Stoeber, *Langmuir*, 2016, **32**, 88–101.
- 6 H. Unni and C. Yang, *Electrophoresis*, 2009, **30**, 732–741.
- 7 H. Unni and C. Yang, *Can. J. Chem. Eng.*, 2007, **85**, 609–616.
- 8 C. Henry, P. Minier and G. Lefevre, *Adv. Colloid Interface Sci.*, 2012, **185–186**, 34–76.
- 9 A. Zaccone, H. Wu, D. Gentili and M. Morbidelli, *Phys. Rev. E*, 2009, **80**, 051404.
- 10 C. M. Cejas, L. Maini, F. Monti and P. Tabeling, *Soft Matter*, 2019, **15**, 7438.
- 11 H. Chen and E. Ruckenstein, *Ind. Eng. Chem. Res.*, 2019, **58**, 3420–3426.
- 12 B. Derjaguin and L. D. Landau, *Acta Phys. Chim.*, 1941, **14**, 633–662.
- 13 E. J. W. Verwey and J. T. G. Overbeek, *Theory of stability of lyophobic colloids*, Elsevier, Amsterdam, 1948.
- 14 H. J. Butt, K. Graf and M. Kappl, *Physics and Chemistry of Interfaces*, Wiley-VCH Verlag GmbH & Co., Weinheim, Germany, Third, Revised and Enlarged Edition edition, 2016.
- 15 J. Israelachvili, *Intermolecular and Surface Forces*, Elsevier, USA, 1991.
- 16 T. Cao, G. Trefalt and M. Borkovec, *Langmuir*, 2018, **34**, 14368–14377.
- 17 B. J. Kirby and E. F. Hasselbrink, *Electrophoresis*, 2004, **25**, 187–202.
- 18 D. Yan, C. Yang, N. T. Nguyen and X. Huang, *Electrophoresis*, 2006, **27**, 620–627.
- 19 B. Kirby and E. Hasselbrink, *Electrophoresis*, 2004, **25**, 203–213.
- 20 A. Khair and T. M. Squires, *Phys. Fluids*, 2009, **21**, 042001.
- 21 M. v. Smoluchowski, *Ann. Phys.*, 1915, **353**, 1103–1112.
- 22 K. Oka and K. Furusawa, *Electrical Phenomena at Interfaces*, Marcel Dekker, New York, 1998.
- 23 M. Minor, A. J. van der Lindner, H. P. van Leeuwen and J. Lyklema, *J. Colloid Interface Sci.*, 1997, **189**, 370–375.
- 24 C. Yang, T. Dabros, D. Li, J. Czarnecki and J. H. Masliyah, *J. Colloid Interface Sci.*, 2001, **243**, 128–135.
- 25 D. Erickson, D. Li and C. Werner, *J. Colloid Interface Sci.*, 2000, **232**, 186–197.
- 26 P. Mela, A. van den Berg, Y. Fintschenko and E. B. Cummings, *Electrophoresis*, 2005, **26**, 1792–1799.
- 27 A. Sze, D. Erickson, L. Ren and D. Li, *J. Colloid Interface Sci.*, 2003, **261**, 402–410.
- 28 F. Bianchi, F. Wagner, P. Hoffman and H. H. Girault, *Anal. Chem.*, 2001, **73**, 829–836.
- 29 A. Garg, C. Cartier, K. Bishop and D. Velegol, *Langmuir*, 2016, **32**, 11837–11844.
- 30 M. Elimelech, *J. Colloid Interface Sci.*, 1991, **146**, 337–352.
- 31 G. Trefalt, F. Javier Montes Ruiz-Cabello and M. Borkovec, *J. Phys. Chem. B*, 2014, **118**, 6346–6355.
- 32 T. Cao, T. Sugimoto, I. Szilagyi, G. Trefalt and M. Borkovec, *Phys. Chem. Chem. Phys.*, 2017, **19**, 15610.
- 33 T. Oncsik, G. Trefalt, Z. Csendes, I. Szilagyi and M. Borkovec, *Langmuir*, 2014, **30**, 733–741.
- 34 A. M. Puertas, A. Fernandez-Barbero and F. J. de las Nieves, *J. Chem. Phys.*, 2001, **114**, 591–595.
- 35 W. Lin, M. Kobayashi, M. Skarba, C. Mu, P. Galletto and M. Borkovec, *Langmuir*, 2006, **22**, 1038–1047.
- 36 M. Trulsson, B. Jonsson, T. Akesson, J. Forsman and C. Labbez, *Phys. Rev. Lett.*, 2006, **97**, 068302.
- 37 P. Sinha, I. Szilagyi, F. J. M. Ruiz-Cabello, P. Maroni and M. Borkovec, *J. Phys. Chem. Lett.*, 2013, **4**, 648–652.
- 38 Z. Adamczyk and T. G. M. van de Ven, *J. Colloid Interface Sci.*, 1981, **84**, 497–518.
- 39 J. H. L. Beal, A. Bubendorfer, T. Kemmitt, I. Hoek and W. Mike Arnold, *Biomicrofluidics*, 2012, **6**, 036503.
- 40 S. H. Donaldson Jr., J. P. Jahnke, R. J. Messinger, A. Ostlund, D. Uhrig, J. N. Israelachvili and B. F. Chmelka, *Macromolecules*, 2016, **49**, 6910–6917.
- 41 M. Lundqvist, J. Stigler, G. Elia, I. Lynch, T. Cedervall and K. Dawson, *Proc. Natl. Acad. Sci. U. S. A.*, 2008, **105**, 14265–14270.
- 42 Z. Adamczyk, T. Dabros, J. Czarnecki and T. V. de Ven, *Adv. Colloid Interface Sci.*, 1983, **19**, 183–252.
- 43 M. M. Fyrrillas and K. K. Nomura, *J. Chem. Phys.*, 2007, **126**, 164510.
- 44 B. H. Devkota and J. Imberger, *Water Resour. Res.*, 2009, **W12406**.
- 45 P. Tabeling, *Introduction to Microfluidics*, Oxford University Press, Oxford, UK, 2005.
- 46 H. Brenner, *Chem. Eng. Sci.*, 1961, **16**, 242–251.
- 47 M. Bevan and D. Prieve, *J. Chem. Phys.*, 2000, **113**, 1228–1236.
- 48 P. Huang and K. Breuer, *Phys. Rev. E: Stat., Nonlinear, Soft Matter Phys.*, 2007, **76**, 046307.
- 49 M. C. Stevenson, S. P. Beaudoin and D. S. Corti, *J. Phys. Chem. C*, 2020, **124**, 3014–3027.

- 50 V. Valmacco, M. Elzvbicciak-Wodka, C. Besnard, P. Maroni, G. Trefalt and M. Borkovec, *Nanoscale Horiz.*, 2016, **1**, 325.
- 51 K. Yao, M. Habibian and C. O'Melia, *Environ. Sci. Technol.*, 1971, **5**, 1105–1112.
- 52 N. Tufenkji and M. Elimelech, *Langmuir*, 2005, **21**, 841–852.
- 53 Y. Wang, L. Wang, M. Hampton and A. Nguyen, *J. Phys. Chem. C*, 2013, **117**, 2113–2120.
- 54 M. Dishon, O. Zohar and U. Sivan, *Langmuir*, 2009, **25**, 2831–2836.
- 55 P. Bacchin, D. Si-Hassen, V. Starov, M. J. Clifton and P. Aimar, *Chem. Eng. Sci.*, 2002, **57**, 77–91.
- 56 M. Soniat, M. Pool, L. Franklin and S. W. Rick, *Fluid Phase Equilib.*, 2016, **407**, 31–38.
- 57 Y. Luo, W. Jiang, H. Yu, A. D. MacKerell and B. Roux, *Faraday Discuss.*, 2013, **160**, 135–149.
- 58 Y. Marcus and G. Hefter, *Chem. Rev.*, 2006, **106**, 4585–4621.
- 59 A. M. Smith, A. A. Lee and S. Perkin, *J. Phys. Chem. Lett.*, 2016, **7**, 2157–2163.

## Supplementary Information

### Colloidal particle deposition on microchannel walls, for attractive and repulsive surface potentials

**T. Porto Santos<sup>\*,a,b,‡</sup>, R. Lopes Cunha<sup>a</sup>, P. Tabeling<sup>b</sup>, and C.M. Cejas<sup>\*,b,‡</sup>**

<sup>a</sup> Department of Food Engineering, Faculty of Food Engineering, University of Campinas, Rua Monteiro Lobato, 80-CEP 13083-862 Campinas, Brazil

<sup>b</sup> Microfluidics, MEMS, Nanostructures Laboratory, CNRS Chimie Biologie Innovation (CBI) UMR 8231, Institut Pierre Gilles de Gennes (IPGG), ESPCI Paris, PSL Research University 6 rue Jean Calvin 75005, Paris, France

<sup>‡</sup> Authors contributed equally to this work

\* Corresponding authors: tatiana.porto90@gmail.com, cesare.cejas@gmail.com

#### A Particle $\zeta$ potential measurements using ZetaSizer

The  $\zeta$  potentials of all colloidal particles used in the experiments (PS-plain, PS-fluo, and PS-amine) are measured using a ZetaSizer Nano Series (Malvern Instruments, UK). Beforehand, the colloidal particles are sonicated (Branson 2800) and diluted in deionized water (1:10000), followed by their insertion inside a zeta cell (DTS1070). The measurements are performed in triplicate. We determine the  $\zeta_p$  for PS-fluo, PS-plain, and PS-amine particles as a function of  $C_{salt}$ . The results are presented in the Fig. 1.

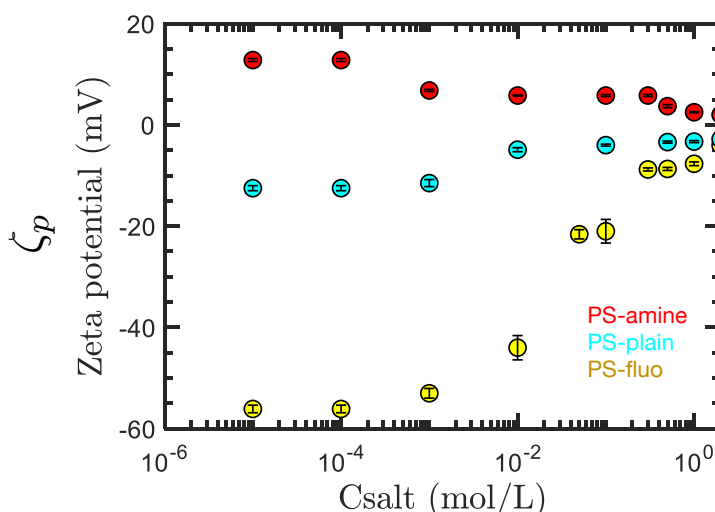


Figure 1: Plot of  $\zeta_p$  for PS-fluo (●), PS-plain (●), and PS-amine (●) as function of  $C_{salt}$  obtained using the Zetasizer.

All three curves exhibit a sigmoidal pattern where there is minimal change at low salt concentrations, followed by a transition, then a constant value at high salt concentrations.

PS-amine exhibits a slightly positive charge due to the amine molecules grafted onto the surface. Thus,  $\zeta_p$  has a smaller value at high ionic strengths and increases positively at lower ionic strengths.

Both PS-plain and PS-fluo exhibit negative surface charges and thus  $\zeta_p$  has a lower value (in terms of mag-



nitude) almost close to zero at high ionic strengths while  $\zeta_p$  becomes increasingly negative at lower ionic strengths. PS-fluo has a higher surface charge density due to the carboxylate anions. This explains why the  $\zeta_p$  for PS-fluo is more negative than that of PS-plain, which is not specifically functionalized.

From our experimental measurements, we find that the  $\zeta_p$  value decreases slowly at low salt concentrations. In some cases, such as PS-plain, the  $\zeta_p$  value does not vary significantly within two orders of magnitude of low salt concentration.

## B Information on numerical simulations

As mentioned in the main manuscript, we perform simulations by expressing the advection-diffusion equation in terms of Langevin equations [1, 2, 3, 4] of the form:

$$\dot{\mathbf{r}}_i(t) = \frac{\mathbf{D}_i \mathbf{F}_i}{kT} + \nabla \cdot \mathbf{D}_i + \mathbf{U}(\dot{\mathbf{r}}_i) + \Delta(t) \quad (1)$$

where  $\mathbf{r}_i$  is the vector position of the  $i$ th particle with respect to time,  $\mathbf{D}_i$  is the anisotropic diffusion,  $\mathbf{F}_i$  is the total force acting on the particle,  $k$  is the Boltzmann constant,  $T$  is temperature,  $\mathbf{U}$  is the contribution of the flow to the particle speed, and  $\Delta(t)$  takes into account the random Brownian displacement, equivalent to  $\sqrt{2D\tau}$ . In non-complex geometries, such as a straight rectangular channel, these quantities are documented in literature. The time derivatives are replaced by a first order discretization. Ideally,  $\tau$  (simulation time step) should be as small as possible. However, taking an even smaller value of  $\tau$  greatly increases computing times. In practice, the values we take for  $\tau$  range between  $0.5 \cdot 10^{-6}$  s and  $1.5 \cdot 10^{-5}$  s, which are well below the characteristic times of the problem. We verify that the results are insensitive to the particular value of  $\tau$  taken within this range.

The Lagrangian approach also makes it easier to compute the Langevin equation, i.e. determining particle trajectory by writing that particle speed is equal to the force applied on it times its mobility [5, 6]. Thus, by applying these general equations to the particular geometry we consider, i.e. long shallow channels with rectangular cross-sections, where geometry is invariant in the  $y$  direction, we obtain the following:

$$\dot{x}(t) = \gamma(z)U(z) + \beta_x(z)\delta(t) \quad (2)$$

$$\dot{z}(t) = \beta_z(z)\delta(t) + \frac{d\beta_z}{dz}D + \beta_z \frac{D}{kT} (F_{vdWz} + F_{elz}) \quad (3)$$

where  $\dot{x}(t)$  and  $\dot{z}(t)$  are vector positions of the particle with respect to time respectively in the  $x$  (along the length of the channel) and  $z$  (along the height of the channel) directions. The  $\dot{x}$  component of the particles, moving along the channel length, have a unidirectional flow speed, scaled by  $\gamma$ . The trajectory along  $x$  has a correction factor,  $\beta_x$ , expressing confinement of the particle diffusion coefficient [6]. The  $\dot{z}$  component of the particles expresses the trajectory along  $z$  dimension with a diffusion component, whose correction factor,  $\beta_z$ , changes with particle distance with respect to the wall.

The expressions for  $\dot{y}(t)$  and  $\beta_y$  convey similar forms [6, 7] respectively to that of  $\dot{z}(t)$  and  $\beta_z$  but is ultimately negligible since we only consider the trajectories of the particles along  $x$  (length) and  $z$  (height), i.e. we analyze the deposition on the channel ceiling and floor, at  $z \pm \frac{h}{2}$ , and neglect the particles on the sidewalls.

In the following subsections, we provide a description of each of the terms in Eq.2 and Eq.3.

### B.1 Calculation of $\gamma$

The parameter  $\gamma$  introduces the ratio between average flow speed and the particle speed near the wall when  $z \approx r$  [7, 8, 9]:

$$\gamma(\eta) = \frac{U_p(z)}{U_r} \quad (4)$$

where  $U_p(z)$  is the average flow speed of the Poiseuille profile,  $U_r = \frac{6Qr}{wh^2} \left(1 - \frac{r}{h}\right)$  is the flow speed at  $z \approx r$ , where  $r$  is particle radius. The parameter  $\gamma(\eta)$  has the following expression as function of  $\eta$ , where  $\eta = \frac{z-r}{r}$ . For  $\eta > 1$ ,

$$\gamma(\eta) = 1 - \frac{5}{16\eta^3} \quad (5)$$

for  $10^{-4} < \eta < 1$ ,

$$\gamma(\eta) = \frac{1}{\eta + 1} \exp(0.68902 + \log(\eta) + 0.072332 \log^2(\eta) + 0.0037644 \log^3(\eta)) \quad (6)$$

for  $\eta < 10^{-4}$ ,

$$\gamma(\eta) = \frac{0.7431}{0.6376 - 0.2 \log(\eta)} \quad (7)$$

We introduce the coordinate:

$$\bar{\eta} = \int_0^\eta \eta \gamma(\eta) d\eta \quad (8)$$

In the case where van der Waals interactions dominate, for example, where  $z - r$  (and thus  $\eta$ ) is relatively small, this solution is not convenient to use, instead opting for an approximate solution by treating  $\gamma(\eta)$  as a constant,  $\gamma(\eta) \sim \gamma^*$ . With this approximation, we obtain:

$$\bar{\eta} \approx \frac{\gamma^*}{2} \eta^2 \quad (9)$$

Comparison between the approximate (Eq.8) and the exact solutions (Eq.9), same as in Ref. [7], show that by treating, for example,  $\gamma^* = 0.7$ , the approximate solution is barely indistinguishable from the exact one within a given range of  $\eta$  between  $10^{-3}$  and 1 (Fig.2). In physical terms, this corresponds to 2.5nm and  $2.5\mu\text{m}$ . Simulations show that below 2.5nm, all of the particles immediately adsorb to the wall, and consequently, the error made on the speed of deposition does not impact significantly the final position of the particle, nor the time it takes for getting adsorbed to the wall.

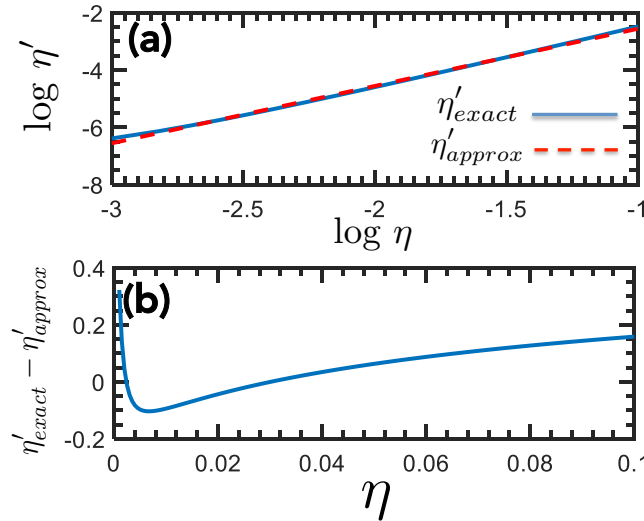


Figure 2: (a) Comparison, on a log log plot, between the approximate expression  $\bar{\eta} = \frac{\gamma^*}{2} \eta^2$  with  $\gamma^* = 0.7$  and the exact solution  $\bar{\eta} = \int_0^\eta \eta \gamma(\eta) d\eta$ . (b) Plot of the difference  $\int_0^\eta \eta \gamma(\eta) d\eta - \frac{\gamma^*}{2} \eta^2$  as a function of  $\eta$ .

## B.2 $\beta_x$ and $\beta_z$

The parameters  $\beta_x(z)$  and  $\beta_z(z)$  are dimensionless functions expressing the dependence of the longitudinal and transverse particle diffusion coefficients with  $z$ , the initial position of the particle with respect to the wall. From literature, the expressions for  $\beta_x$  and  $\beta_z$  are as follows [6, 3, 8, 9]:

$$\beta_x = 1 - \frac{9}{16z} + \frac{1}{8z^3} - \frac{45}{256z^4} - \frac{1}{16z^5} \quad (10)$$

$$\beta_z = \frac{6z^2 - 10z + 4}{6z^2 - 3z - 1} \quad (11)$$

## B.3 $\delta(t)$

As the particles move in the direction of the channel length,  $x$ ,  $\delta(t)$  is a zero mean step random function with amplitude  $\sqrt{2D\tau}$ , where  $\tau$  is the discrete incremental step used to calculate the trajectories. The parameter  $\delta(t)$  is an analogue to  $\Delta(t)$  in Eq.1. This parameter is in fact well-established [10] to take the Brownian movement into account. This makes the equation stochastic and as a result very difficult to solve, except in the case where this term can be neglected.

### B.4 Contribution of other forces

The bulk diffusion coefficient of the particles is represented by the Stokes-Einstein coefficient,  $D$ , while  $F$  is the force acting on the particle, comprising of two components: van der Waals,  $F_{vdWz}$ , and electrostatic forces,  $F_{elz}$ . Both forces act on the  $z$  direction, perpendicular to the wall.

$$F_{vdWz} = -\frac{Ar}{6(z-r)^2} \text{ and } F_{elz} = \frac{\chi}{\lambda_D} \exp\left(-\frac{z-r}{\lambda_D}\right) \quad (12)$$

The Hamaker constant,  $A$ , defines the strength of the surface interactions and can be affected by significant surface roughness [11]. We only consider Hamaker constant values where  $A > 0$ . The parameter  $\chi$  is a dimensionless function showing the product of the  $\zeta$  potential values:

$$\chi = 4\pi\epsilon\epsilon_0\zeta_w\zeta_p r \quad (13)$$

in which  $\epsilon$ ,  $\epsilon_0$  are respectively the relative dielectric constant of the fluid transporting the particles and the permittivity of free space,  $\zeta_w$  and  $\zeta_p$  are respectively the zeta potentials of the channel wall and the particle, and  $r$  is particle radius. Here, we consider both conditions where  $\chi > 0$  (repulsive charges or similar  $\zeta$  signs) and  $\chi < 0$  (attractive charges or opposite  $\zeta$  signs).

The parameter  $\lambda_D$  is the Debye length, (also expressed as  $\kappa^{-1}$ ), which for a monovalent salt follows [12]:

$$\lambda_D = \kappa^{-1} = \sqrt{\frac{\epsilon\epsilon_0 kT}{2(N_{Av})e^2 I}} \quad (14)$$

where  $N_{Av}$  is Avogadro's number,  $e$  is the elementary charge, and  $I$  is the ionic strength ( $\text{mol/m}^3$ ) equivalent to salt concentration in molarity,  $C_{salt}$ .

### B.5 Contribution of surface roughness

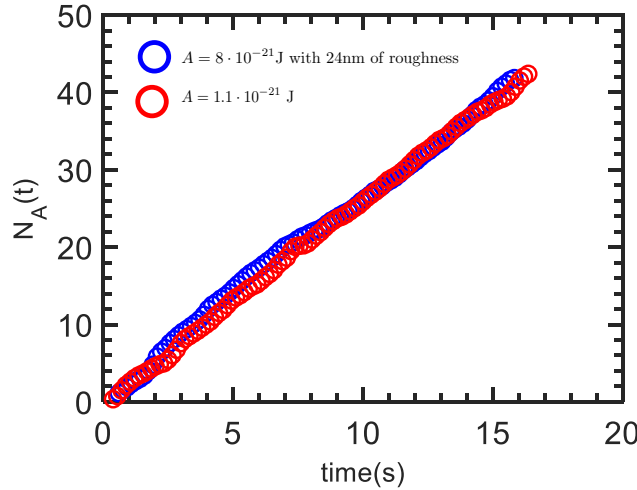


Figure 3: (a) Numerical simulation results of  $N_A(t)$  for  $A = 1.1 \cdot 10^{-21}$  J, which provides the same result as  $A = 8.0 \cdot 10^{-21}$  J with  $R_q = 24\text{nm}$ .

Surface roughness,  $R_q$ , affects surface interactions. Notably, it has been shown [13, 11] that Hamaker constants can vary with a certain degree of surface roughness but are often complex to analytically describe. Hence, surface roughness is usually characterized using AFM. In the theoretical analysis in the main manuscript, we did not introduce any surface roughness effect. This could have been done by modifying extensively the expression of the van der Waals forces but owing to simplicity, we did not do it. In the numerical simulations, however, the roughness effect can be gauged by incorporating it into the particle-surface distance,  $z$ , thereby resulting to a total effective particle-surface distance of  $z + R_q$ .

Take for example PDMS and unfunctionalized particles (PS-plain), in which both are considered smooth or with negligible roughness, the Hamaker constant for this interaction was determined to be  $A = 8.0 \cdot 10^{-21}$  J [7, 5,

14]. If we keep PDMS as the surface and change the particles from PS-plain to PS-fluo, we know that the Hamaker constant for this interaction was experimentally measured to be  $A = 1.1 \cdot 10^{-21}$  J. Using this  $A$  value agrees well with simulations. Moreover, in the simulation for this case,  $R_q$  was set to 0 since we presume that any obtained  $A$  value from the experiments already takes into account the effect of any roughness.

Furthermore, in Fig. 3, we find that the simulation results for  $A = 1.1 \cdot 10^{-21}$  J (red circles) is also equivalent to the results of  $A = 8.0 \cdot 10^{-21}$  J but with an additional 24 nm surface roughness (blue circles). In this regard, this suggests that the functionalization of PS-fluo adds a roughness value that changes the Hamaker constant from  $A = 8.0 \cdot 10^{-21}$  J to an effective value of  $A = 1.1 \cdot 10^{-21}$  J.

## B.6 Glossary of parameters and constants used in the theory and simulation section

Table 1: Nomenclature

Symbol	Definition
$h$	channel height
$w$	channel width
$L$	channel length
$C$	particle concentration in the advection-diffusion equation
$U_p$	average velocity based on Poiseuille profile
$U_r$	flow velocity at distance $z \approx r$
$\dot{x}$	vector position in the $x$ direction
$\dot{z}$	vector position in the $z$ direction
$\gamma$	ratio between $U_p/U_r$
$\beta_x$	dimensionless function expressing dependence of longitudinal particle diffusion coefficient w.r.t wall
$\beta_z$	dimensionless function expressing dependence of transverse particle diffusion coefficient w.r.t wall
$\delta(t)$	zero mean step random function with amplitude, $\sqrt{2D\tau}$
$\tau$	incremental time step
$D$	Stokes-Einstein diffusion coefficient of particle
$A$	Hamaker constant
$r$	particle radius
$k$	Boltzmann constant
$T$	temperature
$\chi$	dimensionless function showing product strength of $\zeta_w$ and $\zeta_p$
$\zeta_w$	zeta potential of the microfluidic channel surface walls
$\zeta_p$	zeta potential of the colloidal particle surface
$\epsilon$	dielectric constant of the fluid
$\epsilon_0$	permittivity of free space
$\lambda_D$	Debye length
$N_{Av}$	Avogadro's number
$e$	elementary charge
$C_{salt}$	salt concentration in molar units
$I$	ionic strength in mol/m <sup>3</sup> units
$F_{vdWz}$	van der Waals forces which act on the $z$ direction perpendicular to wall
$F_{elz}$	electrostatic forces which act on the $z$ direction perpendicular to wall
$S$	collection factor
$z_0$	position of the particle w.r.t wall following its exit trajectory
$\eta$	dimensionless altitude, $\eta = \frac{(z-r)}{\lambda_D}$ , but in definition of $\gamma(\eta)$ , $\eta$ is also dimensionless altitude $\eta = \frac{(z-r)}{r}$
$t$	time
$P$	dimensionless parameter showing strength of van der Waals forces w.r.t Debye forces
$\sigma_L$	dimensionless parameter equivalent to $\sigma_L = \frac{D\chi L}{\gamma_0 U_r \lambda_D r k T}$
$\xi_L$	effective Peclet number
$Q$	flow rate (velocity $\times$ cross section)
$\phi$	experimental particle concentration
$v_p$	spherical volume of the particle
$N_A(t)$	number of adsorbed particles as a function of time
$S_{vdw}$	theoretical expression of $S$ when van der Waals forces dominate (at high ionic strengths)

## C Numerical simulations of $\zeta_w$ and $\zeta_p$ for repulsive charges

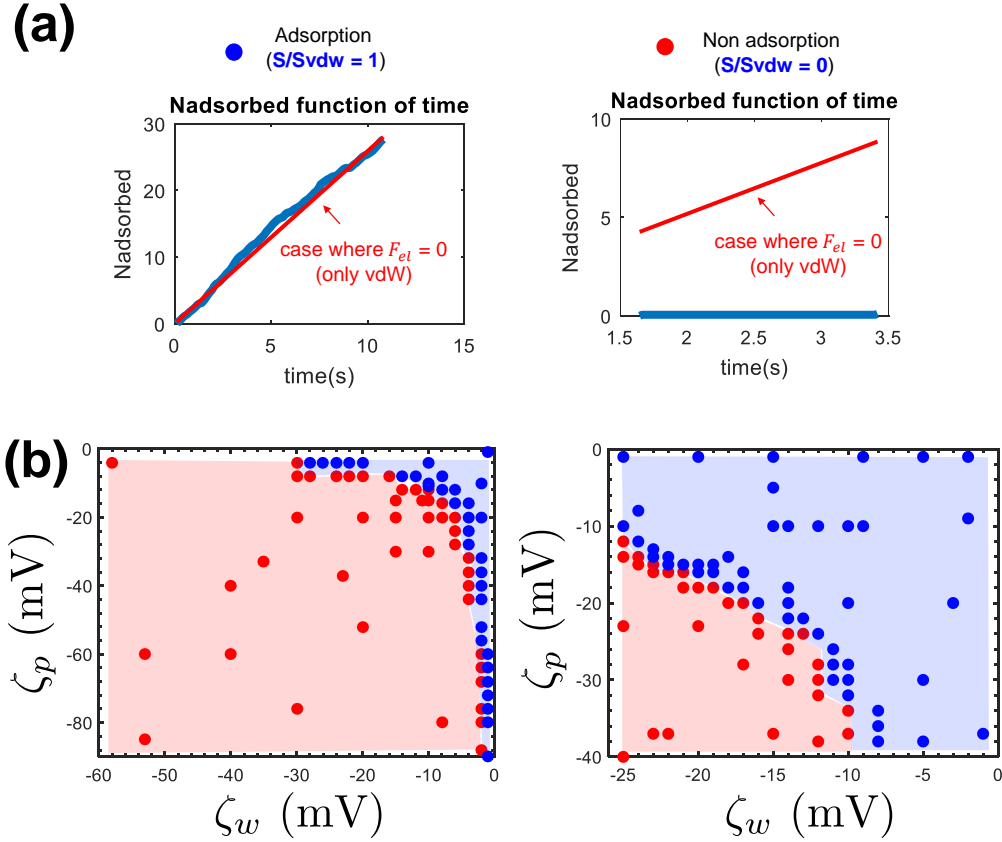


Figure 4: (a) Simulation results based on Langevin equations with adhesion and electrostatic forces. In the case of repulsive charges, results are binary, i.e. deposition/adsorption (●) or no deposition/adsorption (●). When  $S/S_{vdw} = 1$ , the simulation results agree with the theoretical expression, which has been calculated at conditions of high ionic strengths where van der Waals forces control deposition and electrostatic contributions are inexistent. When  $S/S_{vdw} = 0$ , the simulation results do not agree with the theoretical expression, mainly because simulation results show that particles are repelled from the surface. This happens at lower salt concentrations. (b) Some examples of different combinations of  $\zeta_p$  and  $\zeta_w$  for a certain salt concentration. (b, left) 0.01 M NaCl and (b, right) 0.1M NaCl. Blue and red regions represent deposition and no deposition, respectively.

We perform numerical simulations based on Langevin equations and generate a phase diagram of  $\zeta_p$  and  $\zeta_w$  combinations. In this case, for repulsive charges, both  $\zeta_w$  and  $\zeta_p$  have the same sign. The sign is negative (-) for both to mirror that of the typical surface charge under aqueous conditions.

As described, we perform numerical simulations of particle deposition on the microchannel surface taking into account contributions of the different forces such as adhesion (vdW) and electrostatic (Debye). Generally, at a given  $C_{salt}$ , there is a certain  $\zeta_p$  and  $\zeta_w$ . However, depending on the type of particle or channel wall surface, we can also have various combinations of both  $\zeta$  potentials. In these simulations results shown in Fig. 4, we demonstrate different combinations of  $\zeta_p$  and  $\zeta_w$ , where results seem to be binary, i.e. deposition/adsorption (●) or no deposition/non-adsorption (●). This binary result also explains why  $S/S_{vdw}$  is either 0 or 1. When  $\frac{S}{S_{vdw}} = 1$ , this means that the  $S$  value obtained from simulations is equivalent to the theoretical expression,  $S_{vdw}$ , represented by the solid red line in Fig. 4(a, left). This is the theoretical prediction at high salt concentration, typically at concentrations  $\geq 0.1$  M NaCl, where deposition is controlled by van der Waals-adhesion forces and electrostatic forces,  $F_{el} \approx 0$ .

When  $\frac{S}{S_{vdw}} = 0$ , this means that the  $S$  value from simulations is zero as in Fig.4(a, right), i.e. particles are repelled from the surface and thus there is no deposition.

For reference,  $S$  is from Eq.16 and  $S_{vdw}$  is from Eq.13 in the main manuscript.

Results in Fig. 4(b) show that for a wide range of values, the deposition result does not change significantly, i.e. the particles are either attracted (●) to or repelled (●) from the surface. In this example, both  $\zeta_w$  and  $\zeta_p$  possess the same sign (repulsive charges).

Two examples are given in the figure: 0.01M NaCl in Fig. 4(b, left) and 0.1M NaCl in Fig. 4(b, right). In both cases, any combination of  $\zeta_p$  and  $\zeta_w$  that falls within the red zone means that both surface charges repel each other. Hence, the particle does not deposit onto the surface. For example, at 0.1M NaCl, a  $\zeta_w = -15\text{mV}$  and  $\zeta_p = -30\text{mV}$  combination would yield no deposition. However, a combination  $\zeta_w = -20\text{mV}$  and  $\zeta_p = -5\text{mV}$  will result to deposition.

We have also evaluated literature data (e.g. in Ref. [15, 16]) on  $\zeta_p$  and  $\zeta_w$  combinations and the results indeed fall within the shaded region.

## D Numerical simulations of $\zeta_w$ and $\zeta_p$ for attractive charges

We perform additional numerical simulations based on Langevin equations (see Theory and Simulations section in main manuscript; see also Ref. [7, 5, 14]) and generate diagrams of  $\zeta_p$ ,  $\zeta_w$ , and  $S/S_{vdw}$  combinations. In this case, for attractive charges, both  $\zeta_w$  and  $\zeta_p$  have the opposite sign.

As described in the main manuscript, we perform numerical simulations of particle deposition on the microchannel surface taking into account contributions of the different forces such as adhesion (vdW) and electrostatic (Debye). At a given  $C_{salt}$ , we have already experimentally determined  $\zeta_p$  from ZetaSizer measurements (see SI-A).

Knowing the value of  $\zeta_p$  and keeping it constant, we vary  $\zeta_w$  over a wide range (from -100 mV to +100 mV). We further extend the analyses by performing more simulations at two additional (hypothetical)  $\zeta_p$  values. Similarly, we keep these hypothetical  $\zeta_p$  values constant while also varying  $\zeta_w$  over an identical range (-100mV to +100mV). Results are shown in Fig. 5 (PS-fluo and APTES-treated PDMS) and Fig. 6 (PS-amine and plasma-treated PDMS).

The results in Fig. 5 show simulations for PS-fluo (-) on APTES-treated walls (+), taking into account  $A = 1 \cdot 10^{-21} \text{J}$ , as determined experimentally.

Results in Fig. 5 reveal a sigmoidal pattern, where at (-) values of  $\zeta_w$ ,  $S/S_{vdw} = 0$ . This is expected since the particle, PS-fluo, has a negative charge. Thus, two negative surface charges result to repulsion. There is a transition value at low  $\zeta_w$  values, followed by a plateau. Simulations show that for wide range of (+)  $\zeta_w$  values spanning approximately two orders of magnitude, from  $\sim +1 \text{mV}$  to  $+100 \text{mV}$ , the value of  $S/S_{vdw}$  does not significantly change. For example, at 0.01M NaCl (Fig.5(c)) and  $\zeta_p = -44 \text{mV}$  (red circle), a  $\zeta_w$  value of either  $\zeta_w = +18 \text{mV}$  or  $\zeta_w = +100 \text{mV}$ , yields approximately the same value for  $S/S_{vdw} \approx 1.5$ .

In the case of attractive charges,  $S/S_{vdw} \approx 1$  only at higher salt concentrations, 0.1M NaCl (Fig. 5(d)) and 1M NaCl (Fig. 5(e)). For lower ionic strengths,  $S/S_{vdw} \gg 1$ , as also predicted by our experiments. The qualitative trend of increasing deposition at low ionic strengths agrees with experiments, although there is disparity between the actual quantitative values at low salt concentrations (see Experiments: attractive charges section in main manuscript). Our experiments generally predict a smaller  $S/S_{vdw}$  value, probably due to the fact that the simulation does not take into account interparticle interactions once the experiment saturates (too many particles that result to aggregation)

The results in Fig. 6 show simulations for PS-amine (+) on hydrophilic plasma-treated walls (-), taking into account  $A = 0.4 \cdot 10^{-21} \text{J}$ , as determined experimentally.

Results in Fig. 6 also reveal a sigmoidal pattern but in reverse, where at (+) values of  $\zeta_w$ ,  $S/S_{vdw} = 0$ . This is expected since the particle, PS-amine, has a positive charge. Thus, two positive surface charges also result to repulsion. There is a transition value at low negative  $\zeta_w$  values, followed by a plateau at increasingly negative  $\zeta_w$  values.

Simulations show that for wide range of (-)  $\zeta_w$  values spanning approximately from  $\sim -1 \text{mV}$  to  $-100 \text{mV}$ , the value of  $S/S_{vdw}$  does not significantly change. For example, at 0.001M NaCl (Fig.6(b)) and  $\zeta_p = +6.8 \text{mV}$  (red circle), a  $\zeta_w$  value of either  $\zeta_w = -25 \text{mV}$  or  $\zeta_w = -100 \text{mV}$ , yields approximately the same value for  $S/S_{vdw} \approx 5$ .

Similar to the previous case for attractive charges,  $S/S_{vdw} \approx 1$  only at higher salt concentrations, 0.1M NaCl (Fig. 6(d)) and 1M NaCl (Fig. 6(e)). For lower ionic strengths,  $S/S_{vdw} \gg 1$ , as also predicted by our experiments. Similarly, the qualitative trend of increasing deposition at low ionic strengths agrees with experiments, although there is still disparity between the actual quantitative values at low salt concentrations.

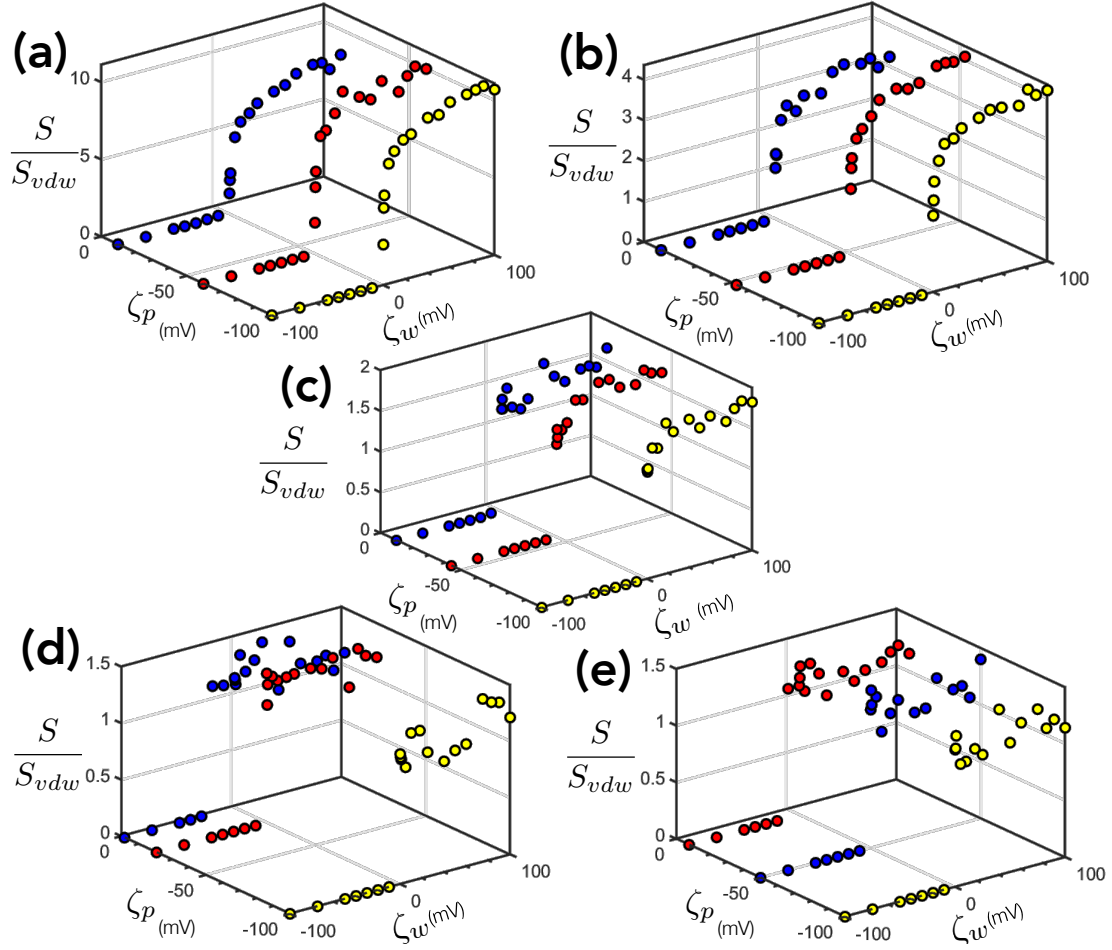


Figure 5: Simulation results based on Langevin equations with adhesion and electrostatic forces for PS-fluo and APTES-treated wall, where surface charges have opposite signs. (a) Results at 0.0001M NaCl. (b) Results at 0.001M NaCl. (c) Results at 0.01M NaCl. (d) Results at 0.1M NaCl. (e) Results at 1M NaCl. In (a-e) (●) are the experimental  $\zeta_p$  values obtained from the ZetaSizer, while (●) and (●) are two hypothetical  $\zeta_p$  values at  $\zeta_p = -10$  mV and  $\zeta_p = -100$  mV respectively. However, in (e) (●) and (●) are two hypothetical  $\zeta_p$  values at  $\zeta_p = -50$  mV instead and  $\zeta_p = -100$  mV respectively.



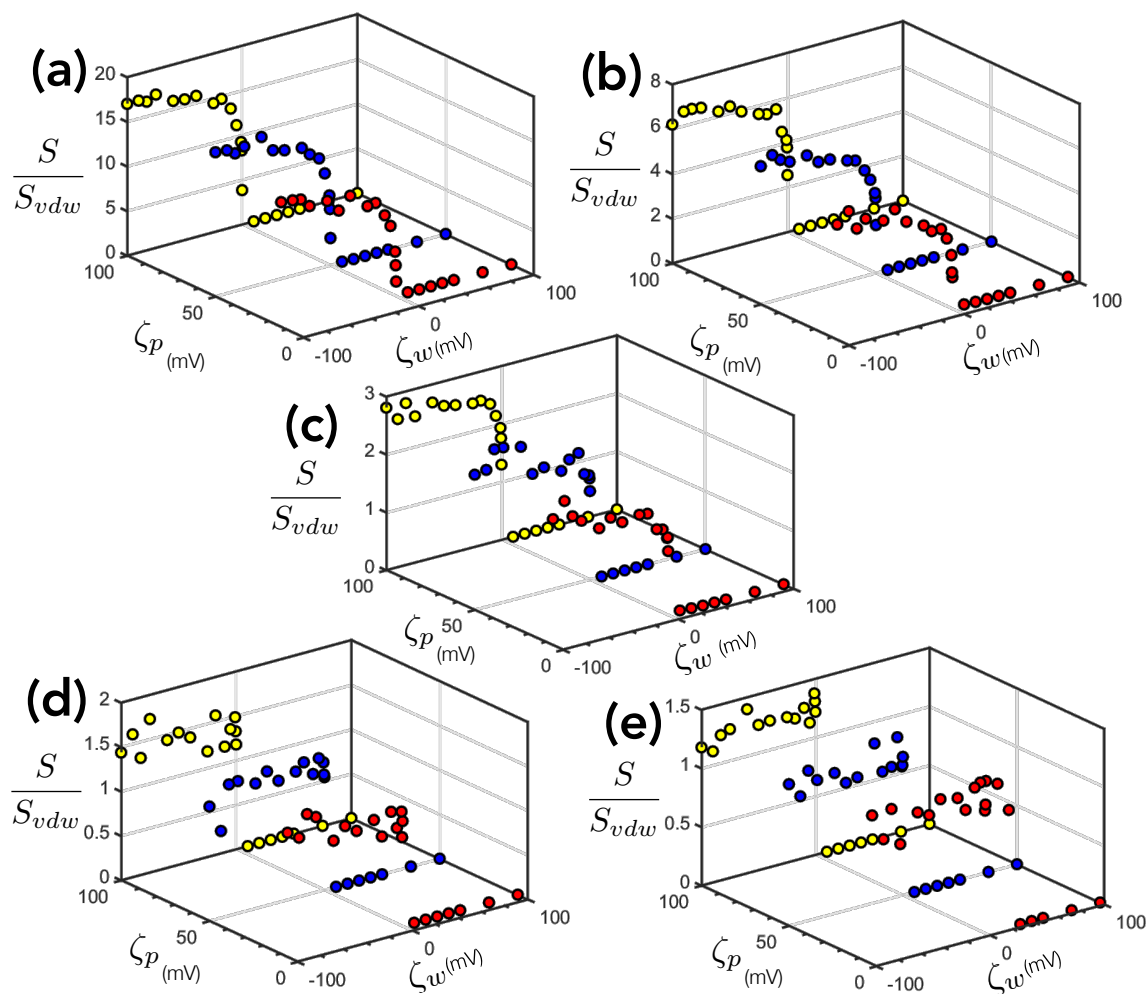


Figure 6: Simulation results based on Langevin equations with adhesion and electrostatic forces for PS-amine and plasma-treated wall, where surface charges have opposite signs. (a) Results at 0.0001M NaCl. (b) Results at 0.001M NaCl. (c) Results at 0.01M NaCl. (d) Results at 0.1M NaCl. (e) Results at 1M NaCl. In (a-e) (●) are the experimental  $\zeta_p$  values obtained from the ZetaSizer, while (●) and (●) are two hypothetical  $\zeta_p$  values at  $\zeta_p = +50$ mV and  $\zeta_p = +100$ mV respectively.

## E Experimental and numerical results for $N_A(t)$ at different ionic strengths for attractive charges

We perform numerous comparisons of experimental and numerical results, in which some examples are shown in Fig. 7 for the number of particles adsorbed as a function of time,  $N_A(t)$  at different salt concentrations.

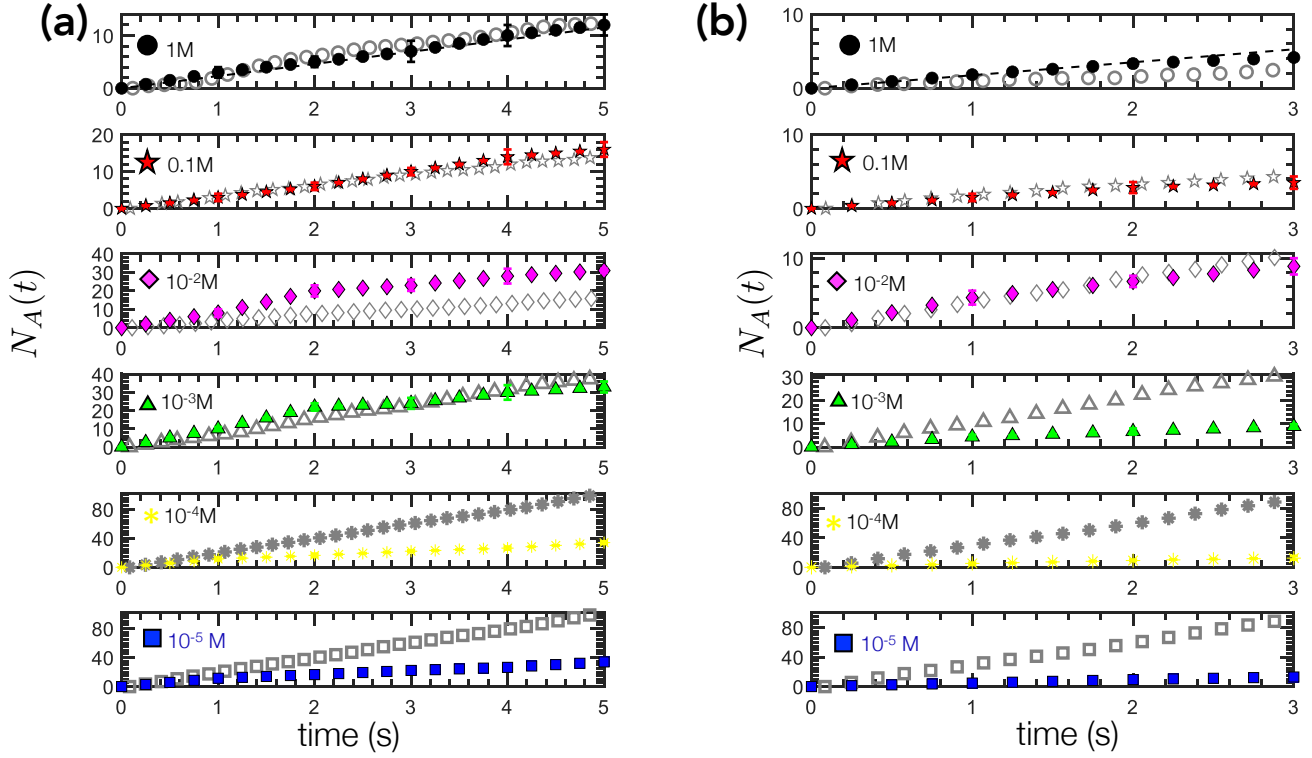


Figure 7: Simulation and experimental results of  $N_A(t)$  at different salt concentrations during initial seconds of deposition. (a) Results for PS-fluo on APTES-treated wall, where  $A = 1.1 \cdot 10^{-21}$  J,  $r = 2.4 \mu\text{m}$ ,  $U = 8 \text{mm/s}$ ,  $\zeta_p$  varies accordingly to the graph in Fig.1 (SI-A), and  $\zeta_w = +1 \text{mV}$  for  $10^{-2} \text{M}$  to  $1 \text{M}$  NaCl,  $\zeta_w = +25 \text{mV}$  for  $10^{-3} \text{M}$  to  $10^{-5} \text{M}$  NaCl. (b) Results for PS-amine on plasma-treated wall, where  $A = 0.4 \cdot 10^{-21}$  J,  $r = 2.4 \mu\text{m}$ ,  $U = 8 \text{mm/s}$ ,  $\zeta_p$  varies accordingly to the graph in Fig.1 (SI-A), and  $\zeta_w = -1 \text{mV}$  for  $10^{-2} \text{M}$  to  $1 \text{M}$  NaCl,  $\zeta_w = -10 \text{mV}$  for  $10^{-3} \text{M}$  to  $10^{-5} \text{M}$  NaCl.

At high salt concentrations, surface charges are screened so their magnitudes are typically smaller while at lower salt concentrations, the magnitude of the charges are larger. From simulations concerning different  $\zeta_w$  values (SI-C and SI-D) for these two different surface treatments, it appears that from a certain value, any further increase in the magnitude of the  $\zeta_w$  no longer has a significant effect on the number of adsorbed particles since the curve of  $S/S_{vdw}$  begins to plateau.

## References

- [1] C. Henry, P. Minier, and G. Lefevre, “Towards a description of particulate fouling: from single particle deposition to clogging,” *Adv. Colloids Inter. Sci.*, vol. 185–186, pp. 34–76, 2012.
- [2] H. Unni and C. Yang, “Kinetics of colloidal particle deposition to a solid surface from pressure driven microchannel flows,” *Can. J. Chem. Engr.*, vol. 85, pp. 609–616, 2007.
- [3] —, “Colloidal particle deposition from electrokinetic flow in microfluidic channel,” *Electrophoresis*, vol. 30, pp. 732–741, 2009.
- [4] Z. Adamczyk, T. Dabros, J. Czarnecki, and T. V. de Ven, “Particle transfer to solid surfaces,” *Adv. Colloids Inter. Sci.*, vol. 19, pp. 183–252, 1983.
- [5] C. M. Cejas, F. Monti, M. Truchet, J. Burnouf, and P. Tabeling, “Universal diagram for the kinetics of particle deposition in microchannels,” *Physical Review E*, vol. 98, p. 062606, 2018.
- [6] P. Tabeling, *Introduction to Microfluidics*. Oxford, UK: Oxford University Press, 2005.
- [7] C. M. Cejas, F. Monti, M. Truchet, J. Burnouf, and P. Tabeling, “Particle deposition kinetics of colloidal particles in microchannels at high ionic strength,” *Langmuir*, vol. 33, no. 26, pp. 6471–6480, 2017.
- [8] H. Brenner, “The slow motion of a sphere through a viscous fluid towards the plane,” *Chem. Eng. Sci.*, vol. 16, pp. 242–251, 1961.
- [9] M. Bevan and D. Prieve, “Hindered diffusion of colloidal particles very near to the wall: revisited,” *J. Chem. Phys.*, vol. 113, pp. 1228–1236, 2000.
- [10] P. Huang and K. Breuer, “Direct measurement of anisotropic near-wall hindered diffusion using total internal reflection velocimetry,” *Phys. Rev. E*, vol. 76, no. 046307, 2007.
- [11] M. C. Stevenson, S. P. Beaudoin, and D. S. Corti, “Toward an improved method for determining the hamaker constant of solid materials using atomic force microscopy. i. quasi-static analysis for arbitrary surface roughness,” *J. Phys. Chem. C*, vol. 124, pp. 3014–3027, 2020.
- [12] A. Khair and T. M. Squires, “The influence of hydrodynamic slip on the electrophoretic mobility of a spherical colloidal particle,” *Physics of Fluids*, vol. 21, p. 042001, 2009.
- [13] V. Valmacco, M. Elzvbiciak-Wodka, C. Besnard, P. Maroni, G. Trefalt, and M. Borkovec, “Dispersion forces acting between silica particles across water: influence of nanoscale roughness,” *Nanoscale Horiz.*, vol. 1, p. 325, 2016.
- [14] C. M. Cejas, L. Maini, F. Monti, and P. Tabeling, “Deposition kinetics of bi- and tridisperse colloidal suspensions in microchannels under the van der waals regime,” *Soft Matter*, vol. 15, p. 7438, 2019.
- [15] A. Garg, C. Cartier, K. Bishop, and D. Velegol, “Particle zeta potentials remain finite in saturated solutions,” *Langmuir*, vol. 32, pp. 11 837–11 844, 2016.
- [16] B. Mustin and B. Stoeber, “Single layer deposition of polystyrene particles onto planar polydimethyl siloxane substrates,” *Langmuir*, vol. 32, pp. 88–101, 2016.

## DISCUSSÃO

Emulsões são sistemas coloidais amplamente difundidos em diversos processos. Em indústrias alimentícias, farmacêuticas e cosméticas geralmente é realizado o desenvolvimento de emulsões visando aplicações tecnológicas. Por outro lado, emulsões também podem ser estruturas inerentemente oriundas de processos biotecnológicos e petrolíferos, sendo nestes casos consideradas indesejáveis, pois aprisionam o produto de alto valor agregado. Independente da aplicação e/ou necessidade de separação de fases, a capacidade de formação e estabilidade são características essenciais a serem estudadas para se entender o comportamento de emulsões. No entanto, ferramentas que permitam uma investigação das emulsões de maneira sistemática são atualmente escassas, fazendo com que a microfluidica manifeste-se como uma estratégia para superar tal limitação. Assim, este estudo surgiu no sentido de analisar a estabilidade de emulsões com base nesta tecnologia, em que os mecanismos de des(estabilização) poderiam ser avaliados em tempo real, bem como seu grau de estabilidade. Apesar de diversos sistemas microfluidicos que levem à desestabilização de emulsões estarem descritos na literatura, ainda se observa um grande desafio em induzir a desestabilização de emulsões desenvolvidas com alta quantidade de estabilizantes com propriedades tensoativas. Além disso, específicas interações entre os componentes das emulsões com a parede dos microcanais ainda possuem diversos fatores a serem revelados.

Isto posto, para melhor entender a discussão relacionada a esta tese, suas respectivas etapas e capítulos experimentais estão descritos na Figura 1. Como mencionado, estes canais seriam testados a priori utilizando emulsões-modelo estabilizadas por compostos fermentativos que foram caracterizadas no *Capítulo 2*, visto que as propriedades tensoativas de tais componentes são pouco conhecidas. Neste estudo, constatou-se a dificuldade em compreender os mecanismos de estabilização de tais emulsões devido à falta de informações sobre a composição dos agentes aplicados, levando à necessidade de se abordar adicionalmente sistemas mais bem estabelecidos na literatura. Desta maneira, para dar continuidade à investigação destes sistemas, foram produzidos tanto canais em PDMS selados ao vidro quanto canais gerados a partir da corrosão de vidro selados ao PDMS, ambos contendo câmaras de expansão visando induzir a aproximação e o choque entre as gotas. Como inicialmente havia o intuito de formar e desestabilizar a emulsão concomitantemente (para simular a re-coalescência de emulsões em processos fermentativos), canais foram desenvolvidos utilizando vidro (propriedades hidrofílicas) esperando-se que produzissem emulsões O/A. No entanto, emulsões A/O foram geradas, provavelmente devido à única superfície de PDMS (hidrofóbico) que

governou a formação de tais emulsões. Destarte, ambos os canais com câmaras de expansão foram empregados para um estudo fundamental (*Capítulo 3*) que concerne à desestabilização de emulsões A/O através de choque induzido. De fato, apesar de emulsões A/O serem geradas nos canais de vidro, as gotas apresentavam uma maior dificuldade na sua formação, não sendo possível a geração de alguns tipos de emulsões, como aquelas que continham hexadecano como fase contínua (mais apolar que os demais óleos). Além disso, a indução do choque possibilitou identificar as emulsões mais susceptíveis à desestabilização. Contudo, pode-se verificar determinadas interações das gotas com a parede dos microcanais, levando à premissa de que, para a utilização de microcanais visando a determinação da estabilidade do sistema coloidal, estes dispositivos não devem interagir com as gotas da emulsão. Porém, se o objetivo é induzir a máxima separação de fases, deve-se utilizar a condição de parede que promova a mais eficiente desestabilização das gotas. Através deste estudo, observou-se que a desestabilização de emulsões em microcanais possui uma complexidade inerente devido às diversas variáveis (propriedades intrínsecas da emulsão e dos microcanais) que afetam o sistema, motivando ainda mais um estudo abrangente englobando, além dos compostos-modelo aplicados em fermentações, surfactantes convencionais conhecidos, focando no entendimento dos fenômenos físico-químicos relacionados à desestabilização de emulsões em microdispositivos.

Devido à impossibilidade de formação de emulsões O/A nos canais previamente expostos, uma segunda estratégia que concerne à utilização de canais capilares de vidro tridimensionais (3D) (*Capítulo 4*) foi dimensionada. Como os canais capilares de vidro são inertes e de natureza hidrofílica, foi possível a produção de emulsões O/A tanto com componentes de processos biotecnológicos quanto com surfactantes convencionais. Através desta análise, constatou-se que os canais 3D não seriam adequados devido à sobreposição das gotas ocasionada no processo, dificultando a visualização dos eventos de desestabilização.

Desta maneira, imergindo os estudos dos *Capítulos 2 e 4* (*in situ* nos canais e *ex situ* com medidas convencionais) foi possível verificar a formação de emulsões O/A com diferentes combinações óleo-antiespumantes/surfactantes, além de mapear as categorias de antiespumantes que promoviam maior ou menor estabilidade ao sistema emulsionado. Sendo assim, de modo geral os estudos nos microcanais corroboraram aqueles com medidas convencionais de estabilidade. Outrossim, similaridades de resultados emergiram-se dos *Capítulos 3 e 4*: foi possível obter *insights* sobre a estabilidade das emulsões baseados em estudos relacionados à formação das gotas e posterior observação da coalescência. No entanto, tais geometrias (canais capilares ou planares contendo câmaras de expansão) não foram suficientes para induzir a desestabilização de emulsões altamente estáveis. Deste modo, apesar

de ser possível a obtenção de indícios da instabilidade, uma nova estratégia se fez necessária para avaliar emulsões com alto grau de estabilidade. Tal estratégia foi baseada na premissa de que sistemas concentrados seriam mais eficientemente desestabilizados devido às interações gota-gota, gota-parede do canal e ao efeito dinâmico da alteração da concentração de surfactantes na interface, além de que outros componentes poderiam ser injetados no interior dos canais para promover a instabilidade interfacial. Este estudo sistemático acarretou em uma melhor compreensão da susceptibilidade das emulsões frente a diferentes compostos e condições de estocagem.

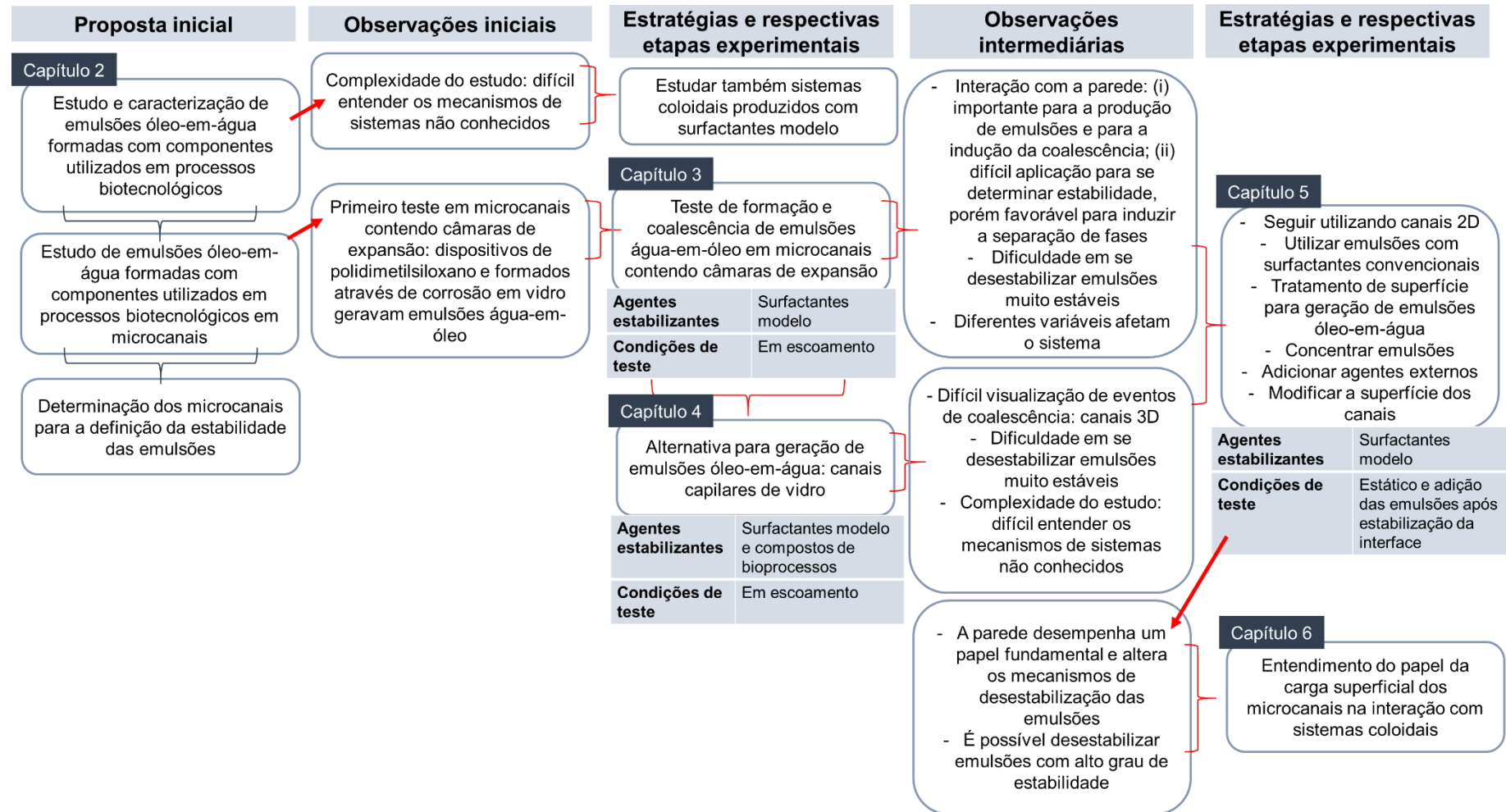
Em vista dos fatores previamente expostos, foram analisados (*Capítulo 5*) sistemas concentrados em câmaras microfluidicas com diferentes propriedades de superfície e com adicional injeção de água ou solução salina. As emulsões foram produzidas utilizando surfactantes convencionais para um melhor entendimento dos mecanismos envolvidos na desestabilização das emulsões. Estas emulsões foram injetadas de maneira passiva (para não comprometer sua estabilidade) após tempo suficiente para a adsorção dos surfactantes na interface (para que uma estabilidade ainda maior fosse avaliada). Ademais, apesar de neste tipo de emulsão altamente estável o estudo de formação não ser relevante, visto que todas as emulsões são facilmente desenvolvidas, deve-se ajustar adequadamente a molhabilidade do canal de acordo com o surfactante (potencial zeta) e a natureza da fase contínua da emulsão (água ou óleo). Assim, através desta análise voltada para emulsões O/A, foi constatado que um vasto número de variáveis afetava os sistemas e, por conseguinte, um estudo adicional foi realizado visando revelar o efeito da carga superficial dos canais em induzir potenciais interações com as partículas (*Capítulo 6*). Desta maneira, foi possível determinar o papel da superfície dos canais, das propriedades das emulsões e dos compostos inseridos no interior da câmara microfluidica em promover a desestabilização das gotas. Ademais, foi alcançada a desestabilização inclusive das emulsões mais estáveis.

Perante o exposto, como cada microcanal se mostrou eficiente para desestabilizar emulsões com diferentes graus de estabilidade, canais em série poderiam ser considerados como uma estratégia interessante. Neste viés, primeiramente a emulsão entraria em contato com um microcanal reto sob condições de escoamento (como os capilares de vidro, porém em 2D) no qual emulsões menos estáveis desestabilizariam quando em contato e choque, podendo-se avaliar os eventos de desestabilização. Aquelas que não fossem desestabilizadas seguiriam para câmaras com expansão (produzidas com superfícies que não interagissem com as gotas, o que sugere que cada tipo de emulsão seria testada em canais específicos). Assim, as emulsões com estabilidade intermediária seriam desestabilizadas e, neste ponto, teríamos os resultados de sua

estabilidade. Por outro lado, as emulsões mais estáveis seguiriam para um próximo canal que promoveria a indução da desestabilização destas emulsões concentradas em contato com agentes que auxiliariam tal ocorrência e, então, sua estabilidade seria determinada. A inserção de emulsões com baixa estabilidade nos microcanais mais eficientes não são sugeridas visto que a desestabilização ocorre facilmente, o que prejudicaria a leitura do grau de estabilidade. Ademais, as câmaras com emulsões concentradas permitiriam entender os mecanismos associados à estabilidade de emulsões quando submetidas a variadas condições ambientais (do meio e da parede dos canais). E claramente, se o objetivo for somente a separação de fases, tais câmaras também seriam mais indicadas.

Para finalizar, entende-se que para os estudos de estabilidade ao longo do tempo se faz necessário o recolhimento das emulsões e posterior injeção das mesmas nos microcanais através de maneiras passivas e que não comprometam a estabilidade da emulsão (ex. baixas pressões). Por outro lado, para os estudos serem correlacionados ao comportamento das emulsões frente aos processos convencionais de formação, estas devem ser formadas e avaliadas concomitantemente nos microcanais. Deste modo, considerando as possíveis aplicações do sistema microfluidico em série, o ideal seria que emulsões geradas nos bioprocessos fossem desestabilizadas nas condições do primeiro canal logo após a formação da gota, indicando re-coalescência durante o processo. Ademais, seria interessante que estas emulsões também fossem avaliadas e desestabilizadas após um determinado tempo, visando a separação do bioproduto. Para aplicações industriais, as emulsões devem possuir um maior grau de estabilidade, não sendo desestabilizadas nas condições dos canais iniciais sendo, portanto, desestabilizadas (ou se possível, não desestabilizadas) na câmara com sistemas concentrados. Da mesma maneira, uma avaliação concomitante à formação indicaria re-coalescência durante a produção da emulsão (gerando sistemas com maior tamanho de gota), enquanto uma avaliação posterior indicaria a estabilidade ao longo do tempo. Finalmente, a geometria final também seria importante para se distinguir a estabilidade da emulsão frente às diferentes condições de estocagem e substâncias, podendo ser utilizada para avaliar o efeito de diversas matrizes e até de compostos desemulsificantes.

**Figura 1.** Detalhamento dos capítulos experimentais da tese, observações e justificativas.





## CONCLUSÃO

Diante dos resultados encontrados ao longo do trabalho, pôde-se verificar que tanto as análises de formação de emulsões em microcanais, quanto as de desestabilização proveem ferramentas relevantes para a aquisição de um maior conhecimento relacionado a estes sistemas coloidais. Além disso, constatou-se o quão complexo é a construção de um microcanal para a avaliação da estabilidade (e dos mecanismos) e indução da desestabilização de emulsões, principalmente devido às inúmeras variáveis inerentes ao processo. No entanto, foi alcançado um maior entendimento associado ao sistema, permitindo sugerir vertentes a serem abordadas para atingir tal desenvolvimento. Ademais, como previamente mencionado, as análises de formação de emulsões em microcanais demonstraram ser relevantes e, neste viés, estudos para se determinar possíveis interações entre os próprios estabilizantes e obter indícios dos mecanismos de estabilização de emulsões (e até das suas potenciais concentrações) podem ser realizados nos microdispositivos. Contudo, deve-se ter em conta que, para a análise de formação das gotas, a natureza da fase contínua das emulsões e da superfície dos microcanais deve ser a mesma (por ex. emulsões O/A formadas em superfícies hidrofílicas) e os estabilizantes devem possuir o mesmo sinal de carga que a superfície dos canais (ex. potencial zeta positivo dos canais com positivo dos estabilizantes é adequado para a formação de gotas). Em se tratando de análises de estabilidade, os canais produzidos em vidro não provocaram interação com os estabilizantes. No entanto, as estruturas capilares não demonstraram ser de grande valia neste tipo de análise pois, apesar de promoverem a coalescência de algumas emulsões via aumento da área dos dispositivos, as gotas fluem através de um sistema 3D e, portanto, pode ser difícil visualizar os eventos de desestabilização. Outrossim, mudar a geometria dos capilares também é um fator limitante. Finalmente, câmaras contendo emulsões concentradas e com injeção de solução aquosa se mostraram eficientes para a avaliação e o entendimento dos mecanismos associados à estabilidade das emulsões, principalmente em se tratando de emulsões altamente estáveis. Não obstante, cabe ressaltar que, se o objetivo for somente promover a desestabilização das emulsões (como nos bioprocessos para a separação eficiente das fases), canais específicos para cada emulsão podem ser aplicados, principalmente considerando-se a estratégia utilizando emulsões concentradas visto que, neste caso, as condições não precisam ser controladas e agentes externos podem ser incorporados para promover a desemulsificação. Por outro lado, para uma comparação eficiente do grau de estabilidade das emulsões, os canais em série seriam mais adequados e, além disso, as interações dos surfactantes/agentes de superfície com a parede dos canais deveriam ser previamente avaliadas. A estratégia considerando emulsões

concentradas também poderia ser aplicada para desvendar tanto os mecanismos associados à desestabilização, bem como a influência de agentes químicos e de diferentes componentes quando adicionados ao sistema. Além disso, esta estratégia se mostra adequada para entender o papel da parede dos canais na desestabilização das emulsões, o que poderia ser extrapolado para condições ambientais ou de estocagem. Por fim, as análises aqui realizadas enfatizaram a importância da funcionalização do canal e mais ainda, da essencialidade do estudo frente à sua utilização.

## REFERÊNCIAS

- AVEYARD, R.; BINKS, B. P.; FLETCHER, P. D. I.; LU, J. R. The resolution of water-in-crude oil emulsions by the addition of low molar mass demulsifiers. **Journal of Colloid and Interface Science**, v.139, p.128-138, 1990.
- BREMOND, N.; THIAM, A. R.; BIBETTE, J. Decompressing emulsion droplets favors coalescence. **Physical Review Letters**, v.100, p.024501, 2008.
- BREMOND, N.; DOMÉJEAN, H.; BIBETTE, J. Propagation of drop coalescence in a two-dimensional emulsion: a route towards phase inversion. **Physical Review Letters**, v.106, p.214502, 2011.
- DENG, N-N.; SUN, S-X.; WANG, W.; JU, X-J.; XIE, R.; CHU, L-Y. A novel surgery-like strategy for droplet coalescence in microchannels. **Lab on a Chip**, v.13, p.3653-3657, 2013.
- FURTADO, G. F.; PICONE, C. S. F.; CUELLAR, M. C.; CUNHA, R. L. Breaking oil-in-water emulsions stabilized by yeast. **Colloids and Surfaces B: Biointerfaces**, v.128, p.568-576, 2015.
- HEERES, A. S.; PICONE, C. S. F.; VAN DER WIELEN, L. A. M.; CUNHA, R. L.; CUELLAR, M. C. Microbial advanced biofuels production: overcoming emulsification challenges for large-scale operation. **Trends Biotechnology**, v.32, p.221–229, 2014.
- HINDERINK, E. B. A.; KAADE, W.; SAGIS, L.; SCHROËN, K.; BERTON-CARABIN, C. C. Microfluidic investigation of the coalescence susceptibility of pea protein-stabilised emulsions: Effect of protein oxidation level. **Food Hydrocolloids**, v.102, p.105610, 2020.
- KREBS, T.; SCHROËN, K.; BOOM, R. A microfluidic method to study demulsification kinetics. **Lab on a Chip**, v.12, p.1060-1070, 2012.
- MAZUTIS, L.; GRIFFITHS, A. D. Selective droplet coalescence using microfluidic systems. **Lab on a Chip**, v.12, p.1800–1806, 2012.
- MCCLEMENTS, D. J. **Food emulsions: principles, practices, and techniques**. 2. ed. Boca Raton: CRC Press, 2005. 632 p.
- MCCLEMENTS, D. J. **Food emulsions: principles, practices, and techniques**, 3. ed. Boca Raton: CRC Press, 2015. 716 p.
- MENG, Q.; ZHANG, Y.; LI, J.; LAMMERTINK, R. G. H.; CHEN, H.; TSAI, P. A. Altering Emulsion Stability with Heterogeneous Surface Wettability. **Scientific reports**, v.6, p.26953, 2016.

SHEN, F.; LI, Y.; LIU, Z-M.; CAO, R-T.; WANG, G-R. Advances in micro-droplets coalescence using microfluidics. **Chinese Journal of analytical chemistry**, v.43, p.1942–1954, 2015.

USHIKUBO, F. Y.; BIRRIBILLI, F. S.; OLIVEIRA, D. R. B.; CUNHA, R. L. Y- and T-junction microfluidic devices: effect of fluids and interface properties and operating conditions. **Microfluidics and Nanofluidics**, v.17, p.711–720, 2014.

## ANEXO 1

## DECLARAÇÃO DE AUTORIZAÇÃO DE USO DE CONTEÚDO



RightsLink®



Home



Help



Email Support



Sign in



Create Account



### Designing biotechnological processes to reduce emulsions formation and improve oil recovery: Study of antifoams application

**Author:** Tatiana Porto Santos, Rosiane Lopes Cunha

**Publication:** Biochemical Engineering Journal

**Publisher:** Elsevier

**Date:** Nov 15, 2020

Copyright © 2020, Elsevier

Please note that, as the author of this Elsevier article, you retain the right to include it in a thesis or dissertation, provided it is not published commercially. Permission is not required, but please ensure that you reference the journal as the original source. For more information on this and on your other retained rights, please visit: <https://www.elsevier.com/about/our-business/policies/copyright#Author-rights>

[BACK](#)
[CLOSE WINDOW](#)

## ANEXO 2

### DECLARAÇÃO DE AUTORIZAÇÃO DE USO DE CONTEÚDO

Unraveling driving regimes for destabilizing concentrated emulsions within microchannels

T. Porto Santos, C. M. Cejas, R. L. Cunha and P. Tabeling, *Soft Matter*, 2021, **17**, 1821

**DOI:** 10.1039/D0SM01674H

If you are not the author of this article and you wish to reproduce material from it in a third party non-RSC publication you must [formally request permission](#) using Copyright Clearance Center. Go to our [Instructions for using Copyright Clearance Center page](#) for details.

Authors contributing to RSC publications (journal articles, books or book chapters) do not need to formally request permission to reproduce material contained in this article provided that the correct acknowledgement is given with the reproduced material.

Reproduced material should be attributed as follows:

- For reproduction of material from NJC:  
Reproduced from Ref. XX with permission from the Centre National de la Recherche Scientifique (CNRS) and The Royal Society of Chemistry.
- For reproduction of material from PCCP:  
Reproduced from Ref. XX with permission from the PCCP Owner Societies.
- For reproduction of material from PPS:  
Reproduced from Ref. XX with permission from the European Society for Photobiology, the European Photochemistry Association, and The Royal Society of Chemistry.
- For reproduction of material from all other RSC journals and books:  
Reproduced from Ref. XX with permission from The Royal Society of Chemistry.

If the material has been adapted instead of reproduced from the original RSC publication "Reproduced from" can be substituted with "Adapted from".

In all cases the Ref. XX is the XXth reference in the list of references.

If you are the author of this article you do not need to formally request permission to reproduce figures, diagrams etc. contained in this article in third party publications or in a thesis or dissertation provided that the correct acknowledgement is given with the reproduced material.

Reproduced material should be attributed as follows:

- For reproduction of material from NJC:  
[Original citation] - Reproduced by permission of The Royal Society of Chemistry (RSC) on behalf of the Centre National de la Recherche Scientifique (CNRS) and the RSC
- For reproduction of material from PCCP:  
[Original citation] - Reproduced by permission of the PCCP Owner Societies
- For reproduction of material from PPS:  
[Original citation] - Reproduced by permission of The Royal Society of Chemistry (RSC) on behalf of the European Society for Photobiology, the European Photochemistry Association, and RSC
- For reproduction of material from all other RSC journals:  
[Original citation] - Reproduced by permission of The Royal Society of Chemistry

If you are the author of this article you still need to obtain permission to reproduce the whole article in a third party publication with the exception of reproduction of the whole article in a thesis or dissertation.

Information about reproducing material from RSC articles with different licences is available on our [Permission Requests page](#).

### ANEXO 3

#### DECLARAÇÃO DE AUTORIZAÇÃO DE USO DE CONTEÚDO

Colloidal particle deposition on microchannel walls, for attractive and repulsive surface potentials

T. Porto Santos, R. L. Cunha, P. Tabeling and C. M. Cejas, *Phys. Chem. Chem. Phys.*, 2020, **22**, 17236  
**DOI:** 10.1039/D0CP01999B

If you are not the author of this article and you wish to reproduce material from it in a third party non-RSC publication you must [formally request permission](#) using Copyright Clearance Center. Go to our [Instructions for using Copyright Clearance Center page](#) for details.

Authors contributing to RSC publications (journal articles, books or book chapters) do not need to formally request permission to reproduce material contained in this article provided that the correct acknowledgement is given with the reproduced material.

Reproduced material should be attributed as follows:

- For reproduction of material from NJC:  
Reproduced from Ref. XX with permission from the Centre National de la Recherche Scientifique (CNRS) and The Royal Society of Chemistry.
- For reproduction of material from PCCP:  
Reproduced from Ref. XX with permission from the PCCP Owner Societies.
- For reproduction of material from PPS:  
Reproduced from Ref. XX with permission from the European Society for Photobiology, the European Photochemistry Association, and The Royal Society of Chemistry.
- For reproduction of material from all other RSC journals and books:  
Reproduced from Ref. XX with permission from The Royal Society of Chemistry.

If the material has been adapted instead of reproduced from the original RSC publication "Reproduced from" can be substituted with "Adapted from".

In all cases the Ref. XX is the XXth reference in the list of references.

If you are the author of this article you do not need to formally request permission to reproduce figures, diagrams etc. contained in this article in third party publications or in a thesis or dissertation provided that the correct acknowledgement is given with the reproduced material.

Reproduced material should be attributed as follows:

- For reproduction of material from NJC:  
[Original citation] - Reproduced by permission of The Royal Society of Chemistry (RSC) on behalf of the Centre National de la Recherche Scientifique (CNRS) and the RSC
- For reproduction of material from PCCP:  
[Original citation] - Reproduced by permission of the PCCP Owner Societies
- For reproduction of material from PPS:  
[Original citation] - Reproduced by permission of The Royal Society of Chemistry (RSC) on behalf of the European Society for Photobiology, the European Photochemistry Association, and RSC
- For reproduction of material from all other RSC journals:  
[Original citation] - Reproduced by permission of The Royal Society of Chemistry

If you are the author of this article you still need to obtain permission to reproduce the whole article in a third party publication with the exception of reproduction of the whole article in a thesis or dissertation.

Information about reproducing material from RSC articles with different licences is available on our [Permission Requests page](#).

## ANEXO 4

## DECLARAÇÃO CADASTRO SISGEN



Ministério do Meio Ambiente  
**CONSELHO DE GESTÃO DO PATRIMÔNIO GENÉTICO**  
 SISTEMA NACIONAL DE GESTÃO DO PATRIMÔNIO GENÉTICO E DO CONHECIMENTO TRADICIONAL ASSOCIADO  
**Comprovante de Cadastro de Acesso**  
**Cadastro nº A937EF7**

A atividade de acesso ao Patrimônio Genético, nos termos abaixo resumida, foi cadastrada no SisGen, em atendimento ao previsto na Lei nº 13.123/2015 e seus regulamentos.

Número do cadastro: A937EF7  
 Usuário: UNICAMP  
 CPF/CNPJ: 46.068.425/0001-33  
 Objeto do Acesso: Patrimônio Genético  
 Finalidade do Acesso: Pesquisa

**Espécie**

*Saccharomyces cerevisiae*  
*Helianthus annuus*

Título da Atividade: DESENVOLVIMENTO DE UM ANALISADOR DE ESTABILIDADE DE EMULSÕES UTILIZANDO MICROFLUÍDICA

**Equipe**

Tatiana Porto dos Santos UNICAMP  
 Rosiane Lopes da Cunha UNICAMP

**Resultados Obtidos**

Divulgação de resultados em meios científicos ou de comunicação  
 Identificação do meio onde foi divulgado: Periódico: Biochemical Engineering Journal

Data do Cadastro: 13/07/2018 09:09:49  
 Situação do Cadastro: Concluído

Conselho de Gestão do Patrimônio Genético  
 Situação cadastral conforme consulta ao SisGen em 11:21 de 08/01/2021.



SISTEMA NACIONAL DE GESTÃO  
 DO PATRIMÔNIO GENÉTICO  
 E DO CONHECIMENTO TRADICIONAL  
 ASSOCIADO - **SISGEN**